NATIONAL COOPERATIVE HIGHWAY RESEARCH PROGRAM

DRAFT FINAL REPORT

ESTIMATION OF SCOUR DEPTH AT BRIDGE ABUTMENTS

NCHRP 24-20

Robert Ettema, Tatsuaki Nakato, and Marian Muste
The University of Iowa
Iowa City, Iowa 52242
USA

Subject Areas
Highway and Facility Design • Bridges, Other Structures, and Hydraulic and Hydrology •Soils, Geology, and Foundations • Materials and Construction

TRANSPORTATION RESEARCH BOARD
WASHINGTON, D.C.
January 2010
www.TRB.org

ESTIMATION OF SCOUR DEPTH AT BRIDGE ABUTMENTS

EXECUTIVE SUMMARY

Problem Statement

The project described herein comprised a comprehensive investigation conducted to meet the overall goal of developing a comprehensive method for estimating abutment scour in compound channels. The method is intended to be readily used by civil engineers, while being cognizant of the diverse combinations of abutment alignment and design, pier proximity, compound-channel form and orientation, and variations in erodibility of channel boundaries.

The investigation reveals abutment scour to entail substantially more complex processes than envisioned at the project's conception, or portrayed in the literature on abutment scour. Consequently, though the project leads a practicable design method, more work is needed to verify aspects of the method. For example, the project's findings show new insights into the geotechnical nature of abutment scour, a major scour aspect heretofore neglected. The insights show that geotechnical failure of the approach embankment commonly limits scour development and depth. Hydraulic processes commence scour, but geotechnical instabilities of channel banks and abutment embankment commonly limit scour extent.

The complexities and uncertainties attendant to abutment scour normally require the design practitioner to apply a safety factor when using an estimation of scour-depth obtained from a general method for estimating scour depth. The project, however, is limited to the objectives listed below and does not expressly address values of safety factor.

Objectives

To produce a practical approach for estimating abutment scour, the project pursued the following series of objectives:

1. Delineate the general features of the flow field in the vicinity of abutments and their approach embankments in compound channels;

2. Explain quantitatively how variations in compound-channel geometry and roughness, as well as in abutment shape, alignment, and extent, influence the flow field in the vicinity of an abutment; and,

3. Obtain qualitative insight into, and formulate, the relationships between abutment scour and –

    i.   Abutment flow field;

    ii. Variations in the material comprising the compound channel and the abutment; and,

    iii. Pier proximity near an abutment.

4. Use the findings from the foregoing objectives to develop a set of scour-depth estimation methods, or an overall approach, readily useable by engineers designing bridge foundations.

The project fulfills the first three objectives, and partially fulfills the fourth. An overall design approach is proposed and detailed. However, the results of work associated with the first three objectives reveal abutment scour to be considerably more complex than envisioned when the objectives were set forth.

Abutment Forms and Construction

The project considered the following common forms and construction features of abutments:

1. Two common abutment forms, spill-through and wing-wall. Spill-through abutments comprise an abutment column at the end of an unconfined earthfill embankment, whereas wing-wall abutments comprise an abutment column formed as a vertical wall confining the end of an earthfill embankment. Variations exist for each common form;

2. Most abutment columns are supported by piles (circular or H) or sheet-piling extending into a floodplain or channel bed;

3. The compacted earthfill embankment approaching the abutment structure is erodible and subject to geotechnical instabilities. A portion of the embankment surrounding spill-through abutments may be riprap protected, and the riprap protection may include an apron;

4. The floodplain (often extensively comprising cohesive soils) may be much less readily eroded than the main-channel bed; and,

5. Frequently, the first pier of a multi-span bridge is located close to a bridge abutment.

Prior studies of abutment scour focused on the simpler and perhaps idealized situations of scour that did not adequately account for important facets of abutment construction. Commensurately, the prior relationships and guidelines apply to simplified abutment situations, such as an abutment placed in a straight rectangular channel, and can only be extended with considerable uncertainty to actual field conditions.

Flume Experiments

Extensive laboratory flume experiments were carried out with spill-through and wing-wall abutments. The variable erodibility of floodplain and embankment at bridge sites were simulated by means of tests utilizing the following arrangements that bracket them:

1. The floodplain and the embankment are fixed, whereby they are taken to be practically erosion resistant relative to an erodible main-channel bed;

2. The floodplain is as erodible as is the main channel bed, and the embankment is erodible but riprap-armored; and,

3. The floodplain, main-channel bed, and the embankment are essentially equally erodible. All are formed of the same non-cohesive sediment as the main-channel bed.

The experiments entailed observation and measurement of abutment flow fields, scour processes, and scour bathymetry. The ranges of parameters varied for the experiments were constrained by the flumes, and time, available. The ranges were selected so as to encompass the main trends anticipated for abutment scour development.

Numerical Experiments

To broaden the range of insight into the flow field around abutments, the flume experiments were augmented with numerical experiments conducted using a depth-averaged numerical model of flow around a spill-through abutment. The numerical model, FESWMS-2D, simulated two-dimensional, depth-averaged flow around abutments in compound or rectangular channels; in this regard, an abutment set well back on a floodplain was treated as in effect being in a rectangular channel. The insights included information on distributions of flow velocity, unit discharge, and bed shear stress for varying lengths of abutment embankment. Additionally, information on flow vorticity is obtained. The numerical values of unit discharge extend those obtained from the laboratory flume.

Scour Conditions and Observations

Abutment form and layout in a channel develop a flow field essentially equivalent to flow through a short contraction. Consequently, the principal features of scour can be described as follow:

1. Abutment scour is essentially a form of scour at a short contraction. Accordingly, scour is closely influenced by flow distribution through the short contraction and by turbulence structures generated, and dispersed, by flow entering the short contraction;

2. For many, if not most abutments, abutment presence contracts flow non-uniformly across a bridge waterway. However, in situations of short embankments, adjoining relatively wide channels, flow contraction scour decreases in accordance with two limits:

   (i) If channel width is constant and embankment length decreases, scour depth at the abutment approaches zero; or,

(ii) For a full abutment form of constant length in a channel of increasing width, scour depth at the abutment approaches a limiting value associated with scour around an abutment in a very wide channel. This scour depth may be estimated approximately in terms of local flow contraction around the abutment itself.

This second limit can be difficult to simulate by means of hydraulic models replicating the full form and usual construction of actual spill-through and wing-wall abutments, because most laboratory flumes are insufficiently wide;

3. Provided that the approach embankment of an abutment does not breach, so that flow passes through it, abutment scour principally develops as a local amplification of contraction scour associated with flow through a long contraction;

4. Abutment scour typically entails hydraulic erosion followed by geotechnical failure of the main-channel bank and earthfill embankment around the abutment column. Normally, an abutment column is a pier-like structure built from concrete or steel, around which an earthfill embankment is formed. The column transfers load from the bridge deck to the foundation in a similar manner as does a pier; and,

5. Abutment scour may involve three distinct scour conditions, herein termed Scour Conditions A, B, and C. These scour conditions were observed in the flume experiments and as well as at actual bridge sites:

- Scour Condition A occurs as scour of the main channel portion of a compound channel;

- Scour Condition B is scour of the floodplain, and occurs for abutments set well back from the main channel; and,

- Scour Condition C is a scour form that develops when breaching of an abutment's embankment fully exposes its abutment-column structure such that scour develops at the abutment column as if it were a pier.

The report extensively illustrates and examines these scour conditions.

Scour Trends

The flume experiments conducted during the project produced the scour trends described below for Scour Conditions A, B, and C. The trends are discussed in terms of flow depth at the location of deepest scour, Y_{MAX}, and flow depth associated with contraction scour, Y_C.

For Scour Condition A, a useful analytical framework with which to relate maximum flow depth (incorporating maximum scour depth), Y_{MAX}, to flow conditions and boundary sediment or soil is to plot the dimensionless parameters Y_{MAX}/Y_C and q_2/q_1. Here, Y_C is the flow depth estimated for live-bed flow through a long contraction; q_2 is the area-average unit discharge of flow through the bridge section; and, q_1 is the area-average unit discharge of flow through the main channel upstream of the bridge site. At lower values of q_2/q_1, scour depth (and Y_{MAX}/Y_C) is governed by the local flow field around an abutment. However, for large values of q_2/q_1, scour development is governed by flow contraction, so that Y_{MAX}/Y_C asymptotically approaches about 1.1. The approximate 10 percent increase is attributable to local concentration of flow and turbulence generated by flow around the abutment.

For Scour Condition B, a useful analytical framework with which to relate maximum flow depth (incorporating maximum scour depth), Y_{MAX}, to flow conditions and boundary sediment or soil is to plot the dimensionless parameters Y_{MAX}/Y_C and q_{f2}/q_f. Here, Y_C is the flow depth estimated for clear-water flow through a long contraction; q_{f2} is the area-average unit discharge of flow through the floodplain portion of the bridge section; and, q_f is the area-average unit discharge of flow over the floodplain upstream of the bridge site. The trend for Y_{MAX}/Y_C versus q_{f2}/q_f is essentially the same for Y_{MAX}/Y_C and q_2/q_1.

For Scour Condition C, scour depths must be estimated in a semi-empirical manner similar to that used for estimating scour depth at a pier of complex geometry. Scour is governed by the highly three-dimensional flow field developed at an exposed pier-like column.

Pier presence does not dramatically affect scour depth at an abutment. However, when a pier is at the toe of a spill-through abutment, pier presence may decrease abutment scour depth by as much as 22%. This reduction occurs because the pier redistributes flow away from the abutment. Because abutment scour dominates scour at a pier close to an abutment, pier-scour equations are not applicable for a pier close to abutments. The flume experiments show that abutment scour influences pier scour when a pier is nominally within 2.5 times bridge-deck width.

Flow-Field Observations

The flow field around an abutment has essentially the same characteristics as flow fields through short contractions. Notably, flow distribution is not uniform and generates large-scale turbulence structures. As embankment length increased, the flow became more uniformly distributed across the main channel through the bridge waterway. The maximum value of unit discharge around the abutment, relative to the section-average value, peaked at about 1.45. Also, the orientation of the flow at the abutment swung more parallel to the abutment before passing around it and entering the bridge opening. The values of flow velocity and unit discharge obtained from numerical simulation concur well with the broader range of trends evident in flow-field measurements taken in the flume.

Scour development at abutments altered the flow field. By increasing the cross-sectional area of flow, on average scour development reduced flow velocities and values of unit discharge. However, it also caused flow to concentrate in the region of scour. This flow concentration locally amplified contraction scour.

Method for Scour Estimation

The observed flow and scour processes led to the formulation of a hydraulic-engineering method for scour-depth estimation that differs fundamentally from that recommended in the current

leading design guides[1]. The method treats flow around an abutment as flow around a short contraction, and consequently estimates

$$\text{abutment scour} = \text{short-contraction scour}$$
$$= (coefficient) \text{ x (long-contraction scour)}$$

Short-contraction scour is an amplification of long contraction scour. The scour amplification occurs near the abutment, and is attributable to non-uniform distribution of flow around an abutment, and to large-scale turbulence structures generated by passing around the abutment. The *coefficient* empirically takes into account the amplifying erosive effects (on scour depth) of non-uniform distribution of flow and of large-scale turbulence.

For a short abutment in a very wide channel, flow contraction occurs locally around the abutment. Additionally, when a short abutment has a continuous, solid-body foundation (e.g., a sheet-pile skirt) set into boundary material, the generated turbulence structures may strengthen as scour forms around the abutment. This manner of scour is akin to scour development around a wide pier.

As abutment length (including embankment) increases, the flow contraction region extends across more of the bridge waterway. At tight contractions of flow through a bridge waterway, short-contraction scour depth approaches long-contraction scour depth.

The customary approach to scour estimation assumes that abutment flow fields can be separated into two distinct parts: a long contraction in which a uniformly wide contracted flow is assumed to pass through the bridge waterway (giving a so-called "contraction scour"); and, a local field of coherent turbulence structures immediately at the abutment (giving an "abutment local scour"). Observations of abutment flow field and scour development show the customary approach to be

---

[1] Richardson, E.V., and Davis, S.R. (2001). "Evaluating Scour at Bridges." *Hydraulic Engineering Circular* No. 18, 4th Ed., Federal Highway Administration, Arlington, VA.
Melville, B.W., and Coleman, S.E. (2000). *Bridge Scour*, Water Resources Publications, Colorado, U.S.A.

physically unfounded. Several prior studies allude to this weakness in the customary approach, and one existing method[2] uses a similar approach to that advocated in the present study.

In accordance with the three Scour Conditions A, B, and C, two maximum depths of scour are of interest for abutment design –

(i). ***Maximum scour as near-abutment amplification of contraction scour***. The flume experiments show that the maximum scour depth develops essentially as a near-abutment amplification of contraction scour, the amplification caused by the increased flow velocity and turbulence local to the abutment and its approach embankment. This depth occurs when an abutment's embankment has not breached, such that the flow is contracted around the abutment.

For an abutment in a compound channel, the deepest scour should be checked at two locations: in the main channel if the abutment is close to the main channel, and, on the floodplain if the abutment is well set back from the main channel. The two locations coincide with Scour Conditions A and B.

(ii). ***Maximum scour as local scour at a fully exposed abutment column***. The experiments show that the deepest scour at the abutment column itself occurs when the embankment has breached so that the abutment column (e.g., standard stub or wing-wall) is fully exposed as if it were a pier; i.e., for Scour Condition C.

Analysis of the flume data produced design curves for estimating scour depth as near-abutment amplification of contraction scour (Scour Conditions A and B) and for local scour of a fully exposed abutment column. The design curves are readily used by engineers estimating scour depth. Additionally, they produce scour-depth estimates that concur well with the few field data on scour depths at actual bridge abutments.

---

[2] Chang, F. and Davis, S., (1999). "Maryland SHA Procedure for Estimating Scour at Bridge Waterways, Part 1 – Live Bed Scour." In *Stream Stability and Scour at Highway Bridges*, (Eds) Richardson, E. and Lagasse, P., American Society of Civil Engineers, Reston VA, pp 401-4011; and,
Chang, F. and Davis, S., (1998). "Maryland SHA Procedure for Estimating Scour at Bridge Waterways, Part 2 – Clear Water Scour." In Proc. Water Resources Engineering '98, American Society of Civil Engineers, Reston VA, pp 169-173.

Geotechnical Limit to Maximum Scour Depth

The maximum scour depth and width attainable at an intact abutment are limited by the geotechnical stability of the channel bank upon which an embankment may be sited, and by the earthfill approach embankment to the abutment.

It is possible to formulate an approximate geotechnical limit to maximum scour depth at an abutment. For pile-supported abutments this limit occurs when scour leads to the geotechnical collapse of the embankment earthfill such that the abutment column becomes exposed. Further scour results in embankment breaching, relaxation of flow through the bridge waterway, and thereby reduced maximum scour depth. For abutments on footing foundations, a limiting maximum scour-depth coincides with the undermining of the footing and the possible geotechnical collapse of the earthfill embankment behind the abutment column. The present report suggests design relationships indicating how these geotechnical limits can be estimated. An important consideration in this respect is the location of deepest scour relative to abutment-column position.

Of considerable practical, design importance, the design relationships associated with the geotechnical limit provide a novel, direct approach to scour-depth estimation. This approach sets aside hydraulics considerations, and thereby simplifies scour-depth estimation. Further work, involving verification using field data, is needed to confirm this approach.

Field Verification

Though the number of well-documented field cases of abutment scour is rather limited, comparisons of existing scour illustrations and scour depths indicate that the proposed relationships for estimating scour depth produce scour forms and depth estimates that reasonably concur with those observed at actual bridge abutments. The estimated scour depths do not excessively exceed the actual scour depths, as do prior methods for estimating abutment scour

depth. There remains a great need for further documentation of scour forms and bathymetries at abutments.

Scale Effects in Flume Experiments on Scour

The project included an auxiliary set of experiments aimed at determining the extent to which similitude of large-scale turbulence is an important consideration influencing equilibrium depth of scour at abutments and similar hydraulic structures. The experiments involved a set of circular cylinders whose diameters varied in size so as to encompass the width of abutments and piers used in the abutment scour experiments conducted for this project.

The results show a direct trend between equilibrium scour depth (normalized with cylinder diameter) and the intensity and frequency of large-scale turbulence shed from each cylinder. The values of normalized scour depth increased when cylinder diameter decreased. Therefore, similitude of large-scale turbulence is important in scour experiments. The writers offer a scour-depth adjustment factor to account for this trend, which essentially is a scale effect incurred with experiments involving three independent length scales: cylinder diameter, bed-particle diameter, and flow depth. The consequent similitude consideration, or scale effect, has general significance for laboratory studies of local scour associated with hydraulic structures in sediment beds. However, the model scale of abutment widths (i.e., 1:30-scale of two-lane road) used for this project is sufficiently large so as not to lead to substantial exaggeration of scour depth. Additionally, the strong role played by flow contraction in abutment scour further minimizes the experimental uncertainty associated with a scale effect owing to under-scaling of large-scale turbulence.

ACKNOWLEDGEMENTS

Panel Members
David Reynaud Senior Program Officer, NCHRP (*Timothy G. Hess, P.E., was initiating Senior Program Officer, NCHRP*)
Riyad M. Wahab, P.E. (**Chair**) State Geotechnical Engineer Illinois Department of Transportation
Mr. Kenneth Akoh-Arrey, P.E. Bridge Hydraulics Engineer Arizona Department of Transportation

Bart Bergendahl Senior Hydraulics Engineer Federal Highway Administration, Colorado Office (*Jorge E. Pagan-Ortiz, P.E., Senior Hydraulics Engineer Federal Highway Administration, Washington, D.C.*, *was initial FHWA member*)
Larry Harrison, P.E. Consultant Lakewood, Colorado
J. Sterling Jones, P.E. Research Hydraulics Engineer Federal Highway Administration, Virginia
Arthur C. Miller, Ph.D., P.E. Professor Pennsylvania State University
Mark A Palmer, C.E.G. Sr. Engineering Geologist California Department of Transportation
Amy Ronnfeldt Assistant Hydraulics Engineer Texas Department of Transportation
Larry J. Tolfa, P.E. Engineer New York State Department of Transportation
Richard Voigt, P.E. Senior Engineer Polaris Group, Minnesota
Njoroge W. Wainaina, P.E. Assistant State Engineering Geologist North Carolina Department of Transportation

ABSTRACT

This report presents the findings from an extensive, laboratory-based project focused on bridge-abutment scour, a common cause of bridge failure. The findings lead to a practical approach for estimating scour depths at abutments. The approach for scour-depth estimation discards the commonly held notion of linearly combining bridge-waterway constriction scour and local scour at the abutment structure, a notion that the project's findings do not support. Instead, the approach entails estimating abutment-induced local amplification of contraction scour at the bridge opening, and separately estimating a maximum local scour depth at the abutment when exposed by embankment failure. Verification with field observations data confirms the efficacy of the new approach.

An important feature of actual bridge abutments is that they comprise a pile-supported structure set amidst an erodible earthfill embankment. This feature has a pronounced set of influences on scour processes at bridge abutments. The project is the first major effort to include considerations of abutment construction, and to consider how these considerations affect scour processes. The project's findings show that abutment scour is as much a problem of embankment geotechnical stability as of hydraulic erosion of the bed or floodplain upon which the abutment and its embankment are placed. The geotechnical stability of an embankment or floodplain bank limits scour depth.

The project entailed experimentation conducted with two laboratory flumes, and abutments of realistic design that were subject to the scour for a range of abutment and flow conditions. The experiments were conducted with abutments with approach embankments configured in a range of erodibility conditions: fixed embankment on fixed floodplain; riprap-protected erodible embankment on readily erodible floodplain; and, unprotected readily erodible embankment on readily erodible floodplain. The flume experiments were supported by numerical simulation of depth-averaged flow around abutments.

TABLE OF CONTENTS

[Note: exact page numbers to be given in galley proofs of Final Report]

LIST OF TABLES

LIST OF FIGURES

LIST OF SYMBOLS

d_{S0pier}	scour depth at pier without the abutment;
d_{Se}	equilibrium scour depth;
E_H	embankment height;
f	Darcy-Weisbach resistance factor;
F_o	densimetric Froude number $= V / \sqrt{(s-1)gd_{50}}$;
F_{fo}	approach Froude number on floodplain;
F_r	Froude number;
F_{rc}	critical Froude number for sediment entrainment;
F_{re}	Froude number with flow obstructed by embankments: $F_{re} = V_e / \sqrt{gY_0}$;
g	gravitational constant;
G_{si}	total sediment flow;
g_{si}	total sediment flow per unit width;
$0.5H$	amplitude of bed forms (H is bed form height);
K_b	alignment factor;
K_I	flow intensity factor;
K_S	abutment shape factor;
K_w	Adjustment factor to account for inadequate similitude of large-scale turbulence structures;
l	length of pier and exposed abutment;
L	length of embankment;
L_p	distance between the pier and abutment toe;
m	ratio of q_{MAX} to $\bar{q}_2$;
m_A	value of m for Scour Condition A;

m_B	value of m for Scour Condition B;
m_S	bridge section ratio between approach section and bridge section;
M	discharge contraction ratio (Sturm and Janjua, 1994);
n_i	Manning's flow resistance coefficient;
q_f	flow rate per unit width on floodplain;
$\bar{q}_f$	average flow rate per unit width on floodplain;
q_i	flow rate per unit width;
q'_i	average flow rate per unit width of i-th stream tube;
q_{MAX}	maximum flow rate per unit width;
Q	total flow rate;
Q_{im}	total flow rate in main channel;
Q_f	total flow rate on floodplain;
Q_a	flow component intercepted by abutment (Kouchakzadeh and Townsend, 1997);
Q_w	flow component related to specific width of channel at end of abutment (Kouchakzadeh and Townsend, 1997);
R	radial distance from abutment column to the location of deepest scour;
s	specific gravity of bed material;
S_0	hydraulic slope;
S_h	abutment shape factor; Eq. (5-25);
ST	spill-through abutment;
t_d	duration of experiment;
t_e	time of embankment breach;
U	depth-averaged flow velocity;

u_*	shear velocity associated with flow;
u_{*c}	critical shear velocity;
u_{*fc}	critical shear velocity in floodplain;
V_{F1}	average flow velocity at upstream end of abutment;
V_{F1c}	critical mean velocity for bed sediment entrainment on approach floodplain;
V_c	critical mean velocity for sediment entrainment;
V_i	mean velocity in the stream wise direction;
V_{MAX}	maximum depth-averaged velocity near abutment face at beginning of scour;
VW	vertical wall abutment;
w	sediment particle fall velocity;
W	abutment top width;
WW	wing-wall abutment;
Y_i	flow depth;
Y_0	initial approach flow depth in main channel;
Y_C	flow depth deepened by contraction scour;
Y_f	initial approach flow depth on floodplain; and,
Y_{MAX}	maximum flow depth where maximum scour depth located

Greek Symbols

α	coefficient or amplification factor;
β	abutment alignment angle;
λ	wave length of bed forms;
γ	angle of attacking flow to pier and exposed abutments;

γ_E	specific weight of earthfill embankment;
ρ	water density;
μ	fluid dynamic viscosity;
θ	Shields parameter $= u_*^2 / \left(s - 1 \right) g d_{50}$;
θ_c	critical Shields parameter for sediment entrainment $= u_{*cr}^2 / \left(s - 1 \right) g d_{50}$;
θ_S	equilibrium slope after development of the scour hole;
σ_g	geometric standard deviation $= d_{84}/d_{50}$;
	particle-drag component of shear stress associated with flow;
τ_1	shear stress associated with flow in approach section in main channel;
τ_2	shear stress associated with flow in bridge waterway;
τ_c	critical shear stress for sediment movement; and,
τ'_f	shear stress associated with flow in approach section on floodplain.

Subscripts

i	1, and 2 for section 1 (approach section), and 2 for section 2 (bridge section), respectively; 3 for section of maximum stream-tube contraction
f	floodplain

CHAPTER 1

INTRODUCTION

1.1 Preamble

Bridge abutments commonly border swift, turbulent flow through bridged waterways, and therefore risk failure by scour. Though abutment scour is an extensively studied topic, the prevailing perception among many hydraulic engineers is that the existing design relationships (derived almost entirely from laboratory flume experiments) significantly over-predict scour depths; the scour depths observed at actual abutments typically are much less than those predicted. The present report, which focuses on scour at abutments in compound channels, suggests that the processes causing scour failure of abutments have been inadequately understood heretofore. The report presents new insights about the processes, and recommends a substantially new method for estimating maximum depth of scour at two common forms and construction configurations of abutment – spill-through abutments and wing-wall abutments – in compound channels. Both abutment forms usually are constructed as a fabricated abutment column supported by piles, and are set amidst a compacted earthfill approach embankment. Figures 1-1 and 1-2, respectively, show representative spill-through and wing-wall abutments.

The design method presented is not entirely new, as is indicated subsequently. However, the method conveys a more comprehensive approach to abutment scour estimation than proposed in prior publications. In developing a new method for scour-depth estimation for abutments in compound channels, the following points must be considered:

1. An emphasis is given to the reasonable *approximate estimation* of scour depth rather than the accurate *prediction* of scour depth. Too many practical factors impede accurate prediction of scour depth;

2. Scour-depth estimation should take into account how an abutment is constructed;

3. The different erosion susceptibility (erodibility) of the bed and floodplain of a compound channel can lead to several scour conditions;

4. For abutments at most bridge waterways, abutment scour cannot be dissociate from so-called contraction scour at a bridge waterway; and moreover,

5. The depth to which scour develops is limited by the geotechnical stability of the earthfill embankment at typical abutments. The report indicates (in Section 9-3) this geotechnical limit to abutment scour.

By and large, the existing methods and guidelines for estimating abutment scour depth inadequately address the complexities associated with real-world channel geometry and boundary material, as well as actual design of abutment. Research to date on abutment scour has focused on the simpler and idealized situations of scour. Commensurately, the existing relationships and guidelines apply to simplified abutment situations, notably abutments placed in straight rectangular channels. Such relationships can be extrapolated only with considerable uncertainty to actual abutment sites. Extrapolation potentially causes existing scour relationships to be questionable, predicting substantially greater extents of scour than actually may occur at many bridge sites. A degree of conservatism in scour-depth estimation is understandable (e.g., basing a design on an upper-bound estimate), but foundations placed substantially deeper than necessary (for load support) incur unwanted additional expense. However, when existing relationships or guidelines inadequately take into account some scour processes, there is a risk that the location of scour failure differs from that assumed for the estimation relationship or guideline. Moreover, none of the current methods accounts for the limited geotechnical stability of the earthfill embankment, for instance.

It is necessary to recognize that numerous practical and seemingly mundane considerations potentially complicate accurate prediction of maximum scour depth and its location relative to an abutment. Many abutments are sited in compound channels whose geometry and hydraulic characteristics are markedly site-specific, and whose boundaries are formed of several types of soils and sediments occupying different locations within a bridge site. Sands and/or gravels may form the bed of a main channel; silts and clays may predominate in riverbanks and underlying floodplains; lenses of clay, rock, and alluvium may interleaf over the depth of a foundation site. Rocks and assorted concrete elements may have been placed as erosion protection for the abutment, as well sometimes along adjoining riverbanks. Vegetation, too, may affect site

1-2

conditions, both as growth around an abutment or as debris accumulated against part of a bridge. Moreover, the abutment foundation arrangement may differ from site to site.

Because of the numerous variables that may influence the depth and location of scour at most actual abutment sites, it is important to realize that any quantitative relationship for use in scour-depth prediction inevitably must be based on a simplification or idealization of the scour type under consideration. Consequently, accurate prediction of scour depth incurs considerable uncertainty. To ensure that the uncertainty errs conservatively from the standpoint of abutment design, quantitative relationships for scour prediction should aim to give upper bound or upper envelope values of scour depth. The values must be realistic, taking into account the major geometric, flow, and soil features of the abutment site, but cannot be expected to take into account second-order features reflecting local variability in, say, riverbank condition or floodplain roughness.

The complexities and uncertainties attendant to abutment scour processes should require the design practitioner to apply a safety factor when using an estimation of scour-depth obtained from a general method for estimating scour depth. The Project, however, is limited to the objectives listed below and does not expressly address values of safety factor. The design relationships proposed in Chapter 12 of the present report do not include a safety factor, but rather are envelop relationships fitted to data obtained from experiments conducted for the Project.

1.2. Scope and Objectives

The Project's scope entailed a comprehensive effort of laboratory research aimed at achieving the overall purpose of developing acceptably accurate, and suitably comprehensive methods for predicting abutment scour at abutments sited in compound channels. Within its scope the Project aimed to produce a practical method for scour-estimation and scour-monitoring for use by civil engineers. The methods link to parallel guidelines developed by companion NCHRP Projects: *Scour at Contracted Bridge Sites* (NCHRP Project 24-14), *Bridge Scour in Cohesive Material* (NCHRP Project 24-15), and *Abutment Scour Countermeasures* (NCHRP Project 24-18).

The research addressed the following set of objectives:

1. Delineate the general features of the flow field in the vicinity of abutments and their approach embankments in compound channels;

2. Explain quantitatively how variations in compound-channel geometry and roughness, as well as in abutment shape, alignment, and extent, influence the flow field in the vicinity of an abutment;

3. Obtain qualitative insight into, and formulate, the relationships between abutment scour and –

    (i)   abutment flow field;

    (ii) variations in the material comprising the compound channel and the abutment; and,

    (iii) pier proximity near an abutment.

4. Develop a scour-depth estimation method readily useable by engineers designing bridge foundations.

Three issues were of key importance in understanding abutment scour and developing useful relationships for predicting maximum depths of scour:

1. Which types of abutment layout, form and construction configuration, and thereby scour conditions, are of essential and practical importance?

2. How do floodplain and main-channel flows combine and contribute to scour at abutments located in compound channels formed of a floodplain flanking a main channel? And,

3. Why do scour-prediction relationships developed from laboratory flumes seem to predict larger scour-depths than the depths observed at actual bridge abutments?

It is pertinent to note at the report's outset that the comprehensive investigation conducted for the Project reveals abutment scour processes to be substantially more complex than envisioned at the Project's conception, or portrayed in the literature on abutment scour. Consequently, though the

report presents a set of practicable design methods, more work is needed to verify the methods. For example the report shows new insights into the geotechnical nature of abutment scour, a major scour aspect heretofore neglected. The insights show that geotechnical failure of the approach embankment commonly limits scour development and depth.

The present report does not directly address abutment scour for conditions when the bridge is submerged. Scour-depth estimation for this situation would use essentially the same method as presented herein for estimating scour.

1.3 Proposed Method

The method for scour-depth estimation presented here is substantially new, relative to the commonly used methods presented in leading scour-related publications such as Richardson and Davis (2001) and Melville and Coleman (2000). It treats flow around an abutment as flow around a short contraction, and consequently estimates

abutment scour   =   short-contraction scour

      =   (*coefficient*) x (long-contraction scour)   (1-1)

Short-contraction scour is an amplification of long contraction scour. The scour amplification occurs near the abutment, and is attributable to non-uniform distribution of flow around an abutment, and to large-scale turbulence structures generated by passing around the abutment. The term "*coefficient*" empirically takes into account the amplifying erosive effects (on scour depth) of non-uniform distribution of flow and of large-scale turbulence. Chapter 4 elaborates on the formulation of the coefficient as pertains to Scour Conditions A and B.

Scour at abutments entails flow contraction around the abutment. At most bridge sites, flow contraction occurs throughout the entire bridge waterway. However, for short embankments in very wide channels, flow contraction may occur only around the abutment itself, with little or no contraction scour occurring across the bridge waterway. For such abutments scour depth also can be estimated as amplification of contraction erosion, though using the flow field locally contracted around an abutment.

The approach presented here departs from the customary approach based on the physically questionable assumption that abutment flow fields can be separated into two distinct parts: a long contraction in which a contracted flow of uniform width is assumed to pass through the bridge waterway (giving a so-called "contraction scour"); and, a local field of coherent turbulence structures immediately at the abutment (giving a "abutment local scour"). Each part is assumed to produce a certain scour depth, and the scour depths of the parts are then linearly combined as

$$\text{abutment scour} = \text{contraction scour} + \text{abutment local scour} \qquad (1\text{-}2)$$

The approach based on Eq. (1-2) is set forth in numerous publications on bridge scour; e.g., Richardson and Davis (1995, 2001), Melville and Coleman (2000), Hoffmans and Verheij (1997), AASHTO (1992), and Neill (1973). While the assumption may be appropriate for estimating scour at bridge piers, it is not supportable for scour at bridge abutments, because, in many abutment situations, the flow field cannot be separated into flow contraction and local regions. Eq. (1-2) only holds when contraction scour (over the bridge waterway) is zero.

The approach expressed as Eq. (1-1), though, is not absolutely new. Chang and Davis (1998, 1999) present a method for estimating abutment scour under clear-water and live-bed scour conditions. Their method forms the basis of ABSCOUR, a procedure for estimating abutment scour. The writers' method, developed independently of that proposed by Chang and Davis, uses essentially a similar premise as used by Chang and Davis: i.e., the coefficient in eq. (1-1) embodies the influences that flow non-uniformity and turbulence exert in amplifying scour depth assessed in terms of flow contraction through a bridge waterway. The method proposed by Chang and Davis is considered further in Chapter 5.

In a further departure, the present approach considers the geotechnical aspects of abutment scour; in particular, for spill-through abutments. Most prior studies focus on maximum scour depth at a simplified, rigid-abutment structure replicated as a flat plate or solid structure that extends at depth into a sand bed (e.g., the studies summarized in Richardson et al., 2001; Melville and Coleman, 2000). Scour depth for such simulations is not limited by considerations of

geotechnical stability of the abutment itself. Typical bridge abutments, however, usually are constructed as a pile-founded column (e.g., standard-stub column used for spill-through abutments) set within a compacted earthfill embankment, as discussed in Chapter 2. Because the embankment is subject to geotechnical instabilities, and is potentially erodible, abutment failure owing to scour involves hydraulic erosion of the channel bed or floodplain near an abutment, followed by geotechnical instability and collapse of the abutment's earthfill embankment, with subsequent further erosion. It is common for field examples of abutment scour to show that the earthfill embankment failed rather than the abutment column failing. Therefore, important considerations influencing abutment scour are the variable and uncertain shear strength of the earthfill forming the embankment, as well as the erodibility and shear strength of the floodplain soil upon which an abutment may be sited.

1.4 Structure of the Report

This report is structured in two parts so as to guide its reader directly to, and through, the new scour-estimation method produced by Project 24-20, yet also to provide the requisite support descriptions and data underpinning the method. Accordingly, the first part of the report briefly outlines the characteristics of common spill-through and wing-wall abutments (Chapter 2). Appendix A briefly summarizes the findings of a survey questionnaire sent to state Departments of Transportation regarding abutment design forms and layouts commonly used. Chapter 3 outlines the main scour processes at common forms and layouts of abutments. The recommended scour-estimation method is outlined next (Chapter 4), and the method's relationship is then compared with prior methods for scour estimation (Chapter 5).

The second part of the report documents the laboratory tests and numerical simulations (Chapters 6 through 11) conducted in developing the method. Appendices B1-B7 give photo sequences of scour development for representative laboratory tests. Appendix C addresses the issue of possible scale-effect concerns for laboratory tests on scour. The results of all these tests and simulations are transitioned to design curves in Chapter 12, which also discusses field validation of the method. Chapter 13 is a design guide for applying the estimation method. The principal conclusions drawn from the laboratory tests and numerical simulations are summarized in Chapter 14.

The Project entailed a comprehensive group of laboratory flume experiments to attain the set of objectives listed in Section 1.2. The numerical simulation, carried out using a two-dimensional, depth-averaged flow model addresses an important specific question at the heart of the relationship between scour depth and flow around an abutment; i.e., What is the maximum velocity (bed-shear stress or unit discharge) developed by flow around an abutment?

Verification of the new method by means of field observations and data is not a straight-forward procedure. There are fairly numerous anecdotal accounts and illustrations of scour at actual bridge abutments. Most accounts anecdotally discuss or illustrate the failure of an abutment, but do not relate the scour depth to flow conditions, thereby, complicating quantitative verification. The scour-estimation method presented in this report is sufficiently versatile that it accounts for the diverse combinations of abutment form and alignment, geometry and hydraulic characteristics of compound channels, channel morphology, proximity of nearby bridge piers, and the sediments and soils comprising channel, floodplain and abutments, and the erodibility of the embankment adjoining an abutment.

1.5 Scale Effects in Flume Tests

Scour of a sediment bed around an abutment involves a complex flow field marked by large-scale turbulence structures generated by flow around the pier or abutment. A concern exists that laboratory-based equations used for estimating scour depths at cylinders inadequately take into account the similitude considerations in the scaling of the frequency and vorticity of large-scale turbulence structures, notably the wake vortices, generated by a cylinder. A consequence of inadequate scaling of large-scale turbulence is that flume experiments with small models can produce larger values of equilibrium scour depth relative to structure size than those found in the field. The consequence may affect the veracity of the scour-estimation methods developed from this Project (and prior methods), and therefore needs to be explored.

As with the present Project, local scour has been studied primarily by means of laboratory flume experiments entailing the use of dimensionless parameters relating maximum scour depth to the mean flow field and the sediment bed in which the pier or abutment is founded. Numerous

flume studies provide semi-empirical equations for the maximum scour depth. A lingering concern is that the available scour equations commonly over-predict scour depths compared to field-observed scour depths. Such overestimation may be due to several reasons, but one substantial similitude effect seems to have been overlooked in prior studies. That effect concerns the scaling of large-scale, turbulence structures formed by flow around a pier or an abutment. The present Project, accordingly, includes a brief investigation of turbulence scaling and its effect on scour. Appendix C presents the findings of this investigation.

1.6 Relationship to Other NCHRP Projects

The Project builds on prior work documented in FHWA Publication No. FHWA-RD-99-156 (2004) "Enhanced Abutment Scour Studies of Four Compound Channels," and prior efforts sponsored by NCHRP. In this respect, it links to NCHRP 24-8 "Scour at Bridge Foundations: Research Needs" and to the Federal Highway Administration's HEC-18 document, "Evaluating Scour at Bridges" (Richardson and Davis 1995, 2001).

It also would link directly to the following three NCHRP studies in the process of being completed during the course of the present Project:

1. NCHRP Project 24-14, "Scour at Contracted Bridge Sites";

2. NCHRP Project 24-18, "Countermeasures to Protect Bridge Abutments from Scour." This project was completed during the latter stage of the present Project; and,

3. NCHRP Project 24-15(02), "Abutment Scour in Cohesive Materials." This project was completed at about the same time as the report for the present project. Consequently, this report does not review Project 24-15(2). Section 4.9 of this report, however, indicates how it relates to the present project.

4. NCHRP Project 24-32, "Scour at Wide Piers and Long, Skewed Piers." This project was underway at the same time as the present project. Section 4.9 of this report indicates how it relates to the present project.

Figure 1-1. A spill-through abutment with earthfill approach embankment on a floodplain

Figure 1-2. A wing-wall abutment with earthfill approach embankment

CHAPTER 2

ABUTMENT FORM AND CONSTRUCTION

2.1 Introduction

The principal design characteristics of an abutment can be described in terms of its form, the overall layout of its approach embankment at a bridge waterway, and the abutment's construction configuration. These characteristics, together with the waterway's channel morphology, boundary sediments and soils, as well as flow-resistance features (e.g., vegetation state of the floodplain), influence abutment flow field, and thereby, scour. However, a striking, and somewhat complicating, characteristic of bridge abutments is that few abutment situations are quite alike. Accordingly, the development of a method for estimating scour depth at abutments requires that the abutment forms, layouts, and construction configurations of common practical importance be identified.

An early task for the Project entailed surveying Departments of Transportation to ascertain the forms, layouts, and construction configurations commonly used for abutments, and obtaining their experience with abutment scour. This task led to a set of representative characteristics for abutment form, layout, and configuration. These characteristics were used in selecting the form, layout, and construction configurations of abutment upon which the Project focused, and the flow conditions simulated during the laboratory tests conducted for the Project. Appendix A summarizes the general findings from the survey.

2.2 Abutment Form

There are two general forms of abutment:

1. spill-through abutments; and,

2. wing-wall abutments.

Figures 2-1a,b illustrate them. Spill-through abutments have sloped sides, whereas wing-wall abutments have a vertical face and wing-walls that retain an earthfill approach embankment. As indicated in Appendix A, a survey of state departments of transportation indicates that spill-through abutments are by far the most common abutment form used in the U.S. The wing-walls can be oriented at various angles to the abutment's central panel, although a 45° angle is representatively common. A wing-wall abutment with wing-walls angled at 90° to its central panel is sometimes called a vertical-wall abutment, and is fairly common for small abutments. Sheet-pile caissons extending in channels also may be viewed as a type of vertical-wall abutment.

2.3 Abutment Layout

In a somewhat simplified manner, it is useful to discuss abutment layout in terms of the length, L, of an abutment plus its approach embankment, floodplain width, B_f, and overall width of the channel at a bridge waterway, B. These variables are indicated in Figure 2-2. Bridge abutments then can be characterized as conforming to the following layout arrangements, which can be characterized in terms of the variables L, B_f, and B:

1. The abutment is located on the floodplain of a compound channel ($L \leq B_f$). This layout is typical for spill-through abutments;

2. The abutment extends up to the main channel ($L \approx B_f$). This layout is typical for wing-wall abutments, especially for channels having a narrow, or no, floodplain. Wing-wall abutments are common for bridges over small streams; and,

3. The abutment is located in a rectangular channel, and no floodplain is present. This layout is not common, although it is essentially similar to a relatively short abutment on a wide floodplain. Also, it is similar to channel-control structures (e.g., spur-dikes, groins, barbs, hard-points) and coffer-dams and construction caissons.

The nature of an abutment inevitably requires that the layout of an abutment be tailored to fit the local topography of a bridge site. Therefore, to varying extents each abutment inevitably differs in layout.

2.4 Abutment Construction

In the U.S., it is usual for the top width of the abutment to accommodate minimally a road width of 24 ft (7.22 m) plus two shoulders of width 8 ft (2.41 m), giving an overall top width of 40 ft (12.04 m). The side-slopes of earthfill approach embankments commonly are set at a 2:1 inclination, though slopes range from about 2 horizontal:1 vertical to 3 horizontal:1 vertical. Figure 2-3 illustrates the embankment geometry used for the spill-through abutments. The embankment geometry for the wing-wall abutments will be essentially similar to that shown in Figure 2-3, except that the vertical face of a wing-wall abutment retains the end of the embankment.

Abutments usually comprise a concrete support wall founded on a pile cap supported by piles or on a spread footing, and adjoin an earthfill approach embankment. Pile supports are more common than are footing supports, unless the abutment is founded directly on rock. Spill-through abutments are formed around a "standard-stub abutment," which comprises a concrete stub supported by a pile cap on two rows of circular piles. The design and dimensions of a standard-stub abutment commonly used by the Illinois, Iowa, and New York DOT's are shown in Figure 2-4. Wing-wall abutments usually have similar foundation layouts as the standard-stub abutments, except that they include wing-walls extending from the central stub. Figure 2-5 shows the design and dimensions of a wing-wall abutment commonly used by the Illinois, Iowa, and New York DOTs.

The elevation of the pile cap and the detailed arrangement of piles may vary from bridge site to bridge site. At some sites, the pile cap is located at, or near, the top elevation of the floodplain, whereas at other sites the piles extend upward through the embankment earthfill. In this latter case, the piles directly support a cross beam, which in turn supports the beams of the bridge deck. Also, for some sites, wing-wall abutments may be supported by sheet piles driven in approximately the same plan layout as the abutment.

2.5 Pier Proximity

Many bridges over rivers are constructed with a comparatively short first deck span, such that a pier is located very close to an abutment. There are structural advantages to having a pier close to the abutment and riverbank, and this arrangement often facilitates a clear span over the river. At times, a high spill-through abutment may cause the first pier to be positioned close to an abutment. These construction considerations, however, raise the question as to whether pier proximity could adversely influence abutment scour. Figure 2-6 depicts a fairly common example of a bridge which has a pier located close to an abutment.

The pier simulated a standard pier design used by the Iowa DOT, shown in Figure 2-7. The pier, as shown in Figure 2-6, has a solid-wall column extending to the bridge deck. This common pier geometry was chosen because it would more markedly affect the flow field and thereby scour than would a pier comprising two, or one, circular columns. The pier has the following features:

1. The deck width of the pier is approximately 12.04m (40ft), in accordance with a two-lane road;

2. Pier thickness is 0.9m (3ft);

3. The pier's support piles are 0.3m (1ft) in diameter, and are spaced 1 to 2m (nominally, 3 to 6ft) apart, in accordance with their layout arrangement; and,

4. The top of the pier's pile cap is at the average level of the main-channel bed.

Pier proximity relative to an abutment can later be discussed in terms of the distance between the pier and the abutment toe, L_p.

2.6 Sediment and Soil

The main-channel, floodplain, and embankment components of a bridge-waterway boundary usually comprise different zones of alluvial sediments and soil, as indicated in Figure 2-8. Abutment scour usually erodes through several zones of sediment and soil, with different processes, and at varying rates of erosion.

The main channel normally has an alluvial bed of noncohesive sediment (sands and gravels), whereas the channel's floodplain may be formed from considerably finer sediments (silts and clays), typically causing the floodplain soil to be more cohesive in character than the bed sediment of the main channel. The banks of the main channel usually are formed of the floodplain soils, and thus also may behave cohesively so as to stand at a fairly steep slope.

Most abutments have an earthfill approach embankment formed of compacted soils. The soils may have been excavated from the floodplain or have been brought to the bridge site from elsewhere. The earthfill embankment is placed and compacted to a specific value of shear strength so as to support the traffic load.

Direct, dynamic simulation of the strength behavior of an earthfill embankment or a floodplain soil poses a practical difficulty for laboratory experiments on scour at bridge abutments. The difficulty is to replicate, at a reduced scale, the shear strength of a representative earthfill embankment. To date, no study appears to have attempted experiments that closely replicated the strength behavior of an embankment or the floodplain.

A preliminary set of tests, conducted before undertaking the flume experiments for the Project, briefly investigated ways to simulate the shear-strength behavior of an earthfill embankment and floodplain. In particular, the tests investigated the effect of additives (fly ash, cement, and clay) applied to sand. However, the additives were found to produce unsatisfactory results, and were abandoned. It was found from tests, though, that model embankments formed of compacted wet sand replicated the essential features of a geotechnical failure behavior of an earthfill embankment next to an evolving scour region; one behavioral difference was that an embankment made of sand failed somewhat faster than that made of a compacted earthfill embankment. It was decided, therefore, to use sand as the model embankment soil.

To address the influences that variable floodplain and embankment conditions would exert on abutment scour, the present study used the following three-condition approach:

1. Fix the floodplain and the embankment, thereby assuming the embankment and floodplain to be far less erodible than the bed sediment in the main channel (Fixed Abutment);

2. Make the floodplain and the embankment erodible, but protect the embankment with a layer of riprap (Riprap Abutment); and,

3. Make the floodplain and the embankment erodible and unprotected (Erodible Abutment).

These three conditions bracket the range of erodibility conditions that likely occur at bridge abutments. As is explained subsequently in Chapter 6, these conditions facilitated the investigation of the scour conditions that occurred at bridge abutments.

2.7 Flow Field

Flow through a bridge waterway narrowed by a bridge abutment and its embankment is akin to flow around a short contraction[3], for which Figure 2-9 schematically illustrates the characteristic flow features. They are intrinsically connected, – the flow width narrows and the flow accelerates through the contraction, generating macro-turbulence structures (eddies and various vortices spun from the contraction boundary) that shed and disperse within the flow. Flow contraction and turbulence at many bridge waterways, though, is complicated by the shape of the channel in which the waterway is located. It is common for waterways to traverse a deeper main channel flanked by floodplain channels, as shown in Figure 2-10.

A further complication for most bridge waterways is that they are erodible contractions. Also, the contraction can be much greater than envisioned in Figure 2-9. Flow may scour the boundary, possibly causing the contraction to fail and widen. Commonly, the bed of the main channel is much more erodible than the floodplain, because the bed is formed of loose sediment, while the floodplain is formed of more cohesive soil often protected by a cover of vegetation. Accordingly, two prime scour regions typically develop (as borne out by field observations of scour):

---

[3] The contraction is short in the streamwise direction

1. Where the boundary is least resistant to hydraulic erosion. This could be the main-channel bed if flow velocities (and unit discharges) are sufficiently large; and,

2. Where the flow velocities (and unit discharges) and turbulence are greatest. This usually is near the abutment.

These regions are indicated in Figure 2-10. Identifying the exact locations of scour can be complicated by the mix of materials forming the compound channel and the embankment approach to the abutment, and by the presence of piers, which locally scour and expose floodplain soils.
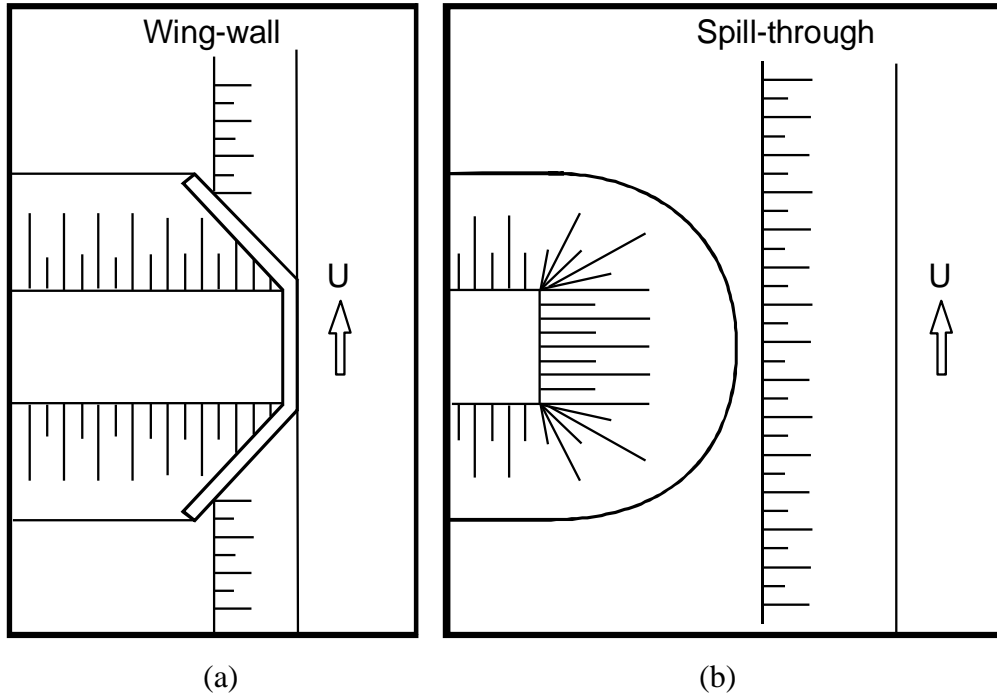
Figure 2-1. Plan views of the two common abutment forms: wing-wall abutment (a), and spill-through abutment (b)
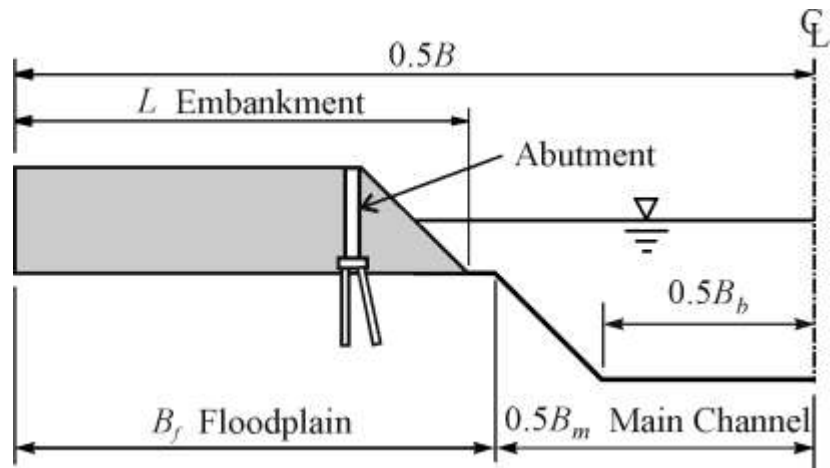
Figure 2-2. A definition sketch showing embankment length extending to the abutment, floodplain width, and main-channel width
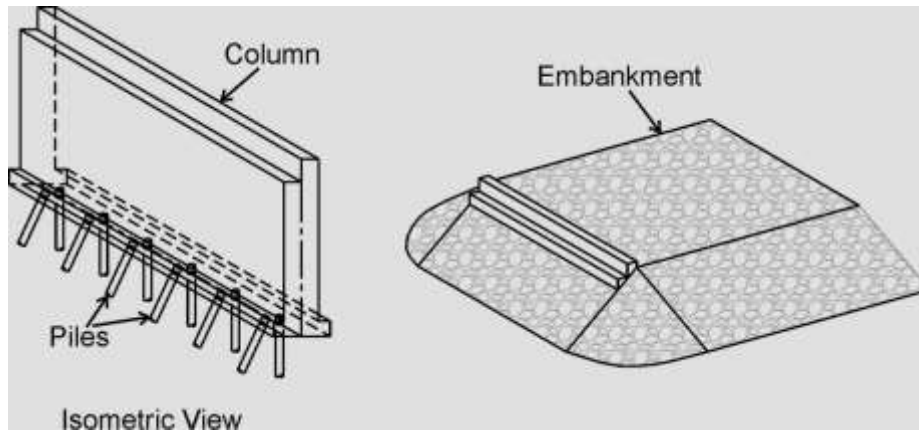
Figure 2-3. Isometric view of spill-through abutment comprising a standard-stub column located within the end of an earthfill embankment
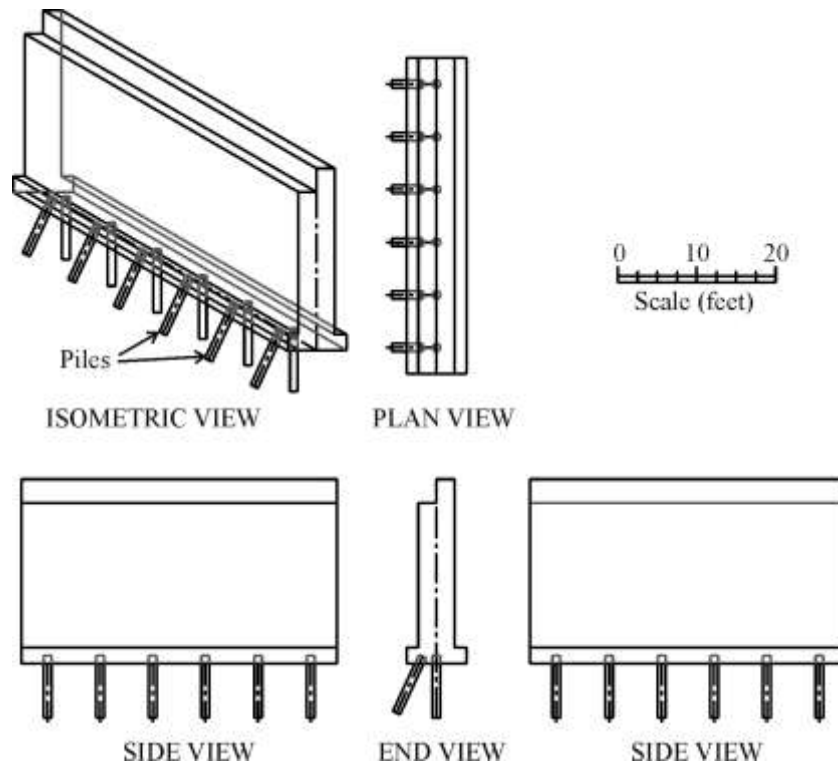
Figure 2-4. The geometry and dimensions of a standard-stub abutment commonly used for spill-through abutments (prototype scale indicated); design provided by the Iowa DOT
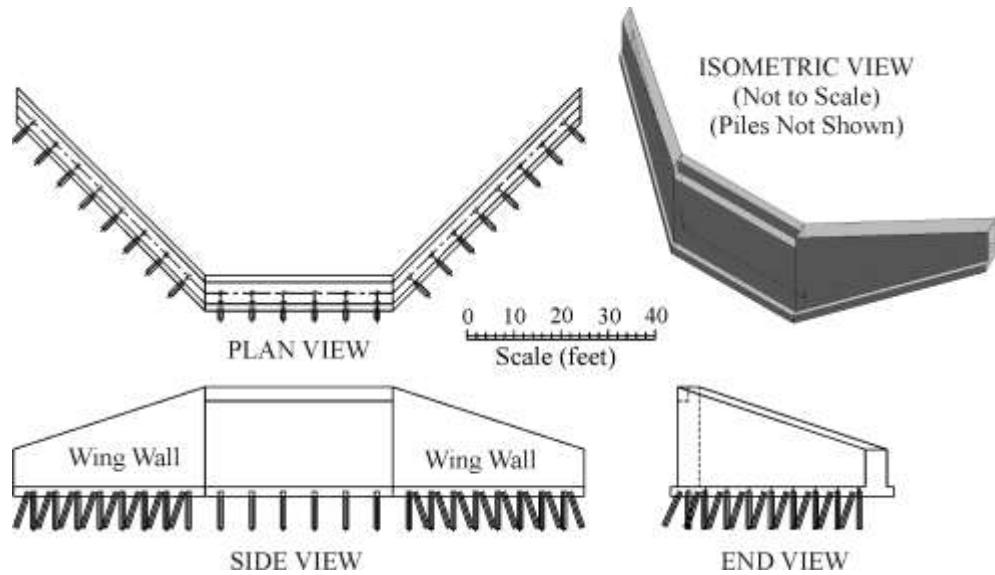
Figure 2-5. The geometry and dimensions of a wing-wall abutment - compacted earthfill embankment extends back from the abutment structure (prototype scale indicated); design provided by the Iowa DOT

Figure 2-6. A spill-through abutment with a pier in close proximity; approximate layout proportions of $L/B_f = 1.0$; $B_f/0.5B \approx 0.7$, and $L/W \approx 1.0$, in which W = abutment top width

ELEVATION VIEW OF BRIDGE PIER

END VIEW OF BRIDGE PIER

0   15   30
Scale (ft)
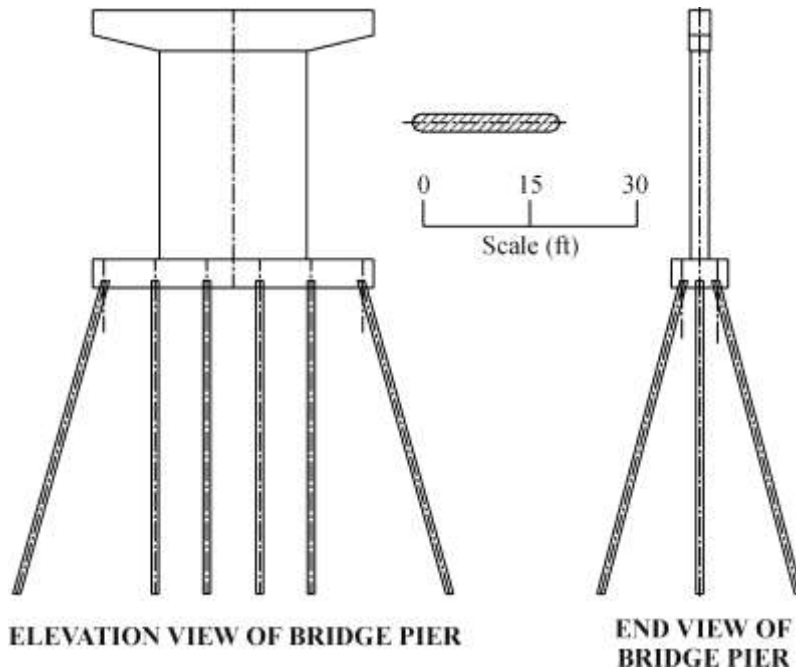
Figure 2-7. The pier form used in the present Project; design provided by the Iowa DOT

Embankment

Abutment

Piers

Compacted Earth Fill

Flood Plain Channel

Main Channel

Flood Plain Channel

Flood Plain Soil

Bed Sediment

Flood Plain Soil
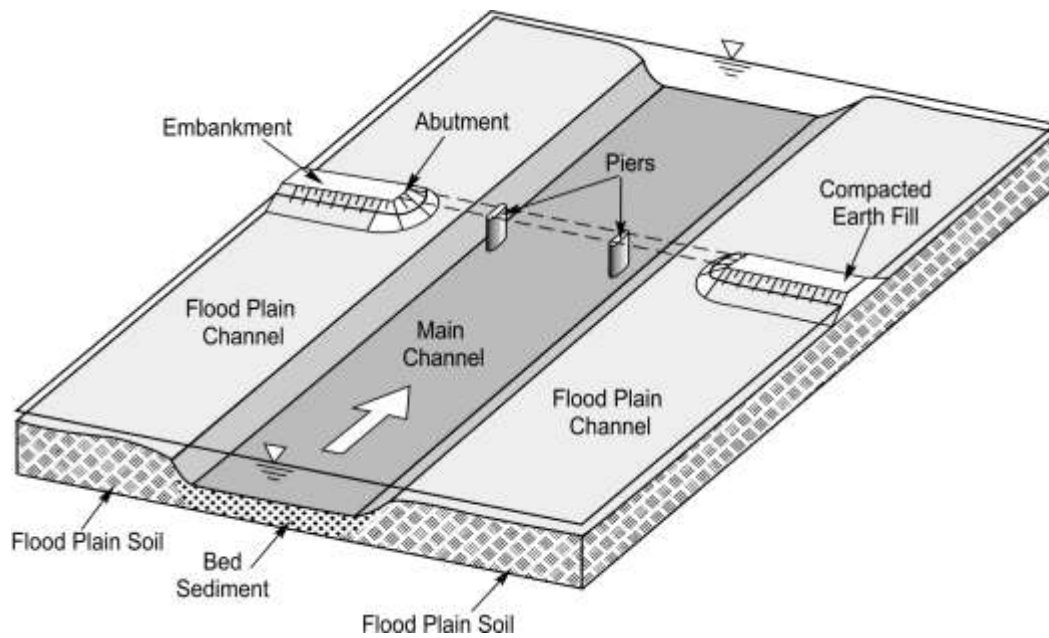
Figure 2-8. Variation of soil and sediment conditions at a bridge waterway
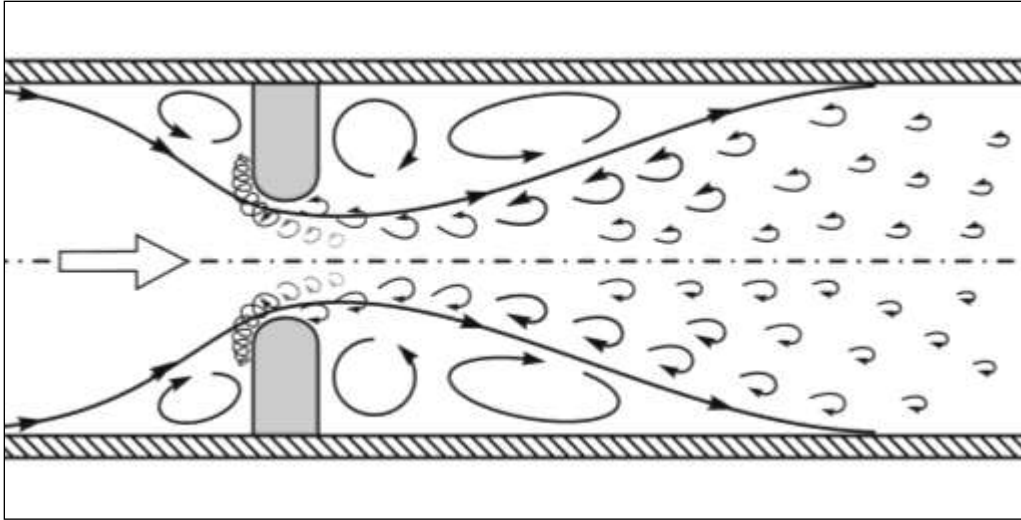
Figure 2-9. Flow around a short contraction
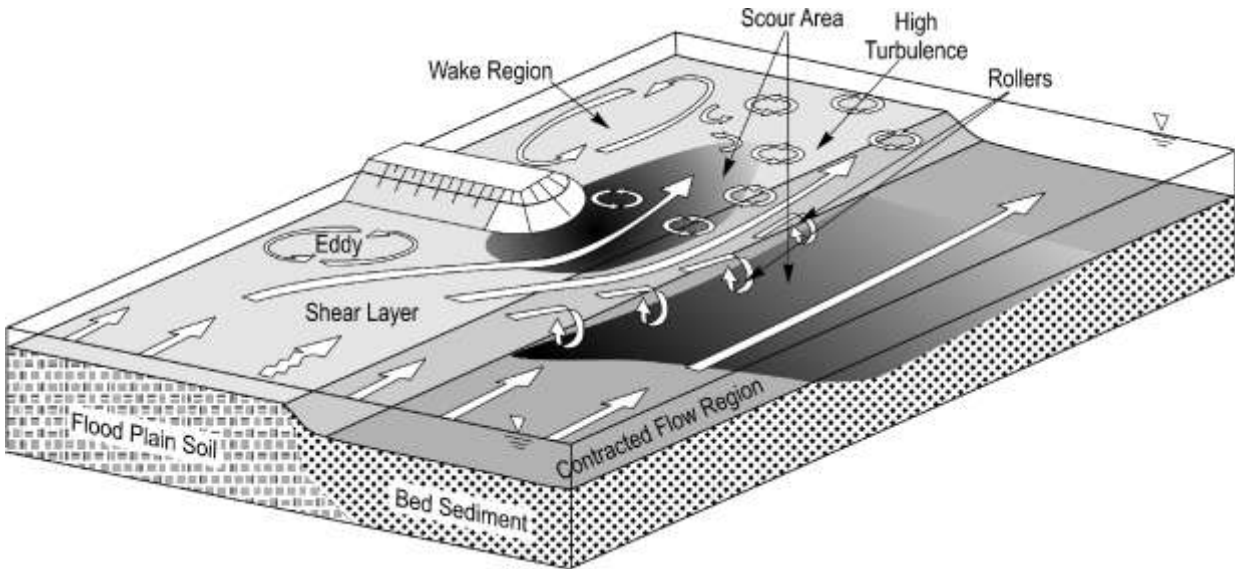
Figure 2-10. Flow around a bridge abutment and embankment in a compound channel

CHAPTER 3

SCOUR AND FAILURE CONDITIONS

3.1 Introduction

In the course of conducting the flume experiments for the Project, three distinct conditions of abutment scour were observed as elaborated in subsequent Section 3.3. The conditions developed in response to the relative erodibility of sediments forming the main-channel bed and soils forming the floodplain, as well as to the shear strength of the compacted earthfill forming the approach embankment. Depending on abutment layout in a channel, the resulting morphology of abutment scour could be transitional between the three distinct scour conditions.

The three scour conditions were developed also in response to the flow field at an abutment. As scour progressed, the flow field adjusted and, for a period, increased its capacity to erode the channel. Eventually, the scour region deepened sufficiently so that the flow field's capacity to erode attained a balance with either the rate of sediment inflow to the scour region (live-bed scour) or the channel boundary's resistance to erosion.

As described in Section 2.7 and illustrated in Figure 3-1, abutments (and approach embankments) commonly may traverse a floodplain and approach a deeper main channel. Though the short-contraction analogy is somewhat simplistic, an important point to be made is that the flow field around an abutment, like the flow field through an orifice, is not readily delineated as a contraction flow field separate from a local flow field limited to the near zone of the abutment. The two flow features (flow contraction and large-scale turbulence) are related and difficult to separate.

Either of the flow features may become more pronounced, depending on the extent of flow contraction and abutment form. When an abutment barely constricts flow through the waterway, scour at the abutment may develop largely in consequence of the local flow field generated by the abutment; this flow field comprises local contraction of flow locally around the abutment, and the generation of large-scale turbulence. For a severely contracted bridge waterway, flow

contraction dominates the flow field, and a substantial backwater rise in water level occurs. In this situation, the approach flow slows as it approaches the upstream side of the bridge, and then accelerates to a much higher velocity as it passes through the bridge waterway. For abutments whose foundation form extends at depth into the channel bed or floodplain, large-scale turbulence structures (vortex structures) may develop and strengthen locally around the base of the foundation; e.g., abutments with sheet-pile support beneath the abutment column, or with a sheet-pile skirt around the base of the spill-slope of a spill-through abutment.

Abutments are potentially erodible short contractions. Higher flow velocities and large-scale turbulence around an abutment may erode the abutment boundary. Commonly, the bed of the main channel is more erodible than the floodplain, because the bed is formed of loose sediment, while the floodplain is formed of more cohesive soil often protected by a cover of vegetation. Accordingly, two prime scour regions typically develop, as borne out by field observations of scour:

1. One region is where the boundary is least resistant to hydraulic erosion. This could be the main bed if flow velocities (and unit discharges) are sufficiently large; and,

2. The other region is where the flow velocities (and unit discharges) and turbulence are greatest. This usually is near the abutment.

These regions are indicated in Figure 3-2. Once scour begins, the geometry of the bridge waterway (as a short contraction) changes. The deepened flow at the scour region draws more flow, because the contraction is locally eased there. This process is explained further in Chapters 7 through 9.

The extent and maximum depth of scour at abutments can be complicated by the mix of materials forming the compound channel and the abutment's embankment, and other considerations such as the proximity of a pier.

3.2 Scour Conditions

Several conditions of abutment scour develop in accordance with the flow field at an abutment, the physical characteristics of an abutment and the waterway in which it is located. For spill-through abutments, three primary scour conditions develop in accordance with the locations of greatest erodibility of flow and least erosion resistance of the channel boundary, as outlined in Figures 3-3a-c.

1. ***Scour Condition A***. Scour of the main-channel bed, when the floodplain is far less erodible than the bed of the main channel. Figure 3-3a illustrates the several-stage failure process, which involves scour leading to potential geotechnical failure of the main-channel bank and the embankment. Hydraulic scour of the main-channel bed causes the bank to become geotechnically unstable and collapse. The collapsing bank undercuts the abutment embankment, which in turn collapses locally. Soil, and possibly riprap, from the collapsed bank and embankment slide into the scour hole. Figure 3-4a shows the main-channel bank erosion that occurred in laboratory tests, and Figures 3-5 and 3-6 illustrate cases where this scour condition occurred;

2. ***Scour Condition B***. Scour of the floodplain around the abutment. This condition also is equivalent to scour at abutment placed in a rectangular channel, if the abutment is set back from the main channel. As the amount of bed-sediment transport on a floodplain usually is quite low, this scour condition usually occurs as clear-water scour. Figure 3-4b shows that the floodplain scours around the abutment, and especially slightly downstream of it. The scour hole locally destabilizes the embankment side slope, causing embankment soil, and possibly riprap, to slide into the scour hole. Figure 3-7 illustrates a case where this scour condition occurred; and,

3. ***Scour Condition C***. Scour Conditions A and B may eventually cause the approach embankment to breach near the abutment, thereby fully exposing the abutment column. For this condition, scour at the exposed stub column essentially progresses as if the abutment column were a pier, as illustrated in Figure 3-4c. For the same reasons as given for Condition B, this scour condition usually occurs as clear-water scour. Figure 3-8 illustrates a case where this scour condition occurred.

These scour conditions may occur for wing-wall abutments. However, a couple of additional erosion processes can result in failure of the main-channel bank and the approach embankment, as illustrated in Figure 3-7:

1. The local flow field generated at the corners of the abutment can cause local scour at those locations; and,

2. Exposure of the piles beneath the abutment pile cap can cause river-banks and embankment soil to be eroded out from beneath the pile cap. Figure 3-4c shows a case where this scour process was a concern entailing careful maintenance inspection.

A scour event (or series of events) at an abutment, may involve a sequence of all three scour conditions. When an abutment is close to the main channel, Condition A may develop relatively quickly, with Condition B occurring at a slower rate. Either, or together, Scour Conditions A and B may eventually cause the approach embankment to undergo a slope-stability failure. If the embankment extensively washes out, so as to expose the abutment structure, scour may then develop at the abutment structure as if the abutment were a form of pier (Condition C). Accordingly, an important design consideration is that the stub or wing-wall abutment should not fail when exposed; i.e., the foundations of the wing-wall should be deep enough that the wing-wall does not fail when exposed to a pier-like scour condition.

For design estimation of scour depth, it is useful to consider the likely rates or sequences in which the three scour conditions developed, and to ask -- What is the greatest scour depth that reasonably could occur near the abutment? Will that scour depth pose a slope-stability problem for the earthfill embankment adjoining an abutment foundation or for the floodplain bank of the main channel? What is the deepest scour that could occur at the abutment column foundation itself, and does that scour occur when the embankment is breached so as to fully expose the abutment column?

The photos in Figures 3-4a-c show the three primary scour conditions, and indicate the different scour depths that may occur at abutments.

3.3 Influence of Pier Proximity

The influence of pier proximity on the three scour conditions is slight, at least for the pier form and construction depicted in Section 2.5. The flume experiments (Chapter 11) show that abutment scour is dominated by the flow field established by an abutment. Once scour initiates, and deepens below the pier's pile cap, pier presence does not substantially increase flow contraction or the strength of large-scale turbulence structures.

For Scour Condition A at spill-through abutments, pier presence may slightly increase maximum abutment scour depth when the pier is close to the abutment toe. For Scour Condition B, however, pier presence slight lessens abutment scour depth. These findings are discussed in Chapter 11.

3.4 Other Scour Processes

Abutment scour may develop consequent to several processes of flow and bed-sediment movement:

1. Scour of the approach embankment flank on the floodplain. This condition, sketched in Figure 3-9, may occur when the floodplain flow converging towards the bridge waterway undercuts the flank of the approach embankment. This scour mechanism differs from those shown in Figures 3-3a-c and 3-4a-c, is less common (no field cases were identified during this Project), and is not discussed in this report;

2. General scour of the main channel bed. This process occurs in response to an overall propensity of the main-channel flow to degrade should an imbalance of sediment supply along the channel occur; and,

3. Localized scour attributable to change in main channel alignment and morphology, which adversely affects abutment location and orientation relative to flow in the main channel. For example, a meander-loop migration may direct flow adversely towards abutments

and piers not designed for a lateral shift in the channel thalweg. The deeper scour commonly resulting from this possibility must be considered in the scour design of abutments and piers.
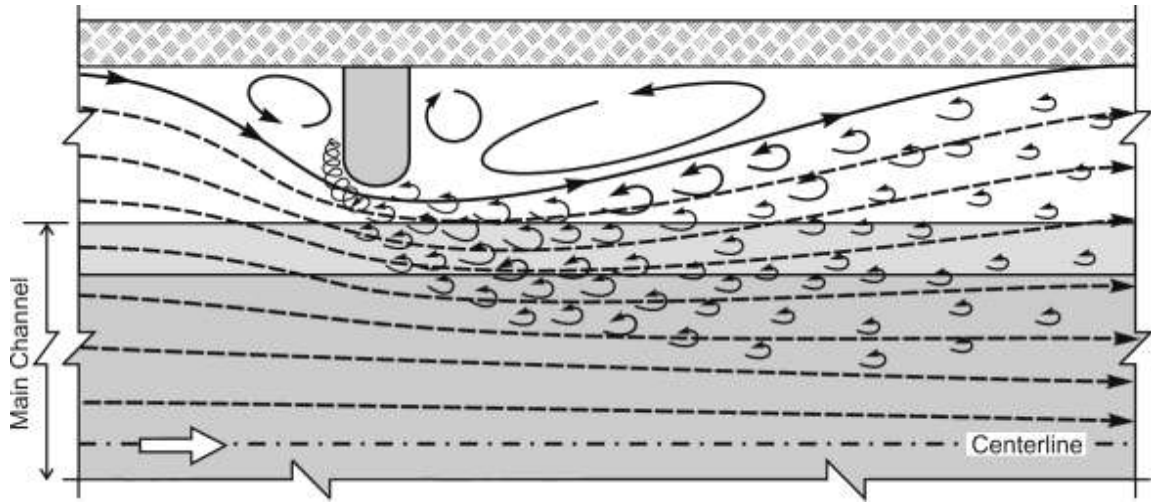
Figure 3-1. Schematic of flow contraction and macro-turbulence generation associated with flow through a bridge waterway in a compound channel (main channel with floodplain)
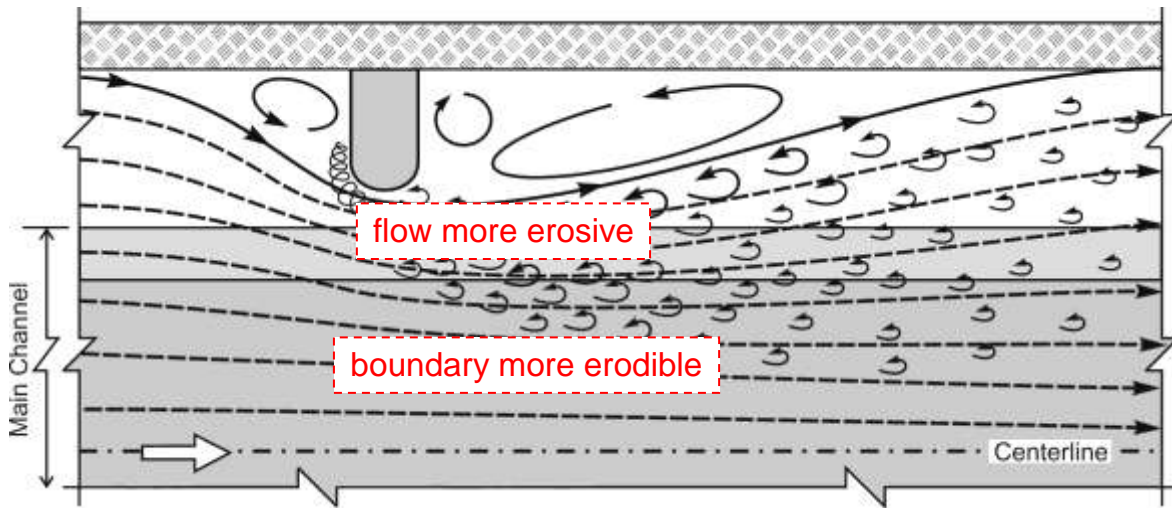
Figure 3-2. A region of possible scour extending across from the abutment
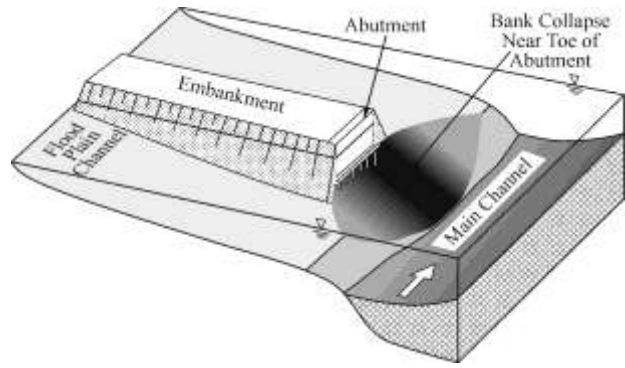
(a)
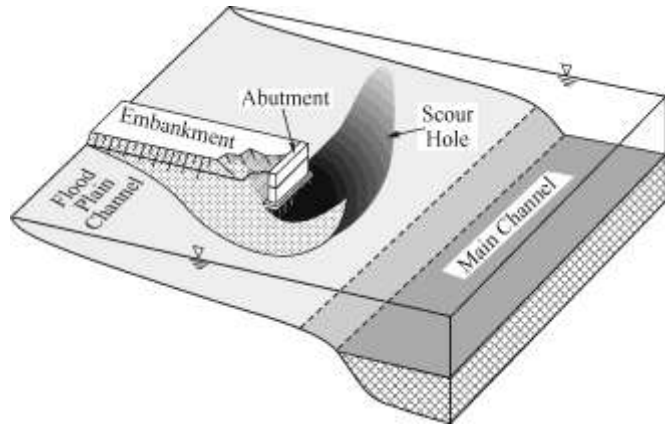
(b)
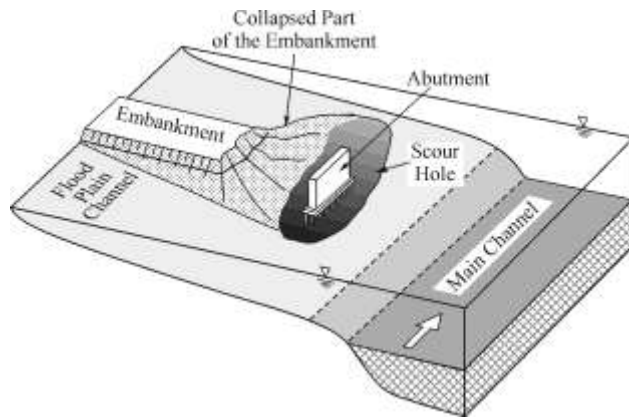
(c)

Figure 3-3. Abutment-scour conditions: Scour Condition A - hydraulic scour of the main-channel bed causes bank failure, which causes a failure of the face of the abutment embankment (a); Scour Condition B - hydraulic scour of the floodplain causes failure of the face of the abutment embankment (b); and, Scour Condition C - breaching of the approach embankment exposes the abutment column so that scour progresses as if the abutment were a form of pier (c)

(a)

(b)

(c)

Figure 3-4. Laboratory views of the three prime scour conditions: Scour Condition A - scour of main channel bed (a); Scour Condition B - scour of floodplain (b); and, Scour Condition C - scour at exposed abutment column (c)

Figure 3-5. Scour Condition A led to failure of the channel bank and road embankment at this spill-through abutment

Figure 3-6. Scour Condition A led to failure of the channel bank and road embankment at this wing-wall abutment

Figure 3-7. Scour Condition B at Interstate-70 Bridge over the Missouri River

Figure 3-8. Scour Condition C at a spill-through abutment
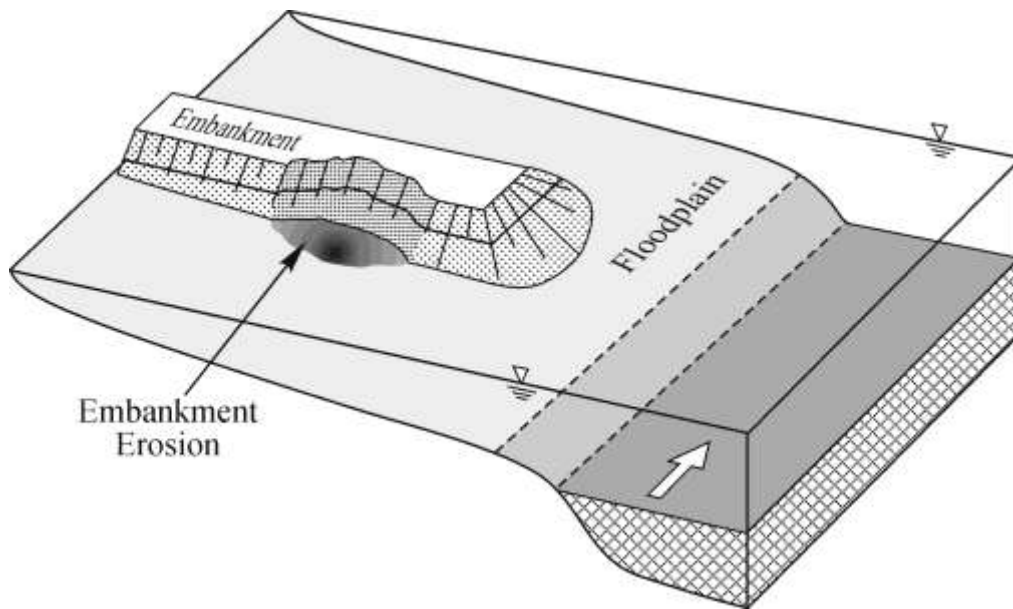
Figure 3-9. Scour of the approach embankment back from the abutment

CHAPTER 4

FORMULATION OF SCOUR-ESTIMATION METHOD

4.1 Introduction

This chapter presents the approach taken to estimate scour depth at abutments. Subsequently Chapter 12 presents the design relations stemming from the approach. The quantitative values recommended for the relationships are determined from the laboratory experiments conducted for this Project.

4.2 Approach

The approach to scour-depth estimation presented here estimates the potential maximum depth of scour that may develop without immediately considering the geotechnical failure of the embankment on floodplain soil. Once this scour depth is estimated, its effect on the geotechnical stability of the main channel bank and embankment should be evaluated. If the bank and embankment were found unstable, they would collapse, relieve flow contraction, diminish macro-turbulence generation, and consequently reduce the maximum scour depth attained. The geotechnical strengths of the embankment and floodplain soils, therefore, may significantly influence abutment scour depth, as well as contribute uncertainty to scour-depth estimation.

The flow chart, given as Figure 4-1, outlines the main considerations involved with the approach. They relate to abutment location on a floodplain, L/B_f, erodibility of floodplain soil at the bridge site, and selection of scour depth for use in designing abutment foundation and analyzing embankment stability. The arrows indicate the sequence of scour conditions to be evaluated. For $L/B_f < 1$, and an erodible floodplain, it is possible that both Scour Conditions A and B may occur. However, Scour Condition B likely may give the deeper scour (based on observations from the writers' experiments); hence, the dotted arrow to Scour Condition A. Figure 4-1 is discussed further in Chapter 13, which presents the design approach.

For the purpose of design estimation of scour depth, it is necessary to consider the absolute depth elevations attained with the scour depths associated with Scour Conditions A through C.

Additionally, the likely rates or sequences in which the scour conditions may develop are important. They give rise to the following four questions:

1. What is the greatest scour depth that reasonably could occur <u>near</u> the abutment?
2. Will that scour depth pose a slope-stability problem for the embankment?
3. What scour depth should be used in estimating the required length of pile support? and,
4. What is the deepest scour that potentially could occur <u>at</u> the abutment column itself? Does that scour occur when the embankment is breached so as to fully expose the abutment foundation?

Figure 4-2 indicates the design concern associated with Scour Condition A. It shows the attendant concerns of main-channel bank collapse and embankment side-slope failure. Scour-depth estimation for a combination of Scour Conditions A and B is complicated by uncertainties in the resulting flow field, as mentioned earlier. The results of the writers' experiments show, however, that combinations of Scour Conditions A and B produce lesser scour depths than if either condition developed independently. This outcome occurs because the development of either Scour Condition A or B diminishes the development of the other condition; scour increases the flow area at the bridge, and thereby reduces flow velocities and relaxes the flow through the bridge.

The essential notion underlying the estimation approach is that the potential maximum flow depth near an abutment can be expressed in terms of an amplified contraction scour estimated in terms of unit-discharge values for flow around an abutment. The maximum scour depth, Y_{MAX}, is estimated as

$$Y_{MAX} = \alpha Y_C \tag{4-1}$$

in which Y_C is the mean flow depth of the contraction scour, and α is an amplification factor whose value varies in accordance with the distribution of flow contracted through the bridge waterway, and on the characteristics of macro-turbulence structures generated by flow through the waterway. Two estimates of αY_C should be considered:

1. Amplification of long-contraction scour; and,

2. Amplification of local scour estimated on the basis of flow contraction locally around an abutment in a channel so wide that flow does not contract through the bridge waterway.

For both estimates, the value of contraction scour depth Y_C can be estimated using one of several methods (e.g., Laursen 1960, 1963). The methods developed by Laursen are used herein, as they are widely employed. The pertinent equation is presented later as Eq. (5-1) in Chapter 5, Review of Prior Studies.

The value of α should be assessed for flow contraction in the main channel (Scour Condition A) and/or near the abutment (Scour Condition B). Abutment shape, along with the aspects of channel morphology and roughness that affect flow through the bridge waterway, influence amplification coefficient α. The ensuing limits apply to α:

1. When the bridge waterway is contracted only locally around an abutment, and contraction scour is negligibly small in the waterway, α is large. Its value depends on the local contraction of flow passing immediately around the abutment, and the turbulence structures generated by the abutment; and,

2. For a severely contracted bridge waterway, α diminishes to a value slightly above 1. At this limit, the bridge creates a substantial backwater effect that impounds water. The bed shear exerted by highly contracted flow is much larger than the erosive forces exerted by turbulence structures generated by the abutment. In some ways, such extreme contraction is similar to scour at a bottomless culvert.

As pointed out in Section 4.5, conduct of laboratory experiments to ascertain exactly the limits to α is complicated by practical considerations of flume widths and lengths available in laboratories.

In developing relationships for estimating the scour depths incurred with Scour Conditions A and B, it is convenient to adapt and extend Laursen's well-known methods for estimating live-bed

contraction scour (Laursen 1960), and for clear-water contraction scour (Laursen 1963). His methods are useful for directly identifying the main parameters associated with abutment scour, though they neglect the influence of macro-turbulence. Other contraction-scour methods could certainly be used. The present formulation assumes live-bed scour conditions for flow in the main channel, and clear-water scour conditions for flow over the floodplain. The relationships apply to scour of cohesive as well as non-cohesive bed and floodplain boundaries.

When discussing flow contraction through a bridge waterway, two limits exist for flow contraction tending to zero. Figure 4-3 indicates the two limits in terms of abutment embankment length and channel half width:

1. For a channel of finite width, flow contraction diminishes as embankment length reduces; or,
2. For an abutment of finite embankment length, flow contraction diminishes as channel width increases.

The two limits give very different values of abutment-scour depth. When abutment embankment length reduces to zero, scour depth tends to zero. However, for a finite-length abutment, scour depth does not tend to zero as channel width increases. Essentially all laboratory experiments to date have used a flume of fixed width. It is very expensive to use a flume of sufficient variable width to attain limit 2.

The ensuing formulations are first presented for the situation whereby flow contraction occurs across the bridge waterway (Sections 4.3 and 4.4 for Scour Conditions A and B, respectively), and then presented (Sections 4.5 and 4.6) for the limiting situation of an abutment of finite length in a very wide channel; i.e., when flow contraction occurs only locally at an abutment.

4.3 Scour of Main-Channel Bed (Scour Condition A)

Scour of the main-channel bed, Scour Condition A, is of concern for abutments located near the main channel (and possibly in it). As sketched in Figure 3-3a, hydraulic erosion of the main channel may destabilize the channel bank and, thereby, the embankment slope. Figures 3-5 and

3-6 illustrate field examples of this scour condition at spill-through and wing-wall abutments, respectively. Scour-depth estimation must account for the flow contraction around the abutment, along with the generation, growth, and dispersion of large-scale turbulence formed as flow passes around the abutment.

Though the waterway flow field is substantially three-dimensional, flow contraction and acceleration around the abutment and through a bridge waterway can be approximated by means of contracting flow streamlines of depth-averaged flow which are superimposed by turbulence structures generated by the abutment as flow enters the waterway. Figure 4-4 schematically depicts flow contraction and the generation of macro-turbulence structures as flow passes around an abutment. By describing the flow and sediment-movement conditions in a single stream tube approaching and passing through the scour region in the bridge waterway, it is possible to formulate, in approximate terms, the depths of flow along a stream tube, and thereby estimate scour depth. Laursen's (1960)[4] approach for estimating live-bed scour depth in a long contraction can be used for estimating scour depth along a contracting stream tube.

For live-bed scour of the main-channel waterway, equilibrium flow depth, and thereby scour depth, along a stream tube in the main channel are governed by mass conservation of sediment transport, G'_s, along the stream tube; i.e., the rate of sediment outflow equals the rate of sediment inflow,

$$G'_{s1} = G'_{s2} = G'_{s3} \tag{4-2}$$

Here, the superscript "$'$" refers to quantities within the stream tube; and, the subscripts 1, 2, and 3 respectively refer to the approach section (away from the influence of the bridge), the bridge section, and the section of the stream tube with the greatest unit discharge, as illustrated in Figure 4-3.

Eq. (4-2) could be restated as

---

[4] Other methods for estimating scour contraction also could be used.

$$g'_{s1}B_1 = g'_{s3}B_3 \tag{4-3}$$

in which g'_s is the rate of bed-sediment transport per unit width of a stream tube; and B is the stream-tube width. Hereafter, the details of the formulation depend on the relationship selected for relating sediment-transport rate to flow rate. The present formulation uses the same relationship adopted by Laursen (1960), as that relationship evidently is familiar to many bridge-scour estimators, and it is fairly simple to use. Also, it enables the present formulation to be compared with the flow-depth estimates obtained using the long-contraction scour relationship developed by Laursen (1960).

The rate of bed-sediment transport can be described in terms of an average sediment concentration, c, conveyed by a unit discharge through the stream tube, q', so that Eq. (4-3) becomes

$$c_1q'_1B_1 = c_3q'_3B_3 \tag{4-4}$$

From Eq. (4-4)

$$\frac{c_1}{c_3} = \left(\frac{q'_3}{q'_1}\right)\left(\frac{B_3}{B_1}\right) \tag{4-5}$$

Laursen (1960) gives

$$c = \left(\frac{d}{Y}\right)^{7/6}\left(\frac{\tilde{\tau}_0}{\tau_c}-1\right)b\left(\frac{u_*}{w}\right)^a \tag{4-6}$$

in which d is bed-particle diameter; Y is flow depth; $\tilde{\tau}_0$ is the portion of flow resistance associated with the bed particles; τ_c is the critical shear stress for bed-sediment movement; b is a

coefficient whose value, along with the value of exponent a, depend on mode of sediment transport, and are functions of the ratio of shear velocity and particle fall velocity, u_* / w.

From Eqs. (4-5) and (4-6),

$$\frac{c_1}{c_3} = \frac{d/Y_1^{7/6} [\tilde{\tau}_0 / \tau_c - 1 \ b \ u_* / w^{\ a}]_1}{d/Y_{MAX}^{7/6} [\tilde{\tau}_0 / \tau_c - 1 \ b \ u_* / w^{\ a}]_3} \tag{4-7}$$

The subscripts 1 and 3 refer to sections 1 and 3. Equating Eqs. (4-4) and (4-7) gives

$$\frac{d/Y_1^{7/6}}{d/Y_{MAX}^{7/6}} = \left(\frac{q_3'}{q_1'} \right) \left(\frac{B_3}{B_1} \right) \frac{[\tilde{\tau}_0 / \tau_c - 1 \ b \ u_* / w^{\ a}]_3}{[\tilde{\tau}_0 / \tau_c - 1 \ b \ u_* / w^{\ a}]_1} \tag{4-8}$$

For there to be continuity of bed sediment transport, the intensity of bed-sediment transport must vary approximately linearly with width of stream tube; i.e.,

$$\frac{[\tilde{\tau}_0 / \tau_c - 1 \ b \ u_* / w^{\ a}]_3}{[\tilde{\tau}_0 / \tau_c - 1 \ b \ u_* / w^{\ a}]_1} = \left(\frac{B_1}{B_3} \right) \tag{4-9}$$

From Eqs. (4-8) and (4-9), and the assumption of uniform bed-sediment diameter,

$$\left(\frac{Y_{MAX}}{Y_1} \right) = \left(\frac{q_3'}{q_1'} \right)^{6/7} \tag{4-10}$$

Eq. (4-10) is arrived at from consideration of flow acceleration through a contracting stream tube. However, because the flow field is three dimensional, and has macro-turbulence structures that disperse across the waterway flow field, Eq. (4-10) should be modified to account for these influences; i.e.,

$$\left(\frac{Y_3}{Y_1} \right) = C_{TA} \left(\frac{q_3'}{q_1'} \right)^{6/7} \tag{4-11}$$

Here, C_{TA} is a term intended to account for the additional scour attributable to macro- turbulence generated by flow passing into the bridge waterway. The value of C_{TA} is influenced by the shape of the abutment and overall waterway entrance; i.e.,

$C_{TA} = function$ (abutment shape, abutment set back from main channel, geometry of main-channel bank, ad-hoc floodplain features)

If all the floodplain flow entered the main channel, in the situation of a long abutment extending practically across the entire floodplain, $q_3' = q_{MAX}' = m_A q_2$ with $q_2 = \ Q_{1m} + Q_f \ / B_2$. Because the average unit discharge of flow limited to the main channel at section 2 is difficult to calculate, q_2 is an estimate of the mean value of the unit discharge through the bridge opening at section 2. Here, q_{MAX} = unit discharge coinciding with the location of deepest scour in the main channel; Q_{1m} is approach flow discharge in the main channel, and Q_f is approach flow discharge over the floodplain. Values of m_A and C_{TA} have to be determined from laboratory or numerical-simulation data. The Project focused further on these parameters. Note that, as the flow features in a short contraction are not meaningfully separated, as shown in Figure 4-3, it is difficult to evaluate m_A and C_{TA} separately.

For the purpose of estimating the maximum scour depth, Y_{MAX} in the main channel, Eq. (4-10) can be restated as

$$Y_{MAX} = Y_1 C_{TA} m_A^{\ 6/7} \left(\frac{q_2}{q_1} \right)^{6/7} \tag{4-12}$$

in which $q_1 = Q_{1m} / B_1$. For a long contraction, $m_A \approx 1$, $C_{TA} \approx 1$, and thus, Eq. (4-12) simplifies to

$$Y_{MAX} = Y_1 \left(\frac{q_2}{q_1} \right)^{6/7} = Y_C \qquad (4\text{-}13)$$

which essentially is the relationship proposed by Laursen (1960) for estimating the scour depth associated with live-bed flow through a long contraction. Comparison of Eqs. (4-2), (4-12), and (4-13) indicates that

$$Y_{MAX} = \alpha_A Y_C = C_{TA} m_A^{6/7} Y_C \qquad (4\text{-}14)$$

In terms of scour depth below the approach-bed level, Eq. (4-13) can be re-written as

$$d_{S\max} = Y_{MAX} - Y_1 = Y_1 \left[C_{TA} m_A^{6/7} \left(\frac{q_2}{q_1} \right)^{6/7} - 1 \right] \qquad (4\text{-}15)$$

The issues now are estimation of q_2, m_A (or q_{MAX}), and C_{TA}. Because there are no direct analytical means for determining these quantities, use must be made of empirical or numerical means to do so. Two approaches are suggested here for estimating[5] q_2 and m_A (or q_{MAX}):

1. Estimate q_2 and m_A (or q_{MAX}) by means of a numerical model that simulates two-dimensional, depth-averaged flow through the bridge waterway under design consideration, or obtain values for ranges of channel and abutment conditions; and,

2. Approximate estimation of q_2 and m_A based on representative values found from laboratory or field data for ranges of channel and abutment conditions. A reasonable

---

[5] Given the various morphologic and flow-resistance irregularities found at many bridge sites, accurate determination of these flow quantities entails large uncertainty. Therefore, the emphasis here is on reasonable estimation rather than accurate calculation.

estimate of q_2 can be made by means of the following approximate relationship, which apportions the flow in accordance with the initial (pre-scour) cross-sectional area of flow through the bridge waterway:

$$q_2 = \frac{Q_{2m}}{B_2} = \left(\frac{1}{0.5B_2}\right)\left[0.5Q_{1m} + Q_f\left(\frac{0.5A_2}{0.5A_2 + A_{f2}}\right)\right] \qquad (4\text{-}16)$$

Figure 4-5 shows the basis for Eq. (4-16). Here, Q_{2m} is the flow discharge through the main channel at the bridge, B is the opening width of the main channel at the bridge (main-channel width – sum of pier widths); A_2 is pre-scour, opening area of the main channel at the bridge (main-channel area - Σ(pier areas); and, A_{f2} is the cross-sectional area of the floodplain immediately upstream of the abutment. This estimate of q_2 is not precise, but the writers' flow measurements indicate it to be acceptably accurate for the purpose of scour-depth estimation.

Whereas Laursen (1960) assumes that bed roughness in the long contraction is about the same as that in the un-contracted approach channel, Y_C could be calculated in either of two ways: using the relationship proposed by Laursen (1960) or a stage-discharge relationship developed for flow in loose-bed channels (e.g., as described in textbooks on loose-bed hydraulics).

To evaluate the overall magnitude of scour for Scour Condition A at an abutment, it is useful to compare the trends for both Y_{MAX} and Y_C versus q_2/q_1, as shown conceptually in Figure 4-6. Initially, for negligible contraction of flow in the main channel through the bridge waterway, $Y_C/Y_1 \approx 1$, and values of Y_{MAX} may approximately equal Y_1 plus the amplitude[6], $0.5H$, of bed forms (dunes) in the main channel. As abutment length approaches floodplain width, the main channel flow contraction, Y_C/Y_1, increases, as does q_2/q_1. Also, the dunes may continue, possibly increasing or decreasing in amplitude. As q_{MAX} exceeds q_2 (enlarged m_A), and because of the

---

[6] Dune amplitude is half dune height (see Figure 4-5a).

influence of turbulence (larger C_{TA}), Y_{MAX}/Y_1 exceeds Y_C/Y_1. However, as flow contraction becomes pronounced, and thereby so do q_2/q_1 and Y_C/Y_1, m_A decreases, and the difference between Y_{MAX}/Y_1 and Y_C/Y_1 diminishes. Further, the bed forms may not occur in the central part of the bridge waterway. In situations where a narrow bridge opening severely constrains and backs up flow, flow through the waterway is highly contracted and relatively uniform in distribution, as indicated by our experiments.

A further issue concerns the inclusion of dune height in the scour depth estimate for Scour Condition A. A realistic assumption is to add dune amplitude (half dune height) to the scour-depth estimate when making a design estimate of maximum scour depth for Scour Condition A. The present experiments showed no consistent variation of dune height and length in the scour region, compared to the approach-flow bed, provided the bottom width of the main channel at the bridge waterway, B_2, exceeded the average width of the dunes on the approach-flow bed. Dune height is not explicitly considered in Eqs. (4-12), (4-14) or (4-15). For the present experiments, dune height $H = 0.09$ m $\pm$ 0.012 m, dune length $L = 1.10$ m $\pm$ 0.12 m, and dune width $= 1.2$ m $\pm$ 0.3 m.

4.4 Scour of Floodplain (Scour Condition B)

Scour Condition B is of primary concern for abutments on wide floodplains, and abutments set well back from the main channel (Figure 3-3b). Because clear-water flow predominantly occurs on floodplains, it is assumed herein that scour of a floodplain at an abutment occurs as clear-water scour. As with Scour Condition A, scour for this condition is influenced by flow acceleration and turbulence generated as flow passes around the abutment, as shown in Figure 4-7. However, now the contraction of interest is near the abutment. Though the flow field is three-dimensional, it is justifiable to formulate the scour by means of a stream tube of flow that passes through the scour region. The stream tube contracts as flow accelerates. Turbulence diffuses through the stream tube.

In accordance with a condition of clear-water scour, equilibrium flow depth and scour depth are governed by the capacity of flow to erode sediment from the floodplain near the abutment. The

rate of sediment inflow into the scour region is considered to be negligible, and dunes are assumed not to occur in the region of deepest scour. For this equilibrium condition, the usual assumption is that the shear stress on the scoured floodplain, τ_2, is equal to the critical shear stress, τ_c, associated with the entrainment of the floodplain sediment;

$$\tau_{f2} = \tau_c \tag{4-17}$$

A significant source of uncertainty in scour depth estimation for Scour Condition B is attributable to uncertainties in estimating τ_c and τ_{f2}. Practical, accurate estimation of them is greatly complicated by the variability of soils, sediments, vegetation, and other aspects of floodplain terrain.

At approach cross section 1 of the floodplain, use of Manning's and Strickler equations to estimate boundary shear stress (as per Laursen 1963) gives

$$\tau_1 = \frac{U_1^2 d^{1/3}}{30 Y_1^{1/3}} \tag{4-18}$$

in which U is depth-average velocity of flow, whose depth is Y, and d is representative median boundary particle diameter. Manning's equation and Strickler equation are commonly cited in books on open-channel flow (e.g. Henderson 1966). For the floodplain at cross section 3,

$$\tau_2 = \frac{U_3^2 d^{1/3}}{30 Y_3^{1/3}} \tag{4-19}$$

Combining Eqs. (4-17), (4-18), and (4-19), then simplifying, leads to

$$\frac{\tau_1}{\tau_c} = \left(\frac{U_1}{U_3}\right)^2 \left(\frac{Y_3}{Y_1}\right)^{1/3} \tag{4-20}$$

From continuity, $U_1 = Q'/Y_1B_1$, and $U_2 = Q'/Y_3B_3$ (4-21)

$$\frac{Y_3}{Y_1} = \left(\frac{\tau_1}{\tau_c}\right)^{3/7}\left(\frac{B_1}{B_3}\right)^{6/7}$$ (4-22)

As $q'_1B_1 = Q, = q'_3B_3$ along the stream tube,

$$\frac{Y_3}{Y_1} = \left(\frac{\tau_1}{\tau_c}\right)^{3/7}\left(\frac{q'_3}{q'_1}\right)^{6/7}$$ (4-23)

However, because the flow field has large-scale turbulence structures that disperse across the waterway flow field, Eq. (4-23) should be modified to account for the influx of turbulence into the stream tube. Eq. (4-23) should be modified to

$$\left(\frac{Y_3}{Y_1}\right) = C_{TB}\left(\frac{\tau_1}{\tau_c}\right)^{3/7}\left(\frac{q_3}{q_1}\right)^{6/7}$$ (4-24)

in which C_{TB} is a term intended to account for the additional scour attributable to turbulence generated by flow passing into the bridge waterway. The value of C_{TB} is influenced by the shape of the abutment and overall waterway entrance.

Replacing subscript "$_1$" with "$_f$" for floodplain, and then considering the maximum depth of flow associated with flow contraction lets Eq. (4-24) be rewritten as

$$\left(\frac{Y_{MAX}}{Y_f}\right) = C_{TB}\left(\frac{\tau_f}{\tau_c}\right)^{3/7}\left(\frac{q_{MAX}}{\bar{q}_f}\right)^{6/7}$$ (4-25)

In a similar manner as done for Scour Condition A, the substitution $q_{MAX} = m_B q_{f2}$ could be made;

$$\left(\frac{Y_{MAX}}{Y_f}\right) = C_{TB}m_B{}^{6/7}\left(\frac{\tau_f}{\tau_c}\right)^{3/7}\left(\frac{q_{f2}}{\bar{q}_f}\right)^{6/7} \tag{4-26}$$

or

$$Y_{MAX} = \alpha_B Y_C = C_{TB}m_B{}^{6/7}Y_{fC} \tag{4-27}$$

where contraction scour depth Y_{fC}, is (Laursen 1963)

$$Y_{fC} = Y_f\left(\frac{\tau_f}{\tau_c}\right)^{3/7}\left(\frac{q_{f2}}{q_f}\right)^{6/7} \tag{4-28}$$

For the moment, the terms C_T and m are used as for Scour Conditions A, but it is anticipated that these turbulence and flow-contraction terms may differ for Conditions A and B.

In terms of maximum scour depth, d_{Smax}, Eq. (4-26) can be re-stated as

$$d_{S\max} = Y_{MAX} - Y_f = Y_f\left[C_{TB}m_B{}^{6/7}\left(\frac{\tau_f}{\tau_c}\right)^{3/7}\left(\frac{q_{f2}}{q_f}\right)^{6/7} - 1\right] \tag{4-29}$$

The values of C_{TB} and m_B may differ from C_{TA} and m_A for Scour Condition A, because of dissimilarities in how flow enters the bridge waterway, and how it flows locally around an abutment. The scour-depth data obtained from our experiments do show this variation. The trends for Y_{MAX}/Y_f and Y_C/Y_f are sketched in Figures. 4-8a-d. If the abutment were located in a wide channel, with little overall flow contraction except immediately around the abutment (Figure 4-8b), the initial greater magnitude of Y_{MAX}/Y_f relative to Y_C/Y_f reflects the magnitude of flow contraction locally around the abutment. Also, because clear-water scour essentially occurs, no significant bed-form trend is included in Figure 4-8a. In some situations, bed forms

could locally develop at an abutment. As the abutment severely contracts the bridge waterway (Figure 4-8d), scour occurs practically uniformly across the main-channel bed.

In summary for Scour Condition B, as for A, the main focus of flow-related uncertainty is the evaluation of terms C_{TB} and m_B. The Project's use of the depth-averaged-flow model FESWMS aimed at providing much of the necessary information regarding m_B values. Evaluation of C_{TB} values will entail comparison of flow depths, m_B values, and ratios of q values. To be sure, other major sources of uncertainty lie in the values quantifying the erodibility of floodplain soil and the shear strength of the earthfill approach embankment. In practical terms, significant uncertainty also attends estimation of τ_f / τ_c, as noted above.

4.5 Limiting Local Scour at Abutment in Very Wide Channel

The limiting situation of local scour at an abutment in a wide channel may occur when only the flow contracted around the abutment erodes the channel bed or floodplain. This situation can occur for Scour Conditions A and B. In terms of scour depth estimation, several concerns arise for this limit:

1. Estimating the maximum velocity of flow locally contracted around an abutment in a very wide channel; and,
2. For abutments with foundations extending into the bed or floodplain (e.g., by way of a caisson structure around the abutment toe), estimating the erosive influence of turbulence structures formed around the abutment foundation.

Given the difficulties associated with constraints on typical flume widths, and on the scaling of flow, abutment, and boundary material, these two concerns must be approached in an approximate sense, as described in the next two sub-sections.

4.5.1 Scour Condition A

For Scour Condition A in a very wide channel not subject to contraction scour, Eq. (4-15) can be used with m_{Aq2} treated as the maximum value of unit discharge at the side of the abutment. A

useful approximation of $m_A q_2$ can be made using potential flow theory. For a cylinder in an unbounded potential-flow field, the maximum velocity around the cylinder is twice the uniform approach velocity (Lamb 1932).

Also for this scour situation, because no contraction scour occurs fully across the channel contraction, $Y_1 = Y_2 = Y_C$; i.e., contraction scour depth $Y_1 - Y_C = 0$. Therefore, $m_A q_2 = 2q_1$, and Eq. (4-14) reduces to

$$\text{(4-30)}$$

Or in terms of flow depth, with $Y_1 = Y_C$,

$$\text{(4-31)}$$

The value of the coefficient reflecting the erosive influence of turbulence, C_{TA}, depends on abutment form and construction.

4.5.2 Scour Condition B

A similar analysis as in Section 4.5.1 can be applied for Scour Condition B. Eq. (4-27) accordingly leads to

$$\text{(4-32)}$$

Like C_{TA} in Eq. (4-32) the value of C_{TB} depends on abutment form and construction.

4.6 Loci of Scour Depth Trends

The relationships in Sections 4.3 through 4.5 for estimating scour depth delineate loci of scour-depth trends. Figure 4-9 indicates the following loci for Scour Condition B:

1. At large increasing flow contractions, Y_{MAX}/Y_C declines towards a value somewhat above 1;

2. For decreasing flow contraction associated with decreasing embankment length L, Y_{MAX}/Y_C declines to 1. As $L \to 0$, $Y_{MAX}/Y_C = 1$. The location of this curve varies with abutment form and construction, as well as with approach flow distribution as related to flow depth and the flow resistance characteristics of the floodplain and channel bank;

3. For decreasing flow contraction owing to increasing channel half width $0.5B$, Y_{MAX}/Y_C, with L fixed, $Y_{MAX}/Y_C \to 1.81C_{TB}$;

4. The shaded region encompasses scour depth variations with adjustments in abutment form and construction, and in flow distribution; and,

5. The upper solid curve can be considered as a design envelop for all q_{2f}/q_f .

The loci of scour-depth trends are based only hydraulic erosion considerations. Further considerations associated with the geotechnical stability of the abutment's embankment may alter the loci. Section 9-3 elaborates the geotechnical considerations incurred with scour development.

4.7 Scour at Exposed Abutment Column (Scour Condition C)

Scour of the floodplain at an abutment may cause the abutment's embankment slope to become unstable and fail, and eventually to breach, as illustrated in Figures 3-4c and 3-8. Scour-depth prediction for this condition has to rely on an empirical relationship, owing to the complexity of flow and sediment entrainment from an abutment structure exposed once the approach embankment has been breached. In simple terms, the exposed abutment column (e.g., as in Figure 3-8) assumes the form of a pier.

The appropriate approach for scour-depth estimation should then be essentially that used for estimating maximum scour depth at a bridge pier. Accordingly, scour depth at the exposed abutment column (pier),

$$d_{S\max} = K_I K_\beta d_{S0column} \tag{4-33}$$

Here, $d_{S0column}$ is the maximum depth of local scour at the abutment column when aligned with the flow direction ($\beta = 0$); and flow intensity parameter $u_* / u_{*c} = 1.0$, the value at which local scour depth normally is a maximum; K_I is a flow intensity coefficient; and K_β is an alignment coefficient. Values of K_I can be determined from essentially the identical curves developed to give the influence of u_* / u_{*c} on pier scour (e.g., Melville and Coleman, 2000; Richardson and Davis, 1995); and, K_β can be obtained from curves to be determined by means of flume experiment for the standard-stub columns (spill-through abutment) and wing-wall columns (wing-wall abutments). Flume experiments are needed to obtain reliable values of $d_{S0column.}$ Note that shear velocity relates to boundary shear stress as $u_* = \sqrt{\tau / \rho}$, with τ = boundary shear stress and ρ = water density.

For short abutments built with solid-body foundations (e.g., a footing surrounded by sheet piles) extending deeply into a floodplain or rectangular channel, as modeled in numerous prior laboratory studies (e.g. summarized in Melville and Coleman, 2000), the macro-turbulence structures at the abutment can deepen scour at the abutment's leading corner. This situation is essentially the same as Scour Condition C. The experiments conducted for Project 24-15(02) used model abutments of this form, and thereby led to a scour estimation expression similar to that used for pier scour.

4.8 Influence of an Adjacent Pier

The presence of a pier close to an abutment modifies the abutment flow field, and, in effect, may also modify the abutment as an overall structure. The influence of pier proximity is best handled by means of a possible adjustment to the scour-amplification factors α_A and α_B, in Eqs. (4-14) and (4-27). This influence, or set of influences, must be evaluated from laboratory experiments, because the adjustments to flow field and overall abutment stability cannot be determined á priori. Chapters 11 and 12 elaborate pier influence on abutment scour depth.

Of commensurate practical importance is the influence of abutment presence on scour depth at a nearby pier. The flume experiments conducted for the present Project investigated this influence, along with the other influences on factors α_A and α_B.

4.9 Influence of Foundation Soil

The present project focuses on scour of non-cohesive sediment at bridge abutments. Moreover, it takes into account how abutments are typically constructed, including their foundations. The modeled abutments simulate pile and sheet-pile support for abutment columns, and attempt to replicate the behavior of earthfill embankments. However, abutments often are sited in cohesive soils, and sometimes have a solid foundation perimeter around the abutment and extending deeply into the soil. A solid foundation in a cohesive soil may modify abutment scour development compared to the results presented in this report.

For example, the end of a spill-through abutment may be protected by a sheet-pile skirt as in Figure 4-10. When such a solid foundation perimeter extends into cohesive soil, the scour process may develop in the manner studied for NCHRP Project 24-15(02), "Scour at Abutments in Cohesive Materials." A boundary of cohesive soil, or clay, may erode differently than would a boundary of non-cohesive sediment, or sand. The manner whereby fragments of clay erode from the scour region is more complicated than erosion of sand. Material failure considerations like oscillatory loading are important for clay, which commonly fails in fragments. Also, the duration needed for scour to develop may be substantially longer than for scour in sand. Consequently, the scour region may remain close to the abutment and does not extend outwards as readily as does scour in non-cohesive sediment. Further, the solid form of the abutment foundation strengthens the local flow turbulence structures within the scour region as it deepens, and augments the scouring role of flow contraction. The solid form of the abutment and its foundation ensure that the abutment is not subject to the limits of embankment geotechnical instability. The resulting scour therefore may remain more localized at the solid abutment, and assume the appearance of scour at a wide pier. Figure 4-10 illustrates the resulting scour form.

Methods for estimating scour at a solid abutment (with solid foundation form) in a clay boundary are proposed in the report (yet to be finalized) for NCHRP Project 24-15(02). Methods for estimating scour depth at wide piers are being proposed by NCHRP Project 24-32, "Scour at Wide Piers and Long, Skewed Piers." The present report, focused on scour of non-cohesive

sediment at abutments of common, realistic construction, does not provide an estimation method for the scour situation where an abutment has a solid-form foundation.

Consideration 1: Embankment Length (L) and Floodplain Length (B_f)

If $L/B_f \geq 0.75$

If $L/B_f < 0.75$

0.5B

L

Embankment

B_f
Floodplain

0.5B_m
Main Channel

0.5B

L

Abutment

Embankment

B_f
Floodplain

0.5B_m
Main Channel

Consideration 2: Floodplain Erodibility

Fixed

Erodible

Scour Condition A

- Estimate the maximum scour depth likely to occur in the main channel.
- Given the estimated scour depth, check the geotechnical slope stability of the main channel bank and the abutment's embankment.

If the channel bank and the embankment are unstable or a conservative design is preferred, consider an abutment exposed by embankment breach.

Scour Condition B

- Estimate the maximum scour depth likely to occur in the floodplain.
- Given the estimated scour depth, check the geotechnical slope stability of the abutment's embankment.

If the channel bank and the embankment are unstable or a conservative design is preferred, consider an abutment exposed by embankment breach.

Scour Condition C
Estimate scour depth at exposed abutment foundation.

Consideration 3: Foundation and Embankment Design

- Select design elevation associated with scour depth estimate. Compare three Scour Locations and decide which scour depth to use in designing the abutment's foundation. For conservative estimation, select the scour producing the absolute lowest elevation near the abutment.

- Check whether abutment embankment stability should be increase to ensure abutment foundation not to be exposed. The embankment of a new abutment should remain stable to Scour Conditions A and/or B.

Figure 4-1. Flow chart outlining considerations in estimating scour depth around abutment; note that this figure is elaborated in Chapter 13, which applies the design approach
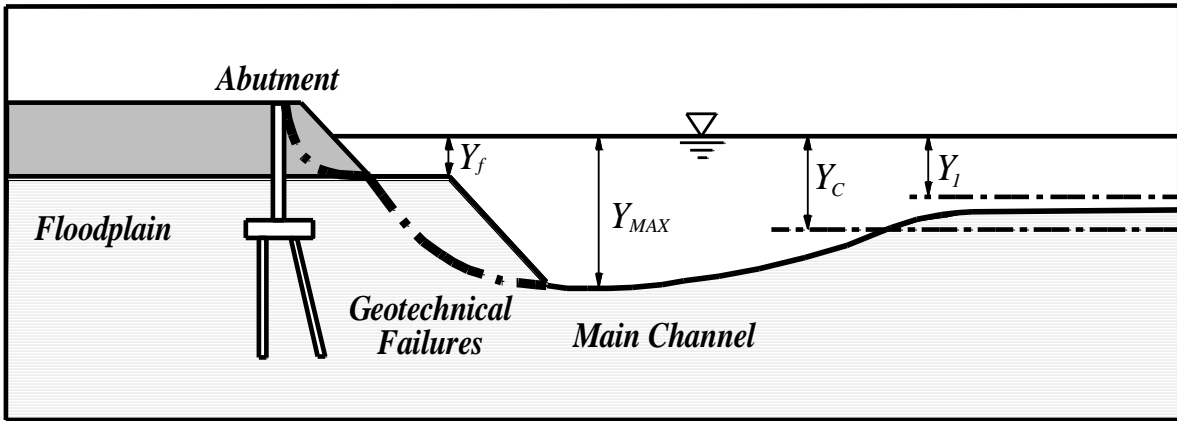
Figure 4-2. Short contraction scour as locally amplified contraction scour (Scour Condition A), and conceptual soil-failure circles. Note that banks and embankments also may undergo under-cutting and block failure; Y_C is flow depth associated with long contraction, and Y_1 is mean depth of the approach flow
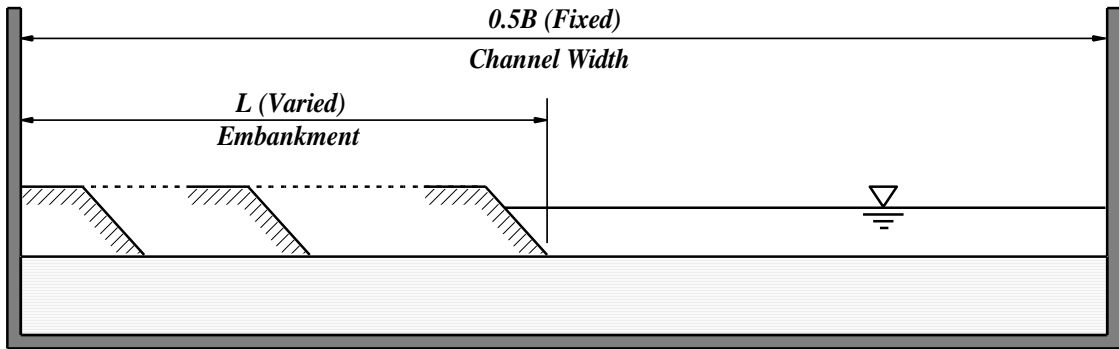
(a). Embankment length, L, reduces in a channel of fixed half width, $0.5B$
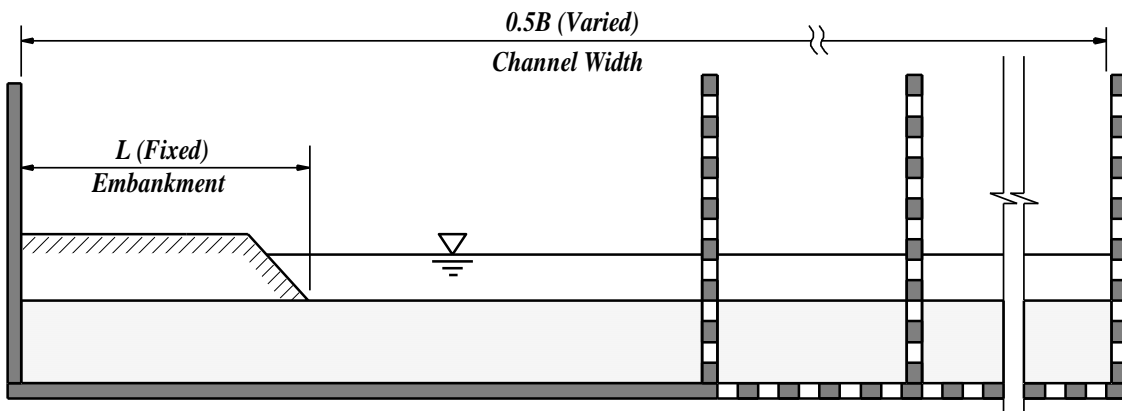
(b). Channel half width, $0.5B$, increases while embankment length, L, is fixed

Figure 4-3. Two limits whereby flow contraction tends to zero (or $Y_C/Y_1 \to 1$) for an abutment embankment in a channel: (a) abutment shortens, and (b) channel widens. Laboratory testing for situation (b) is considerably more expensive than situation (a)
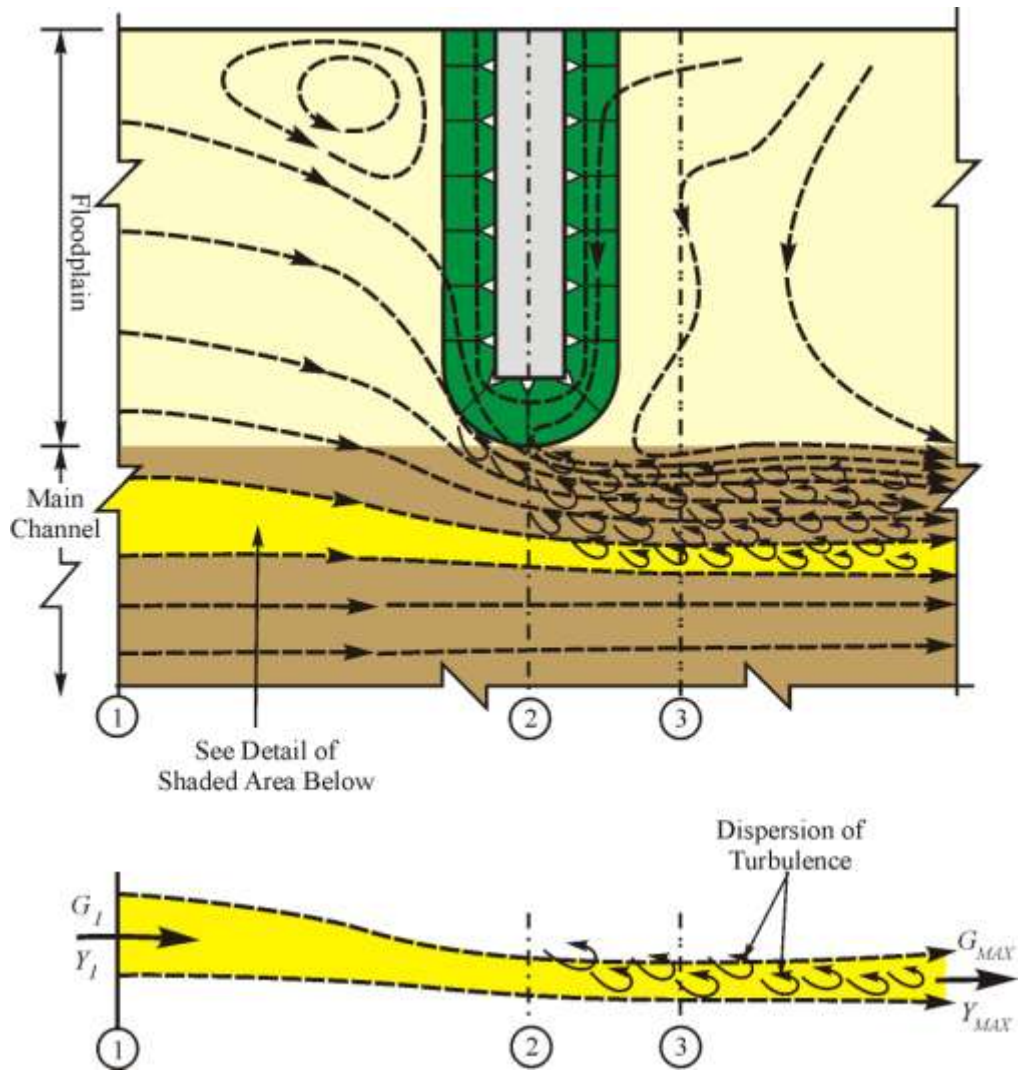
Figure 4-4. Schematic plan view of flow field around a spill-through abutment. The detail shows live-bed flow through a contracted stream tube in the main channel. Section 3 is at greatest unit discharge (q') in the stream tube
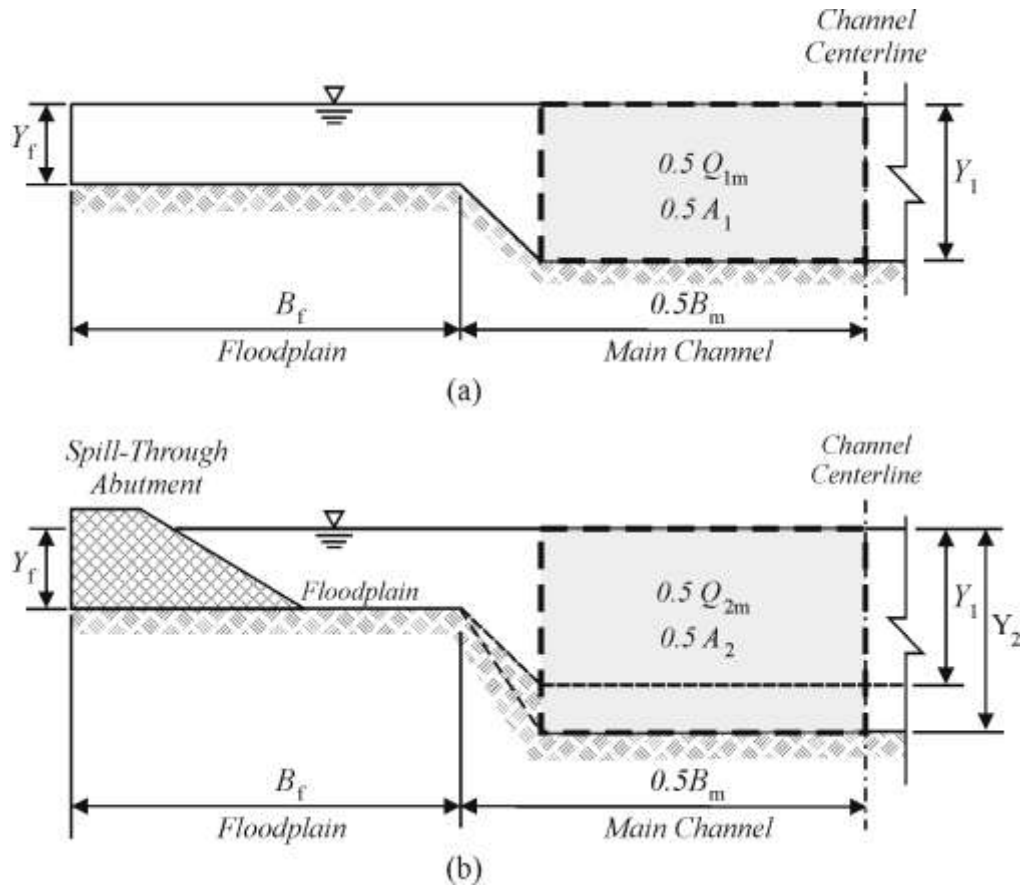
Figure 4-5. Approximate basis for estimation of flow in main channel through bridge waterway: at section 1 upstream from the bridge (a); and, at section 2 for spill-through abutment (b)
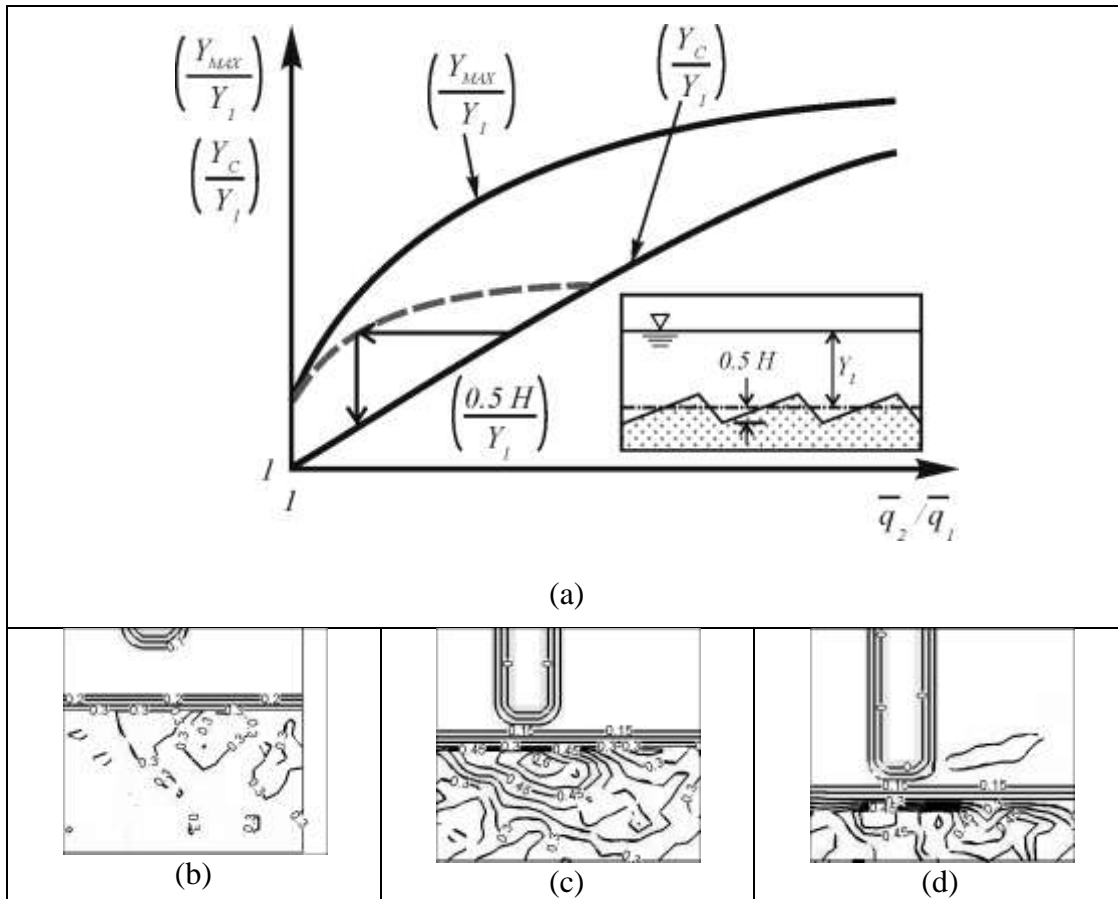
Figure 4-6. Conceptual variation of maximum flow depth, Y_{MAX}, and long-contraction flow depth, Y_C, (relative to approach flow depth Y_1), with ratio of unit discharges for Scour Condition A. Abutment length decreases in a channel of fixed width: (a); no effect on flow in main channel (b); some contraction effect (c); and, major contraction of flow in main channel (d). Note that figure (a) indicates the influence of dune amplitude, $0.5H$, on Y_{MAX}/Y_1.
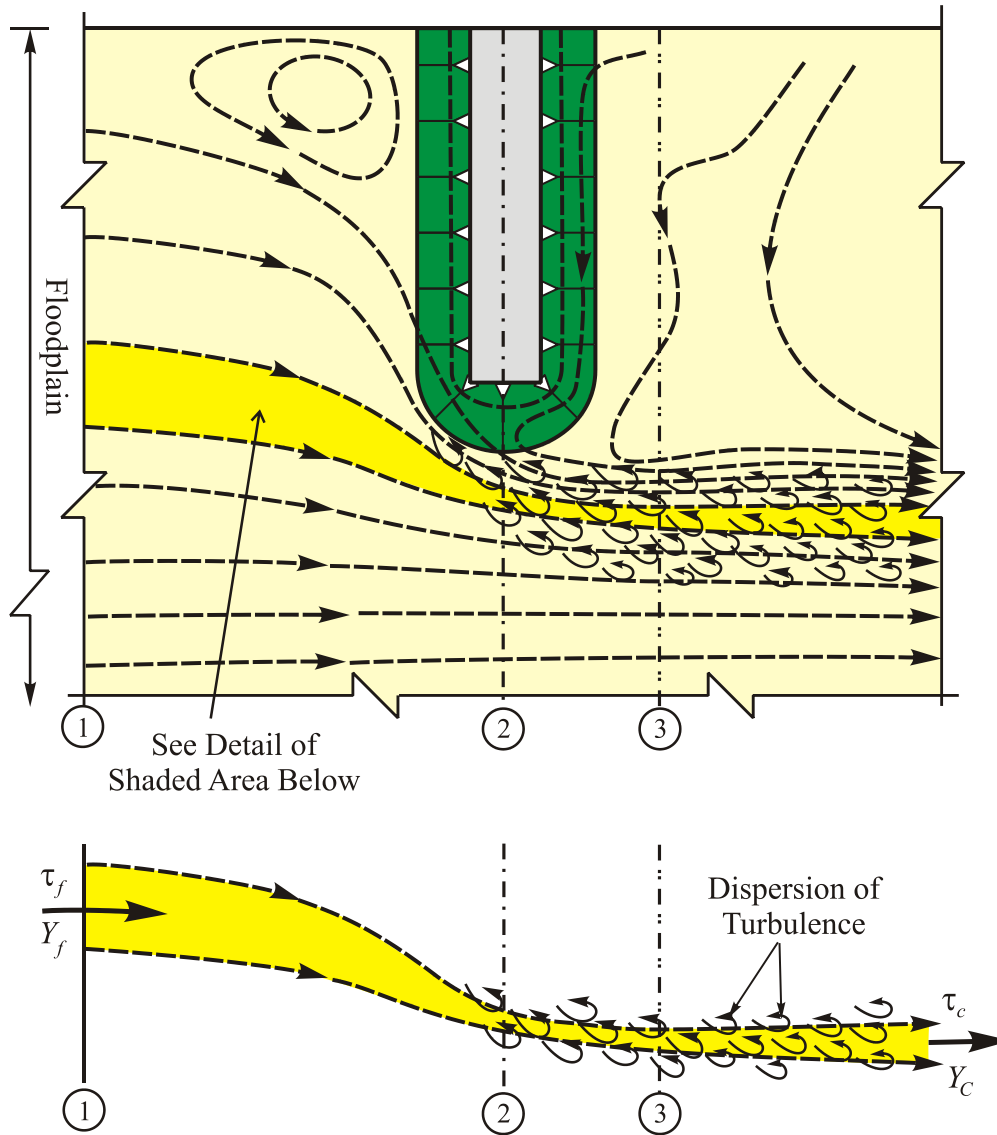
Figure 4-7. Schematic plan view of flow field around a spill-through abutment set back on a floodplain. The detail shows clear-water flow through a contracted stream tube near the abutment.
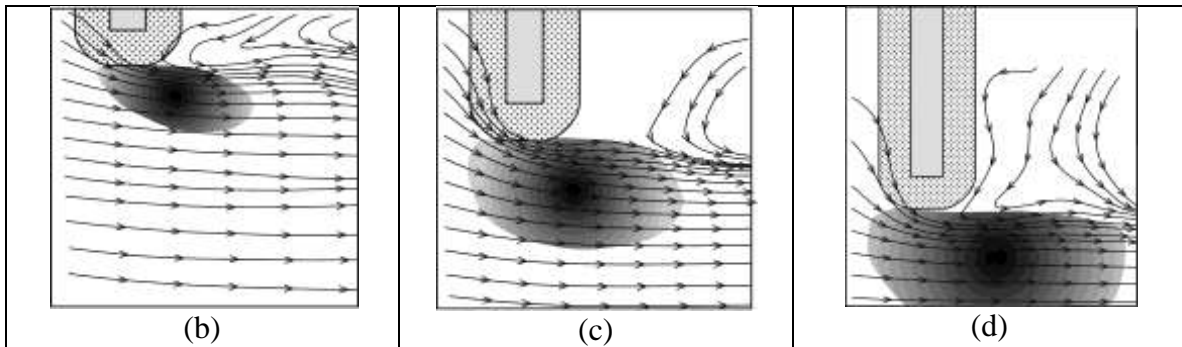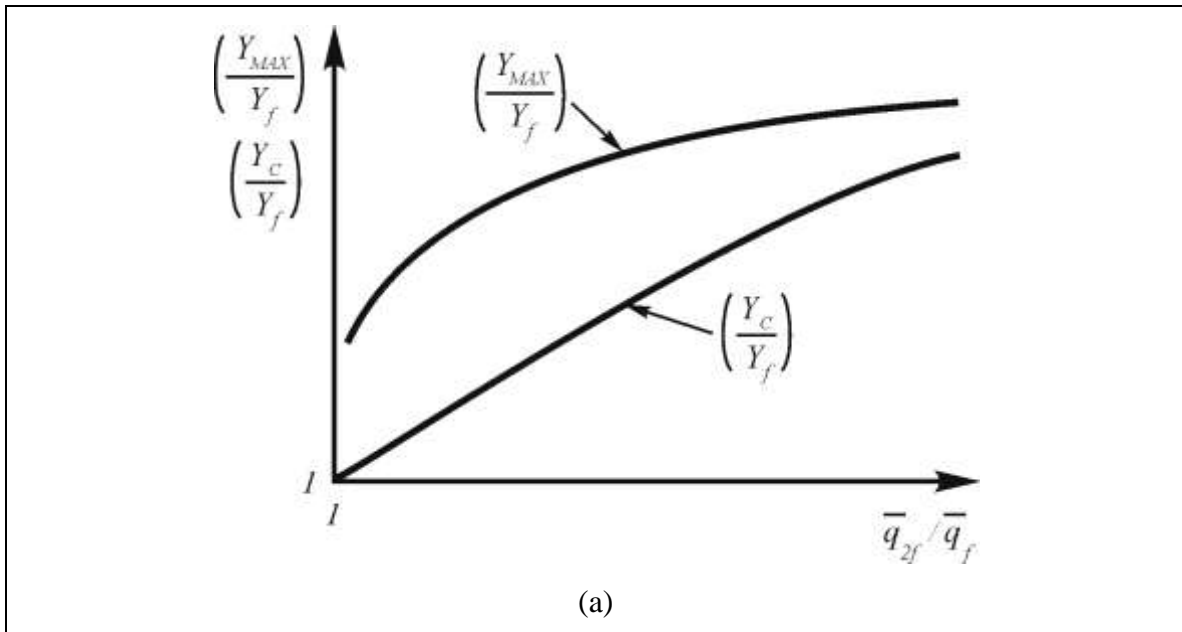
Figure 4-8. Conceptual variation of maximum flow depth, Y_{MAX}, and long-contraction flow depth, Y_C, (relative to approach flow depth, Y_1) with ratio of unit discharges, for Scour Condition B. Abutment length decreases in a channel of fixed width: (a) The lateral extent of scour increases as flow contraction and q_{2f}/q_f increase: localized contraction (b); greater contraction (c); and, major contraction of flow (d)
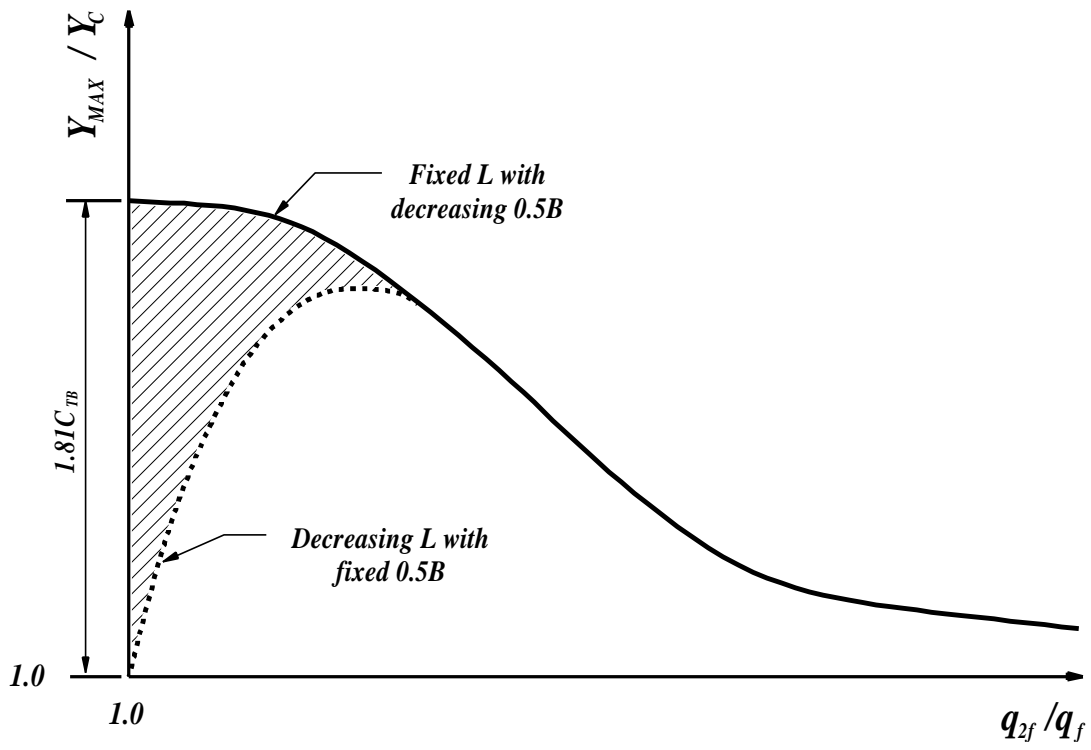
Figure 4-9. Loci of scour depth trends delineated in terms of Y_{MAX}/Y_C and q_{2f}/q_f for Scour Condition B
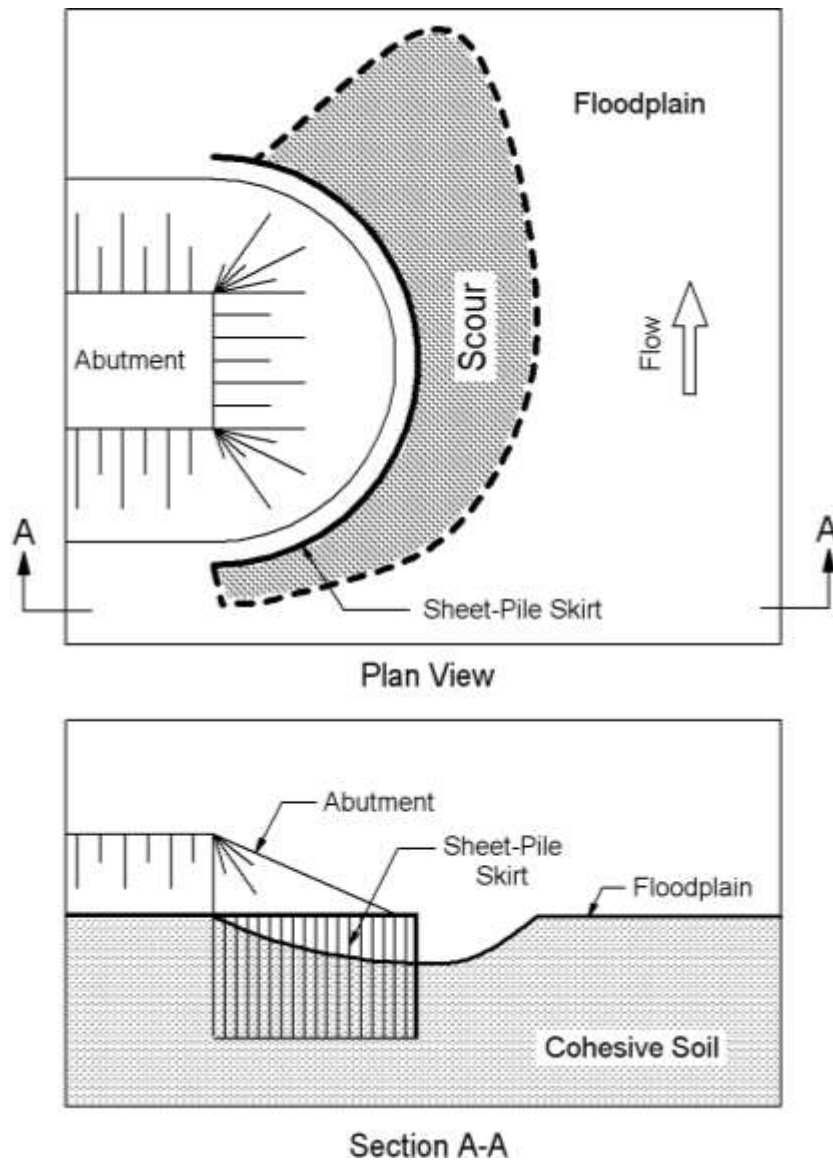
Figure 4-10. Scour at an abutment with solid-form foundation (shown here as a sheet-pile skirt) set in cohesive soil, which erodes in a different manner than non-cohesive sediment. This situation is examined in NCHRP Project 24-15(02)

CHAPTER 5

PARAMETERS AND PRIOR STUDIES

5.1 Introduction

The body of prior studies documenting studies on abutment scour lacks information regarding the circumstances leading to abutment Scour Conditions A, B, and C, as introduced in Chapters 3 and 4. Especially lacking are considerations of the actual ways whereby abutments are constructed, and consequently of how scour progresses and scour failures of abutments occur. The great majority of prior studies treat abutments and their earthfill embankments as being fixed structures that extend without limit into the sediment forming the bed of a channel or a floodplain. Though many aspects of the physical processes attendant to abutment scour are known and documented, prior predictor relationships for abutment-scour depth lack a general level of accuracy because they do not relate sufficiently to common structural configurations of abutment.

Moreover, only a few prior studies include a comprehensive accounting of the many parameters potentially influencing abutment scour. Indeed, a daunting consideration for abutment scour studies is the number of such parameters, some of which are difficult to replicate adequately in laboratory experiments; e.g., the influence of varying combinations of boundary sediments and soils at abutment sites.

This chapter briefly reviews the extent of knowledge developed by prior studies, the predictive accuracy of leading prior predictor methods, and indicates how the present Project expands that knowledge. This review is structured in the following manner:

1. Parameters;

2. Scour in a long contraction;

3. Scour locally at abutments;

4. Separation of contraction and local scour;

5. Field data observation; and,

6. Summary.

As the present Project focuses on scour at abutments, it is useful to consider prior studies dealing with so-called contraction scour attributable to flow acceleration through a contracted bridge opening, and with what is termed local scour at abutments. A dimensional analysis frames the review of each scour situation. The two resulting sets of parameters provide a useful filter through which the current state of knowledge about scour at abutments can be viewed. This approach has the advantage of revealing unexplored parametric influences of potential significance to scour. It is an approach that is useful for examining Scour Conditions A, B, and C. Scour Condition B here also includes abutments in rectangular channels.

The present review of prior studies briefly surveys a selection of quite widely cited laboratory studies, and does not attempt to review all prior studies. Table 5-1 lists them approximately in terms of Scour Conditions A, B, and C. Most studies, though, do not exactly align with these scour conditions. This table also includes a several studies of local scour at spur dikes (also known as groins, wing dams and jetties). Table 5-2 summarizes two leading predictive relationships for contraction scour. Listings of prior scour-depth relationships for Scour Condition B are given in Table 5-3. Each table briefly provides the details associated with each equation. Table 5-4 is a partial list of the symbols used in this chapter. Table 5-5 compares the range of variable values used in prior laboratory experiments producing scour condition approximately similar to Scour Conditions A and B.

5.2 Parameters

An immediate challenge confronting an effort to understand and discuss abutment scour is the potentially large number of variables that may influence scour. Many of the variables are well known (e.g., Melville and Coleman (2000), who provide the most extensive extant review). However, the full influences of some variables are unclear. Additionally, as mentioned above, there is lack of clarity about how to meaningfully characterize some influences exerted by some variables. Also, no relationship addresses the effect on scour depth of embankment failure, and thus the geotechnical strength properties of the earthfill.

5.2.1 Parameters for Abutment Scour

For scour near an abutment, the following somewhat simplified analysis that identifies and combines the variables into a reasonably comprehensive set of dimensionless parameters. Figure 5-1 indicates the variables for an idealized site. The variables can be grouped as follow

Water properties: ρ = density; μ = dynamic viscosity

Channel boundary properties: d and d_f = representative boundary particle diameter for bed and floodplain, respectively; ρ_s = density of boundary particles; u_{*c} = the critical value of shear velocity associated with entrainment of particles forming the main-channel bed; u_{*fc} is the critical shear velocity associated with the floodplain soil. (Note that shear velocity $u_* = (gS_0Y_1)^{0.5}$, and depth-average velocity of flow in the approach main channel, $U_1 = u_*(8/f)^{0.5}$ relate via the Darcy-Weisbach resistance coefficient $f = \varphi_1 \, d/Y_1$ in fully turbulent flow (a similar relationship between shear velocity and depth-average velocity exists for the depth-average flow on the floodplain). The present Project was limited to noncohesive sediment forming the main channel bed and the floodplain, though the Project also ran tests with erosion-resistant floodplains, as elaborated in Chapter 6.

Water flow geometry: S_0 = energy gradient; Y_1 = flow depth in main channel; Y_f = flow depth on floodplain; g = gravitational acceleration; $0.5B$ = half width of main channel upstream of the bridge site (the channel is assumed symmetrical about its centerline); B_f = width of floodplain. The floodplain is taken to have a flat transverse slope.

Abutment and embankment properties: L = embankment length; W = abutment top width; E_H = embankment height at the abutment; K_S = abutment shape factor (including construction configuration); L_p = distance from abutment column to first pier; and, β = abutment alignment relative to approach flow. The geotechnical strength properties of the abutment's earthfill embankment can be characterized in terms of shear strength, σ_E, and the specific weight of earthfill soil, γ_E.

By way of dimensional analysis using three dependent variables reflecting length, time, and mass units, the aforementioned 22 variables and their influences can be expressed in terms of the 19 independent parameters (for three quantities: length, time, and mass) given in the functional relationship below for maximum, scour-associated flow depth at the bridge axis, Y_{MAX}:

$$\frac{Y_{MAX}}{Y_1} = \varphi_2 \left(\frac{u_{*1}}{u_{*c}}, \frac{u_{*f}}{u_{*fc}}, \frac{u_{*c}}{u_{*fc}}, \frac{u_{*1}f^{0.5}}{\sqrt{gY_1}}, \frac{u_{*f}f^{0.5}}{\sqrt{gY_f}}, \frac{\rho U_1 Y_1}{\mu}, \frac{\rho U_f L}{\mu}, \frac{d_f}{d}, \frac{L}{d}, \frac{L}{Y_1}, \frac{W}{Y_1}, \right.$$
$$\left. \frac{L_p}{Y_f}, K_S, \beta, \frac{L}{B_f}, \frac{B_f}{0.5B}, \frac{Y_f}{Y_1}, \frac{Y_f}{k_p}, \frac{\sigma_E}{\gamma_E E_H} \right)$$

(5-1)

Quite numerous other variables could be considered (e.g., transverse slope of floodplain, geotechnical shear strength of floodplain soil, abutment riprap armor properties; patterns of flow resistance on the floodplain), thereby quickly demonstrating the innate complexity of many abutment sites.

Especially important are parameters involving embankment length, L. There is considerable debate (e.g., in the conference proceedings edited by Briaud and Chen 2002) about how equilibrium scour depth relates to L. A practical concern is that existing predictor relationships tend to give large values of scour depth, d_S ($= Y_{MAX} - Y_1$) relative to L. The present Project addresses this concern by using the ratio of area-averaged discharges to and through the bridge waterway, as Chapter 4 formulates. In this manner, the influences of several parameters are merged to reflect their combined effect on scour.

Alternative parameters could be identified for Eq. (5-1). Indeed, the various predictor methods use variations of the essential set of parameters given in Eq. (5-1). For example, several methods use one or other form of Froude number, $F_r = U/(gY)^{0.5}$. Also, various coefficients (or K factors) expressing parameter influences are often used.

Note that the ensuing discussion of prior studies uses slight differences in symbols for variables. The variables, defined in each section (and in the List of Symbols), remain essentially those used in the prior studies. The potentially large overall number of variables needed to characterize

differences in abutment sites, and the various site geometries assumed by prior studies, make in more convenient to use more-or-less the same symbols adopted by each of the prior studies.

Eq. (5-1) is useful for identifying some of the important gaps in knowledge, and, thereby, the limitations in predictive relationships regarding scour at abutments. Insofar as Melville and Coleman (2000) provide a useful comparison of the three relationships, and arguably have themselves proposed the most comprehensive relationship (in terms of the number of parameters considered), Section 5.3 begins with their proposed relationship.

5.2.2 Parameters for Long-Contraction Scour

The ostensibly simpler flow and erosion situation of scour in a long contraction involves a subset of the variables in Figure 5-1, and with some approximation it can be described using the following functional relationship of six significant parameters expressing turbulent, sub-critical flow depth through the long contraction:

$$\frac{Y_2}{Y_1} = \varphi_2 \left(\frac{u_{*1}}{u_{*c}}, \frac{B_f}{B_{m1}}, \frac{Y_f}{Y_1}, \frac{Y_f}{k_p}, \frac{L}{B_f}, \frac{B_{m2}}{B_{m1}} \right) \tag{5-2a}$$

The parameters can be restated in somewhat simpler terms, and terms more familiar with those used by Laursen (1960, 1963), as

$$\frac{Y_2}{Y_1} = \varphi_2 \left(\frac{u_{*1}}{u_{*c}}, \frac{B_f}{B_{1m}}, \frac{Q_F}{Q_1}, \frac{n_1}{n_2}, \frac{B_{m1}}{Y_1}, \frac{B_{m2}}{b_{m1}} \right) \tag{5-2b}$$

The parameters are combined from the variables used to constitute Eq. (5-2a) in which B_{m1} and B_{m2} are the widths of the main channel upstream of the contraction and through the contraction, respectively; Q_1 and Q_F are the water flow rates in the main channel and the floodplain upstream of the contraction, respectively; n_1 and n_2 are the values of Manning's flow resistance coefficient in the main channel upstream and through the contraction; and, Y_1 is the flow depth in the main channel. The shear stress on the bed at section 1 is τ_1, and the critical shear stress associated with erosion of the bed is characterized using τ_c. Flow rate through the contraction $Q_2 = Q_1 +$

$2Q_f$. Alternative variables, and resultant parameters, may be used rather than those in Eq. (5-2). For example, Darcy-Weisbach resistance coefficient, f, could be used instead of Manning's n.

5.3 Predictors for Long-Contraction Scour

As the present Project focuses on both scour types at abutments, it is useful to consider prior studies of contraction scour attributable to quickened flow through a long, contracted channel, such as has customarily been assumed representative of bridge openings. Prior studies of direct use for the present study include Laursen (1960, 1963), Laursen and Toch (1956), Richardson and Davis (1995) and Melville and Coleman (2000). This section considers live-bed and clear-water modes of scour through a long contraction. Discussed then is the difficulty of separating contraction scour and scour local to an abutment scour.

The studies by Laursen (1960, 1963) are considered in this section, because the estimation methods that they described are extended in the scour-depth formulation presented in Chapter 4.

5.3.1 Live-Bed Long-Contraction Scour

Laursen (1960) proposed a one-dimensional contraction scour formula for live-bed scour of the main channel of a compound channel with a long contraction section. His study was conducted in an experimental flume, as shown in Figure 5-2. The flume has two sections, such as an approach section (section1) which has a floodplain and a main channel, and a contraction section (section 2) which has only the main channel. To formulate a prediction equation, Laursen made the following assumptions:

1. Equilibrium scour depth in the long contraction is based on the principle of continuity applied to water and sediment flow through the bridge water way; and,

2. No sediment transport occurs on the approach floodplain at section 1.

Based on the above assumptions and laboratory experiments, Laursen proposed the following equation for long-contraction scour:

$$\frac{Y_2}{Y_1} = \left(\frac{Q_2}{Q_1}\right)^{6/7} \left(\frac{B_{m1}}{B_{m2}}\right)^{k1} \left(\frac{n_2}{n_1}\right)^{k2} \tag{5-3}$$

where Q_i is water discharge, Y_i is the water depth, B_{mi} is width of main channel in each section, and n_i is the Manning's coefficient. Laursen recommends $k_1 = 0.59$ to 0.69, and $k_2 = 0.066$ to 0.37, depending on values of shear velocity, and falling velocity. Suffixes 1 and 2 refer to sections 1 and 2, respectively (Figure 5-1). Laursen indicates that Eq. (5-1) can be modified with some simplification:

1. Usually, it can be considered that the Manning's coefficient does not change substantially in the different sections;

2. Also it can be assumed that the width of the main channel in each section is the same; and,

3. The flow forces exerted on the bed of the main channel are uniformly distributed across the main channel.

Therefore, Eq. (5-3) becomes

$$\frac{Y_2}{Y_1} = \left(\frac{Q_2}{Q_1}\right)^{6/7} \tag{5-4}$$

This equation is the most simplified relationship for deriving the contraction scour depth for live-bed conditions. It estimates the flow depth, Y_2, for uniform flow along a narrowed long channel. However, as illustrated in Chapter 4, flow through a short contraction is not uniformly distributed. Moreover, large-scale turbulence structures develop and disperse across the contracting flow, and affect sediment movement.

5.3.2 Clear-Water Long-Contraction Scour

Laursen (1963) proposed a formula for one-dimensional contraction scour occurring under the clear-water flow condition. His study used an experimental set up comprising an un-contracted

section and a contracted section (section 1 and 2, respectively) as shown in Figure 5-3. Unlike the experimental set up that he had used for the live-bed condition, this study was conducted using a rectangular channel. He adopted the following assumptions to formulate an equation for contraction scour:

1. Equilibrium scour depth in the long contraction is attained when critical bed shear stress develops along the bed of the contracted section;

2. Dunes and other bed forms are neglected; and,

3. The local head loss, due to flow entering the contraction, is negligible.

These assumptions, with appropriate formulation, lead to the following equation for flow depth in the contraction, Y_2:

$$\frac{Y_2}{Y_1} = \left(\frac{u_{*1}}{u_{*c}}\right)^{6/7} \left(\frac{B_{1m}}{B_{2m}}\right)^{6/7} \tag{5-5}$$

The same comment pertains here as for the live-bed contraction scour; i.e., this equation estimates the flow depth, Y_2, for uniform flow along a narrowed long channel. It does not include the flow features associated with a short contraction: non-uniform flow distribution, and large-scale turbulence.

5.4 Predictors for Scour near Abutments

An immediate challenge confronting an effort to understand and discuss abutment scour is the potentially large number of parameters that may influence scour near abutments (Eq. (5-1)). The influences of many of the parameters are well known (e.g., Melville and Coleman, 2000). However, the full influences of some of them are unclear. Additionally, as mentioned above, there is lack of clarity about how to meaningfully characterize some influences exerted by some variables. Moreover, no relationship addresses the effect on scour depth of embankment failure.

All of the predictor methods are empirical, to varying extents. The methods are based largely on laboratory flume experiments, and attempt to estimate scour depth separate from a depth attributable to flow contraction around an abutment. No method purports to estimate a scour depth ascribable to the combined effects of flow contraction and the turbulence structures generated by flow around an abutment.

The predictor methods are here discussed in terms of

1. Scour Condition B – the simpler condition of abutments located in rectangular channels (or well set back on floodplains);

2. Scour Condition A – scour of the main-channel bed for abutments close to the main-channel bed; and,

3. Scour Condition C – scour of an exposed abutment column.

Some predictors pertain to Scour Conditions A and B, none to all three conditions.

5.4.1 Scour Condition B (Rectangular Channel)

Fairly numerous laboratory studies on abutment scour in rectangular have been conducted over the years. Most of the studies have been conducted with abutments simulated with rigid-forms, and not the earthfill and abutment-column structures indicated in Chapters 3. Table 5-1 lists studies that have contributed laboratory flume data for each condition of abutment scour. The approach taken herein is to focus on the predictive relationships commonly used for estimating scour depth. The relationships are those proposed by

1. Liu et al. (1961) [also Field (1971)];

2. Froehlich (1989);

3. Richardson and Davis (1995, 2001);

4. Chang and Davis (1998, 1999); and,

5. Melville and Coleman (2000)

These five methods present relationships developed from laboratory data and a very modest amount of field data. Actually, the methods proposed by Froehlich (1989) and Richardson and Davis (2001, 1995) have much in common, insofar that they relate scour depth primarily to a Froude number and structurally are similar to the relationships proposed by Liu et al. (1961). Only the method presented by Chang and Davis (1998, 1999) treats abutment scour as being intrinsically linked to contraction scour. Their method, called ABSCOUR, is further discussed in Section 5.7.

Lui et al. (1961) proposed the following relationship based on the results of laboratory flume experiments:

$$\frac{d_S}{Y_1} = 1.1 \left(\frac{L}{Y_1} \right) F_r^{0.22} \tag{5-6a}$$

in which d_S = scour depth below the un-scoured bed at the bridge centerline. For wing-wall abutments, scour depth is increased in accordance with

$$\frac{d_S}{Y_1} = 2.15 \left(\frac{L}{Y_1} \right) F_r^{0.33} \tag{5-6b}$$

For L/Y_1 greater than about 25, Liu et al. recommend using $\dfrac{d_S}{Y_1 F_r^{0.22}} = 4$, and $\dfrac{d_S}{Y_1 F_r^{0.33}} = 7.8$ for Eqs. (5-6a) and (5-6b), respectively. These equations apply for both clear-water and live-bed local scour. Field (1971) developed a design chart based on the data published by Liu et al. The chart is included herein as Figure 5-4.

Froehlich (1989) proposed the following relationship for estimating local scour at bridge abutments:

$$\frac{d_S}{Y_1} = 2.27 K_S' K_\beta' \left(\frac{L \sin \gamma}{Y_1} \right) F_{re}^{0.61} \tag{5-7}$$

in which Y_1 is approach-flow depth in the main channel, $K_S{}'$ is an abutment-shape factor, $K_\beta{}'$ is a factor accounting for abutment alignment to the flow, and $F_{re} = V_e / \left(gY_1\right)^{-0.5}$ where $V_e = Q_e/A_e$, with Q_e is flow obstructed by the abutment and its approach embankment, and A_e is the flow area corresponding to Q_e.

Froehlich's relationship, which is similar in structure to those by Liu et al. (1961), was developed from an extensive multiple linear-regression analysis of some 334 measurements from laboratory experiments on Scour Condition B at abutments and spur dikes. In total, 164 and 170 cases, respectively, of clear-water and live-bed scour were used in the regression. Many of the data sources used by Froehlich are listed in Table 5-1.

In effect, Eq. (5-7) by Froehlich is an envelope fitted to the scour data from diverse flume experiments, including those by Liu et al. (1961). Froehlich's (1989) arrival at Eq. (5-7), however, is a little disconcerting. He presented rather boldly without much consideration of the parameters involved in scour, and without much discussion of similitude considerations.

Eq. (5-7) is intended for live-bed scour, and has been adopted for use in HEC-18. Froehlich also proposed an equation for clear-water scour

$$\frac{d_S}{Y_0} = 2.27 K_S{}' K_\beta{}' \left(\frac{L\sin\gamma}{Y_1}\right)^{0.63} F_{re}{}^{1.16} \left(\frac{Y_1}{d_{50}}\right)^{0.43} \sigma_g{}^{-1.87} \tag{5-8}$$

The relationship is an effort to take into account, for scour estimation, the combined influences of floodplain and main channel flows through the use of a Froude number.

Richardson and Davis (1995) in HEC 18 suggest Eq. (5-7) be modified as

$$\frac{d_S}{Y_1} = 2.27 K_S{}' K_\beta{}' \left(\frac{L\sin\gamma}{Y_1}\right) F_{re}{}^{0.61} + 1 \tag{5-9}$$

in which the term "+1" is added, though the reason for so doing is unclear.

Richardson and Davis (1995) recommend use of a relationship only slightly adjusted from Eq. (5-6b) proposed by Liu et al. (1961):

$$\frac{d_S}{Y_1} = 7.27 K_S'' F_r^{0.33}$$

(5-10)

Here, K_s'' is an abutment-shape factor generally comparable to K_S' and K_s. This equation applies to abutments for which L/Y_1 exceeds about 25. It also applies only for live-bed scour, which arguably develops the greater scour depths at actual bridges.

Melville and Coleman (2000) propose that scour depth be estimated as

$$d_S = K_{yL} K_I K_d K_S K_\gamma K_G K_t$$

(5-11)

in which the *K* factors embody the following influences:

K_{yL} = flow depth relative to abutment size, L/Y_0;

K_I = flow intensity, u_{*0}/u_{*c};

K_d = sediment size relative to structure size, L/d;

K_S = abutment shape;

K_γ = abutment alignment, γ;

K_G = shape of compound channel; and,

K_t = time factor

The influence of each factor is expressed in a curve based on data from several laboratory flume studies. The curves are provided by Melville and Coleman (2000) and are not reproduced herein.

Melville (1992, 1995) introduced the concepts under-girding Eq. (5-11). A substantial number of the flume experiments used in preparing the curves for it are documented in Dongol (1994) and Kwan (1984). The method follows an approach that is applicable for estimating pier and abutment scour. Melville (1992) suggests that, for the purpose of scour estimation, abutments can be divided into three categories: long, intermediate, and short abutments. The three equations associated with each category are

$$\frac{d_S}{Y_1} = 10 K_I K_d K_\sigma K_\gamma K_G \qquad \text{when } \frac{L}{Y_o} > 25 \qquad (5\text{-}12)$$

$$\frac{d_S}{\sqrt{LY_1}} = 2 K_I K_d K_\sigma K_s^* K_\gamma^* K_G \qquad \text{when } 1 \le \frac{L}{Y_o} \le 25 \qquad (5\text{-}13)$$

and,

$$\frac{d_S}{L} = 2 K_I K_d K_\sigma K_s K_G \qquad \text{when } \frac{L}{Y_o} < 25 \qquad (5\text{-}14)$$

Depending on whether an abutment is long, intermediate, or short, the appropriate equation listed above is used to calculate the depth of abutment scour. The superscript in each term shows slightly different factors from that without the superscription. Those are shown in Table 5-4.

5.4.2 Predictors for Abutment Scour Condition A-B (Compound Channels)

Three reasonably concerted research efforts have been conducted to elucidate Scour Conditions B and A-B for abutments in compound channels. The efforts (listed in Table 5-1) are usefully discussed in terms of the principal investigator and their home institutions:

1. Sturm at Georgia Institute of Technology, US; and,

2. Townsend at the University of Ottawa, Canada.

Each of these efforts has produced several papers on Scour Condition B or the combination Scour Condition A-B, comprising scour of the floodplain and main channel near an abutment. A series of brief appraisals of the studies ensues below.

The studies conducted by Sturm and colleagues at the Georgia Institute of Technology have focused on the clear-water state of Scour Condition B. In their studies the floodplain simulated typically is wide compared to main-channel width. This arrangement is especially so for the earliest set of experiments (Sturm and Janjua 1993, 1994), for which the main-channel widths, B_m, are 0.2 m and 0.3 m, and floodplain widths, B_f, are 2.6 m and 2.5 m, respectively. These widths yield B_f/B_m ratios of 13.0 and 8.3, respectively. Table 5-5 summarizes the test conditions of the experiments.

Sturm and Janjua (1993, 1994) began their study by proceeding through a dimensional analysis that resulted in the formulation of the functional relationship

$$\frac{d_S}{Y_{Fo}} = \varphi \left[\frac{V_{F1}}{\sqrt{gY_{F1}}}, \frac{d_{50}}{Y_{F1}}, m_S, \frac{B_m}{B_f}, \frac{B_f}{Y_{F1}}, \frac{Y_1}{Y_{F1}} \right] \tag{5-15}$$

in which d_S = scour depth at abutment; Y_1 = approach flow depth in main channel; Y_{F1} and V_{F1} = approach flow depth, and average flow velocity upstream of the end of abutment; d_{50} = median grain size of bed sediment; m_S = geometric contraction ratio. Eq. (5-15), however, is incomplete, when compared with Eqs. (5-2a-b). It does not include sufficient parameters for characterizing the larger-scale turbulence features generated by the abutment or within the interacting flows passing in the main channel and the floodplain.

Sturm and Janjua (1993) propose that abutment scour depth should not depend directly on abutment length, but rather on the effect abutment length exerts on flow redistribution in the contracted section of a compound channel. Therefore, Sturm and Janjua (1993, 1994) replace the geometric contraction ratio, m_s, with a discharge contraction ratio, $M = Q_o/Q$, with Q_o being the portion of the flow in the approach section with a width equal to the opening width and Q being the total discharge.

They further reasoned that, since M is related to the last four dimensionless variables in Eq. (5-15), it may be postulated that the primary influence on these variables is embodied in M. Based on this reasoning, Sturm and Janjua (1993) arrive at the functional relationship

$$\frac{d_{Se}}{Y_{F1}} = \varphi \left[F_{F1}, M, \frac{d_{50}}{Y_{F1}} \right] \tag{5-16}$$

where F_{F1} = approach Froude number on the floodplain, and is defined by the velocity and flow depth upstream of the end of the abutment, and d_{Se} = equilibrium abutment scour depth. From their experimental data, Sturm and Janjua obtain

$$\frac{d_{Se}}{Y_{F1}} = \varphi \left[\frac{F_{F1}}{M} - 0.18 \right] \tag{5-17}$$

This equation is derived from a least-square regression analysis of flume data. The equation neglects an influence of d_{50}/Y_{F1}. The Sturm and Janjua argue that the sediment ratios of their data were large enough such that relative-roughness effects were negligible.

In their later work, Sturm and Janjua (1994) include d_{50}/Y_{Fo1} by using the argument by Jain (1981) that d_{50}/Y_{F1} could be replaced by the critical Froude number at the initiation of sediment motion, F_c. With this assertion, they formulated a functional relationship slightly different from Eq. (5-17), resulting in

$$\frac{d_S}{Y_{Fo}} = \varphi \left[F_{F1}, F_C, M \right] \tag{5-18}$$

where F_C = critical approach Froude number for sediment entrainment.

The authors proposed formulation of an appropriate equation to determine abutment scour depth on a floodplain using a contraction theory. Here, their arguments become rather vague and

confusing. They claimed to use the long contraction equation proposed by Laursen (1963) to determine an equation that relates scour depth, d_S to the flow property.

$$\frac{d_S}{Y_{F1}} + 1 = 0.57 \frac{\left(\dfrac{F_{F1}}{m_S}\right)^{6/7}}{\left(\dfrac{d_{50}}{Y_{F1}}\right)^{2/7}} \tag{5-19}$$

This equation is followed by an equation proposed by Jain (1981) to relate F_c to d_{50}/Y_{F1}

$$F_C = 1.93 \left[\frac{d_{50}}{Y_{F1}}\right]^{1/3} \tag{5-20}$$

By substituting Eq. (5-20) into Eq. (5-19), Sturm and Janjua were able to derive an equation for use to calculate abutment scour on a floodplain

$$\frac{d_S}{Y_{Fo}} + 1 = \left[\frac{F_{F1}}{m_S F_C}\right]^{6/7} \tag{5-21}$$

This equation derived from consideration of flow contraction theory is clearly similar to that obtained using dimensional analyses Eq. (5-21) except for the difference in the geometric and flow contraction ratios. Sturm and Janjua suggest that m can simply be replaced by M at this point.

They plotted their experimental data relating d_S/Y_{F1} to F_{F1}/MF_c and obtained the following empirical equation:

$$\frac{d_{Se}}{Y_{F1}} = 7.70 \left[\frac{F_{F1}}{MF_C} - 0.35\right] \tag{5-22}$$

The correlation coefficient and standard error in d_{Se}/Y_{F1} are 0.91 and 0.37, respectively.

The experiments conducted by Sturm and Janjua (1993, 1994) involved a short flume of overall length only 5.18 m. One feature of the study is that there is negligible change in flow depth at the contracted section of the flow. This is because the tail water in the short flume drowns the influence of the abutment. To explore whether the backwater effect caused by the abutment would have any influence on the depth of scour, Sturm and Sadiq (1996) and Sturm (1998) conducted additional studies using a longer flume (17 m), and a marginally smaller B_f/B_m ratio. They used arguments on critical velocity for flow entrainment of bed sediment Laursen (1963) used with a long contraction theory and the continuity equation for the floodplain from the approach to the contracted section to derive a functional relationship with which they fitted the following equation:

$$\frac{d_{Se}}{Y_{F1}} = 8.14 \left[\frac{q_{F1}}{Mq_{F1c}} - 0.40 \right]$$

(5-23)

where q_{F1} (= $V_{F1}.Y_{F1}$) = flow rate at the beginning of scour (with water backup due to abutment); $q_{F1c} = V_{F1c}Y_{F1}$; and V_{F1c} = critical mean velocity for bed sediment entrainment on the approach floodplain. The authors suggested that q_{F1} could be determined from a one- or two-dimensional numerical simulation of the water surface profile of the river (with floodplain and abutment). The correlation coefficient and standard error in d_{Se}/Y_{Fo} are 0.86 and 0.68, respectively. The data used in fitting the above equation also include those by Sturm and Janjua (1993, 1994). An interesting result from this study is that the earlier empirical Eq. (5-21), for which backwater is absent, provides just as good a prediction as obtained using Eq. (5-23).

In yet another formulation, Sturm (1998) considered the possibility of relating the depth of abutment scour with the maximum depth-average velocity, V_{max} near the abutment face at the beginning of scour (without scour). He utilized the depth-averaged, k-ε turbulence model proposed by Biglari and Sturm (1998) to determine the flow field around an abutment founded on the floodplain of a compound channel. With such an output, he was able to determine the maximum velocity, with which he fitted his empirical scour data to obtain the following functional relationship

$$\frac{d_{Se}}{Y_{F1}} = \varphi\left(\frac{V_{max}}{V_C} - 1\right) \qquad (5\text{-}24)$$

Sturm found that the experimental data fitted well with the above parameter. This is despite the fact that although he obtained a second parameter (Y_{MAX}/Y_{Fo}) in his dimensional analysis, it is absent from his final equation. He claimed that the influence of this second is significant. He did not provide a mathematical equation for the function in Eq. (5-24) and the data were only presented graphically. It is reproduced in Figure 5-4.

The work at the University of Ottawa is presented in three separate papers by Kouchakzadeh and Townsend (1997a-b, 1998). It is not dissimilar to those carried out at Georgia Institute of Technology. However, the duration of their experiments of 5 hours is even shorter than that used by Sturm and his co-workers. From another perspective, the data of the University of Ottawa are more extensive in that four abutment shapes were used. The ratio of the width of the floodplain and that of the main channel, B_f/B_m is 0.93, lower than those used at the Georgia Institute of Technology.

By conducting a dimensional analysis, Kouchakzadeh and Townsend (1997a) obtained the following functional relationship:

$$\frac{d_{se}}{Y_{F1}} = \varphi\left(F_c, F_{F1}, \frac{Q_a}{Q_w}, S_h\right) \qquad (5\text{-}25)$$

where Q_a = flow intercepted by abutment length and diverted towards main channel; Q_w = flow related to a specific channel width at the abutment end; and Sh = abutment shape factor. Eq. (5-25) insufficiently characterizes the flow field at an abutment in a compound channel. Somewhat like Eq. (5-15), it does not capture the parameters needed to account for the effects on scour of the larger-scale features of flow turbulence.

Comparison of Eq. (5-25) with the functional relationships proposed by Sturm and Janjua (1993, 1994) -- Eqs. (5-15) and (5-18) -- reveals these relationships to be similar. An exception is the parameter used to describe the lateral momentum transfer. The former relationship uses a Q_a/Q_w ratio while the latter a discharge contraction ratio, M. As can be seen in the definitions of Q_a and Q_w stated above (which is the exact wording in Kouchakzadeh and Townsend 1997a), they are at best vague. In fact, it is not at all clear from their paper how these values were measured. For the sake of clarity, the definition sketch of Q_a and Q_w is reproduced as Figure 5-5. Using this somewhat ambiguous approach of obtaining Q_a/Q_w and their own fitted shape adjustment factor, the authors obtained the following empirical equation for calculating the scour depth of a semi-circular abutment on a floodplain:

$$\frac{d_{Se}}{Y_{F1}} = 13.5 \left(\frac{Q_w}{Q_a} \right)^{3.9} F_{F1}^{1.17} F_c^{-0.25} \tag{5-26}$$

It must be pointed out that the shape adjustment factor used in their study is different from those listed in Melville and Coleman (2000).

Using the same data set, Kouchakzadeh and Townsend (1997b, 1998) reported in separate papers that for abutments terminating in the floodplain, the lateral momentum transfer, which is characteristic of severely compounded flow field, could cause an increase of 15 to 30% of the depth of scour.

5.5 On the Separation of Contraction and Local Scour

The difficulty of separating contraction and local scour is mentioned in several articles. Benedict (2003) and Mueller and Wagner (2005) pointed out this issue in their report of the field studies, but do not pursue it. From a practical point of view, in terms of field measurements, it is almost impossible to define contraction scour by bathymetry measurements.

Laursen and Toch (1956) conducted scour experiments with multiple cylinders in a channel. Cylinders of a diameter of b were evenly placed across the flow for obtaining the appropriate bridge opening. Figure 5-6 shows the depth of scour around multiple cylinders. Here in this

figure, the horizontal axis represents β, which related to the ratio of bridge opening. The vertical axis represents scour depth normalized with water depth. The curves in this figure are estimated by the experimental result. Among them, at the bottom in the series of curves, there is a calculation result shown as long contraction. This curve is based on the following equation, originally proposed by Straub (1934):

$$\frac{d_s}{y} = \frac{1}{1 - \beta^{\frac{9}{14}}} - 1 \qquad\qquad (5\text{-}27)$$

Here, $(1-\beta)$ is the ratio of the width of the approach section, B_1, to that of bridge section, B_2. This curve represents the case where pier width is zero. Accordingly, the data on this curve includes no local scour around pier; only contraction scour. Therefore, two bias examples are drawn in this figure:

1. The case with <u>no contraction scour</u> as the curve of $y/b = 1/8$ at the top of the curves, whose scour depth is independent from the contraction scour; and,

2. The case with <u>no local scour</u>, as already described for Eq. (5-30).

The offset between these two curves represents the scour depth, which is, probably, observed in actual bridge sites. As shown in these curves, the scour depth is a function of both y/b and $\hat{a}$. This evidence indicates that each depth cannot be distinguished as either purely contraction scour or local scour. As discussed further in Section 5.7, the concept that contraction and local scour are essentially inseparable has been expanded upon by Chang and Davis (1998, 1999).

5.6 Field Data and Observation

Many field data observations have been measured by, mainly, United States Geological Survey (USGS). Mueller and Hitchcock (1998) measured scour depth during the flood on the several bridges in Minnesota. Parts of those data are well described in the report of Mueller and Wagner (2005). Holnbeck (1993) provides additional useful data and comparisons with design methods. Benedict (2003) intensively surveyed the bathymetry around 146 bridges in South Carolina. The objectives of his work were as follow:

1. Evaluate techniques for collecting clear-water contraction and abutment scour data;

2. Compare theoretical estimates of clear-water contraction and abutment scour depth with observed data;

3. Select for further analysis data from field data sets; and then,

4. Develop envelope curves from observed data.

In pursuit of these objectives, he observed 146 bridges in North Carolina during the flood of 1996 to 1999. Two broad types of bed material were encountered: one being cohesive soils, and the other sandy soils.

The possible failure, and even breaching of bridge embankment, was not taken into account by Benedict in formulating his prediction equation. However, the occurrence of bridge failure with the embankment breaching is common. For example, during floods in October 1990, 80 bridge failures were reported. Of these 80 bridge failures, 79 were caused by embankment failure, and partial or complete breaching.

Benedict compared of field data and predicted value of maximum scour depth. He used the scour equations recommended in HEC-18. The equations used were those by Laursen (1960) and Laursen (1963) for live-bed and clear-water contraction scour. Froehlich (1989) for live-bed abutment scour, and HIRE by Richardson et al. (1990). Benedicts' study concluded these conventional prediction equations poorly estimate the maximum scour depth, compared with values measured in the field.

To address the deficiency of the existing prediction equations, Benedict proposed two types of envelope curves, such as the maximum scour depth by the 100-year flood with the function of length of abutment, and the function of geometric contraction ratio as shown in the following equations:

$$d_S = 0.0338L \qquad\qquad\qquad L \le 426 \qquad\qquad\qquad\qquad (5\text{-}28)$$

$$d_S = 14.4 + 0.00131\ L - 426 \qquad\quad 426 \le L \le 7{,}440 \qquad\qquad\qquad (5\text{-}29)$$

where d_S is the upper limit for the range of anticipated abutment-scour depth, in feet, and L is the 100-year-flow embankment length (in feet);

$$d_S = 29.62 m_S{}^3 - 10.182 m_S{}^2 + 5.538 m_S \qquad\qquad\qquad\qquad (5\text{-}30)$$

Where d_S is the upper limit for the range of anticipated abutment-scour depth, in feet, and m_S is the 100-year-flow geometric-contraction ratio, where $m_S = B_1/B_2$.

5.7 ABSCOUR Method

Insofar that contraction scour and local abutment scour are essentially inseparable, for abutments as are commonly constructed, the existing method closest to the hydraulic method presented in this report is the ABSCOUR method presented by Chang and Davis (1998, 1999). Therefore, it is useful to devote a full section to their method. It estimates flow depth at the location of greatest scour as

$$\overline{}\qquad\qquad \overline{} \qquad\qquad\qquad\qquad\qquad\qquad\qquad\qquad (5\text{-}31)$$

Here, Y_1 is flow depth in the approach channel, and Y_2 is flow depth estimated using Laursen's relationships (Laursen 1960, 1963) for contraction scour; q_1 and q_2 are section-average values of unit discharge through the upstream approach and the contracted section at the bridge, respectively; and k_v and k_f are coefficients.

The ratio of flow velocity at the abutment toe relative to the mean velocity in the contracted section at the bridge is

$$\overline{\hspace{2em}} \tag{5-32}$$

If the flow is not contracted through the bridge waterway, $k_v = 1.8$. For increasing contraction, k_v diminishes, such that for severe contraction asymptotes to $k_v = 1.0$. The coefficient k_f expresses the influence of what Chang and Davis term spiral flow at the abutment toe, and is set as

$$\overline{\hspace{3em}} \tag{5-33}$$

for clear-water scour, and for live-bed scour as

$$\overline{\hspace{3em}} \tag{5-34}$$

Chang and Davis suggest that k_f be limited to the range 1.0 to 3.2; at larger contractions, k_f approaches 3.2 This coefficient is expressed in terms of   , the section average Froude number for the approach flow to the bridge. However, as indicated in Appendices B (Scale Effects Associated with Scour Experiments) of the present report, the scour effects of large-scale turbulence structures (spiraling flow, as referred to by Chang and Davis) are better described using the vorticity-similitude parameter   (here, W = a characteristic width of abutment in the streamwise direction) rather than Froude number, because the scaled erosiveness of turbulence structures depends upon their vorticity.

The values used in forming Eq. (5-29) pertain to vertical wall abutments, and are based on laboratory experiments with abutments modeled as solid structures extending to depth within a channel (Palaviccini 1995, Sturm 1997). For scour at spill-through or wing-wall abutments, Chang and Davis refer to a recommendation in Richardson and Davis (1995, 2001; see also Table 5-3) that Eq. (5-30) be modified as

$$\overline{\hspace{1em}} \qquad \overline{\hspace{1em}} \tag{5-35}$$

where k_s is a factor accounting for abutment shape (= 0.55 for spill-through abutments, 0.82 for wing-wall abutments); and k_α = 1.08 abutments at 30° skew, 1.15 for 60° skew. ABSCOUR provides a convenient spreadsheet procedure for scour estimation.

Scour depth is determined as

$$ \text{(5-36)} $$

where Y_0 is the flow depth through the bridge waterway prior to scour. The scour-depth relationships in Eqs (5-30) through (5-36) are further considered in Chapters 7 through 9 when discussing the results of the present study.

5.8 Summary: Useful Parameters and Knowledge Limits

Eq. (5-1) comprehensively delineates the numerous parameters influencing abutment scour, but it is unwieldy for developing a practicable design method. Moreover, some parameters are difficult to assess for many bridge sites. A simpler, though approximate, approach is to estimate scour depth in terms of a sub-set of parameters readily determined: i.e.,

$$ \text{(5-37)} $$

in which q_1 and q_2 are the section average values of unit discharge in the approach channel and through the bridge waterway (at the bridge centerline). The experiments carried out for the present Project worked mainly with these parameters.

The limits to the extent of knowledge about abutment scour can be summarized as follow:

1. The manner whereby so-called local scour and contraction scour actually combine. – The usual assumption for design purposes (e.g., Richardson and Davis, 1995, 2001; and Melville and Coleman, 2000) is that depths of local and contraction scour can be added linearly, at least for abutments in rectangular channels. For abutments in compound

channels, that assumption is open to debate because the flow field at the abutment is more complex than for rectangular channels. Several studies (Laursen 1960, Kouchakzadeh and Townsend 1997a, Melville and Coleman 2000, Benedict 2003), infer, but do not expressly state, the inherent combination of contraction and local scour at abutments. The method proposed by Chang and Davis (1998, 1999) directly assumes contraction and local scours to be inseparable;

2. How the geotechnical failure of the abutment's embankment affects scour dept and location – It is common (e.g., as illustrated in Figure 4-2) for scour developed at an abutment to cause the embankment slope to become unstable and fail. In many cases, the abutment column itself does not fail; rather the embankment breached immediately in a region behind the abutment;

3. The incomplete state of knowledge concerning the multiple factors influencing scour processes at abutments – The literature is unclear as to the influences on scour depth of embankment length and orientation. Moreover, the literature says little or nothing about the influence on scour depth of the geotechnical strength of embankment and floodplain soils;

4. The difficulties in characterizing some processes in a practical manner (e.g., convergence of flow at an abutment;

5. The role of large-scale turbulence structures generated by the flow at an abutment;

6. The absence of laboratory studies or field observations for Scour Condition C; and,

7. The lack of data on velocity fields near an abutment – Knowledge about the velocity field is needed in order to apply an erosion relationship. In this regard, lingering basic questions concern the flow concentration around abutments, and the generation of large-scale turbulence as flow passes around an abutment.

Table 5-1. Commonly used sources of laboratory data for abutment scour conditions

Abutment scour condition	Reference (partially grouped in terms of hydraulics lab – several studies reflecting a concerted study effort)
A	Nanyang University, Singapore: Yu and Lim (2002) --- HR Wallingford, UK: Cardoso and Bettess (1999)
B (in a compound channel)	Georgia Tech University, USA: Sturm and Janjua (1993, 1994); Sturm and Sadiq (1996); Sturm and Chrisochoides (1997, 1998a, 1998b); Sturm (1998) --- HR Wallingford, UK: Cardoso and Bettess (1999) --- University of Ottawa, Canada: Kouchakdeh and Townsend (1997a, b, 1998)
B (in a rectangular channel)	Karaki (1959), Liu et al. (1961), Garde et al. (1961), Laursen (1960, 1963), Sastry (1962), Dietz (1969), Gill (1970, 1972), Zaghloul (1983) Auckland University, New Zealand: Kwan (1988), Kandasamy (1995) Nanyang University, Singapore: Lim (1997)
C	None

Table 5-2. Relationships for estimation of contraction-scour depth

Reference	Equation with Standard Format	Notes
Laursen (1963)	$\dfrac{Y_2}{Y_1} = \left(\dfrac{Q_2}{Q_1}\right)^{6/7}\left(\dfrac{B_{1m}}{B_{2m}}\right)^{k1}\left(\dfrac{n_2}{n_1}\right)^{k2}$	For clear-water scour
Laursen (1960)	$\dfrac{Y_2}{Y_1} = \left(\dfrac{\tau_0'}{\tau_C}\right)^{3/7}\left(\dfrac{B_1}{B_2}\right)^{6/7}$	For live-bed scour

Table 5-3. Local abutment scour under clear-water condition

Reference	Equations	Notation/Notes
Lim (1997)	$\dfrac{d_{se}}{y_{mo}} = 0.9\left\{ \theta_c^{-0.375}\, F_{oe}^{-0.75}\left(\dfrac{d_{50}}{y_{mo}}\right)^{0.25}\left[0.9\left(\dfrac{L_e}{y_{mo}}\right)^{0.5}+1\right] - 2\right\}$	θ_c = critical Shields parameter, where $$\theta_c = \dfrac{u_{*c}^2}{\sqrt{(S-1)gd_{50}}}$$
Froehlich[*3] (1989)	$\dfrac{d_S}{Y_0} = 2.27 K_S' K_\beta'\left(\dfrac{L\sin\gamma}{Y_0}\right) F_{re}^{0.61}$	$F_{re} = V_e / \left(gY_0\right)^{0.5}$
Sturm and Janjua (1993)[*4]	$\dfrac{d_{Se}}{Y_{Fo}} = \varphi\left[\dfrac{F_{Fo}}{M} - 0.18\right]$	
Sturm and Janjua (1994)[*4] Sturm and Sadiq (1996)[*4]	$\dfrac{d_{Se}}{Y_{Fo}} = 7.70\left[\dfrac{F_{Fo}}{MF_C} - 0.35\right]$	
Sturm and Sadiq (1996)[*4], Sturm (1998)[*4]	$\dfrac{d_{se}}{y_{fo}} = 8.14\left[\dfrac{q_{f1}}{Mq_{fc}} - 0.40\right]$	
Sturm (1998)[*4]	$\dfrac{d_{Se}}{Y_{Fo}} = \varphi\left(\dfrac{V_{max}}{V_C} - 1\right)$	

Kouchakza deh and Townsend (1997)	$\dfrac{d_{Se}}{Y_{Fo}} = 13.5\left(\dfrac{Q_w}{Q_a}\right)^{3.9} F_{Fo}^{1.17} F_c^{-0.25}$	F_{Fo} = approach Froude number on floodplain.(Experi mental data were adjusted for time and shape factor)
Gill (1972)	$d_{sl} = y_{m1}\left[8.375\left(\dfrac{d_{50}}{y_{m1}}\right)^{0.25} \beta^{\frac{6}{7}}\left(\dfrac{\tau_1}{\tau_C}\right)^{\frac{3}{7}} - 1\right]$	$\beta = \dfrac{B_m}{B_m + L}$
Laursen (1963)	$d_{sl} \approx 1.89L\left(\dfrac{y_{mo}}{L}\right)^{0.5}$	Abutment encroaching into the main channel
Liu et al. (1961)	$\dfrac{d_S}{Y_0} = 1.1\left(\dfrac{L}{Y_0}\right) F_r^{0.22}$	

Note:
*3 Additional explanations for Froehlich's Equation

Factor	Symbol	Method of Estimation	
Shape	K_S	Vertical-wall abutment	1.00
		Vertical-wall abutment with wing walls	0.82
		Spill-through abutment	0.55
Alignment	K_γ	$K_\gamma = \left(\dfrac{\gamma}{90}\right)^{0.13}$	

*4, All these empirical equations were fitted to data obtained with limited time duration, and therefore, equilibrium conditions were unlikely reached

Table 5-4. *K* factor in Eqs. (5-11), (5-12), (5-13), and (5-14)

Factor	Symbol	Method of Estimation						
Depth size	K_{yL}	$K_{yL} = 2L \qquad\qquad L/Y_0 < 1$ $K_{yL} = 2\,Y_0 L^{0.5} \qquad 1 < L/Y_0 < 25$ $K_{yL} = 10 Y_0 \qquad\qquad L/Y_0 > 25$						
Flow intensity	K_I	$K_I = \dfrac{V-(V_a-V_c)}{V_c} \qquad \dfrac{V-(V_a-V_c)}{V_c} < 1$ $K_I = 1.0 \qquad\qquad\qquad \dfrac{V-(V_a-V_c)}{V_c} \geq 1$						
Sediment size	K_d	$K_d = 0.57 \log\left(2.24\dfrac{L}{d_{50}}\right) \qquad \dfrac{L}{d_{50}} \leq 25$ $K_d = 1.0 \qquad\qquad\qquad \dfrac{L}{d_{50}} > 25$						
Shape (shorter abutment)	K_S	Vertical-wall				1.00		
		Wing-wall				0.75		
		Spill-through - 0.5:1.0 (H:V)				0.60		
		Spill-through - 1.0:1.0 (H:V)				0.50		
		Spill-through - 1.5:1.0 (H:V)				0.45		
Adjusted shape (for longer abutment)	K_S^*	$K_S^* = K_S \qquad\qquad\qquad\qquad\qquad L/Y_0 \leq 10$ $K_S^* = K_S + 0.667\left[1-K_S\right]\left(0.1\dfrac{L}{Y_0}-1\right) \quad 10 < L/Y_0 < 25$ $K_S^* = 1.0 \qquad\qquad\qquad\qquad\qquad L/Y_0 \geq 25$						
Alignment (longer)	K_β	β	30°	45°	60°	90°	120°	135°	150°
		K_β	0.90	0.95	0.98	1.0	1.05	1.07	1.08
Channel geometry	K_G	$K_G = 1.0$				Scour condition B		
		$K_G = \sqrt{1-\left(\dfrac{B_f}{L}\right)\left[1-\left(\dfrac{Y_F}{Y_1}\right)\left(\dfrac{n}{n_f}\right)\right]}$				Scour condition A when $L/B_f \gtrless 1$		

Table 5-4. Continued

Adjusted alignment (shorter)	$K_\gamma{}^*$	$K_\gamma^* = K_\gamma$ $\qquad\qquad\qquad\qquad\qquad L/Y_0 \geq 3$ $K_\gamma^* = K_\gamma + \left(1 - K_\gamma\right)\left(1.5 - 0.5\dfrac{L}{Y_0}\right) \qquad 1 < L/Y_0 < 3$ $K_\gamma^* = 1.0 \qquad\qquad\qquad\qquad\qquad L/Y_0 \leq 1$
Time	K_t	$K_t = 1.0$ (time factor relation not presently defined yet)

Source: Melville, B.W. and Coleman, S.E. (2000). *Bridge Scour*, Water Resources Publications.

Table 5-5. Summary of data ranges produced from prior flume experiments for Scour Conditions A, and B

Reference	Scour Condition	B_m (m)	B_f (m)	B_f/B_m	H_{fp} (mm)	y_{fo} (mm)	y_{mo} (mm)	α	L (m)	Type	d_{50} (mm)	σ_g	Time (hrs)	No. of Tests
Sturm & Janjua (1993,1994)	2	0.300	2.49	8.3	210	51	261	90°	0.58	VW	3.3	1.20	10~12	29
		0.200	2.59	13		76	286		1.14					8
						102	312		1.55					
Sturm & Sadiq (1996); Sturm & Chrisochoides	2	0.270	0.93	3.4	152.4	20~59	172.4~211.4	90°	0.152 / 0.305 / 0.457	VW	3.3	1.20	12~16	31
Sturm and Chrisochoides (1997, 1998a, 1998b); Sturm	2	0.550	3.66	6.7	150	NA	NA	21°	0.80 / 1.60 / 2.40 / 3.22	ST (2H:1V)	3.3 / 2.7 / 1.2	1.30	24~36	NA
Yu & Lim (2002)	1	0.600	1.00	1.67	0.15	NA	NA	90°	1	VW	0.93	1.17	7~21 days	NA
Kouchakzadeh & Townsend (1997)	2	0.406	0.381	0.94	104	38 / 28.5~42	142 / 132.5~146	63° (1H:2V)	0.09 / 0.15 / 0.21	WW* / VW / ST*	0.7 / 0.5	1.16 / 1.13	5** / 5**	12 / 12
Cardoso & Bettess (1999)	1 & 2	1.640	0.80	0.49	0.08	31~88	111 ~168	45°	0.147~0.80	VW	0.835	1.26	56~142	14

Note:
*   The side slope of the wing-wall and the spill-through abutments is 1H:1.175V.
** Scour depth was artificially adjusted to equilibrium.
NA: Not available

Figure 5-1. Variables influencing scour at abutments

Figure 5-2. Definition sketch for a long contraction for live-bed scour experiments (Laursen 1960)
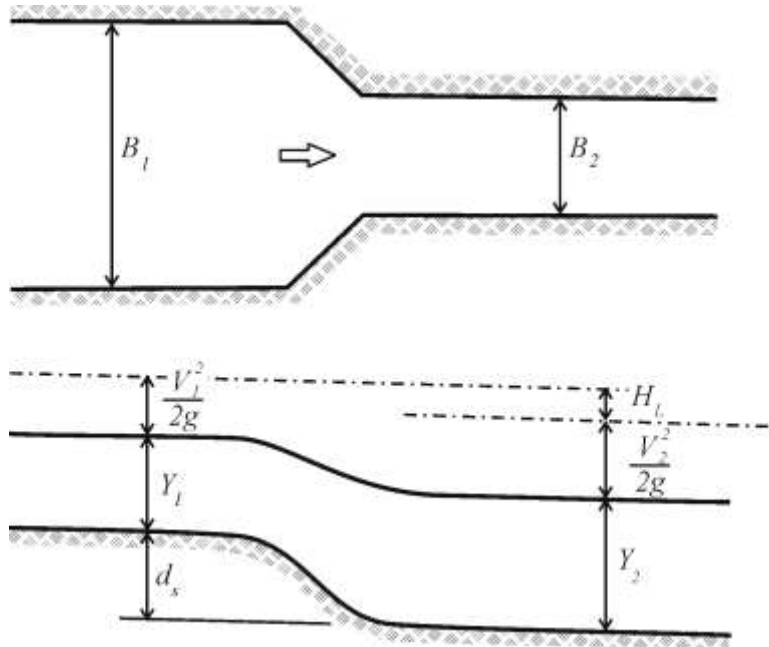
Figure 5-3. Definition sketch for long contraction for the clear-water scour experiment (Laursen 1963)
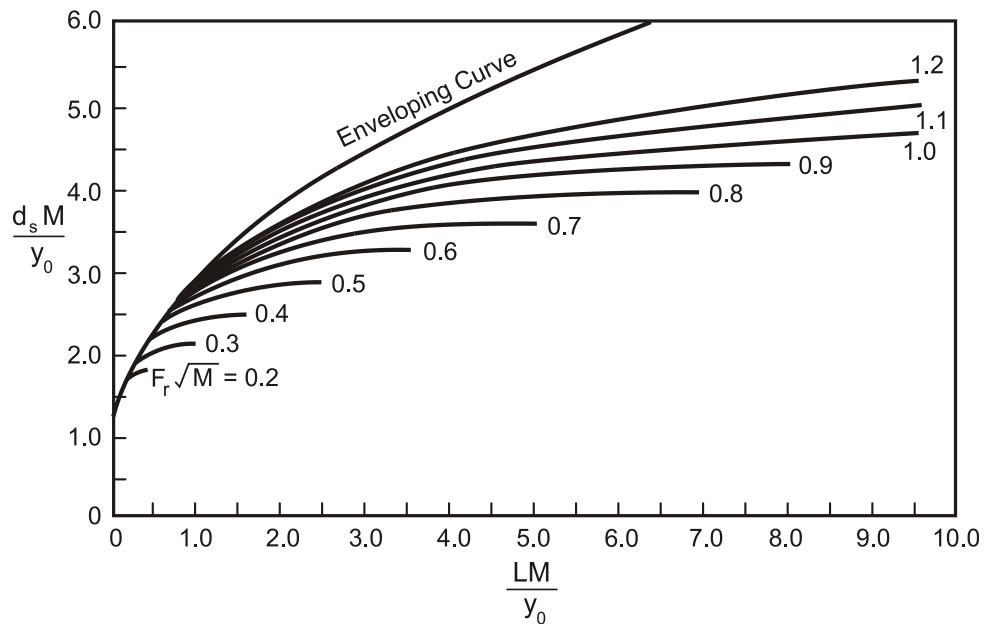
Figure 5-4. Field's graphical adaptation of flume data published by Liu et al. (1961). Note that $M = (B_m + 2B_f)/B_m$ (Field 1971).
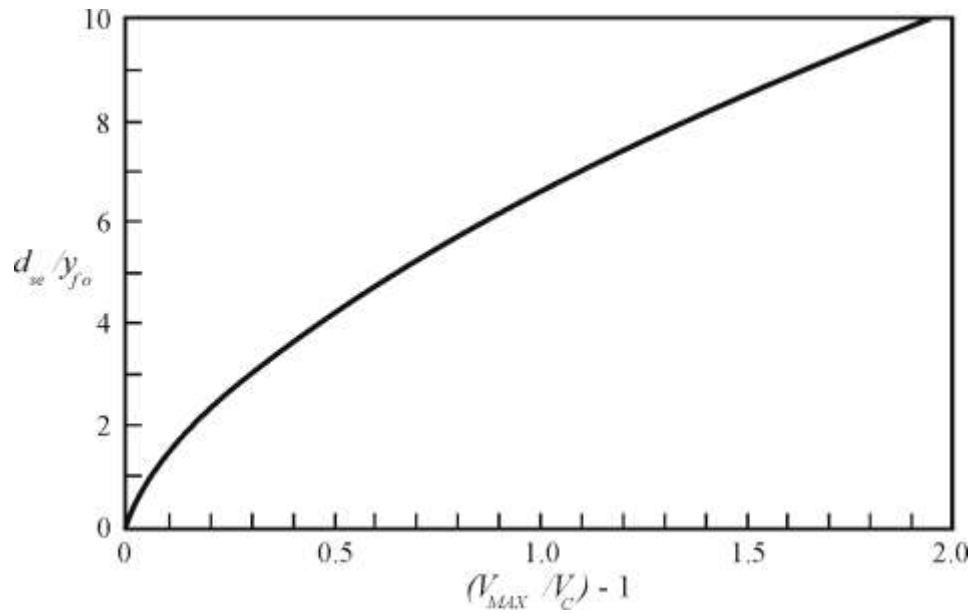
Figure 5-5. Equilibrium scour depth (Scour Condition A) as a function of local flow variables (figure taken without data from Sturm 1998)
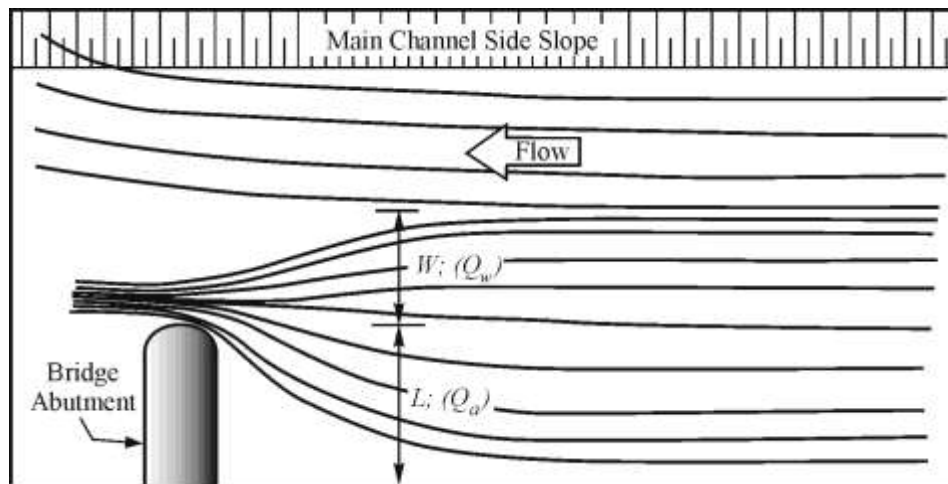
Figure 5-6. Surface flow pattern in floodplain; figure illustrates the definition of Q_a and Q_w (Kouchakzadeh and Townsend 1997a). The flow pattern corresponds to presence of a scour hole, not depicted in the figure.
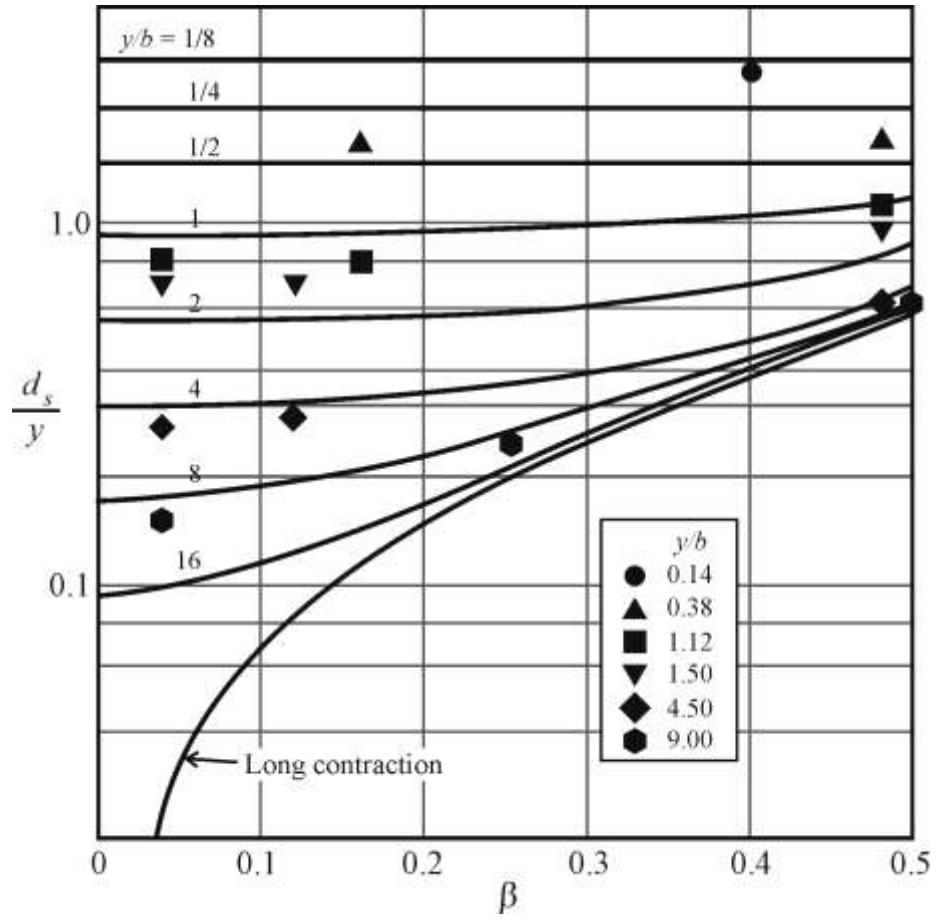
Figure 5-7. Depth of scour around multiple cylinders (Laursen and Toch 1956)

CHAPTER 6

EXPERIMENTS

6.1 Introduction

This chapter describes the program of laboratory experiments, laboratory facilities, model layouts, model bed materials, instrumentation, procedures, and test matrices of variables, associated with the laboratory experiments completed for the Project. The experiments were performed in two flumes located at IIHR – Hydroscience & Engineering (IIHR), the University of Iowa.

Also described here is the program of numerical experiments conducted with a numerical model of depth-averaged flow around abutments. These experiments were aimed at obtaining insight into abutment flow fields, and especially to address the important fundamental question as to how the flow distribution parameter q_{MAX}/q_2 (i.e., m) varied with the abutment length parameter, L/B_f.

6.2 Program of Laboratory Experiments

The Project's program of experiments entailed five groups of laboratory experiments.

1. **Scour at an abutment located in a compound channel (Scour Conditions A and B)**. The major part of the Project's experiments focused on scour at a single abutment in a straight channel comprising a main channel and a floodplain. The findings of these experiments are reported in Chapters 7 and 8;

2. **Scour at an abutment set back on the erodible floodplain of a compound channel, or located in a rectangular channel, subject to clear-water scour (Scour Condition B).** A substantial part of the Project's experiments focused on scour at a single abutment set well back on the floodplain of a compound channel, and subject to clear-water flow (i.e., no approach-flow transport of bed sediment), or in a rectangular channel subject to clear-water flow. The findings of these experiments are reported in Chapter 9;

3. **Scour at an exposed abutment column (Scour Condition C)**. Field experience shows that scour development commonly results in a failure of an abutment's earthfill embankment, often causing the embankment to be breached and fully exposing the abutment column founded in an erodible floodplain. Accordingly, it is of interest to ascertain the scour depths at exposed standard designs of the abutment column. Chapter 10 reports the findings of these experiments;

4. **Scour at an abutment with an adjacent pier (Scour Conditions A and B with a pier in close proximity)**. Because a pier often is located comparatively close to an abutment, it was necessary to complete a series of experiments aimed at determining how pier proximity affects abutment scour location and depth. Also, of interest was the influence of abutment proximity on scour depth at an adjacent pier. Chapter 11 reports the findings; and,

5. **Uncertainties associated with length-scale effects in scour experiments**. Because existing scour-prediction methods (based almost entirely on flume experiments) tend to over-estimate scour depths, a brief series of experiments were conducted to examine the effects of length scale on the relative magnitude of scour depths obtained from laboratory flume experiments. Appendix C presents an extensive discussion of the findings.

The experiments investigating Scour Conditions A and B were conducted using a flume replicating a channel of fixed overall width. Of focal interest was abutment scour development subject to variations of the following parameters identified in Eq. (5-1):

$$\frac{L}{B_f}, \frac{B_f}{0.5B}, K_S, \frac{u_{*c}}{u_{*fc}}, \beta, and \frac{L_p}{Y_f}$$

The first two parameters express relative lengths of abutment embankment, floodplain, and overall channel width, as defined in Figure 2-2. The third parameter characterizes abutment shape, the fourth differentiates the relative erodibility of main channel and floodplain, and the fifth defines abutment alignment relative to approach flow. The relative distance from abutment

toe to an adjacent pier is expressed by the sixth parameter. Approach flow depths in the main channel and on the floodplain were held constant for the experiments.

The findings from the program of experiments are analyzed so as to produce the design guide introduced in Chapter 12.

6.3 Abutments on Floodplains of Variable Resistance to Erosion

Series of experiments were conducted with simulated spill-through and wing-wall abutments at the end of an embankment located in compound channel whose floodplain had variable resistance to erosion: floodplains substantially resistant to significant erosion (e.g., a vegetated floodplain formed of a cohesive soil), and floodplains equally prone to erosion as the main channels (e.g., un-vegetated floodplains formed of the same alluvium as bounds the bed of the main channel).

As part of the overall effort to determine how abutment scour develops, and to obtain laboratory data on scour depths, the experiments had the following specific objectives:

1. For the two principal abutment forms (spill-through and wing-wall), determine how an abutment's embankment length influences scour depth, for a range of floodplain widths and erosion resistivity; and,

2. Determine how scour depth and location are affected by the erodible conditions of main-channel bed and floodplain.

6.3.1 Model Channel
The experiments were conducted using a model channel fitted in a sediment-recirculating flume, 21.3-m long, 4.0-m wide, and 1.0-m deep. The flume, shown in Figure 6-1, was designed and built specifically for the Project, and accommodated the half width of a compound channel; i.e., the flume's width = 0.5B, where B is the entire width of the compound channel. Figure 6-2 is a cross-sectional view of the half channel. The width of the floodplain was adjustable, and the floodplain surface could be fixed or erodible. The main channel had a bed of uniform medium

sand. As the slope of the flume itself was fixed at zero, the hydraulic gradient of the flow was controlled by the difference in water surface elevations between the head box and the tail box; given the flume's relatively short length compared to flume width and depth, the difference in elevation did not adversely affect the flow field locally around the abutment. One wall of the flume was fitted with glass walls at the model abutment section to aid viewing of the flow and scour-process visualizations, as indicated by Section A-A in Figure 6-1.

The variable erodible natures of floodplain and embankment at bridge sites were simulated by means of tests with the model channel configured in the following arrangements that bracket the variable erodibility of floodplain and embankment:

1. Fixed floodplain and the embankment, both taken to be practically resistant to erosion, whereas the main-channel bed was erodible. This arrangement was used only when studying Scour Condition A;

2. Erodible floodplain and main channel bed (the two being formed of the same noncohesive sediment and equally erodible), with the embankment being erodible but armored with riprap stone; and,

3. Erodible floodplain and main-channel bed, with the embankment unarmored. The abutment was formed of the same noncohesive sediment as the main-channel bed.

These states of floodplain and embankment erodibility led to the three primary conditions of abutment scour explained in Chapter 4.

The main channel bed was formed from medium, uniform-sized sand whose size frequency curve is shown in Figure 6-3. The median diameter, d_{50}, was 0.45 mm and the geometric standard deviation, σ_g, was 1.4. The specific gravity of the sand was 2.65.

The channel's floodplain was formed from plywood roughened by a coating of the sand used for the main-channel bed. For the experiments simulating abutments on an erodible floodplain, the model abutments were placed in a recess area containing the same sand. The experiments were conducted for three different floodplain lengths relative to the main channel's half width, i.e.,

$B_f/(0.5B)$ = 0.23, 0.43, and 0.63. The commensurate half width of the main-channel bed relative to half-channel width, $B_B/(0.5B)$ = 0.70, 0.50, and 0.30; as indicated in Figure 6-2.

To prevent excessive bed scouring at the entrance of the main channel, and to reduce non-uniformity in velocity distributions immediately downstream from the head box, concrete baffle-blocks were installed. Furthermore, a perforated plate, with 50-percent opening, was installed at the outlet of the head box to control flow velocity over the floodplain. A trial-and-error procedure was employed to produce the required velocity distributions for the floodplain and the main channel. A sand trap was placed at the upstream end of the floodplain and the downstream end of the flume to avoid excessive sediment accumulation on the simulated floodplain.

6.3.2 Model Abutments

Abutments usually comprise a concrete support wall founded on a pile cap supported by piles or on a spread footing, and adjoin an earthfill approach embankment. Pile supports are more common than are footing supports, unless the abutment is founded directly on rock. Spill-through abutments are formed around a "standard-stub abutment," which comprises a concrete stub supported by a pile cap on two rows of circular piles. The elevation of the pile cap and the detailed arrangement of piles may vary from bridge site to bridge site. At some sites, the pile cap is located at, or near, the top elevation of the floodplain, whereas at other sites the piles extend upward through the embankment earthfill. In this latter case, the piles directly support a cross beam, which in turn supports the beams of the bridge deck. The model spill-through abutments were constructed around the same standard-stub abutment structure, shown in Figure 6-4, which shows the design and dimensions of a standard-stub abutment commonly used by the Illinois, Iowa, and New York Departments of Transportation (DOTs).

Wing-wall abutments usually have similar foundation layouts as the standard-stub abutments, except that they include wing-walls extending from the central stub. The embankment geometry for the tests with the wing-wall abutments is shown in Figure 6-5; the design and dimensions shown therein are those commonly used by the Illinois, Iowa, and New York DOTs.

The following prototype considerations and dimensions were used in selecting the model layout, length scale, and dimensions for both types of abutments:

- A road width of 40ft (12.0m) (, in accordance with standard prototype two-lane roads. The road width includes 24ft (7.22m) plus 8ft (2.7m) -wide shoulders, a total width of 40 ft (12.0m);

- Pile spacing of 6.6ft to 9.8ft (2m to 3m);

- Pile diameter of 1ft (0.3m);

- The base of the pile cap submerged approximately 3.3ft (1.0m) below the original level of the floodplain bed;

- A 2-horizontal:1-vertical (2H:1V) constructed side slope of the earthfill embankment connected to the abutment; and,

- A 2H:1V slope of the bank between the floodplain and the main channel

Considerations of the flume's size led to selection of a geometrically undistorted length scale of 1:30 for the experiments. A view of the model standard-stub abutment is given in Figure 6-6, while Figure 6-7 gives the corresponding view of the model wing-wall abutment.

The model wing-wall abutments had the following additional features:

- They extended from a center body of streamwise width identical to the stub abutment;

- They were set at an angle of 45 degrees;

- They met the bottom end of the spill-through abutment slope; and,

- A sub-set of tests was done with a wing-wall abutment supported by sheet piles.

Figures 6-8 and 6-9 show model layouts of the spill-through abutment and the wing-wall abutment for $B_f/(0.5B) = 0.43$ and $B_B/(0.5B) = 0.50$. Here, $L/B_f = 1.00$ for a spill-through abutment, and $L/B_f = 1.18$ for a wing-wall abutment.

The riprap armor layer placed on the model abutment comprised rough-edged, irregularly-shaped stone having an equivalent median diameter of 6.6 mm and a specific gravity of 2.65. The stone was placed as a single layer over the full-length of each model embankment.

The model test section was prepared in three different states for a spill-through abutment and a wing-wall abutment as follows:

1. **Fixed embankment and fixed floodplain** -- the floodplain and the embankment were fixed; thereby, assuming the embankment and the floodplain to be far less erodible than the bed sediment in the main channel, as shown in Figures 6-10a-b;

2. **Riprap-protected embankment and erodible floodplain** -- the floodplain and the embankment were erodible, but the embankment was protected with a layer of riprap, as shown in Figures 6-11a-b. The experiment with a rectangular channel was also included in this state, as shown in Figures 6-12a-b. Also two types of wing-wall abutment were employed; and,

3. **Erodible embankment** -- the floodplain and the embankment were both erodible and unprotected, as shown in Figures 6-13a-b.

6.3.3 Flow Conditions

The flow conditions for the experiments were selected so that a live-bed flow condition prevailed in the main channel and a clear-water flow condition occurred on the floodplain. The main variable adjusted during the experiments was floodplain width, and thereby, main-channel width.

Approach flow depths were kept constant throughout the experiments. The approach flow depth was 0.30 m in the main channel, and 0.15 m on the floodplain, as depicted in Figures 6-8 and 6-9. This relative magnitude of floodplain flow depth to main-channel flow depth enabled the experiments to replicate a suitably broad range of extents whereby an abutment contracts flow through a bridge waterway. For each experiment, the main-channel bed was kept in a dune-bed

mode. The flow depth in the main channel was taken relative to the bed's average (or level-bed) elevation.

Accurate simulation of a flow by means of a hydraulic model required that certain dimensionless parameters describing the geometric and dynamic properties of the flow assume equal values in the model and at full scale. This requirement usually is not fully achieved, because of natural limitations in fluid properties and the smaller size of non-cohesive sediment. Consequently, judicious compromises need to be made in order that the dominant processes are replicated in the model. As described in Section 5.3, the basic similitude requirements for modeling free-surface flow and sediment-transport processes in an alluvial channel lead to the following similitude criteria:

1. Dynamic similitude is based on the flow intensity parameter u_*/u_{*c} ; and,

2. Undistorted geometric similitude based on length scale governed by flume size and abutment width.

Appendices B elaborate how this common pair of criteria results in an under-scaling of the vorticity associated with turbulence structures generated by flow passing around a model structure (abutment or pier) in a sand bed.

6.4 Scour at Abutments with an Adjacent Pier

Selected experiments with the single abutment were repeated with a pier located near the abutment. These experiments had the following specific objectives:

1. Determine how the distance between pier and abutment influences scour depth at the abutment and at the pier, for a range of floodplain widths and abutment shapes; and,

2. Determine how scour depth and location are affected by the erodible conditions of main-channel bed and floodplain.

These experiments were conducted using the same model channel and abutments, as well as flow conditions, described in Section 6.2.

6.4.1 Model Pier

The pier simulated a standard pier design used by the Iowa DOT. The pier, as shown in Figure 6-14, which gives the main features and dimensions of the pier, had a solid-wall column extending to the bridge deck. This common pier geometry was chosen because it would markedly affect the flow field and thereby scour more than would a pier comprising one, or two, circular columns. Note that the top of the pier's pile cap was located at the average level of the main-channel bed.

With the pier positioned relative to the abutment in the manner shown in Figure 6-15, the experiments entailed varying the distance between the pier and the abutment, L_p, for selected abutment length, L, on a floodplain length relative to half width of channel, $B_f/(0.5B)$. Two states of abutment and floodplain resistance to erosion were used: fixed floodplain and abutment; and, erodible floodplain with riprap-protected embankment. Figures 6-16a-b depicts the two states of model floodplain with a spill-through abutment and an adjacent pier. An additional test was conducted for which the embankment was not protected with riprap.

The duration of the experiments was selected so as to ensure that an equilibrium bed condition was attained. Based on scour's temporal progress, as measured by way of the ADV and viewed through the observation windows, the time to reach the equilibrium condition was determined for each test condition. The time was longer than 24 hours for abutments on the fixed or erodible floodplains, but not much longer than about 4 hours for the unprotected embankments on erodible floodplains.

Table 6-1 summarizes the ranges of variables for the experiments conducted in the present study. Recall that only one side of the compound channel was simulated in the study. It was assumed that the entire flow is a mirror image of the half width flume.

6.5 Scour at Exposed Abutment Columns

This brief series of experiments examined scour depths at standard stub and wing-wall abutment columns fully exposed following erosion and breaching of an earthfill embankment. Scour at an exposed abutment is similar to scour at a pier subject to local scour. Because no prior study has investigated scour at an exposed abutment, the present experiments investigated the following influences on scour depth at exposed standard-stub and wing-wall abutments:

1. Flow intensity, u_*/u_{*c}; and,

2. Abutment-column alignment, β.

Two laboratory flumes were used for these experiments, so that they could be conducted in parallel with the experiments focused on abutment scour.

6.5.1 Model Channel

IIHR's flow-recirculating flume, 21m long, 3.3m wide, and 2.3m deep, was used as the model channel for these experiments. The layout and principal dimensions of the flume and the experiment set-up in it are shown in Figure 6-17. A view of the model in the flume is given by Figure 6-18. The flume was fitted with an elevated fixed-bed approach section upstream of a 1-m deep, 4.8-m long, sand-bed test section, a sediment trap downstream, and a tailgate to control water-surface elevations. The flow depth was set at 0.53 m. The approach flow was calibrated using roughness elements so that approach-flow velocity profile conformed to that for a fully developed turbulent flow.

6.5.2 Model Abutment Structures

The abutment structures were the same as depicted in Figures 6-4 and 6-5, except that the column portion was lengthened to accommodate the greater flow depth (0.53 m) in the present flume. Figure 6-19 shows the experiment layout used for the wing-wall column. Essentially the same layout arrangement was used for the standard-stub column. The alignment of each column relative to the flow direction was varied from 0 to 90°.

6.6 Scale-Effect Experiments

Scour of a sediment bed around a bridge abutment involves a complex flow field marked by large-scale turbulence structures generated by flow around an abutment; notable structures include rollers and wake vortices. It is important to take into account the similitude considerations in the scaling of the frequency and vorticity of large-scale turbulence structures, notably the wake vortices, generated by the simplest of structures, a vertical circular cylinder. A consequence of inadequate scaling of large-scale turbulence is that flume experiments with model-scale abutments may produce larger values of equilibrium scour depth relative to abutment length or flow depth than are found at prototype-size abutments. This concern is explained by Ettema and Muste (2004), who studied scale effects on flow around laboratory models of spur-dikes and wing-dams; they used flat plates to simulate these structures.

To investigate the possible influence of vorticity similitude on scour depths obtained for the present experiments, a brief series of experiments was conducted using a set of circular cylinders, and the flume described in Section 6.4. The experiments entailed a simple scour case: clear-water scour at a uniform-diameter cylinder set in a planar bed of uniform sediment. These tests should reveal the same fundamental scale effect as exists for scour at structures of more complex geometry. The results of the experiments are reported in Appendices B.

The relaxation of some parameters in the scour experiments potentially causes the scour equations to be inaccurately scaled from laboratory to the field dimensions. Based on a simple similitude analysis of the scour problem (Chapter 5 and Appendices B), two parameters generally overlooked in the past studies have an important effect on the equilibrium scour depth. The parameters are Reynolds number-like and Froude number-like dimensionless parameters. Based on this hypothesis, in a simple experimental setup, series of cylinder put in the same flow condition, the net effect of two parameters on the equilibrium scour depth was shown. Further experiments showed that the frequency of vortex shedding and the vorticity field behind the cylinders has an important role in the turbulent scour process. Frequency of the vortex shedding was obtained from power spectrum plots of ADV velocity recordings in the wake, and vorticity field plots were obtained from large scale PIV application on the surface of the wake. Flow

visualization further showed the importance of the vortex structures in the scour process, which are caused by the vorticity flux fed by the turbulent boundary layer separation from the cylinders.

6.7 Instrumentation

Various instrumentation devices were used to measure flow velocities and patterns, as well as channel bathymetry and scour depth details during the experiments.

Water-surface elevations along the flume were measured using a series of piezometer taps spaced at 1.5-m intervals along the simulated floodplain. A vernier scale, with a resolution 0.3 mm, was used to determine water levels.

An Acoustic Doppler Velocimeter (ADV) was used to measure flow velocities and depths. This instrument is capable of measuring velocities ranging from 1 mm/s to 2.5 m/s, with a sampling rate and error up to 2 Hz and 1%, respectively.

Large-Scale Particle Image Velocimeter (LSPIV) was used to obtain two-dimensional flow patterns and velocities at the water surface around each model abutment. LSPIV is a non-intrusive technique using digital recordings of tracer-particle displacement. The software developed at IIHR enables the velocity field to be obtained from the displacements divided by the time difference of each video image. Additionally, the software facilitates adjustment of the oblique-angle video images taken with a digital video camera located above the flume. The camera used for this study had a resolution of 640x480 pixels. LSPIV images were taken at night, when the laboratory housing the flume could be darkened, and suitable lighting could be focused on the flow field around a test abutment. Figure 6-20 shows the overall arrangement used for obtaining the LSPIV images.

To determine how the flow-field evolved as scour developed, measurements of flow velocity and flow patterns were made at the pre-scour and the equilibrium condition. LSPIV measurements were made with the boundary conditions of the fixed embankment and floodplain and the riprap-protected embankment.

Bathymetry data at the scour region were taken after water was drained from the flume. These data were obtained in 0.2 m by 0.2 m grids in the far field, and in finer grids, 0.1 m by 0.1 m, around the model abutment, as depicted in Figure 6-21. The data were obtained using a point gauge whose measurement accuracy was 0.5 mm.

6.8 Numerical-Simulation Experiments

The laboratory tests described earlier in this chapter showed that magnitude and location of deepest scour, and flow depth, for Scour Conditions A and B correlate with the magnitude and location of q_{MAX} for each scour condition. To estimate the magnitude and location of q_{MAX}, and to relate q_{MAX} to the average unit discharge through the bridge waterway, q_2, require knowledge of the flow field through the bridge waterway. Although the laboratory tests produced values for q_{MAX} and q_{MAX}/q_2, the number of values obtained was quite limited, and the validity of the values required further evaluations.

A series of numerical-simulation experiments, employing a 2-dimensional, depth-averaged, model, FESWMS-2D, was used to provide further information regarding the flow field approach to, and around, the abutment and embankment configurations that were tested in the laboratory experiments. This information significantly aided understanding of the flow field and, thereby, diagnosis of scour processes at the test abutments. Commensurately, this information confirmed the flume trends obtained for the variation of q_{MAX}/q_2 with variations in abutment-embankment length and floodplain extent.

The extensive work completed with FESWMS-2D is fully documented in by Morales and Ettema (2010), a companion report to the present report. A depth-averaged numerical model of flow in open channels, FESWMS-2D, was configured to simulate the flow field around abutments in situations subject to Scour Conditions A and B. The following considerations were of particular interest:

1. The influence of abutment length and channel geometry (compound and rectangular) on flow field and scour;

2. How abutment length affects the flow distribution at a bridge waterway (distributions and information on unit discharge, depth-averaged velocity, vorticity and bed shear stress), information needed for design considerations; and,

3. The sources of uncertainty associated with the use of common numerical models like FESWMS. This effort will guide modelers in the selection of an optimum mesh size to adequately and accurately simulate flows using this computational tool.

6.8.1 FESWMS-2D

FESWMS-2D is a computer program developed for the Federal Highway Administration to model flows at bridge waterways, where complex hydraulic conditions limit the applicability of the traditional one-dimensional analysis. The program is capable of simulating two-dimensional, depth-averaged, steady and unsteady free-surface water flows in channels containing abutments.

6.8.2 Model Development

The process of developing a numerical model using FESWMS-2D for the present Project can be summarized as the following set of tasks:

1. Definition of geometry and boundary conditions;

2. Selection of Manning's flow-resistance coefficient, n, and eddy viscosity, V_t; and,

3. Selection of mesh type and size, and estimation of grid uncertainty.

The area of interest for flow around the test abutments is 16-m long and 4-m wide. However, the numerical model was set for longer dimensions. Froehlich (2002) recommends extending the boundaries further away from the areas where accurate solution is needed. Figure 6-22 shows the typical extent of the numerical model and grid used to simulate the flume experiments. The location and dimensions of the abutment, as well as bed elevations, were established in accordance with actual values recorded in each experiment. The boundary conditions are in accordance with the experimental settings.

A key concern in modeling is selection of roughness and eddy-viscosity variables. The ensuing discussion is intended to illustrate something of the concern. Hobbs (2005) performed a sensitivity analysis of FESWMS with regard to Manning's roughness coefficient, n, and eddy viscosity, V_t. Hobbs found that the FESWMS model is very sensitive to changes in these parameters, and n and V_t should be estimated accurately. Methods for determining Manning's coefficients are well established in the literature, e.g. Chow, 1959, Rice et al. 1998, and tested successfully in field and laboratory applications. Values of n and V_t in this study were determined using the ADV velocity measurements in the flume experiments.

Structured and unstructured meshes were used in preliminary runs before selecting the final grid design to be used in the simulations. Structured grids lead to a regular matrix of equations which can be solved faster than those obtained for unstructured grids. However, Ferziger and Peric (2002) state that unstructured grids are best adapted to finite-element methods because of their flexibility to fit any shape and because there is no limit in the number of neighbor elements or nodes. Preliminary tests for the present Project showed that unstructured meshes yielded the optimum running times with adequate level of accuracy. Accordingly, unstructured meshes were selected for use. Figure 6-22 illustrates a typical mesh used. Figure 6-23 is a detailed view of the mesh used for one abutment layout.

Table 6-1. Range of parameters in flume experiments; X indicates test conducted

$B_f/0.5B$	L/B_f	u_*/u_{*c} Main-Channel Bed	Fixed Floodplain	Erodible Floodplain, Riprap-Protected Embankment	Erodible Floodplain, Unprotected Embankment
			Spill-through Abutments		
1.00	0.69	0.90	-	X	-
	0.60	0.90	-	X	-
	0.51	0.90	-	X	-
	0.34	0.90	-	X	-
	0.24	0.90	-	X	-
	0.18	0.90	-	X	-
0.63	1.20	1.20	X	-	-
	1.10	1.20	X	-	-
	1.00	1.20	X	X	-
	0.75	1.20	X	X	-
	0.63	1.20	X	-	-
	0.50	1.20	X	X	-
	0.35	1.20	X	X	-
0.43	1.38	1.20	-	-	X
	1.00	1.20	X	X	X
	0.75	1.20	X	X	X
	0.63	1.20	X	X	-
	0.50	1.20	X	X	X
0.23	2.13	1.20	X	-	-
	1.49	1.20	X	-	-
	1.00	1.20	X	X	-

$B_f/0.5B$	L/B_f	u_*/u_{*c} Main-Channel Bed	Fixed Floodplain	Erodible Floodplain, Riprap-Protected Embankment	Erodible Floodplain, Unprotected Embankment
	0.75	1.20	X	X	-
	0.63	1.20	X	X	-
	0.50	1.20	X	-	-
	0.40	1.20	-	X	-
	0.30	1.20	-	X	-

Table 6-1 continued

Wing-wall Abutments					
$B_f/0.5B$	L/B_f	u_*/u_{*c} Main-Channel Bed	Fixed Floodplain	Erodible Floodplain, Riprap-Protected Embankment	Erodible Floodplain, Unprotected Embankment
1.00	0.67	0.90	-	X	-
	0.59	0.90	-	X	-
	0.42	0.90	-	X	-
	0.14	0.90	-	X	-
0.63	1.12	1.20	X	X	-
			X	X	-
0.43	1.18	1.20	X	X	X
	1.18	1.30	-	X	-
	1.18	1.40	-	X	-
0.23	1.33	1.20	X	X	-
$B_f/0.5B = 0$, with $B_m/B = 0.95$		1.20	X	X	

Note:

- When $B_f/0.5B = 0$, only the floodplain slope (2:1) extends into the main channel, exposing full wing-wall to the flow
- When $B_f/0.5B \leq 1.0$, and main channel flow set at $u_*/u_{*c} = 1.20$, floodplain flow at $u_*/u_{*c} = 0.90$

- When $B_f/0.5B = 0.63$, and main channel flow set at $u_*/u_{*c} = 1.30$, floodplain flow at $u_*/u_{*c} = 1.00$
- When $B_f/0.5B = 0.63$, and main channel flow set at $u_*/u_{*c} = 1.40$, floodplain flow at $u_*/u_{*c} = 1.05$
- Several runs were repeated, to assess repeatability
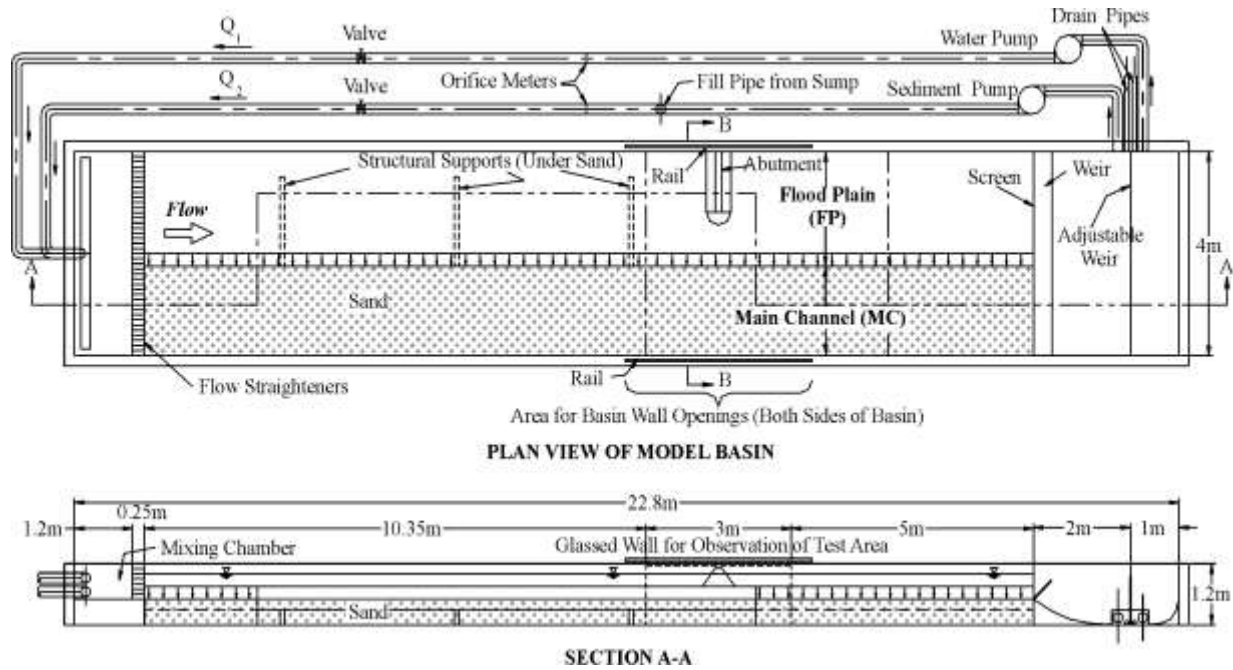
Figure 6-1. Plan and elevation of the compound open-channel flume used in the present investigations
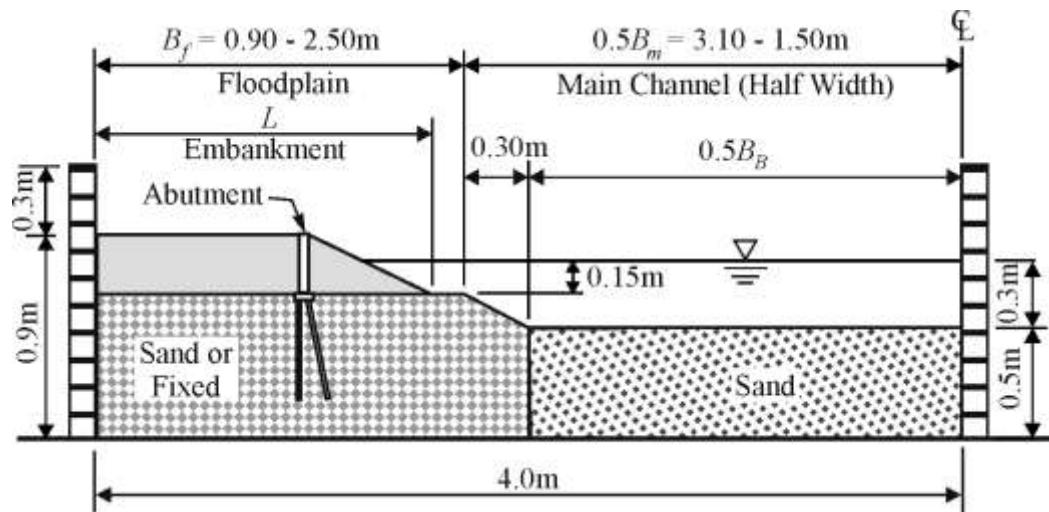
Figure 6-2. Cross section showing layout of experimental set up in the lab flume. Indicated are abutment and embankment length, floodplain width, and channel half width.
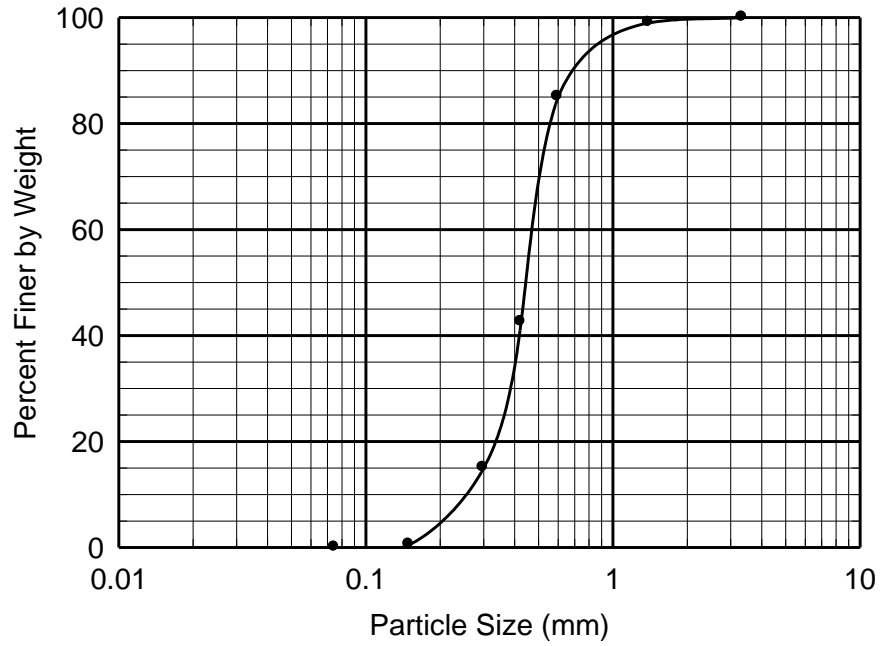
Figure 6-3. Particle size distribution of bed sand used in experiments in 4-m wide flume
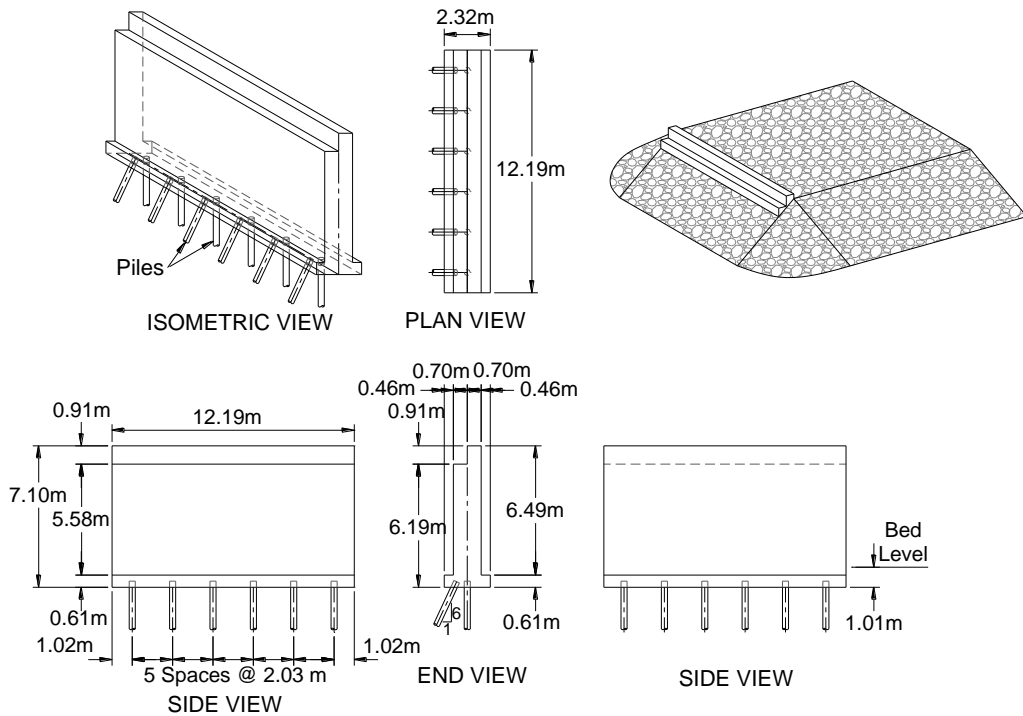
Figure 6-4. Prototype dimensions of a pile-supported standard-stub column for spill-through abutments. The model-scale dimensions are 1/30th of these dimensions.
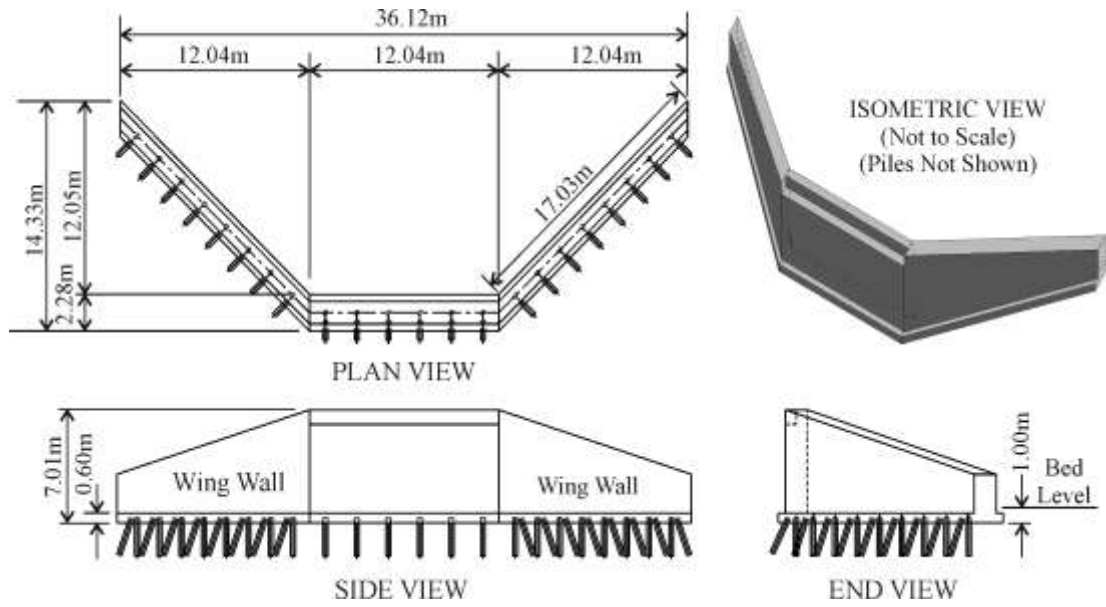
Figure 6-5. Prototype dimensions of a pile-supported wing-wall column for wing-wall abutments. The model-scale dimensions are $1/30^{th}$ of these dimensions.

Figure 6-6. Model standard-stub column (1:30 scale)

Figure 6-7. Model wing-wall column (1:30 scale)
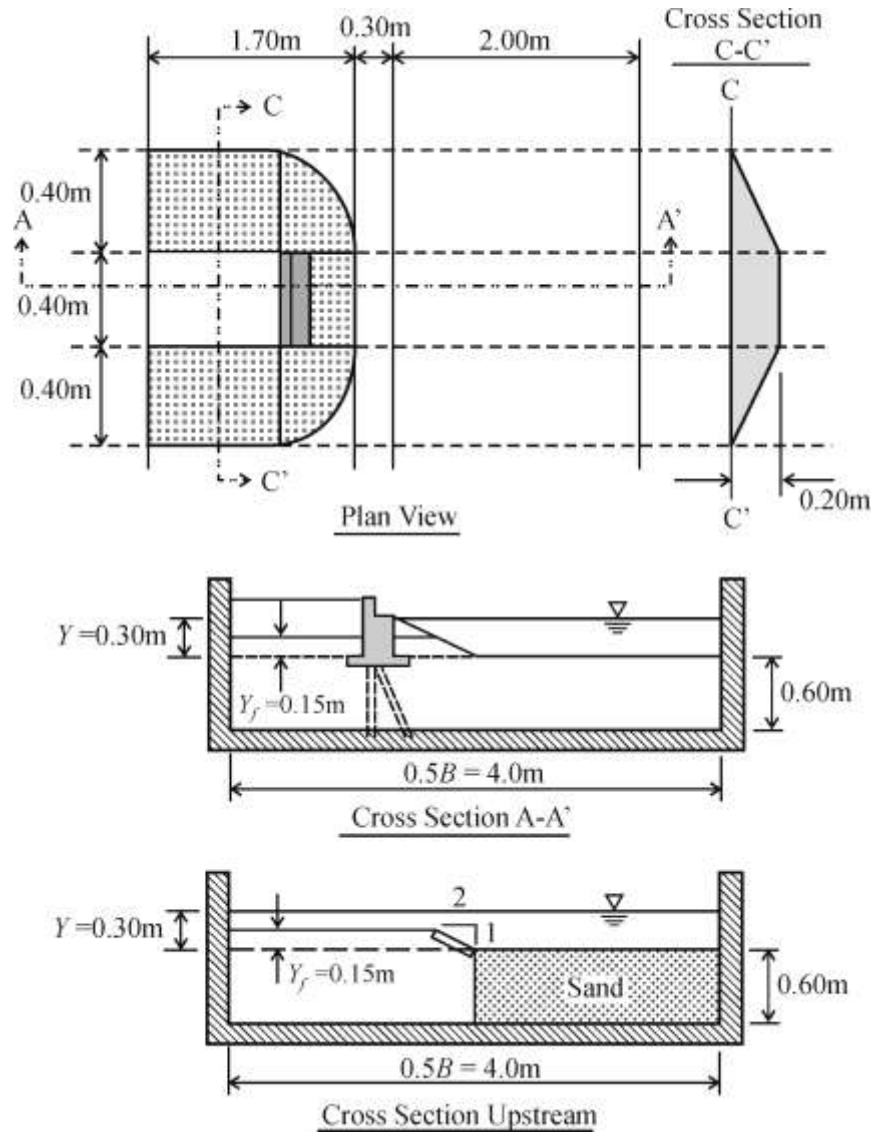
Figure 6-8. Model layout and dimensions of the spill-through abutment ($B_f/(0.5B)$ = 0.43 and L/B_f = 1.00)
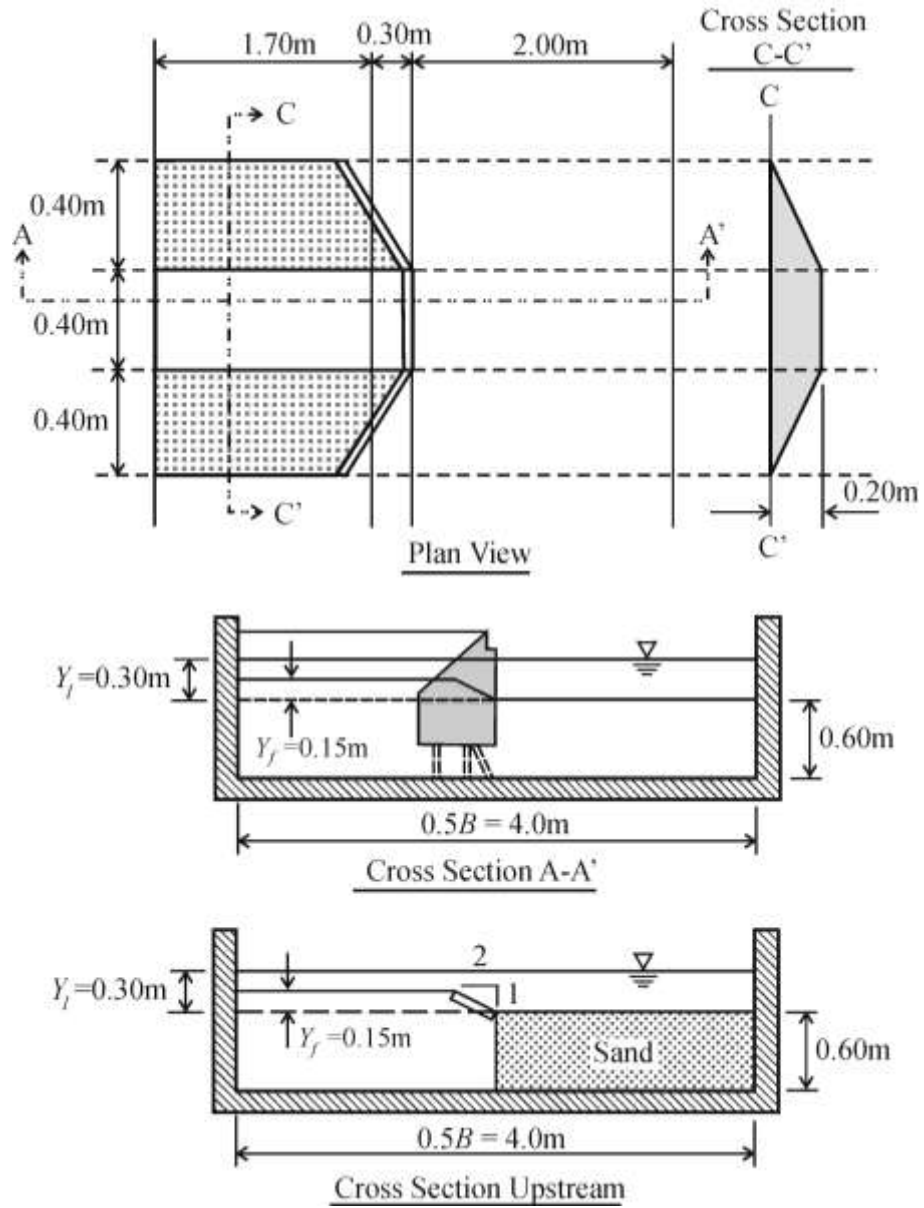
Figure 6-9. Model layout and dimensions of the wing-wall abutment
($B_f/(0.5B) = 0.43$ and $L/B_f = 1.18$)

Figure 6-10. Photos showing initial set up for experiments with fixed embankment over floodplain: (a) spill-through abutment, and (b) wing-wall abutment – dark lines are drawn to indicate the sloping bank.
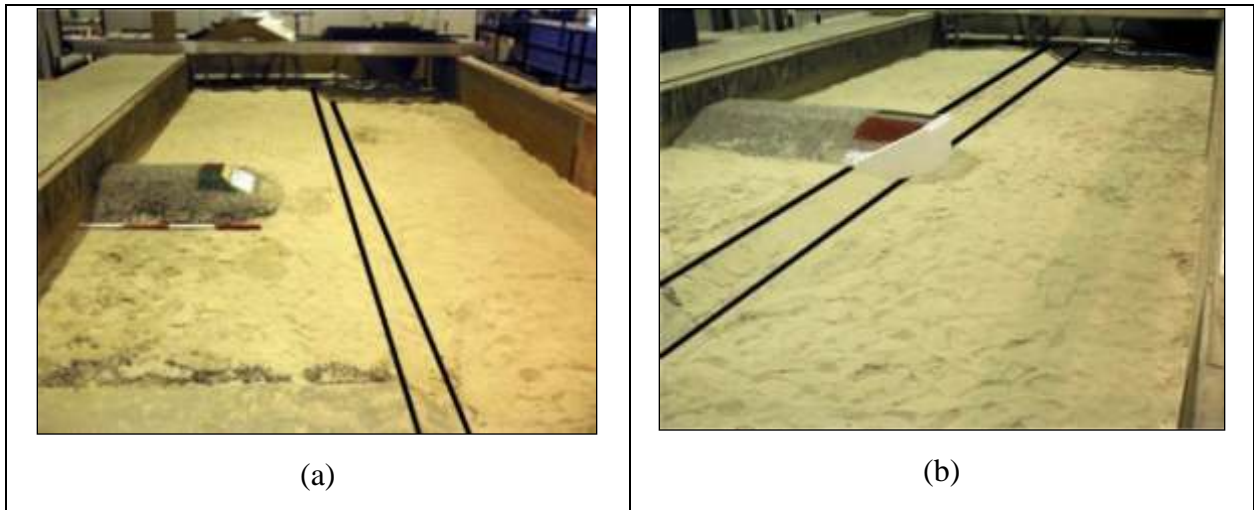
Figure 6-11. Photos showing initial set up for experiments with a riprap-protected embankment over floodplain in the compound channel: (a) spill-through abutment, and (b) wing-wall abutment – dark lines are drawn to indicate the sloping bank.
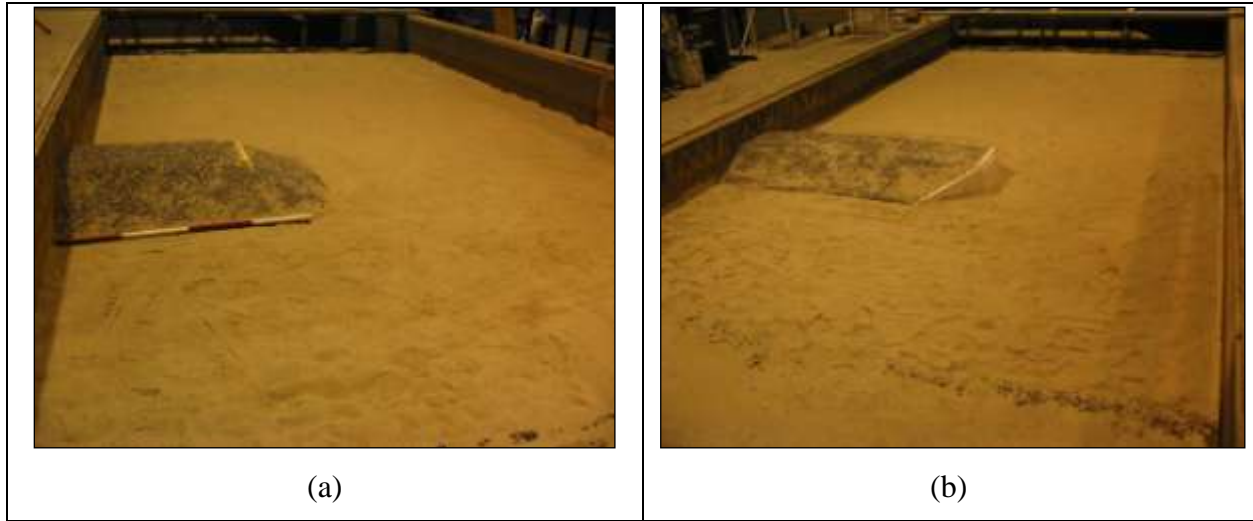
Figure 6-12. Photos showing initial set up for experiments with a riprap-protected embankment in the rectangular channel: (a) spill-through abutment, and (b) wing-wall abutment
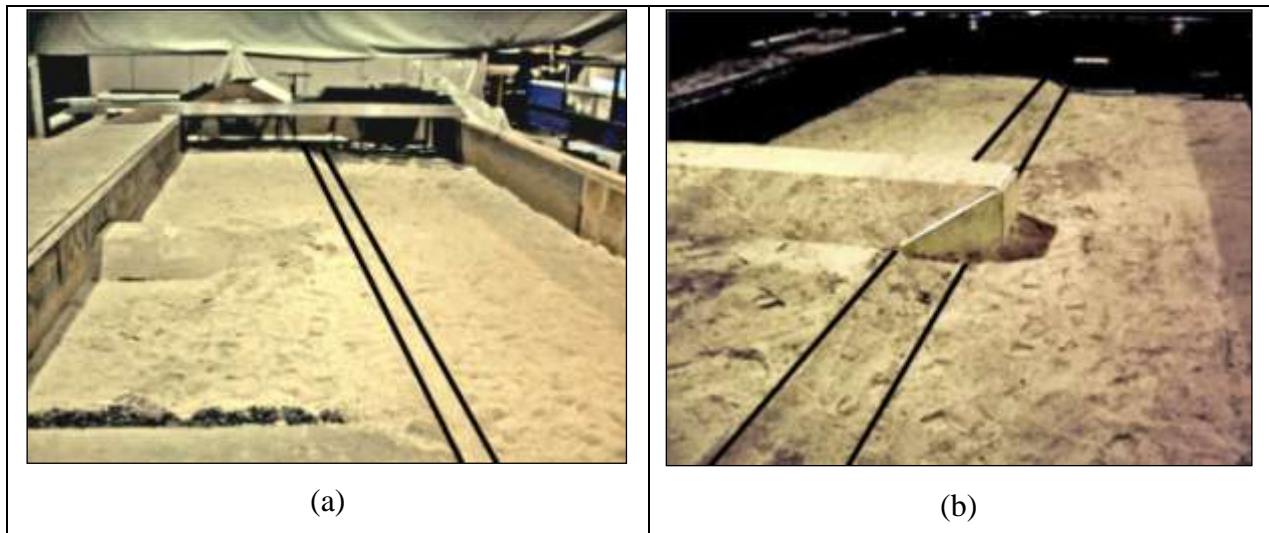
Figure 6-13. Photos showing initial set up for experiments with an unprotected embankment on an erodible floodplain: (a) spill-through abutment, and (b) wing-wall abutment – dark lines are drawn to indicate the sloping bank.
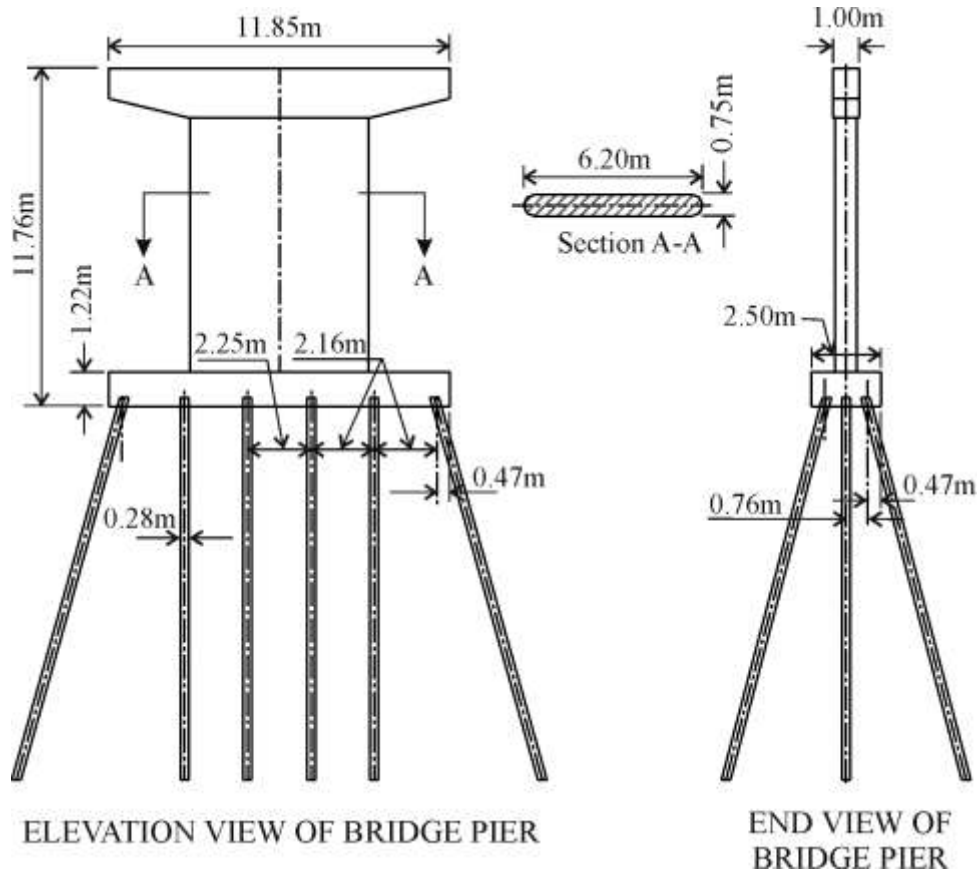
Figure 6-14. Prototype dimensions of the pile-supported pier used. The model-scale dimensions are $1/30^{th}$ of these dimensions.
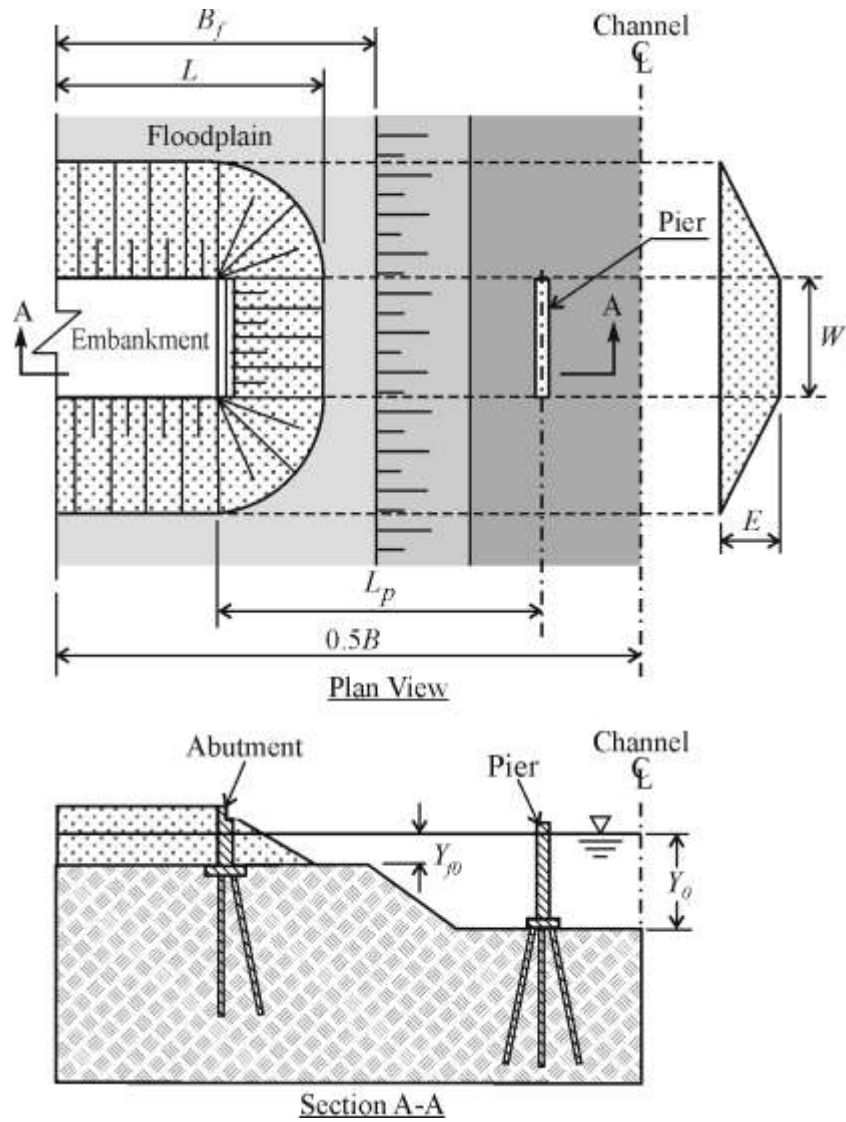
Figure 6-15. Model layout of pier adjacent to abutment

(a)   (b)

Figure 6-16. Initial set up for spill-through abutments with an adjacent pier: (a) fixed abutment and floodplain, and (b) erodible embankment and floodplain
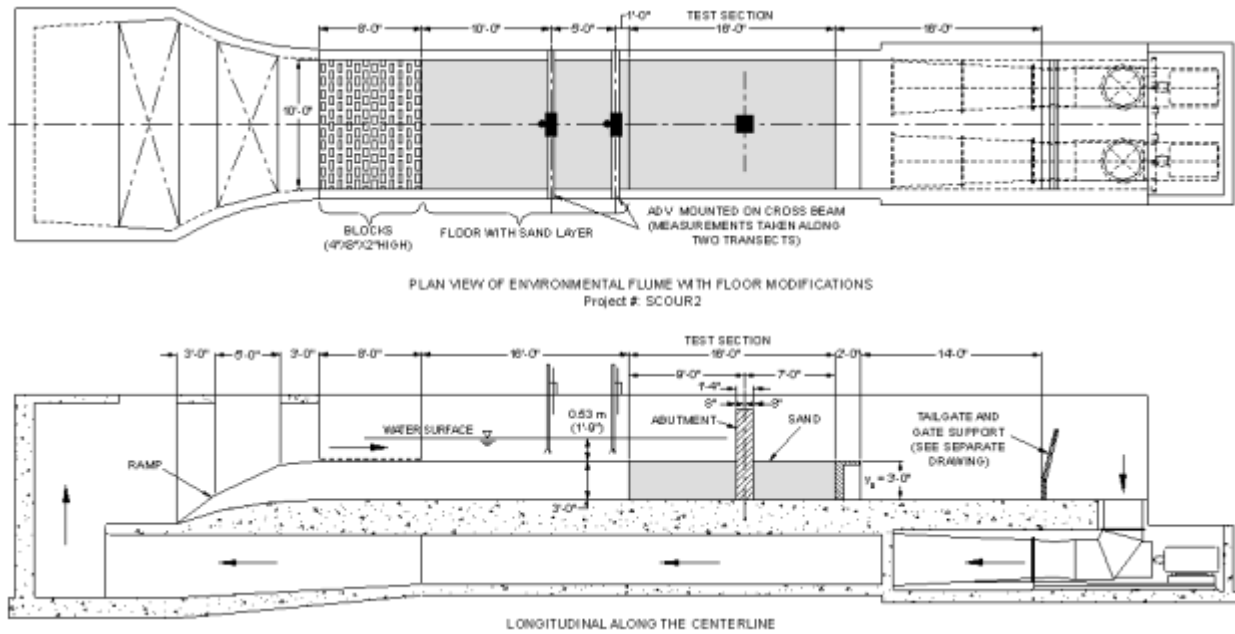
Figure 6-17. Layout and dimensions of flume used for experiments on exposed abutment columns, and for the scale-effect experiments

Figure 6-18. View of model of exposed wing-wall column in the flume shown in Figure 6-17
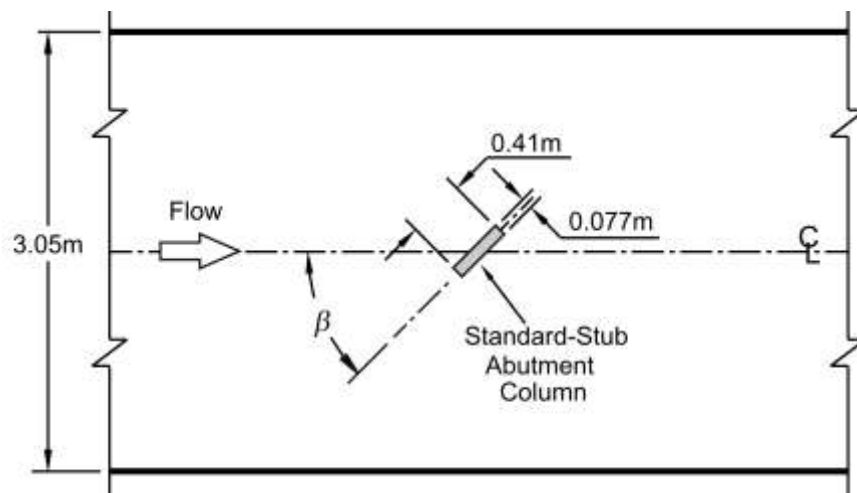
Figure 6-19. Plan layout of standard-stub column in the flume

Figure 6-20. Photo showing the experimental flume and LSPIV set up
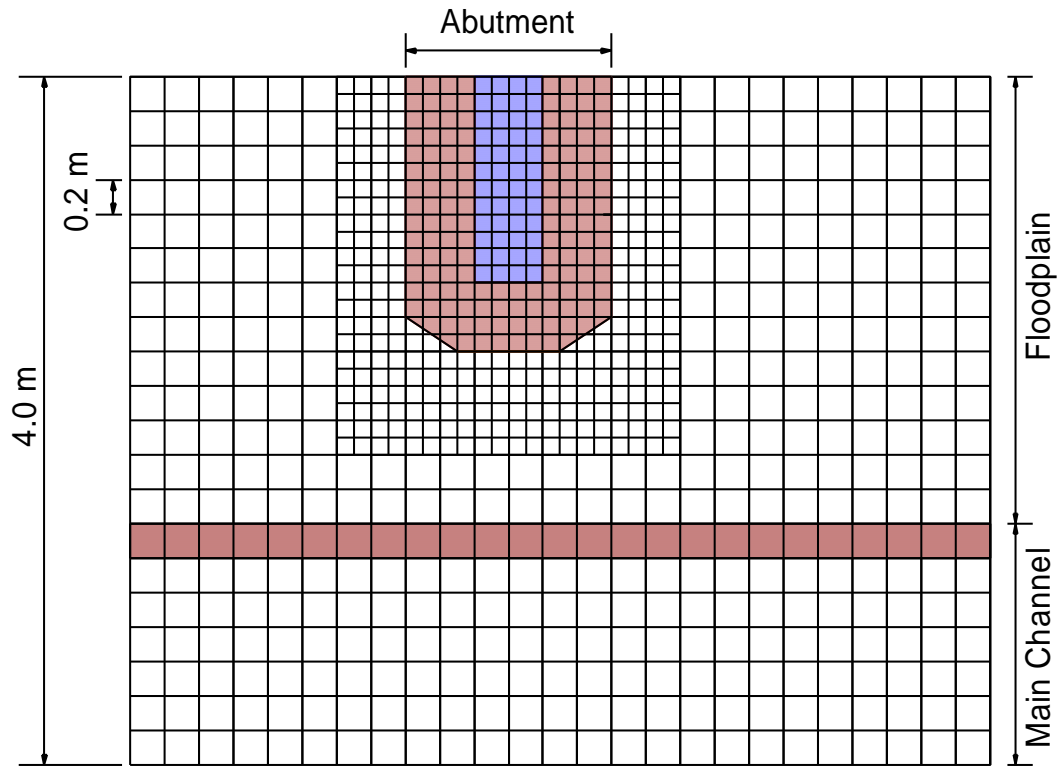
Figure 6-21. Grids for flow velocity and bathymetry measurements around the model abutment in the flume
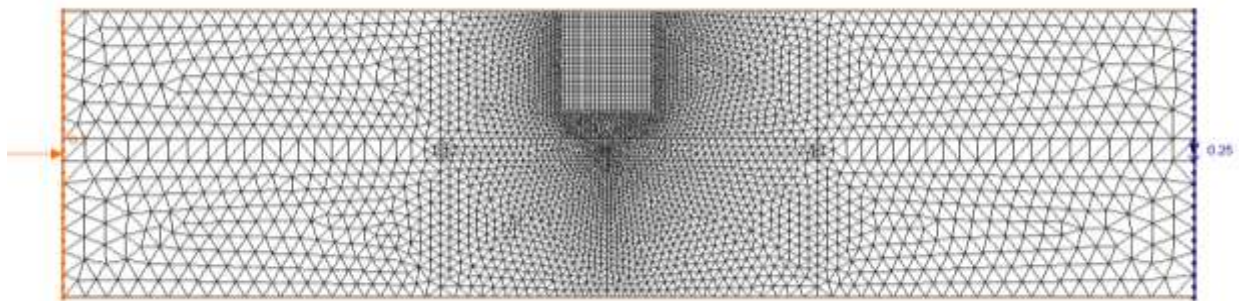
Figure 6-22. Schematic showing the mesh selected for the numerical model. Note that the abutment length and floodplain width were varied in the numerical tests, and a series of tests also was done for spill-through and vertical-wall abutments in equivalent rectangular channels.

6-33
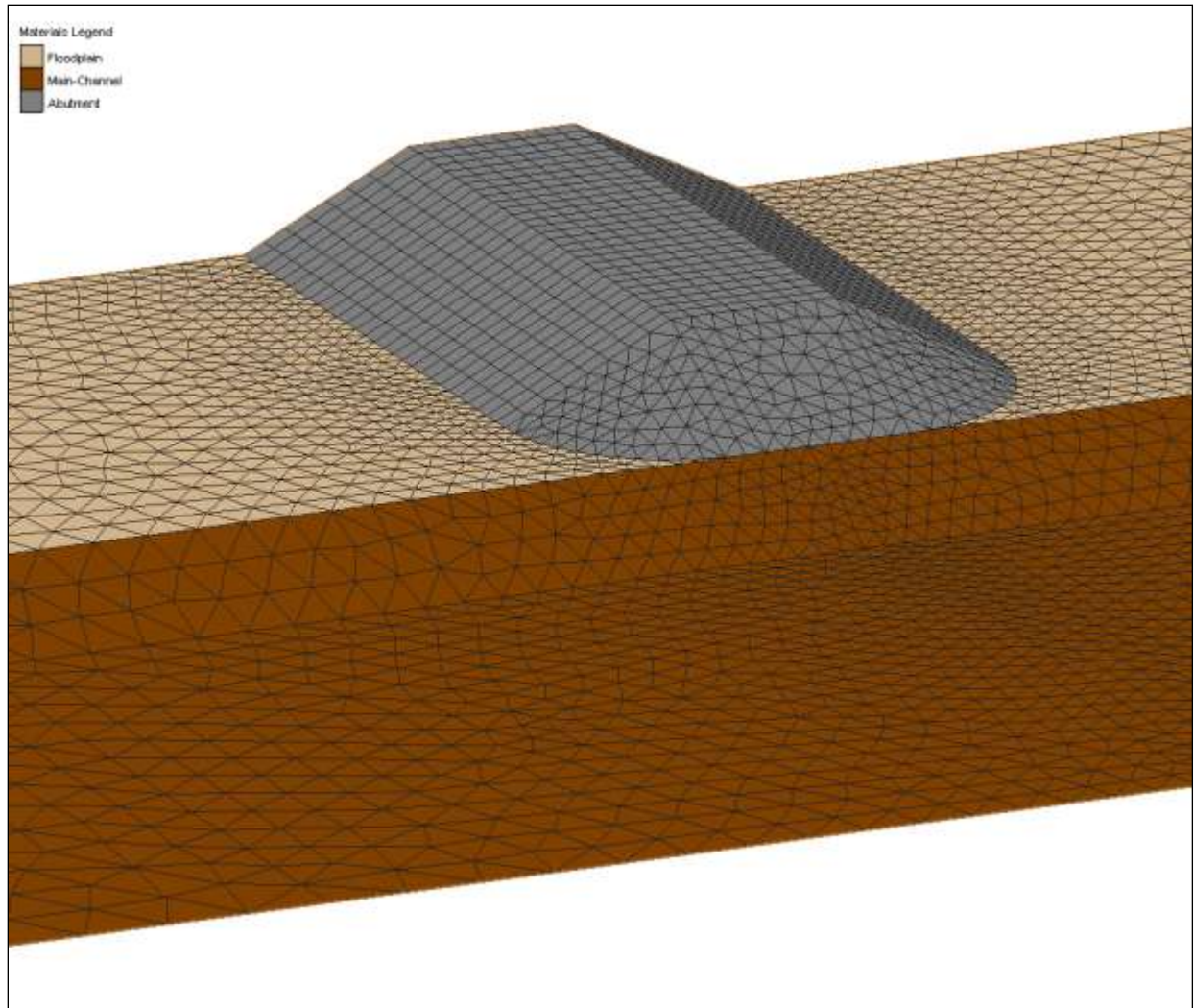
Figure 6-23. Enlarged, three-dimensional view of the unstructured mesh around one configuration of model spill-through abutment, floodplain, and main channel of a compound channel

CHAPTER 7

LABORATORY RESULTS FOR SCOUR CONDITION A AT SPILL-THROUGH ABUTMENTS

7.1 Introduction

This chapter presents the results of the flume experiments associated with Scour Condition A for spill-through abutments in compound channels. For Condition A, scour occurs only in the main-channel bed when the channel's floodplain is sufficiently erosion resistant (or fixed), or scour extends from the main channel into the floodplain when the floodplain is as erodible as the main-channel bed. This latter situation merges Scour Conditions A and B; where Condition B is scour limited to a single channel. Figure 7-1 illustrates how Scour Condition A potentially may adversely affect the geotechnical stability of the main-channel bank and abutment's embankment. It also illustrates the principal scour variables discussed in this chapter. They include maximum flow depth at the location of maximum scour, Y_{MAX}, and an estimated hypothetical, long-contraction scour depth, Y_C. Also measured was the location of Y_{MAX}, relative to the abutment's centerline axis.

The results were obtained for fixed spill-through abutments on fixed floodplains; and, for riprap-protected, pile-supported abutments with erodible (sand) embankments built on erodible (sand) floodplains. The abutment columns for these model layouts are illustrated in Figures 6-4 and 6-5. The results obtained with the model layout comprising an unprotected (no riprap) abutment on an erodible floodplain are presented in Chapter 10, which discusses scour at exposed abutment columns. Chapter 11 presents further data for Scour Condition A for the layout situation when a pier is located adjacent to a spill-through abutment.

7.2 Scour-Depth Trends

The scour experiments led to definite trends for maximum scour depth, discussed in terms of an overall maximum flow depth, Y_{MAX}, normalized with long-contraction scour depth, Y_C, and plotted versus unit-discharge ratio, q_2/q_1, for the fixed and erodible states of floodplain. The

parameter q_2/q_1 usefully expresses the flow-contraction aspects implied by the combination of parameters L/B_f, $B_f/0.5B$, and Y_f/B_f. The values of Y_C were estimated using Laursen's (1960) long-contraction relation, herein given as Eq. (5-3). Table 7-1 summarizes the scour-depth data.

7.2.1 Abutment on Fixed Floodplain

Figure 7-2 shows the trends obtained for Y_{MAX} versus q_2/q_1 with the simulated spill-through abutments on fixed floodplains. Also plotted in this figure are the values of Y_C. The trend is usefully re-plotted as Figure 7-3 in terms of the depth-amplification factor, $\alpha_A = Y_{MAX}/Y_C = C_T m^{6/7}$, expressed in Eq. (4-14), versus q_2/q_1, for the fixed floodplain and embankment state. Observations regarding the scour processes underlying the trend in Figure 7-3 are discussed in Sections 7.3 and 7.4, where the resulting scour forms and flow fields associated with the trend also are illustrated and explained.

Figure 7-3 provides the following insights into the scour-depth trend:

1. The overall trend shown by the data in Figure 7-3 delineates the conceptual relationship presented in Figure 4-5, though there is a consistent slight shift with values of $B_f/0.5B$ (floodplain width divided by half width of whole channel including the main channel and the floodplain);

2. At small values of q_2/q_1 (and small flow contraction), $Y_{MAX}/Y_C > 1$. This portion of the trend is attributable to the local change in bed-form height in the contraction, combined with the erosive influence of turbulence structures generated as flow passes around the abutment and over the edge of the main-channel bank. The bed forms were predominantly dunes. Table 7-1 also summarizes, for varying q_2/q_1, the major amplitude measured for the one or two dunes near the abutment;

3. Eventually as the bridge waterway becomes more contracted, and q_2/q_1 further increases, the values Y_{MAX}/Y_C attain a peak of around 1.6 to 1.7 when $q_2/q_1 \approx 1.2\sim1.3$;

4. When extrapolated to $q_2/q_1 \approx 1$ for the limiting condition of a finite-length abutment in a very wide channel, the peak value obtained for the Y_{MAX}/Y_C data aligns with the estimate $1.81C_{TA}$ given by Eq. (4-32), especially if the turbulence coefficient C_{TA} is not much larger than 1;

5. For the higher values of q_2/q_1, Y_{MAX}/Y_C reduces asymptotically towards approximately 1.1. This portion of the trend reflects the dominance of scour caused primarily by flow contraction, with some influence of turbulence; and,

6. The parameter, $B_f/0.5B$, exerts a small, but discernable, influence on Y_{MAX}/Y_C, especially in the range of maximum values of Y_{MAX}/Y_C. The maximum value of Y_{MAX}/Y_C is slightly larger for the smaller value of $B_f/0.5B$. This influence is attributable to the fact that, in absolute lengths, the abutment is closer to the main channel, thereby causing floodplain flow to enter the main channel more readily, and more of the turbulence generated by the abutment to be diffused into the main channel.

The flow-depth values associated with long-contraction scour, Y_C, were calculated using Laursen's (1960) formulation, and therefore would include some uncertainty, given the approximations inherent in estimating the relationship between flow depth and unit discharge for loose-bed channels. One consideration introducing some inaccuracy is that the dimensions of the dunes in the contracted portion of the flow around the abutment varied as q_2/q_1 varied. Laursen's formulation (leading to Eq. (4-13) for Y_C) assumes that Manning's flow resistance coefficient, n, remains constant between the approach channel and through the waterway. However, the dimensions of the dunes on the main-channel bed increased where flow contracted around the abutment, as evident in Table 7-1.

7.2.2 Pile-Supported Abutment on Erodible Floodplain

The manner of scour development, and equilibrium scour bathymetry, altered somewhat when the floodplain comprised the same erodible sediment as the bed of the main channel (i.e., sand), and the abutment's embankment was erodible though riprap covered. Scour of the main-channel bed, along with erosion of the floodplain between the main channel and the abutment, essentially

merged or combined Scour Conditions A and B. Such overlap is illustrated schematically and described earlier in Figure 4-2.

Figure 7-4 plots the values of Y_{MAX}/Y_C versus q_2/q_1 obtained for spill-through abutments on erodible floodplains. This figure also indicates the upper-bound envelope to the data obtained for Scour Condition A when the abutments were on fixed floodplains (shown in Figure 7-3). Also included in this figure are two data obtained with the abutment aligned $\pm 30^o$ to the approach flow direction; i.e., $\beta = 30^o$ and 150°, as defined in the insert to Figure 7-4. The following results are evident in Figure 7-4:

1. For small values of q_2/q_1, and thereby small flow contraction through the main channel, $Y_{MAX}/Y_C > 1$. Moreover, for some experiments with small q_2/q_1, the value of Y_{MAX}/Y_C equaled or marginally exceeded that obtained when the floodplain was fixed. For these latter experiments, the resultant scour was predominantly Scour Condition B, and produced a deeper scour than Condition A when the floodplain was fixed;

2. As values of q_2/q_1 increased, the merging of Scour Conditions A and B increased the flow cross-sectional area at the abutment, and, thereby, relaxed the flow contraction. In turn, this effect resulted in a leveling off of Y_{MAX}/Y_C at the scour location;

3. The scour of the floodplain near the abutment effectively steepens the embankment side slope, and poses an issue for the embankment's geotechnical stability;

4. Abutment alignment did not appreciably affect Y_{MAX}/Y_C for the range of abutment layouts investigated. The variations in Y_{MAX}/Y_C were well within the amplitude variation of dune height; and,

5. Extrapolation of the peak value obtained for the Y_{MAX}/Y_C data would fall below the estimate $1.81 C_{TA}$ given by Eq. (4-32) for the limiting condition of a finite-length abutment in a very wide channel.

Several of the flume tests were repeated to ensure consistency of results. Minor variations occurred owing to slight differences in dune bathymetry in the main channel near the abutment. The repeated tests are for the two conditions: $B_f/0.5B = 0.43$ and 0.63 ($B_B/0.5B = 0.50$ and 0.70)

7.2.3 Comparison with ABSCOUR

As mentioned in Section 5.7, the ABSCOUR method developed by Chang and Davis (1998, 1999), like the approach taken for the method developed in the present project, treats abutment scour as essentially inseparable from contraction scour. It is useful to compare the scour predictions obtained from ABSCOUR with the data and trends in Figure 7-4. Because the scour processes envisioned in the development of ABSCOUR may differ from Scour Condition A, the comparison likely cannot be entirely complete. Therefore, of interest is a comparison of data magnitude and trends.

The comparison uses Eq. (5-35), modified as follows:

$$Y_{MAX}/Y_C = (Y_{MAX}/Y_1)/(Y_C/Y_1) \tag{7-1}$$

In which $Y_{MAX}/Y_1 = Y_2/Y_1$ in Eq. (5-35). Given that the embankment construction technique used in the present project (i.e., the abutment and embankment did not extend as a solid body into the bed or floodplain) did not produce the large-scale turbulence structures (spiraling flow) assumed in the development of ABSCOUR, the adjustment coefficient for spiral flow is set at $k_f = 1$. Also, an adjustment factor of 0.55 is used for spill-through abutment form (Table 5-3).

Figure 7-5 shows that the overall magnitudes of Y_{MAX}/Y_C estimated using ABSCOUR are reasonably close, allowing for the approximate nature of the comparison. The ABSCOUR trend for Y_{MAX}/Y_C, though, differs from that shown by the data. For the larger values of q_2/q_1, the ABSCOUR trend shows Y_{MAX}/Y_C gradually increasing, whereas the data show Y_{MAX}/Y_C reducing.

The difference in trend is attributable to several considerations, including the differences in abutment construction used for the present experiments.

7.3 Observations of Scour at Spill-Through Abutments

Observations of the scour processes and of equilibrium scour bathymetry shed useful explanatory insights regarding the foregoing trends for equilibrium flow (and scour) depth.

7.3.1 Spill-Through Abutment on Fixed Floodplain

A selection of three sets of figures is presented here to illustrate Scour Condition A (fixed floodplain) when the contraction of flow extended passed the abutment was minor, moderate, and substantial. The three sets coincide with the values $B_f/0.5B = 0.23$, 0.43, and 0.63; and, $L/B_f = 1.00$ in Figures 7-6, 7-7, and 7-8, respectively. The corresponding values of the parameter q_2/q_1, which expresses the extent of contraction, are 1.18, 1.31, and 1.56, respectively.

The set of figures shows the following points:

1. The location of deepest scour commonly was where the axis of the abutment intersected with the bank of the main channel;

2. The scour depth (and thereby flow depth) is not uniformly distributed across the main channel bed for the lower values of q_2/q_1. For small q_2/q_1, the region of deepest scour is close to the bank of the main channel; and,

3. As q_2/q_1 increased from 1.2 to 1.6, flow constriction at the abutment increases, and scour at the abutment axis becomes increasingly more uniform across the main-channel bed.

Figures 7-6a, b depict the resultant equilibrium scour hole that formed when $B_f/0.5B = 0.23$, $L/B_f = 1.00$, and $q_2/q_1 = 1.18$. The scour hole is viewed from upstream of the abutment. The main channel bed at the embankment axis was dune covered. Also the maximum scour depth is located at the embankment axis.

When L/B_f remained at 1.00, but $B_f/0.5B$ increased to 0.43 with $q_2/q_1 = 1.31$, scour extended proportionately further across the main channel, though the deepest scour remained at the main-channel bank. Figures 7-7a,b depict the resultant equilibrium scour hole formed for this condition. The line indicated along the centerline of the main-channel bed in Figure 7-7b shows that the contraction scour did not extend to the centerline of the main channel (represented by the flume's far wall). The scour hole is viewed from upstream of the abutment. As mentioned in Section 7.2, the amplitude of the dunes enlarged slightly because of the somewhat greater contraction of flow passing around the abutment.

When $B_f/0.5B$ was increased to 0.63, with L/B_f remaining at 1.00, and $q_2/q_1 = 1.56$, the scour region practically covered the entire bed of the main channel at the abutment, as shown in Figures 7-8a, b. The line indicated along the centerline of the main channel bed indicates the amount of contraction scour there. Also noticeable is the substantial increase in dune amplitude in the vicinity of the abutment. The larger discharge, and thereby drag exerted on the bed, led to larger dunes, as the data in Table 7-2 list.

The bathymetry measurements corresponding to the set of scour photographs in Figures 7-6 through 7-8 are given in Figures 7-9a-c, which show a series of views of the scour bathymetry for $L/B_f = 1.00$ and varying $B_f/0.5B$. The following general features can be drawn from Figure 7-8:

1. The geometries around the abutment are similar with the location of maximum scour as described for Figures 7-6 through 7-8;

2. The maximum scour depth became deeper as $B_f/0.5B$ increased;

3. When $B_f/0.5B = 0.23$ and 0.43, the scour area expanded from the point of the maximum scour to the downstream with an oblique angle; and,

4. When $B_f/0.5B = 0.63$, the whole bed of the main channel at the embankment axis was scoured, as if it were essentially a contraction scour. The maximum scour depth coincided with the trough elevation of dunes formed in the scour region.

7.3.2 Pile-Supported Abutment on Erodible Floodplain

When the riprap-protected abutment was located on a floodplain as erodible as the bed of the main channel, Scour Condition A quickly led to the geotechnical failure of the main-channel bank and, then, the embankment, as well as erosion of the floodplain immediately around the abutment. The consequent development of scour for a pile-supported abutment on an erodible floodplain is illustrated in Figure 7-9, for which $B_f/0.5B = 0.43$ and $L/B_f = 1.00$. Appendix B1 depicts scour development over time for a similar layout of spill-through abutment.

Scour development occurred chiefly as follows:

1. Initially, the scour hole deepened in the main channel until the main-channel bank and the abutment's upstream side slope shoulder became geotechnically unstable and failed, exposing most of the abutment column and its pile cap;

2. The failed side slope slumped as a rounded shoulder protected by riprap stone, which also dispersed as a fan over part of the scour region; and,

3. The abutment's re-shaped and riprap-armored shoulder guided flow past the abutment in a more streamlined manner, and pushed the region of deepest scour to form at a location in the main channel adjacent to the abutment's downstream corner.

For cases where an abutment was slightly set back from the main channel, the floodplain surface also eroded around the abutment. This erosion, together with scour of the main-channel bed, merged Scour Conditions A and B. Figures 7-11a,b through 7-13a,b illustrate the resulting scour bathymetries for $B_f/0.5B = 0.23$, 0.43, and 0.63, and $L/B_f = 0.75$, respectively. These pairs of photographs depict the abutment before and after scour. To illustrate the bathymetry variation associated with these scour views, Figure 7-14 plots the bathymetry data corresponding to the scour developed when $B_f/0.5B = 0.43$ and $L/B_f = 0.75$. The black dots in this figure indicate the dispersion of riprap stone displaced from the embankment slope. The maximum scour was located at the abutment's downstream corner. Inside this scour area, no dunes were observed. Two cross sections of the scour bathymetry are given in Figure 7-15.

In a series of plan views of the scour bathymetry associated with variable abutment length and variable floodplain width, Figure 7-16 summarizes the variation of scour forms. From the top to the bottom of the array of views, L/B_f increases from 0.35 to 1.0. Similarly, the column from left to right composed to $B_f/0.5B$ increases from 0.23 to 0.63. In each view, the area in between the two lines indicates the initial slope between the floodplain and the main channel. The contour lines start from 0 m (at the water surface) to the maximum depth of the scour hole, with level increments of 0.05m.

Figures 7-11 through 7-16 indicate that scour and embankment failure, for abutments set back from the main channel, occur much the same way as described for Figure 7-10 for abutments right at the main channel. Several differences are evident, however:

1. The floodplain surface scoured around the abutment concurrently as Scour Condition A developed in the main channel. Scour of the floodplain directly enlarged the flow area at the abutment axis, thereby reducing flow contraction around the abutment, and reducing floodplain flow into the main channel;

2. Scour of the floodplain caused the region of deepest scour to move closer to the abutment than when the floodplain was fixed for the same abutment layout;

3. As scour of the floodplain progressed, it caused the embankment slope to fail geotechnically, and riprap stone from the embankment's shoulders slid into the scour region;

4. When the abutment was set back on the floodplain, the location of major failure of the abutment was at the abutment's upstream shoulder. There, the abutment column was most exposed, as evident especially in Figures 7-13 and 7-14;

5. The absolute deepest scour remained located immediately downstream from the abutment's downstream corner, where flow contraction was greatest, as explained subsequently in Section 7.4. The failed riprap covered and partially protected the upstream portion of the scour region;

6. As L/B_f decreased, where the abutment was further distant from the main channel, Scour Condition B developed increasingly independently of Scour Condition A. Because, in

the present experiments, the floodplain comprised the same sand as the main-channel bed, the floodplain between the abutment and the main channel eroded;

7. When $L/B_f \leq 0.67$, the region of deepest scour formed in the floodplain;

8. For the abutment layouts with $L/B_f > 0.67$, the region of deepest scour extended from the floodplain into the main channel;

9. Embankment erosion became more severe as both L/B_f and $B_f/0.5B$ increased. When $L/B_f = 1.00$ and $B_f/0.5B = 0.63$ embankment breaching occurred; and,

10. As elaborated in Chapter 12, which discusses field verification of the laboratory findings, the scour bathymetry obtained in the flume is similar in appearance to that for scour failures observed in the field.

Figure 7-17 compares the locations of deepest scour, Y_{MAX}, for spill-through abutments on erodible and fixed floodplains. Whereas Y_{MAX} was located quite close to the centerline axis abutments built on fixed floodplains, for abutments on erodible floodplains its location moved slightly downstream of the abutments. This downstream shift is attributable to scour re-shaping of the upstream corner of the abutments.

A set of photographs comprising Figure 7-18 show both the initial and equilibrium scour states of a spill-through abutment built at three alignments on an erodible floodplain. For each alignment, scour led to a slope failure of the embankment's upstream corner, and the formation of a similarly rounded, riprap-protected shoulder there. Flow and scour practically re-shaped, or streamlined, the abutment so as to better pass flow around the abutment for the three alignments. Consequently, the value of Y_{MAX} did not change substantially when the abutment's alignment varied from 30° to 150°, relative to the channel axis.

7.4 Flow-Field Observations

The LSPIV and ADV measurements of the flow-field observations lent useful insight as to how Scour Condition A developed around the abutments. Though not revealing the full, three-dimensional flow around the abutments, giving instead the flow distribution at the water surface,

the measurements provide sufficient information to explain the scour bathymetry and scour-depth trends described in Sections 7.2 and 7.3. For many test cases, the surface flow pattern around the test abutment was measured initially before scour commenced, and then once equilibrium scour had been attained. The initial flow fields apply to both the fixed and the erodible floodplain states. However, depending on floodplain erodibility, the equilibrium flow field differed with scour bathymetry.

7.4.1 Spill-Through Abutment on Fixed Floodplain

Figures 7-19a-f show initial distributions of q_2/q_1 and streamlines before scour began for the spill-through abutments in a compound channel set at $B_f/0.5B = 0.63$, and relative abutment lengths $L/0.5B = 0.30$, 0.50, 0.63, 0.75, 1.00, and 1.10. The values of unit discharge were determined from LSPIV measurements. Of interest is the relationship between the maximum value of unit discharge around the abutment, q_{2MAX}, relative to the area-average value through the centerline axis of the abutment, q_2, for varying q_2/q_1. Figure 7-20 shows this relationship. As explained in Section 4.3, the variation of q_{MAX}/q_2 expresses the variation of factor m in the scour-depth estimation equation, Eq. (4-14).

Figures 7-19 and 7-20 indicate the following variations in flow-field with increased embankment length (or L/B_f):

1. The magnitude of the q_2/q_1 increased;

2. The orientation of flow near the embankment on the floodplain swung more parallel to the embankment axis;

3. The flow became more uniformly distributed across the main channel through the bridge waterway;

4. The data trend in Figure 7-20 supports the conceptual trend shown in Figure 7-3 for Y_{MAX}/Y_C. Values of m_A initially are level, or increase very slightly, then asymptote down to about 1.1, as q_2/q_1 increases. The greater values for Y_{MAX}/Y_C in Figure 7-3, than m_A in Figure 7-22, are interpretable as the influence of dunes and the erosive effects of large-

scale turbulence (vortices) generated by flow around the abutment, as expressed with the parameter C_{TA} in Eq. (4-14).and,

5. These general features are typical of flow through a short contraction, such as one sketched in Figure 2-11.

The LSPIV measurements show that, once scour began in the main channel, flow was found to concentrate in the scour region locally when the abutment-length parameter L/B_f exceeded about 0.63. No significant flow concentration was detected in the main channel for L/B_f less than 0.63, however. The pair of LSPIV photographs in Figure 7-21 depicts how flow concentrated in the scour region. The large wake eddy downstream of the abutment grew and extended into the main channel as scour progressed. The eddy's lateral extent reflects the contraction of flow passing around the abutment. No such concentration of flow occurred when all the approach flow (in the main channel and over the floodplain) passed through the main channel, notably when $L/B_f \cong 1.00$.

The scour bathymetry shown in Figure 7-22, for the same conditions indicated in Figure 7-21, shows that the maximum scour area corresponded to the area where flow concentrated. This figure shows values of q_2/q_1 for $B_f/0.5B = 0.63$, and $L/B_f = 0.75$. As evident from the pathlines drawn in this figure, the bulk of the flow passed through the main channel, and the wake region extended to the main channel.

The influence on Y_{MAX} of the aforementioned flow features can be summarized as follows:

1. For small L/B_f, such that q_2/q_1 is low, the deepening of the bed near the abutment was due to the passage of dune troughs. When $0 < L/B_f < 0.63$, for $B_f/0.5B = 0.63$, flow did not concentrate over the main channel (at least, it was not observed in the LSPIV measurement). As L/Bf increased, Y_{MAX} increased;

2. For $0.63 \leq L/B_f < 1$, flow concentration (as observed by LSPIV measurement) produced scour substantially deeper than that attributable to flow contraction, Y_C.;

3. When $L/B_f \geq 1.00$, the approach flow fully passes through the main channel, such that no flow concentration in the scour region was observed in the LSPIV measurements. Though Y_{MAX} increased, it did not increase as rapidly as for the lesser values of L/B_f. The increase essentially followed the increase in long-contraction scour, Y_C, because the main channel opening narrowed as L/B_f increased;

4. The foregoing influences hold in overall mechanistic terms, but the values of L/B_f at which scour-induced flow concentration occurs may vary with the flow-depth parameter Y_f/B_f. This influence can be taken into account by means of q_2/q_1, which expresses the concentration of flow (floodplain and approach main channel) through the bridge waterway; and,

5. The old hydraulics adage, "depth attracts flow," seems indeed to hold for Scour Condition A.

7.4.2 Spill-Through Abutment on Erodible Floodplain

The trends described above for spill-through abutments on fixed floodplains basically also occurred for the spill-through abutments on erodible floodplains, though with the following differences evident in Figure 7-23:

1. Because the floodplain could erode, and thereby laterally increase the cross-sectional area of flow at the abutment axis, less flow was drawn towards the scour region in the main channel. Instead, flow was drawn towards the abutment;

2. Erosion of the floodplain shifted the region of greatest scour closer to the abutment, and resulted in a broader, shallower scour region than when the floodplain was fixed; and,

3. The lateral extent of the wake region downstream of the abutment became much smaller than when the floodplain was fixed.

These effects can be illustrated by viewing the flow field development at a representative layout of spill-through abutment on erodible floodplain. Figure 7-23 shows water-surface velocities,

values of q_2/q_1, and pathlines for flow around the spill-through abutment when $B_f/0.5B = 0.63$, and $L/B_f = 0.50$, before and after scour. The changes in distributions of q_2/q_1 are made clear in Figure 7-24, which presents lateral distributions of q_2/q_1, before scour, and after scour, through a transect at the location of maximum scour. As illustrated by these figures, the flow distribution changed markedly as scour progressed. Before scour, the values of q_2/q_1 were largest in the main channel. As scour progressed, and the floodplain eroded, the flow re-distributed, becoming more uniform and aligned with the channel axis, as well as reduced in magnitude. Also, the extent of the wake region downstream of the abutment diminished, reducing considerably from when the floodplain was fixed. These figures show that, unlike for the fixed-floodplain case, flow did not concentrate in main channel, as scour developed. Consequently, as is evident in Figure 7-4, Y_{MAX}/Y_C was less than for the fixed-floodplain case.

The preceding flow-field figures indicate that the trend in values of q_2/q_1 agree with that of Y_{MAX}/Y_C for spill-through abutments. The velocity data obtained from the ADV measurements also support the trend. Figures 7-25a-c give values of local average velocity normalized by the bulk velocity of flow through the main channel near the abutment; i.e, $\sqrt{V_x^2 + V_y^2}/\overline{V}$, where V_x and V_y are the streamwise and normal components of the local velocity vector. The velocity ratio $\sqrt{V_x^2 + V_y^2}/\overline{V}$ approximates the parameter q_2/q_1. These figures also show the scour bathymetry. The $\sqrt{V_x^2 + V_y^2}/\overline{V}$ values for each abutment configuration suggest that the maximum values of q_2/q_1 are about 1.2~1.3 in the main channel, thereby further suggesting that $m_A \approx 1.2$~1.3. The further amplification of Y_{MAX}/Y_C beyond about 1.2~1.3 likely is owing to the influence of turbulence generated as flow passes around the abutment.

The locations of higher value of flow velocity, or unit discharge, do not exactly correspond to the location of the maximum scour hole, but generally the higher value of the m_A coincides with the location of deepest geometry. The presence of dunes in the main channel, however, introduced some local variability in this relationship.

7.5 Numerical Simulation of Flow Field

To provide important additional diagnostic insights into the flow field associated with scour development, series of numerical experiments were performed using the two-dimensional, depth-averaged model FESWMS produced flow fields showing the distribution of unit discharge, q, as well as depth-average velocity and bed shear stress, commensurate with flow around spill-through abutments sited on the floodplain of compound channels. The findings of work with FESWMS are fully documented in the companion report by Morales and Ettema (2010). A summary is provided here.

Flow field insights were obtained from simulations run for a range of L/B_f values up to $L/B_f = 0.95$. Figures 6-22 and 6-23 earlier show an example of the computational mesh used for one configuration of spill-through abutment and compound channel. The simulations are for flat-bed, or pre-scour flows, in compound and rectangular channels.

The cross-channel distribution of unit discharge, q_2, for flow around ten configurations of spill-through abutments ($L/B_f = 0.20$ through 0.95), are presented in Figures 7-26 for $B_f/0.5B = 0.65$. Similar general trends occur for other values of $B_f/0.5B$. The distributions, taken along the centerline axis of the bridge, reveal the following aspects flow around the abutments:

1. The peak value of q_2 near the abutment increases when L/B_f increases, with channel width remaining constant;

2. The peak value of q_2 in the main channel also increases when L/B_f increases;

3. The distribution q_2 over the narrow region immediately in front of the abutment corresponds to a portion of the wake flow (and flow separation) that extends up along part of the abutment face (e.g., as evident in Figure 7-18). The size of the flow-separation region increases mildly with increasing L/B_f (as also evident in Figure 7-18);

4. For abutments set such that $L/B_f > 0.70$, the distribution of becomes is slightly more complicated, because the peak for q_2 near the abutment extends over the main-channel bank interacts with the main channel flow; and,

5. When $L/B_f > 0.80$, the peak for q_2 near the abutment becomes increasingly comparable to the peak magnitude for q_2 in the main channel.

In the main channel at the bridge axis, the maximum value q_2, expressed as q_{MAX}/q_2, remained at about 1.2, for the ranges of q_2/q_1 (i.e., L/B_f and $B_f/0.5B$) values simulated numerically (Figure 7-27). The laboratory flume values of obtained for q_{MAX}/q_2, concur with the numerical values, over the same range of q_2/q_1 values, but decrease to about 1.1 for larger values of q_2/q_1. This latter trend shown by the flume results can be explained in terms of flow distribution for flow forced through relatively severe short contractions (analogous to flow through a short outlet pipe) in which lateral distribution of flow is constrained because flow velocity profiles are not fully developed (e.g. Rouse 1950).

Over the floodplain at the bridge axis, values of q_{MAX}/q_2, increases from a value marginally above 1.0 for short spill-through abutments to approach asymptotically a value of 1.2 when the abutment extends substantially across the floodplain; i.e., when $L/B_f > 0.70$. This trend, along with that for q_{MAX}/q_2 in the main channel, indicates peak values of unit discharge or depth-average velocity being about twenty percent above the cross-sectional average values at the bridge axis.

Table 7-1. Spill-through abutments on fixed floodplains

$B_f/0.5B$	L/B_f	q_2/q_1	Y_{MAX} (m)	Y_C (m)	Y_{MAX}/Y_C	Maximum Dune Height H (m)	Maximum Dune Length λ (m)
0.63	1.20	2.35	0.698	0.617	1.13	0.070	0.762
	1.10	2.02	0.630	0.561	1.12	0.057	1.20
	1.00	1.66	0.570	0.463	1.23	0.062	1.07
	1.00	1.66	0.572	0.463	1.24	0.062	1.07
		1.49				0.064	1.11
	0.75	1.33	0.568	0.382	1.50	0.057	1.22
	0.625	1.21	0.540	0.352	1.53	0.110	0.90
	0.50	1.11	0.410	0.327	1.25	0.058	0.09
	0.35	1.01	0.353	0.301	1.17	0.063	0.90
0.43	1.00	1.30	0.615	0.375	1.64	0.093	0.90
	1.00	1.30	0.616	0.375	1.64	0.093	0.90
	0.75	1.17	0.550	0.344	1.60	0.102	0.68
	0.625	1.12	0.440	0.330	1.33	0.076	0.76
	0.50	1.07	0.385	0.318	1.21	0.102	0.90
0.23	2.13	1.87	0.605	0.453	1.34	0.110	0.91
		1.54			1.32	0.096	0.90
	1.49	1.28	0.600	0.361	1.66	0.057	0.760
	1.00	1.14	0.545	0.336	1.62	0.075	1.00
	1.00	1.14	0.545	0.336	1.62	0.077	1.01
	0.75	1.08	0.460	0.321	1.44	0.075	1.20
	0.625	1.06	0.395	0.314	1.26	0.090	0.850
	0.50	1.03	0.355	0.308	1.15	0.076	1.07

Table 7-2. Riprap-protected spill-through abutments on erodible (sand) floodplain

| $B_f/0.5B$	L/B_f	q_2/q_1	Y_{MAX} (m)	Y_C (m)	Y_{MAX}/Y_C
	1.0	1.66	0.505	0.463	1.09
0.63	1.0	1.66	0.490	0.463	1.05
	0.75	1.33	0.530	0.382	1.39
	0.625	1.21	0.496	0.352	1.41
	0.50	1.11	0.380	0.327	1.16
	0.35	1.01	0.420	0.301	1.40
	0.00	1.00	0.300	0.300	1.00
	1.0	1.30	0.485	0.375	1.29
0.43	1.0	1.30	0.487	0.375	1.30
	0.75	1.17	0.475	0.344	1.38
	0.625	1.12	0.435	0.330	1.32
	0.5	1.07	0.435	0.318	1.37
	0.35	1.03	0.470	0.321	1.46
	0.00	1.00	0.300	0.300	1.00
	1.0	1.14	0.485	0.336	1.44
0.23	1.0	1.14	0.483	0.336	1.43
	0.75	1.08	0.470	0.321	1.47
	0.625	1.06	0.410	0.314	1.31
	0.50	1.04	0.505	0.305	1.66
	0.35	1.02	0.490	0.299	1.64
	0.00	1.00	0.300	0.300	1.00
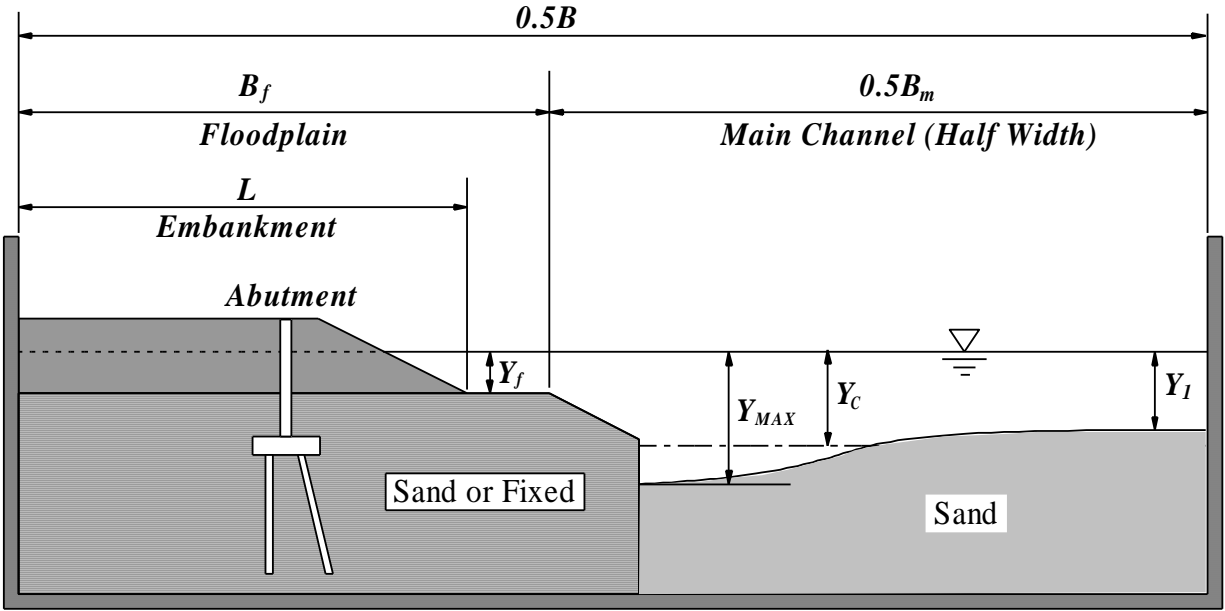
Figure 7-1. Principal variables measured for spill-through abutments subject to Scour Condition A
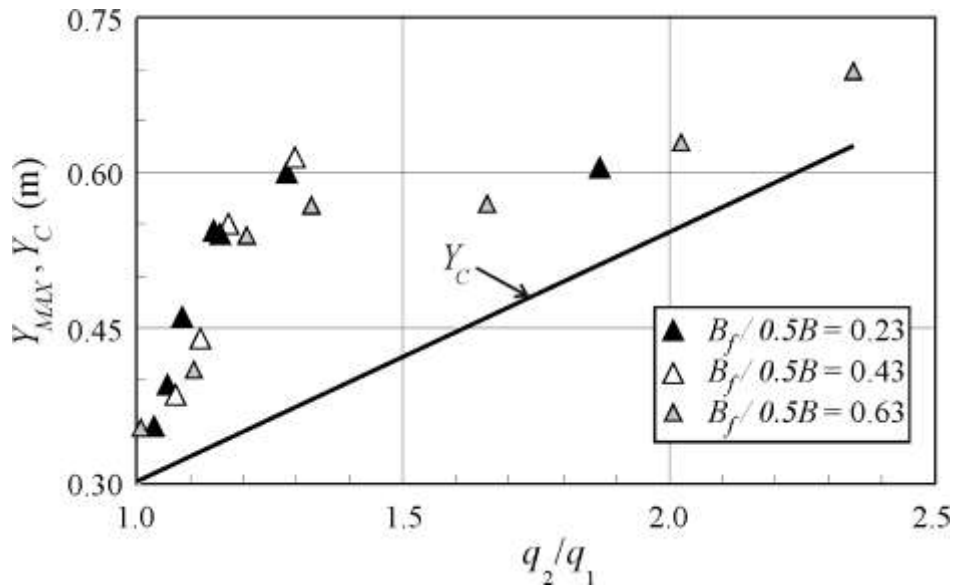

Figure 7-2. Variations of Y_{MAX} and Y_C with unit-discharge ratio q_2/q_1 for Scour Condition A at spill-through abutments on fixed floodplains
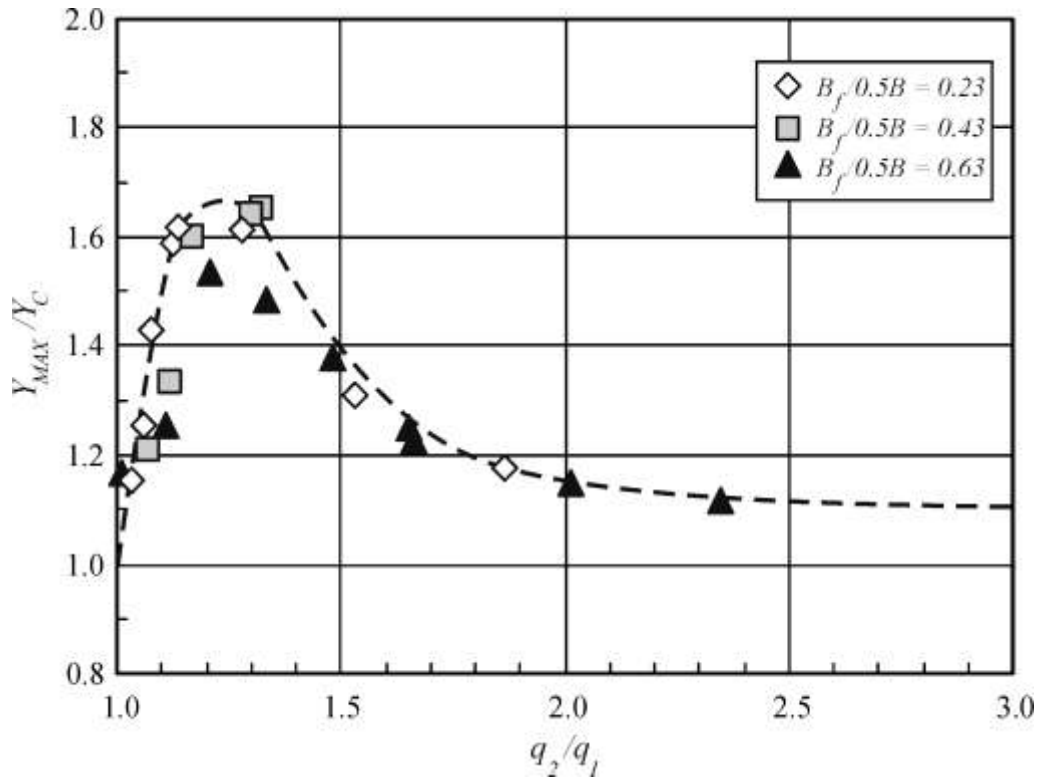
Figure 7-3. Variation of Y_{MAX}/Y_C with q_2/q_1 for Scour Condition A at spill-through abutments on fixed floodplains
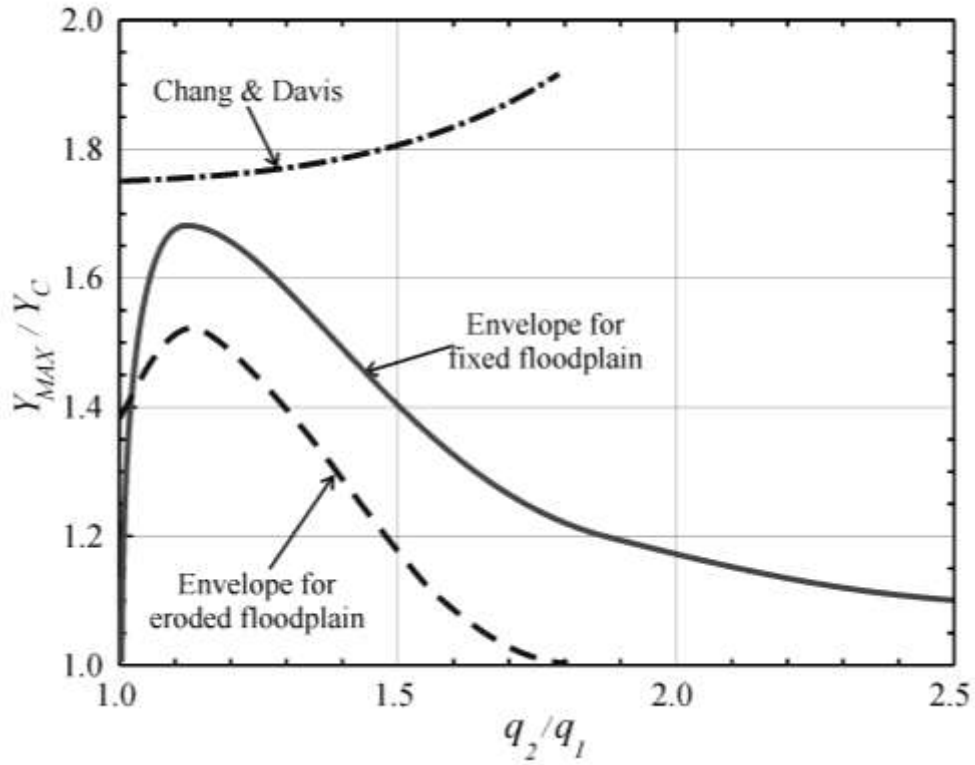
Figure 7-4. Variation of Y_{MAX}/Y_C with q_2/q_1 for Scour Condition A at spill-through abutments armored with riprap on erodible floodplains. The envelope is for the data given in Figure 7-3; i.e., fixed floodplains. The data include abutments aligned at $30°$ and $150°$ to the approach flow direction.

Figure 7-5. Comparison of trends for variation of Y_{MAX}/Y_C with q_2/q_1 for Scour Condition A: data envelopes from Figures 7-3 and 7-4, and curve from method proposed by Chang and Davis (1998, 1999).
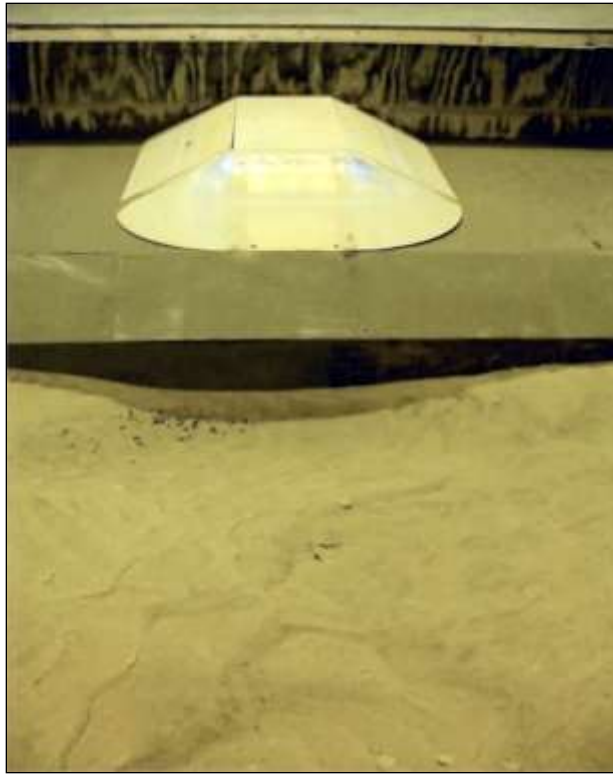
(a)

(b)

Figure 7-6. Scour at spill-through abutment for $B_f/0.5B = 0.23$ and $L/B_f = 1.00$: (a) a frontal view of scour hole, and (b) a downstream view of scour hole
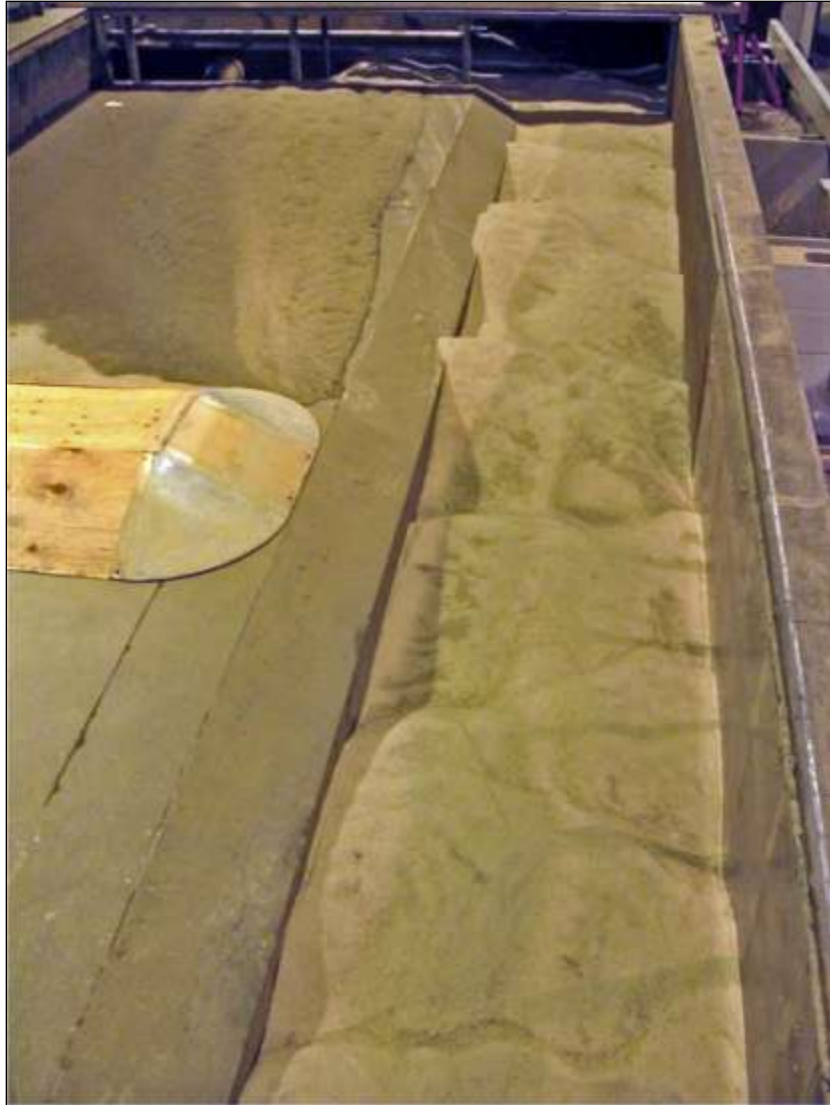
(a)

(b)

Figure 7-7. Scour at spill-through abutment for $B_f/0.5B = 0.43$ and $L/B_f = 1.00$: (a) a downstream view, and (b) a downward view
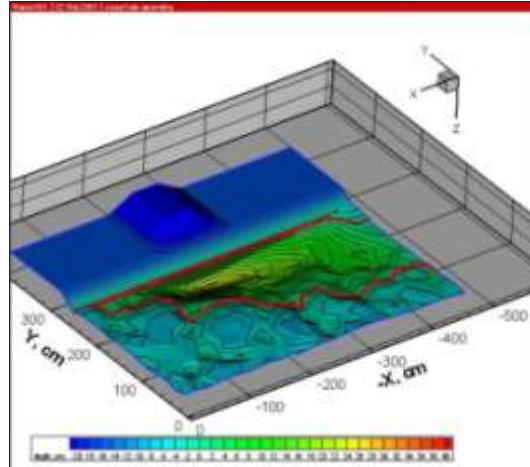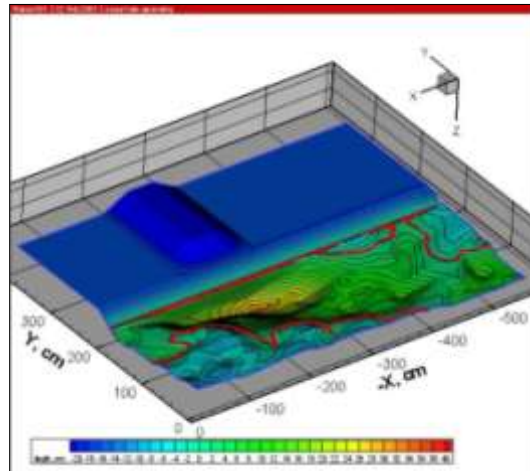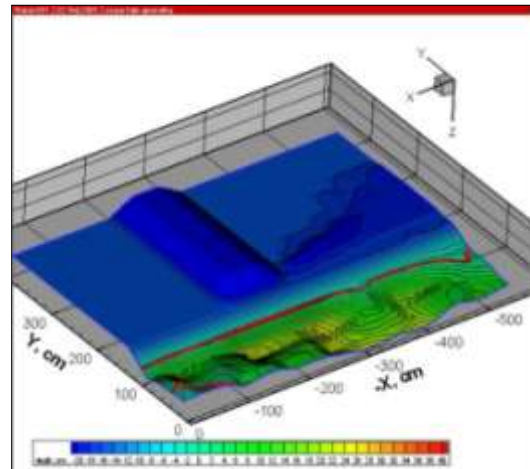
(a)

(b)

Figure 7-8. Scour at spill-through abutment for $B_f/0.5B = 0.63$ and $L/B_f = 1.00$: (a) a downstream view, and (b) a downward view

(a)

(b)

(c)

Figure 7-9. Bathymetry contours of scour holes: L/B_f = 1.00 when $B_f/0.5B$ = 0.23 (a), 0.43 (b), and 0.63 (c)

(a)

(b)

Figure 7-10. Initial condition (a), and resulting scour hole of spill-through abutment (b) for B_f /$0.5B$ = 0.43 and L/B_f = 1.00
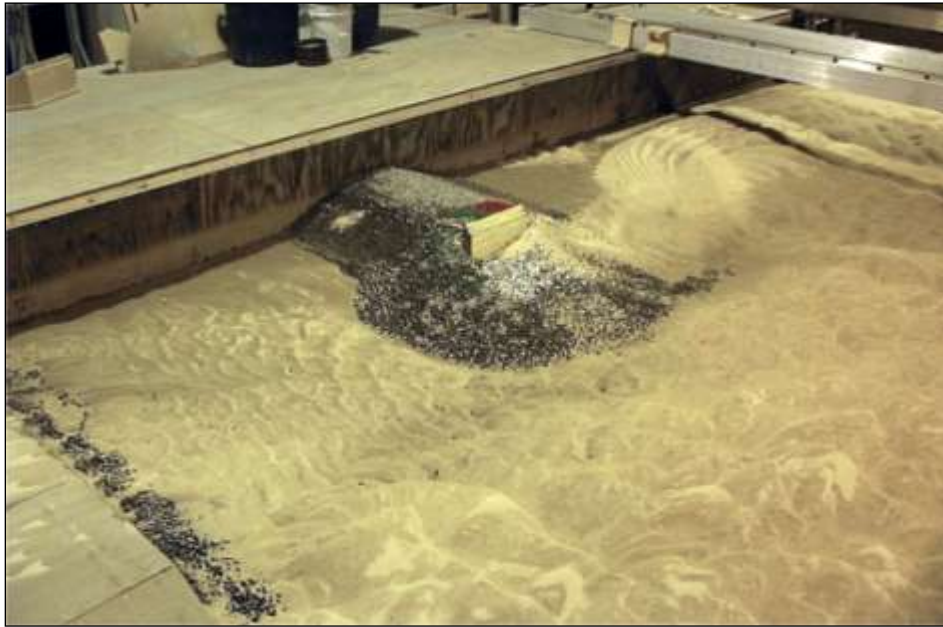
(a)

(b)

Figure 7-11. Initial condition (a), and resulting scour hole of spill-through abutment (b) for $B_f/0.5B = 0.23$ and $L/B_f = 0.75$
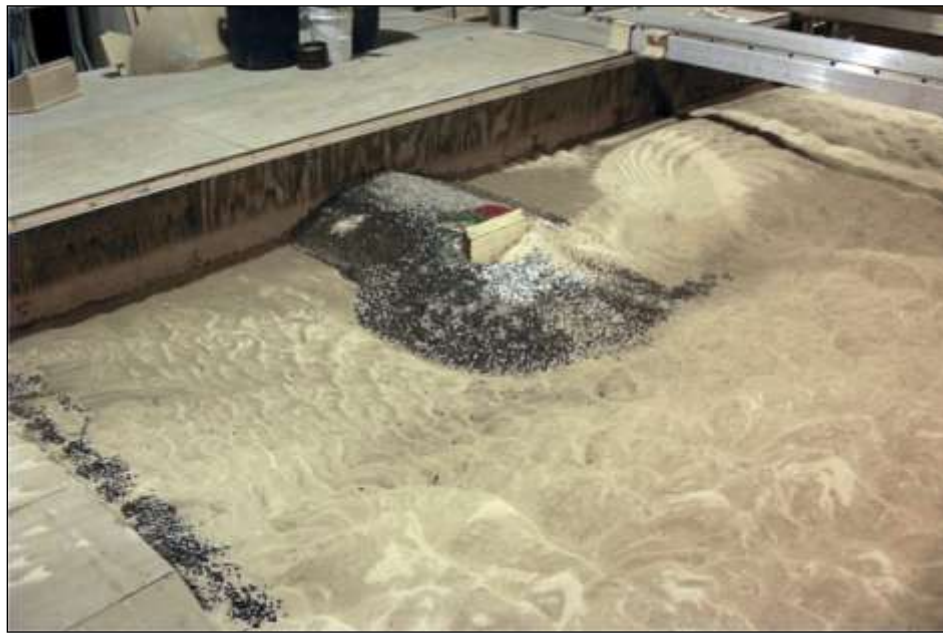
(a)

(b)

Figure 7-12. Initial condition (a), and resulting scour hole of spill-through abutment (b) for B_f $/0.5B = 0.43$ and $L/B_f = 0.75$ – sloping main-channel bank boundaries are shown in dark lines.

(a)

(b)

Figure 7-13. Initial condition (a) and resulting scour hole of spill-through abutment (b) for $B_f/0.5B = 0.63$ and $L/B_f = 0.75$ – sloping main-channel bank boundaries are shown in dark lines.
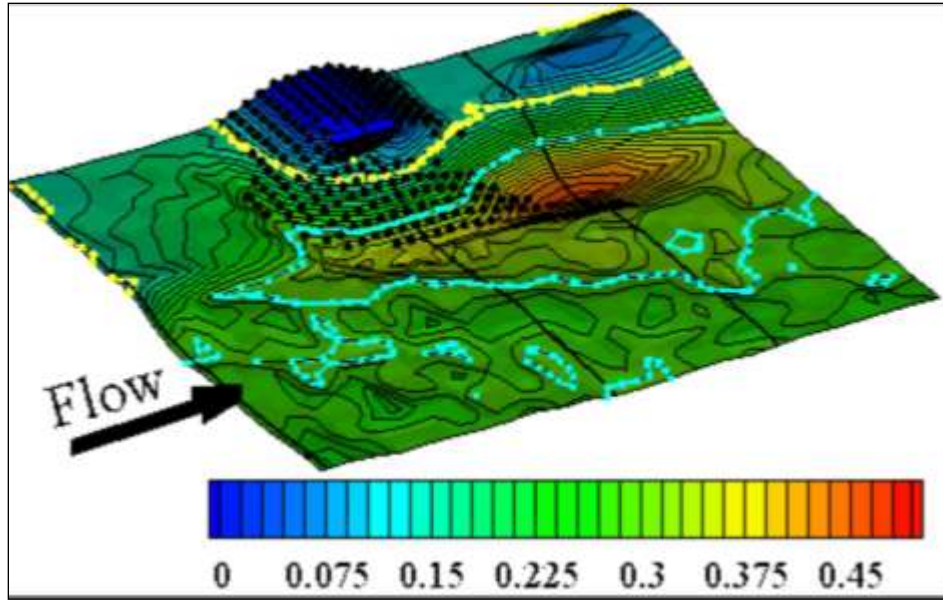
Figure 7-14. Contour plot of the resulting scour hole ($B_f/0.5B = 0.43$ and $L/B_f = 0.75$). The black dots indicate riprap-stone disposition. A yellow curve with circles, and a cyan curve with square dots indicate 0.15 m from water surface (initial bed level of floodplain), and 0.30 m from water surface (initial bed level of main channel), respectively.
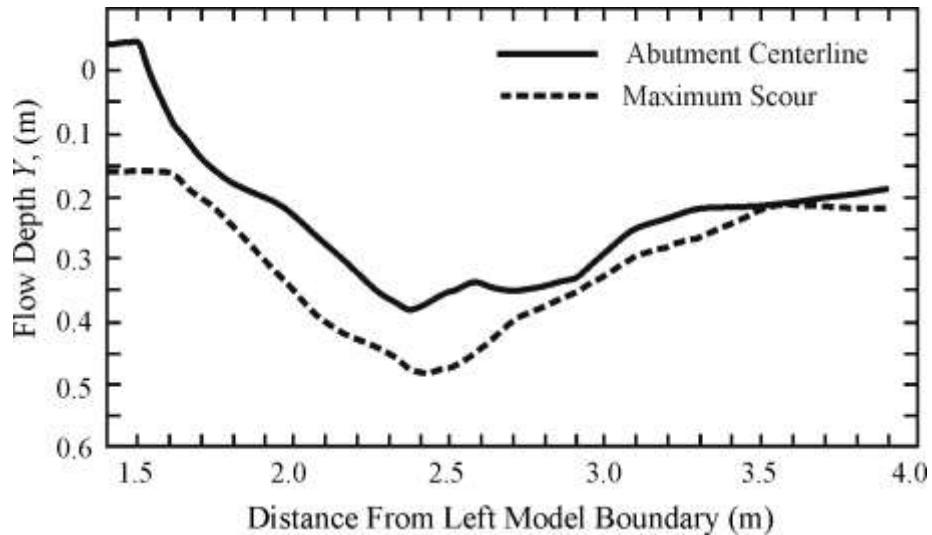

Figure 7-15. Longitudinal changes in bed profile between the two cross-sections shown in Figure 7-13

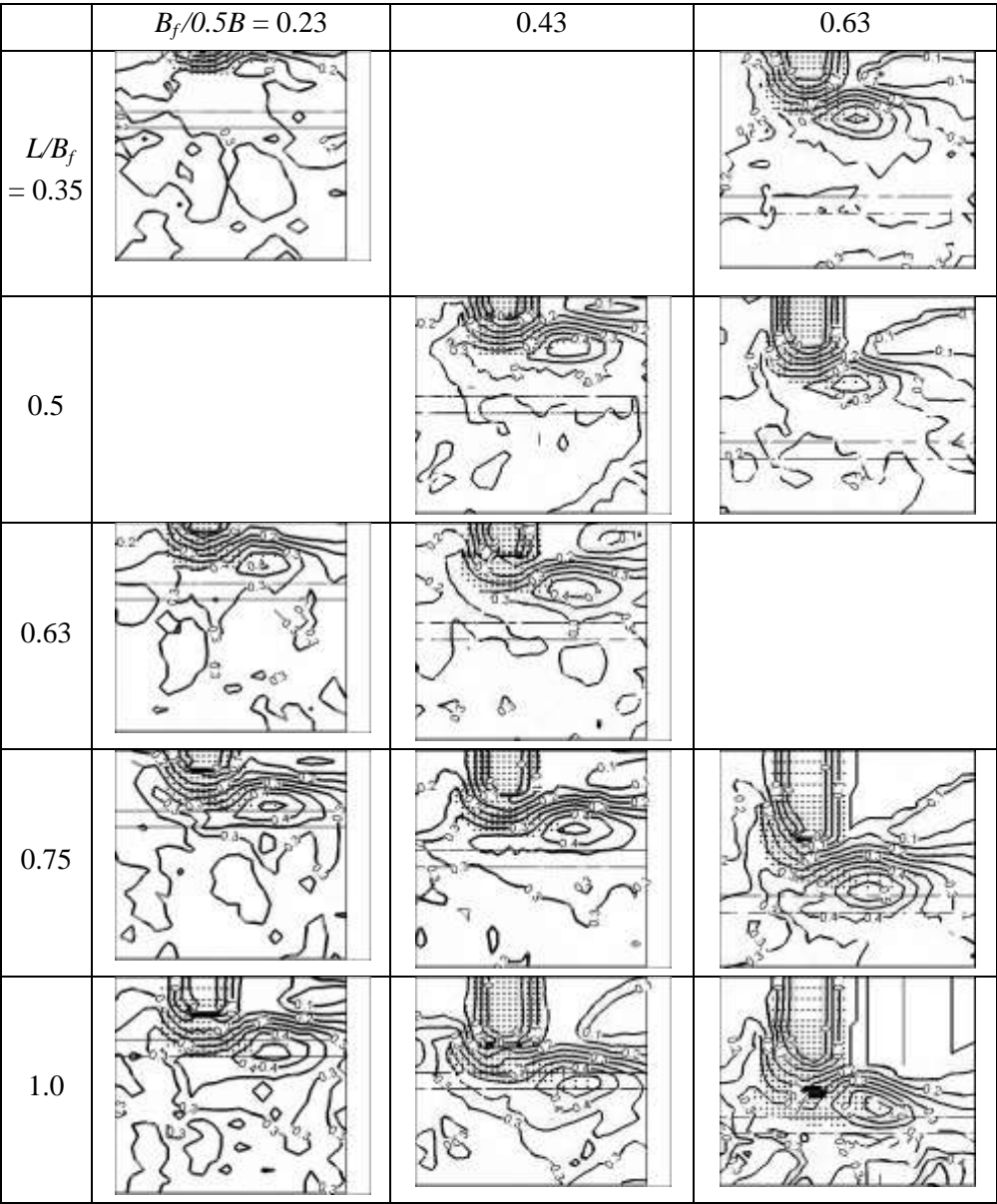|	$B_f/0.5B = 0.23$	0.43	0.63
L/B_f = 0.35			
0.5			
0.63			
0.75			
1.0			

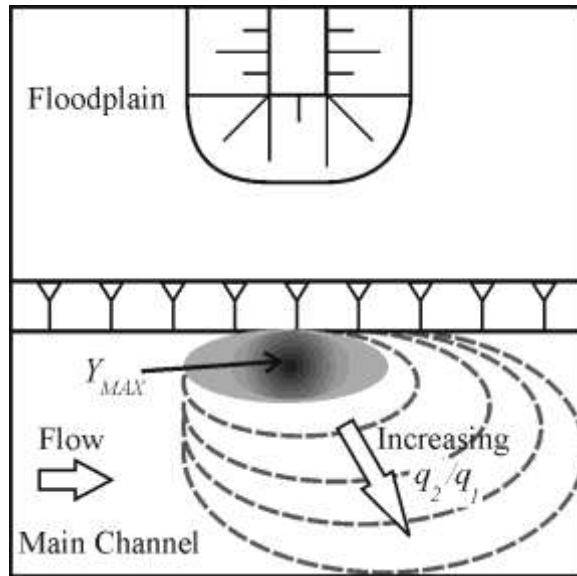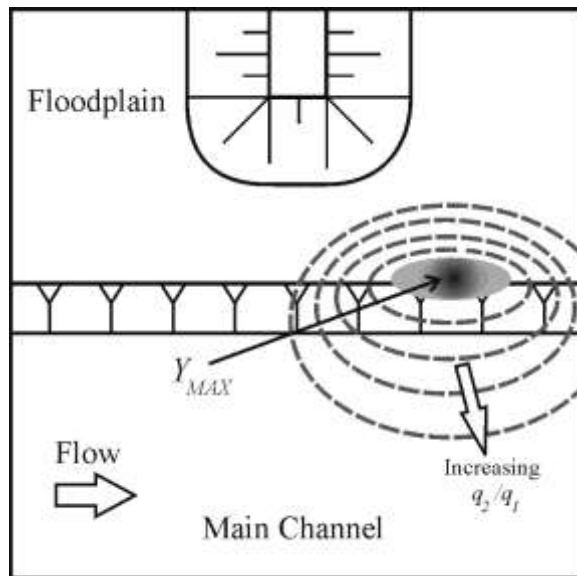Figure 7-16. Contour plots of the resultant scour geometry for spill-through abutments on erodible floodplains; $L/B_f = 0.35 \sim 1.0$ and variable $B_f/0.5B = 0.23 \sim 0.63$, contours are drawn from water surface to maximum scour depth with an increment of 0.05 m.

(a)

(b)

Figure 7-17. Location of deepest scour, for spill-through abutments on fixed floodplains (a), or erodible floodplains (b)

(a) Initial

(a) Scoured

(b) Initial

(b) Scoured
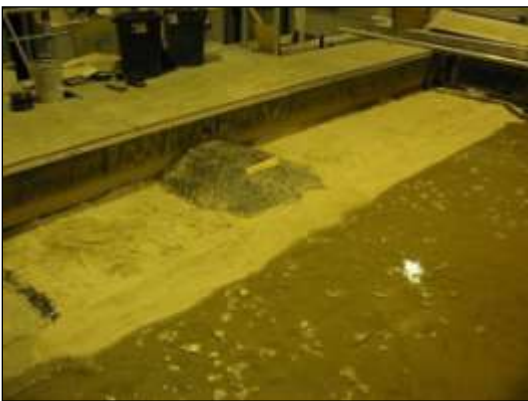
(c) Initial

(c) Scoured

Figure 7-18. Views of scour around spill-through abutment set at three alignments (initial and scour conditions); $\beta = 30°$ (a), 150° (b), and 0° (c), relative to the channel axis with $B_f/0.5B = 0.23$ and $L/B_f = 1.00$
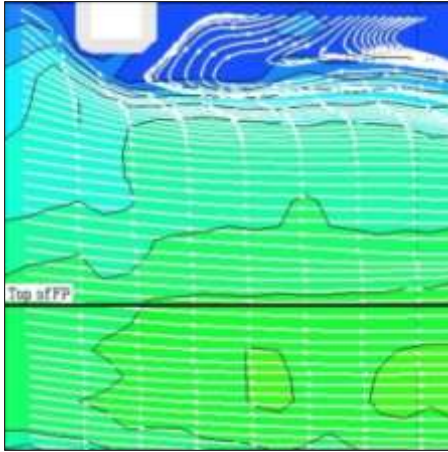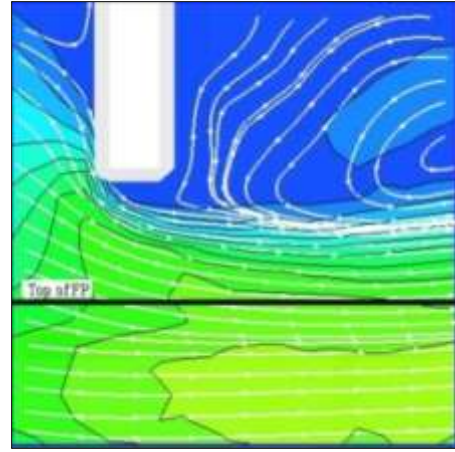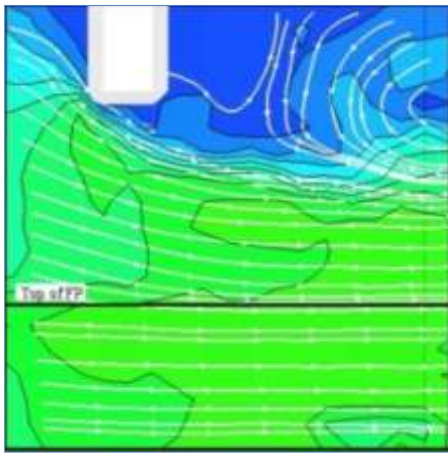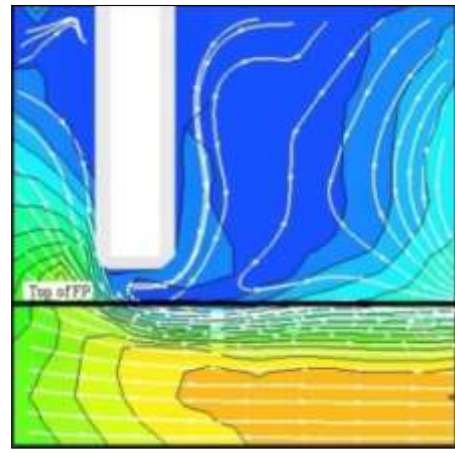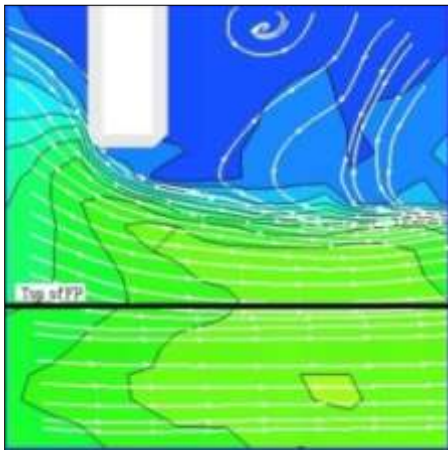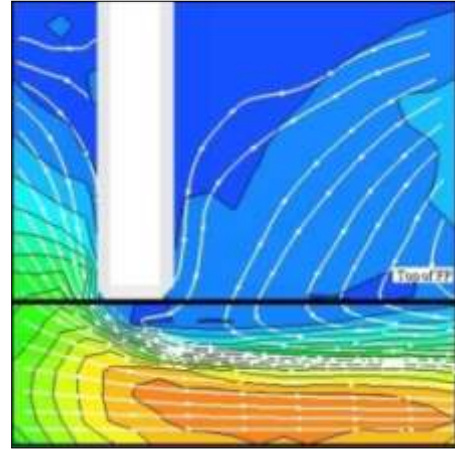
Figure 7-19. Comparisons of surface flow patterns at the start of experiment; spill-through abutment, $L/B_f = 0.30$ (a), 0.50 (b), 0.63 (c), 0.75 (d), 1.00 (e), and 1.10 (f), with $B_f/0.5B = 0.63$. The contours show values of q_2/q_1.
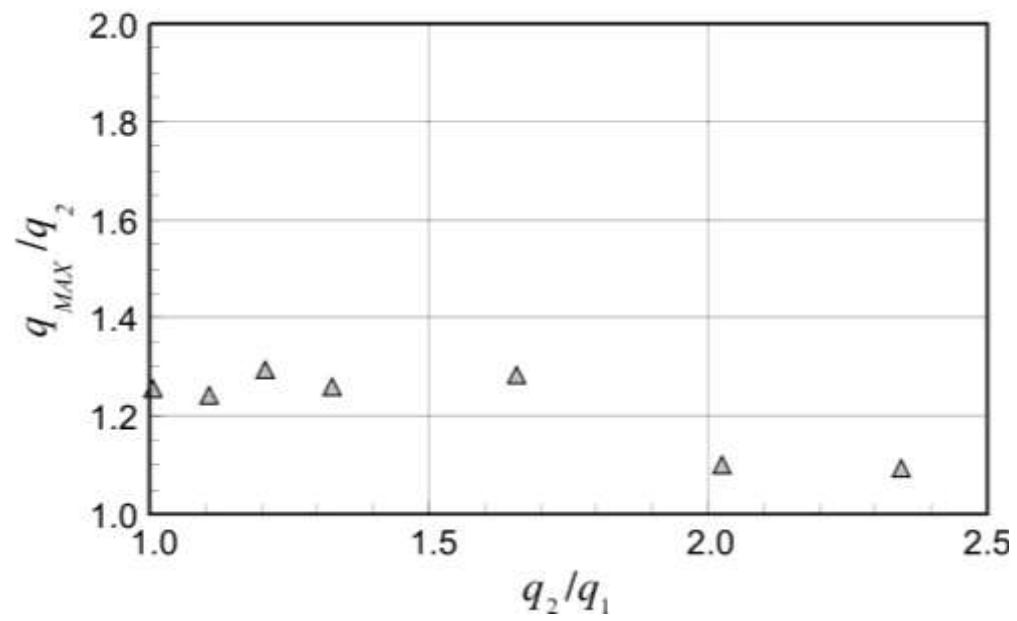
Figure 7-20. Variation of $q_{MAX}/q_2 = m_A$, for spill-through abutments on a fixed floodplain with $B_f/0.5B = 0.63$
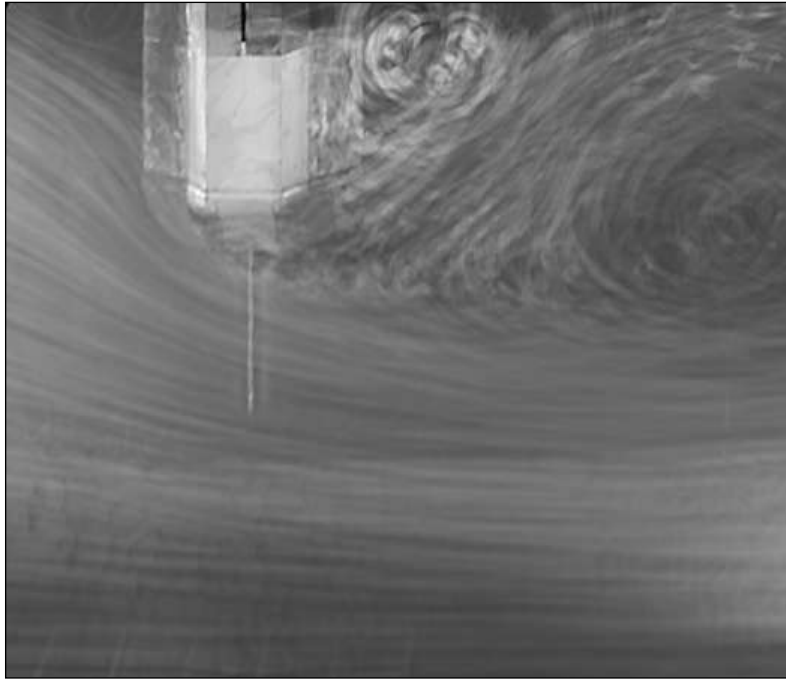
(a)
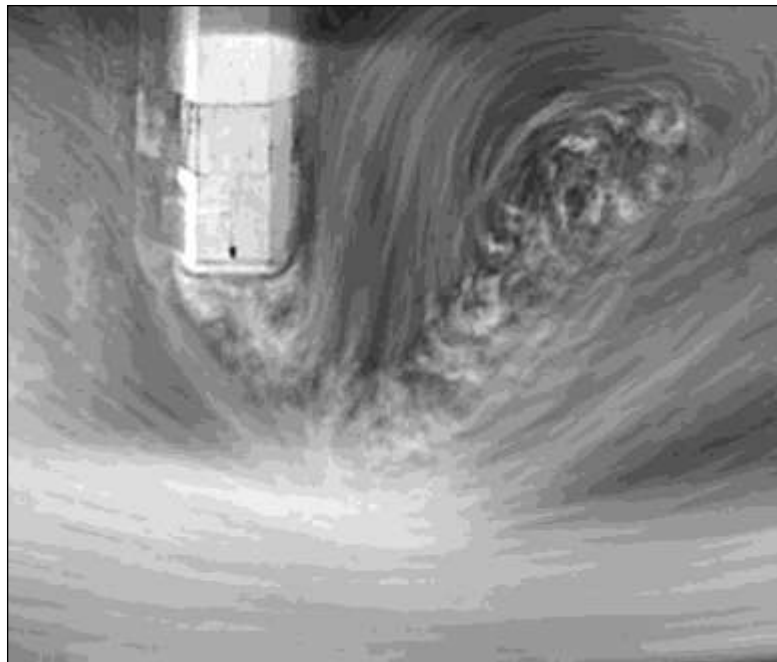
(b)

Figure 7-21. Surface flow patterns under Scour Condition A for L/B_f = 0.75 and $B_f/0.5B$ = 0.63 with fixed floodplain - flow distribution alters as scour develops; (a) shows flow field before scour, (b) shows how flow becomes concentrated in the scour region (flow direction is from left to right)
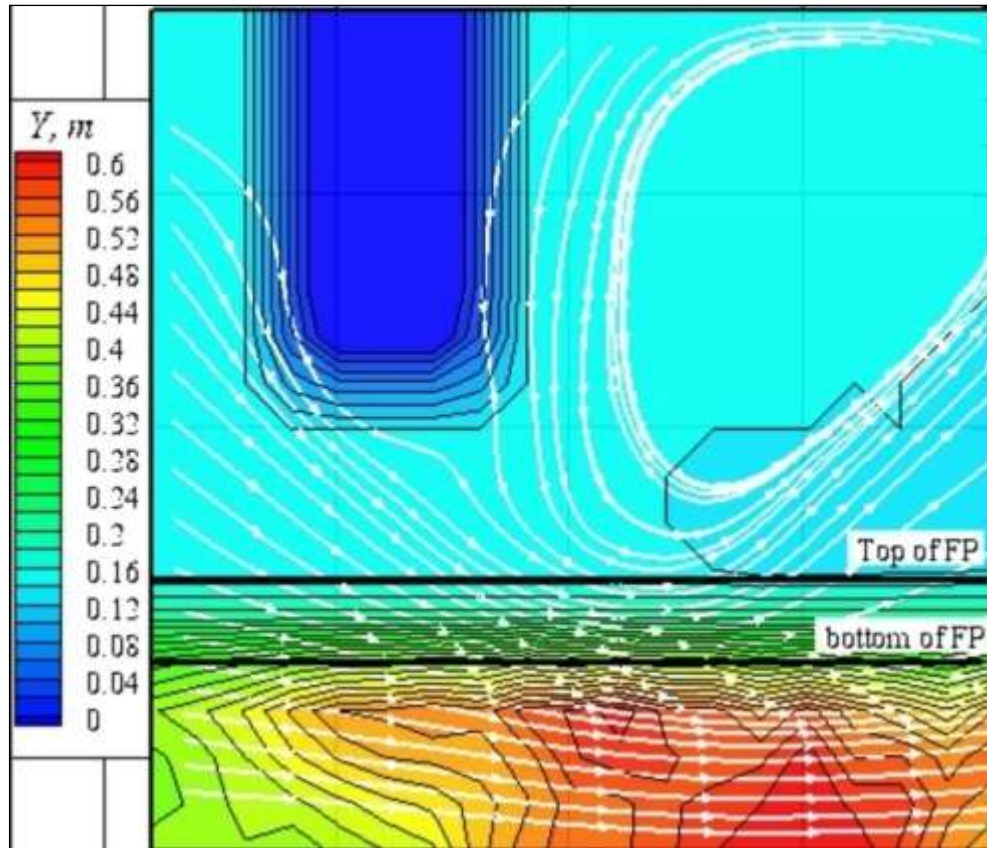
Figure 7-22. Flow pathlines and equilibrium scour bathymetry for $L/B_f = 0.75$ and $B_f/0.5B = 0.63$; compare these with those in Figure 7-19d.
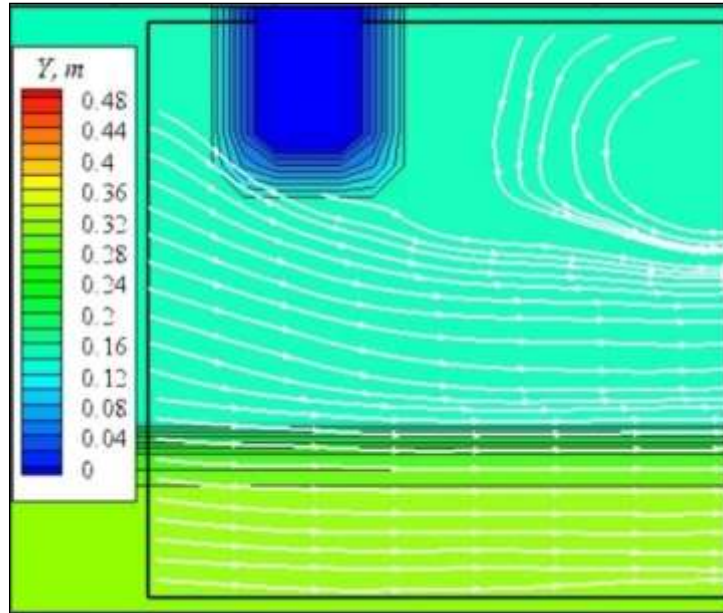
(a)
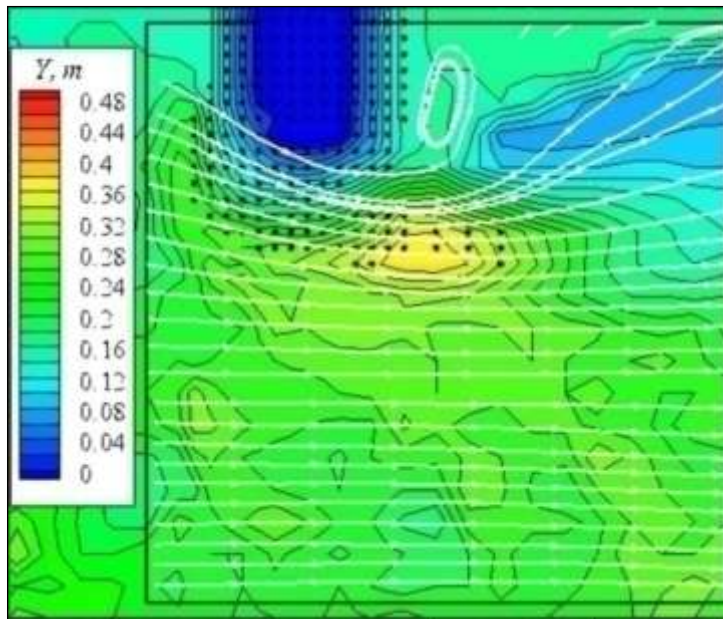
(b)

Figure 7-23. Flow pathlines and channel bathymetry before scour (a), and after scour (b) for spill-through abutment on erodible floodplain with $L/B_f = 0.50$ and $B_f/0.5B = 0.63$
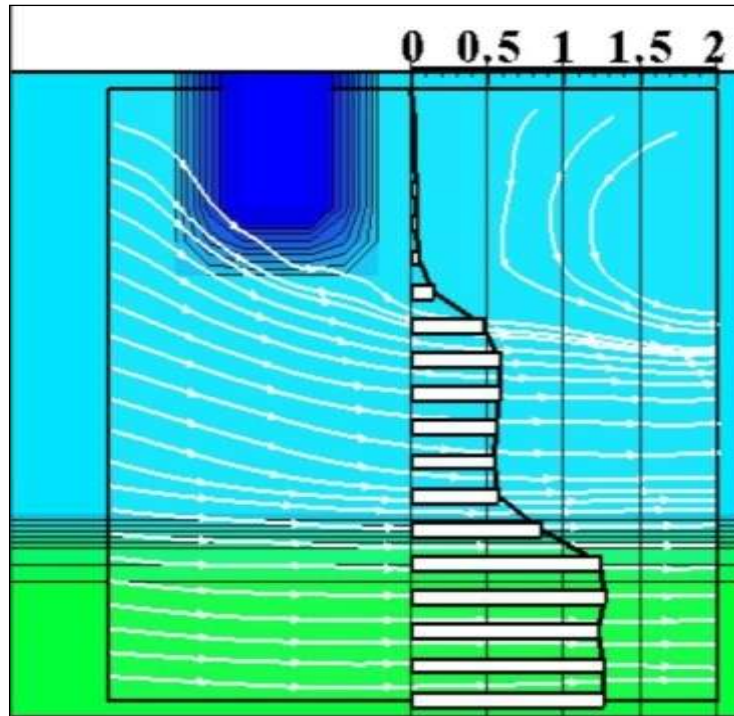
(a)
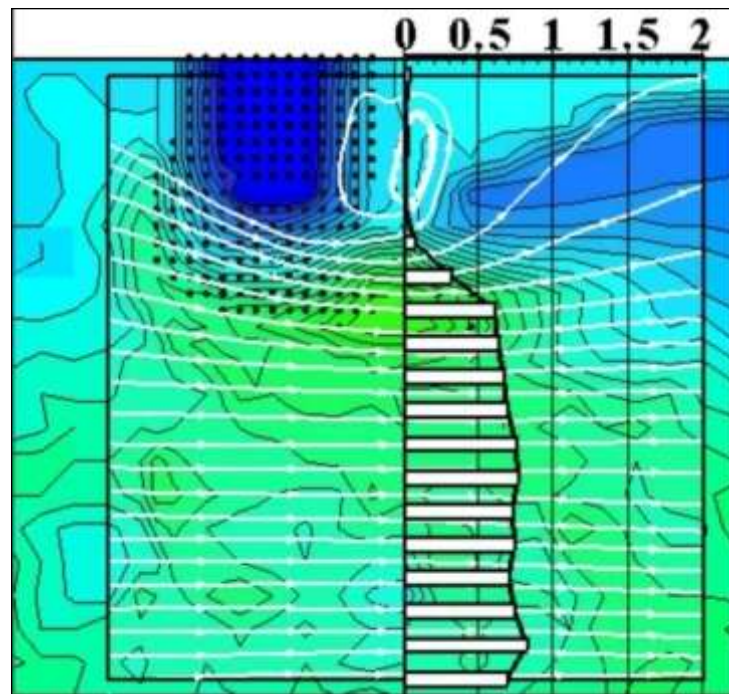
(b)

Figure 7-24. Comparison of distributions of discharge ratio, q_2/q_1, at the location of deepest scour before scour (a), and at equilibrium scour (b) with $L/B_f = 0.50$ and $B_f/0.5B = 0.63$
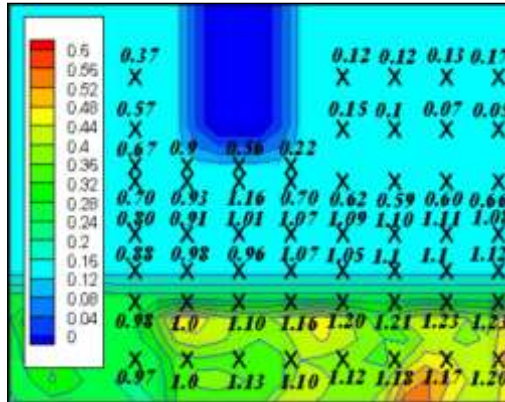
(a)
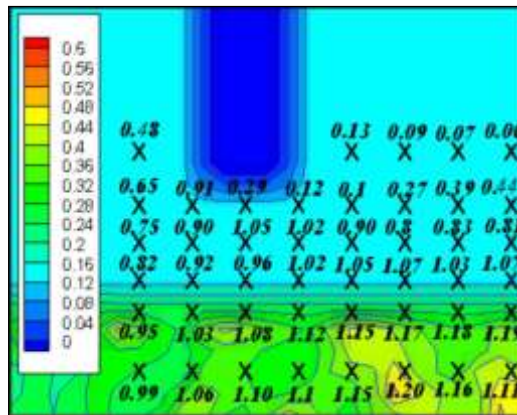
(b)
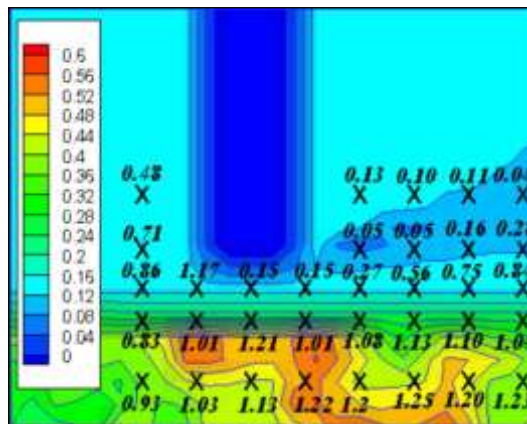
(c)

Figure 7-25. Distributions of average velocities normalized by the bulk velocity, the contour lines, and equivalent bed geometries for experimental conditions of $B_f/0.5B = 0.63$, and $L/B_f = 0.63$ (a), 0.75 (b), and 1.00 (c)
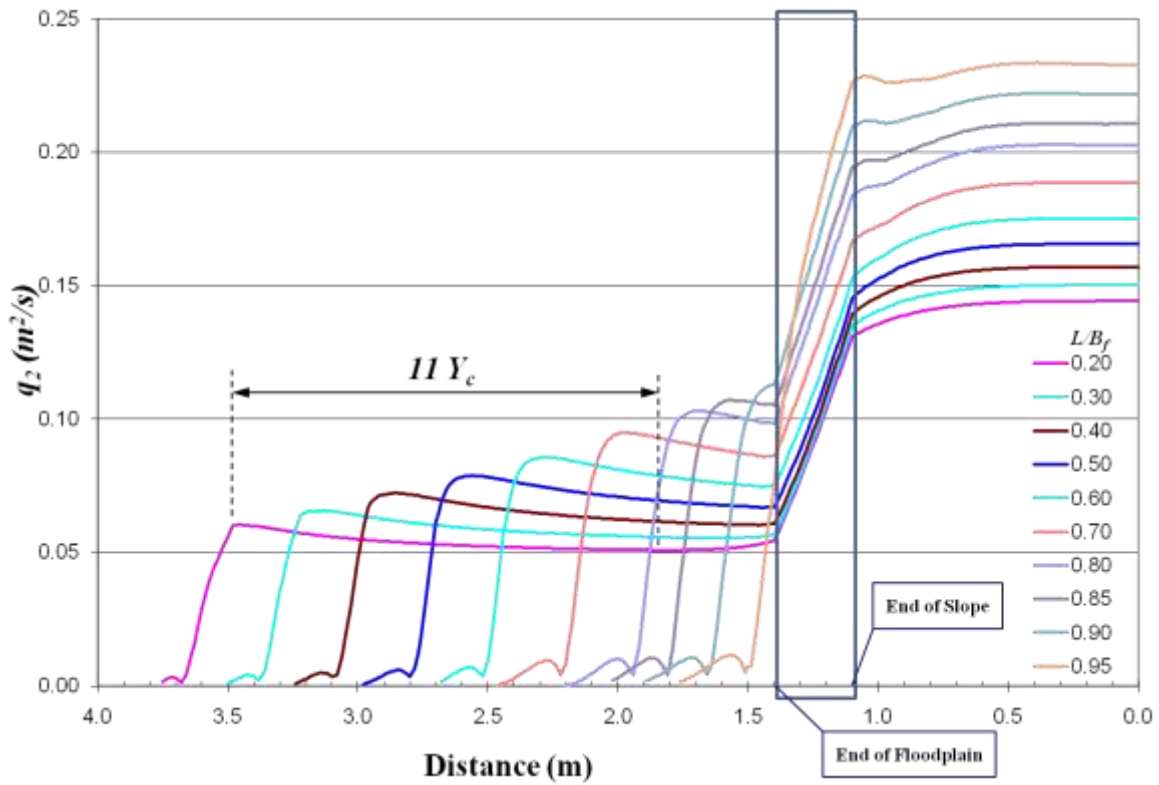
Figure 7-26. Numerical simulation (FESWMS) results for transverse distributions of unit discharge at the abutment axis, q_2, versus distance across the compound channel for varying values of L/B_f. Here, distance is measured from the flume wall opposite the abutment. The range $11Y_c$ is discussed in Section 11.5
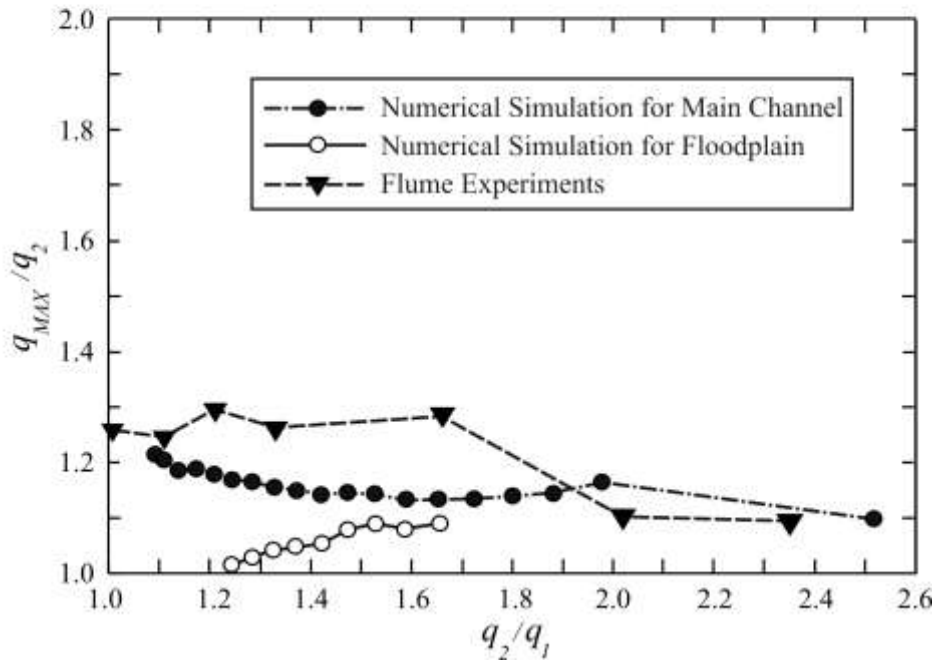
Figure 7-27. Variations of q_{MAX}/q_2 with q_2/q_1, as obtained from the numerical simulation and flume experiments

CHAPTER 8

LABORATORY RESULTS FOR SCOUR CONDITION A AT WING-WALL ABUTMENTS

8.1 Introduction

This chapter presents the laboratory data and observations on scour and flow field at wing-wall abutments subject to Scour Condition A. The flume experiments simulated wing-wall abutments located at the main-channel bank of a compound channel, the common location for wing-wall abutments. For this layout, the abutment's earthfill approach embankment extends fully across the floodplain to the abutment column. Accordingly, $L/B_f > 1.0$, for these experiments (Figure 2-2). A few additional experiments were conducted with the approach embankment extended into the main channel. These experiments enable extrapolation of scour data for q_2/q_1 values greater than those developed by the abutment located at the edge of the floodplain.

As for the experiments conducted with the spill-through abutments, the floodplain of the compound channel was treated as being either fixed (relatively erosion resistant) or erodible. For the erodible floodplains, the wing-wall abutments were supported on circular piles, as shown in Figure 6-5, and the simulated earthfill embankment was covered by a layer of riprap stone. Additional experiments also were run simulating wing-wall abutments supported by sheet piles: The principal variables measured during the experiments are indicated in Figure 8-1.

The results obtained with the model layout comprising unprotected (no riprap) wing-wall abutments on erodible floodplains are presented in Chapter 10, which discusses scour at exposed abutment columns. Chapter 11 presents further data for Scour Condition A for the layout situation when a pier is located adjacent to a wing-wall abutment.

8.2 Scour-Depth Trends

The trends for maximum scour expressed in terms of flow depth, Y_{MAX}, are given here for fixed wing-wall abutments founded on a fixed floodplain, pile-supported abutments, and abutments supported on sheet piles. Table 8-1 summarizes the scour-depth data.

8.2.1 Wing-Wall Abutment on Fixed Floodplain

Figure 8-2 presents the scour data as Y_{MAX}/Y_C versus q_2/q_1, for the wing-wall abutments located on a fixed floodplain. For the purposes of comparison, Figure 8-2 includes an envelope delineating the Y_{MAX}/Y_C data determined for the spill-through abutments (see Figure 7-3).

The figure gives the following insights regarding scour-depth trends:

1. The data for the wing-wall abutment adhere to the same trend shown in Figure 7-3 for Scour Condition A at spill-through abutments. Collectively, the data for the wing-wall and spill-through abutments conform to the conceptual curve shown as Figure 4-5 (Chapter 4) for Y_{MAX}/Y_C versus q_2/q_1;

2. The largest value of Y_{MAX}/Y_C for the wing-wall abutments, however, is slightly larger than that for the spill-through abutments, for the present range of experiments;

3. As obtained for the spill-through abutments, the sharp increase in Y_{MAX}/Y_C values for small q_2/q_1 is attributable to scour caused by the flow field locally around the abutment, and by the passage of dune troughs along the main channel. The estimated value of long-contraction scour (Y_C) is small;

4. When extrapolated to $q_2/q_1 \approx 1$ for the limiting condition of a finite-length abutment in a very wide channel, the peak value obtained for the Y_{MAX}/Y_C data aligns with the estimate $1.81C_{TA}$ given by Eq. (4-32), especially if the turbulence coefficient C_{TA} is not much larger than 1;

5. As $B_f/0.5B$ increases (with the abutment extending to the floodplain toe), flow contraction increases to the extent that, eventually with increasing q_2/q_1, scour is largely attributable to flow contraction. Accordingly, values of Y_{MAX}/Y_C then approached unity; and,

6. For $q_2/q_1 = 2.49$, the biggest value tested, the value of Y_{MAX}/Y_C is about 1.1. The trend for yet larger values of q_2/q_1 is for Y_{MAX}/Y_C to remain at about this value, as is the case for spill-through abutments.

8.2.2 Pile-Supported Wing-Wall Abutment on Erodible Floodplain

When the pile-supported wing-wall abutment, with riprap armored embankment, was placed on an erodible floodplain, scour deepened at two to three locations, giving local maximum values of Y_{MAX}/Y_C as indicated in Figure 8-3. The maxima were consequent to three scour processes:

1. In the main channel, just out from the wing-wall abutment, as occurred for scour at abutments on the fixed floodplains;

2. Immediately at the front of the wing-wall abutment, when the main-channel bank eroded; and,

3. Immediately downstream of the abutment, when its approach embankment breached.

The occurrence of the three scour-depth maxima depended on the extent of flow contraction (i.e., q_2/q_1) around the abutment. The overall maximum scour depth developed at the front of the abutment, except for the case of greatest flow contraction. For this latter case, the scour region was sufficiently extensive so that more-or-less the same scour depth occurred at the three locations. For the experiments, the embankment breached immediately behind the abutment. Because the scour depths were greater than those for the spill-through abutments, scour at the wing-wall abutments resulted in the complete collapse and breach of the embankment immediately at the abutment.

An important mechanism contributing to embankment failure and breaching was erosion of embankment sediment from beneath the pile cap. This mechanism, not observed for the spill-through abutments, is illustrated in Section 8.3. The depth of scour at the front of the abutment quickly progressed to a level below the pile cap, and exposed the piles.

Figure 8-4 presents the values of Y_{MAX}/Y_C versus q_2/q_1 for the pile-supported wing-wall abutments located on an erodible floodplain. The data in this figure show somewhat reduced scour depths compared to scour at wing-wall abutments (and spill-through abutments) on fixed floodplains, and the resulting scour bathymetries reflect the effect of combined Scour Conditions A and B. Floodplain erosion around the abutment, and failure of the embankment side slope increased the cross-sectional area of flow passed the abutment. The greatest reduction in Y_{MAX}/Y_C occurred for the widest floodplain ($B_f/0.5B = 0.63$), because this layout resulted in the largest breach through the embankment. When $B_f/0.5B = 0.23$ and 0.43, the three local maxima occurred for Y_{MAX}. However, when $B_f/0.5B = 0.63$, the flow depth at the three maxima was practically the same, because scour was dominated by flow contraction. The largest value of Y_{MAX} is used in Figure 8-4 for each experiment. The scour depths, though, were larger than obtained with the spill-through abutments on erodible floodplains (see Figure 7-4).

8.2.3 Sheet-Pile-Supported Abutment on Erodible Floodplain

Figure 8-5 indicates the same Y_{MAX}/Y_C trend for wing-wall abutments supported by sheet piles as does Figure 8-4 for pile-supported abutments. However, the magnitudes of Y_{MAX}/Y_C exceed those for pile-supported abutments. This result was because sheet-piling helped retain the embankment sediment immediately behind and below the abutment, thereby preventing erosion of sediment from beneath the pile cap. In so doing, the sheet piles prevented or retarded breaching of the embankment immediately behind the abutment. When $B_f/0.5B = 0.63$, the embankment did breach, though.

The data in Figure 8-5 align very closely with the data for the wing-wall abutments on fixed floodplains. The values of Y_{MAX} did not increase when the embankment was lengthened. However, this apparent trend is based on only three data, and does not take into account the effect of embankment breaching on scour development when $B_f/0.5B = 0.63$. Embankment breaching relieved flow around the abutment, and resulted in a lesser scour depth. To determine scour depth when the embankment did not breach (as could be the case for an embankment formed from compacted earthfill more erosion resistant than the floodplain) this test was continued with a breach-prevention plate placed in the center of the embankment. The resulting scour was deeper than when the embankment breached, as indicated in Figure 8-5.

Together, Figures 8-5 and 8-4 provide the following information on scour depth at wing-wall abutments on an erodible floodplain:

1. The values of Y_{MAX}/Y_C follow essentially the same trend as shown in Figure 8-3 for wing-wall abutments on a fixed floodplain;

2. The values also follow the conceptual trend indicated in Figure 4-5;

3. The values of Y_{MAX}/Y_C for the abutments on sheet piles are practically the same as for the abutments on fixed floodplain. The abutments on piles produced lesser maximum values of Y_{MAX}/Y_C, principally because of embankment breaching.

4. A check on the temporal development of scour in front of the abutment, for $B_f/0.5B = 0.63$, revealed that, for the abutment on sheet piles, scour became deeper before the embankment breached than was the case for the abutment on piles. The time to breaching limited the time available for scour deepening. This point is discussed further in Chapter 9.

8.2.4 Comparison with ABSCOUR

The ABSCOUR method (Chang and Davis, 1998, 1999) produces scour depth estimates and values of Y_{MAX}/Y_C exceeding those shown in Figure 8-2, 8-4, 8-5. This finding can be attributed to several factors, notably the different model-abutment constructions upon which ABSCOUR is based. The closest comparisons occur for small values of q_2/q_1; e.g., when $q_2/q_1 = 1.32$, ABSCOUR indicates $Y_{MAX}/Y_C = 2.67$, when $k_f = 1$, whereas the data point for a wing-wall abutment on sheet piles in an erodible floodplain is $Y_{MAX}/Y_C = 1.76$ (Figure 8-5).

8.3 Observations of Scour at Wing-Wall Abutments

Presented here are observations of equilibrium scour forms and the development of scour at wing-wall abutments subject to Scour Condition A in compound channels.

8.3.1 Wing-Wall Abutment on Fixed Floodplain

The wing-wall abutments on the fixed floodplains produced essentially the same scour bathymetry as did the spill-through abutments on fixed floodplains, except the scour depths were somewhat larger. Figures 8-6 and 8-7 depict the resultant equilibrium scour region developed with the wing-wall abutment on a fixed floodplain when $B_f/0.5B = 0.43$ and 0.63. The bathymetry measurements corresponding to the layout $B_f/0.5B = 0.63$, given in Figure 8-8, show that the maximum scour occurred in front of the abutment and that substantial scour of the entire main-channel bed occurred. The line drawn in Figure 8-7b indicates the overall lowering of the bed. The overall scour form is similar to that shown in Figure 7-7 for the spill-through abutment in an equivalent layout. This observation holds also for $B_f/0.5B = 0.23$ and 0.63.

A pronounced feature of the scour region for both abutment forms is the enlarged dunes that developed in the scour region as q_2/q_1 increased, which remained stationary once formed. Upstream of the abutment, when $B_f/0.5B = 0.63$, the dunes averaged a 90-mm wave length and a 76-mm height. The dunes in the region of greatest flow contraction were 1.40-m long and 120-mm high.

8.3.2 Pile-Supported Wing-Wall Abutment on Erodible Floodplain

Scour at the pile-supported wing-wall abutments progressed essentially in the same manner as for the pile-supported spill-through abutments on erodible floodplains. One difference is that the width of embankment breach behind wing-wall abutments typically was wider than for spill-through abutments. This difference is attributable to the greater breadth of wing-wall abutments.

Figure 8-9 depicts the resultant equilibrium scour region formed by flow at the wing-wall abutment on cap and piles. This figure is a view from upstream of the abutment. As mentioned above, a feature of scour is the breaching of the embankment behind the wing-wall abutment. Most riprap stone spilled into the scour area at the base of the abutment. Also evident in the figures are dunes about 1.0-m long and 0.9-m high. Figures 8-10 and 8-11 show much of the same features evident in Figure 8-9, with the exception that the extent of scour increased across the main channel as the abutment lengthened. The lines drawn in Figures 8-10 and 8-11 show how the bed was lowered by flow contraction.

The bathymetry measurements corresponding to the photographs in Figures 8-9 through 8-11 are shown in Figures 8-12a-c. The black dots indicate the presence of riprap stone. The measurements show that the maximum depth of scour occurred at the front of the abutment.

The observations of scour development show that scour began at the abutment's upstream corner, and then evolved around the abutment. The sequence of photographs in Appendix B2 illustrates the time development of scour in greater detail. In particular, it illustrates the geotechnical failure of the embankment at the abutment's upstream corner, a common feature of scour at wing-wall abutments. It is useful, in this respect to observe how well the failure process illustrated in Appendix B2 compares with the actual abutment case illustrated in Figure 3-6.

As scour deepened sufficiently to expose the piles beneath the abutment pile cap, sediment was eroded from the core of the embankment below the pile cap. This mechanism has not been reported heretofore, largely because it is difficult to observe. It occurred as follows. As the scour deepened to below the pile cap and exposed the piles, the embankment's earthfill was eroded out from beneath the pile cap. Gradually, a cavity developed within the embankment, undermining the embankment immediately behind the abutment. This development is depicted in Figures 8-13a-c. Eventually scour deepening caused the embankment side slopes to become unstable and slide into the scour hole, whence sediment was removed by the flow. As the embankment collapsed, the flow passed around the exposed abutment and resulted in a scour form somewhat similar to that observed at the failed bridge depicted in Figure 3-6.

8.3.3 Sheet-Pile-Supported Wing-Wall Abutment on Erodible Floodplain

The scour forms associated with the sheet-pile-supported wing-wall abutments are virtually the same as those when the abutments were pile-supported, except that the sheet piles blocked the erosion of sand from behind the abutment column, and retarded embankment breaching. This effect, portrayed in Figure 8-14, enabled the scour to develop deeper than when the abutment was pile-supported. The commensurate bathymetry is given in Figure 8-15.

When the embankment behind the wing-wall abutment on sheet piles breached, it did so in a way that differed somewhat from that for the abutment on piles. Breaching of the sheet-pile-supported abutment only occurred when $B_f/0.5B = 0.63$. Because the sheet piles retained the embankment, riprap stone did not slide beneath the pile cap, but instead slid from the abutment's shoulders. This was a slow process. It took approximately 20 hours for the sheet-pile-supported abutment to breach, in contrast to about 1 hour for the pile-supported abutment to breach.

The scour bathymetries obtained with the sheet-pile-supported abutments are summarized in Figure 8-16, which also presents photos of the resulting scour forms. These results are compared further in Figure 8-17 with the bathymetries obtained with the wing-wall abutment on piles. The following features emerged from Figures 8-17:

1. The scour bathymetry reflects the innate combination of contraction scour and local scour characteristic of abutment scour as short-contraction scour;

2. Scour was accompanied by changes in dune dimensions, as evident in Figures 8-15a, d, and e, especially between the channel center (bottom of each figure) and the nose of the wing-wall abutment;

3. For the sheet-pile-supported wing-wall abutments, Y_{MAX} occurred close to the abutment, and always in front of the abutment. This observation commonly held for the pile-supported abutments, though occasionally was at their downstream corner;

4. Embankment breaching occurred when $B_f/0.5B = 0.23$, 0.43 and 0.63 for the wing-wall abutment on piles. It occurred when $B_f/0.5B = 0.63$ for the wing-wall abutment on sheet piles; and,

5. When an embankment breached, scour also developed behind the embankment. For some cases, this scour was almost as deep as at the front of the abutment.

8.4 Flow-Field Observations

Observed from above, the flow around the wing-wall abutments had the same overall features of flow contraction, along with turbulence generation and dispersion, as did the flow around the spill-through abutments (see Section 7.4). For example, Figures 8-18a-d show the initial and the

eventual flow fields around the pile-supported wing-wall abutment when $B_f/0.5B = 0.63$. These figures illustrate how flow initially contracted around the abutment, then relaxed as scour developed, especially once the embankment breached. The flow field for the equilibrium scour resembles flow around a spill-through abutment with adjacent pier. This flow field is discussed further in Chapter 11.

Table 8-1. Data summary for wing-wall abutments on fixed floodplains

						Bed-form Height	Bed-form Length
			Y_{MAX}	Y_C		H	λ
$B_f/0.5B$	L/B_f	q_2/q_1	(m)	(m)	Y_{MAX}/Y_C	(m)	(m)
0.63	1.12	2.49	0.59	0.54	1.09	0.08	0.91
0.63	1.12	2.49	0.62	0.54	1.14	0.10	1.02
0.43	1.18	1.56	0.62	0.44	1.40	0.12	1.17
0.23	1.33	1.32	0.63	0.37	1.71	0.09	1.06
0.23	1.33	1.32	0.62	0.37	1.67	0.09	1.06
0.00	0.00	1.00	0.30	0.30	1.00	0.09	1.07
$B_f/0.5B = 0$, with $B_m/B = 0.95$		1.12	0.49	0.31	1.61	0.09	1.07

Fixed Floodplain (title row, first table)

Riprap-Protected Embankment on Erodible Floodplain — Abutment Column on Piles							
0.63	1.12	2.49	0.62	0.54	1.15	0.07	0.61
0.43	1.18	1.56	0.53	0.44	1.41	0.10	1.02
0.23	1.33	1.32	0.57	0.37	1.54	0.09	1.07
0.23	1.33	1.32	0.56	0.37	1.52	0.09	1.06
0.00	0.00	1.00	0.30	0.30	1.00	0.09	1.07

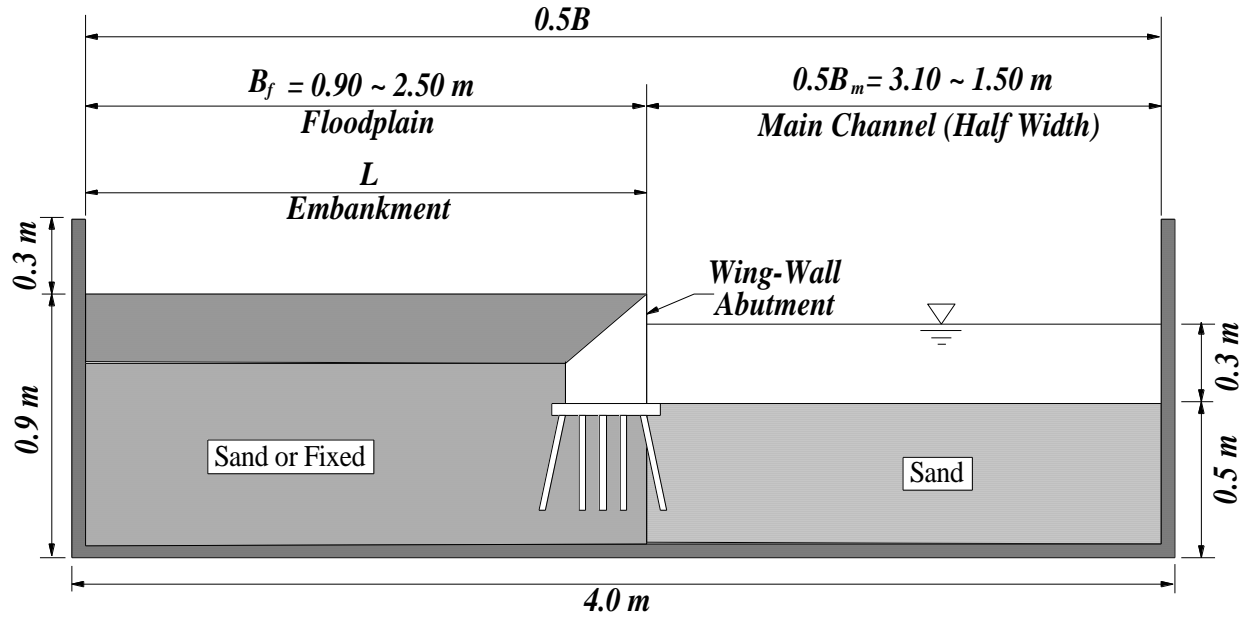| Riprap-Protected Embankment on Erodible Floodplain — Abutment Column on Sheet Piles							
0.63	1.12	2.49	0.62	0.54	1.07	0.08	0.90
0.43	1.18	1.56	0.62	0.44	1.42	0.13	1.20
0.23	1.33	1.32	0.65	0.37	1.76	0.08	1.20
0.00	0.00	1.00	0.15	0.15	1.00	0.09	1.07

Figure 8-1. Principal variables measured for wing-wall abutments subject to Scour Condition A, scour of the main-channel bed adjoining a much more erosion-resistant floodplain
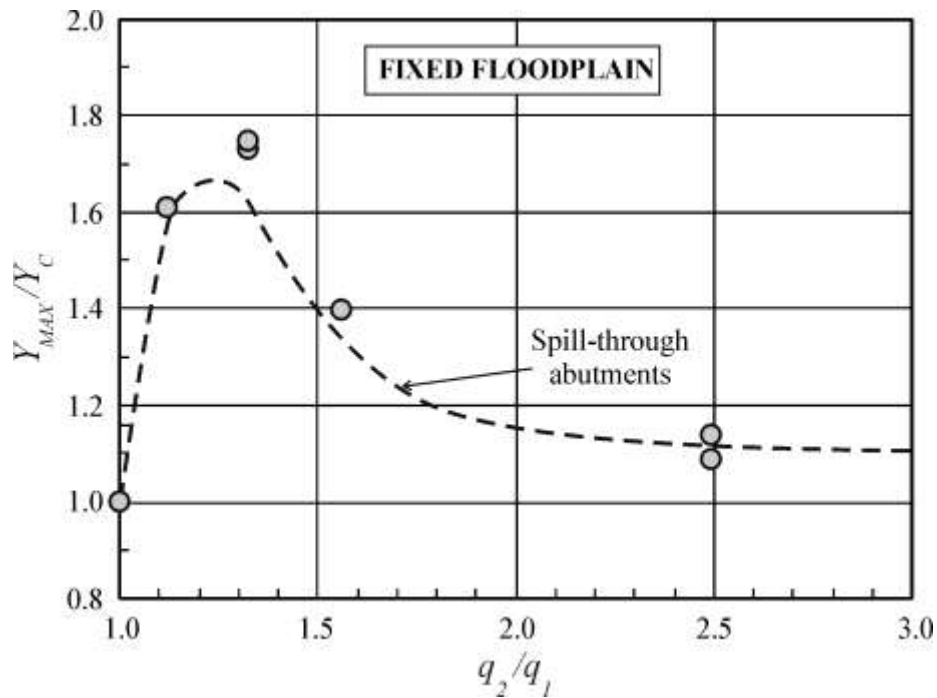

Figure 8-2. Variation of normalized maximum scour depth, Y_{MAX}/Y_C, for wing-wall abutments on fixed floodplains (Scour Condition A). Also shown is an envelope encompassing the data obtained for the spill-through abutments on fixed floodplains
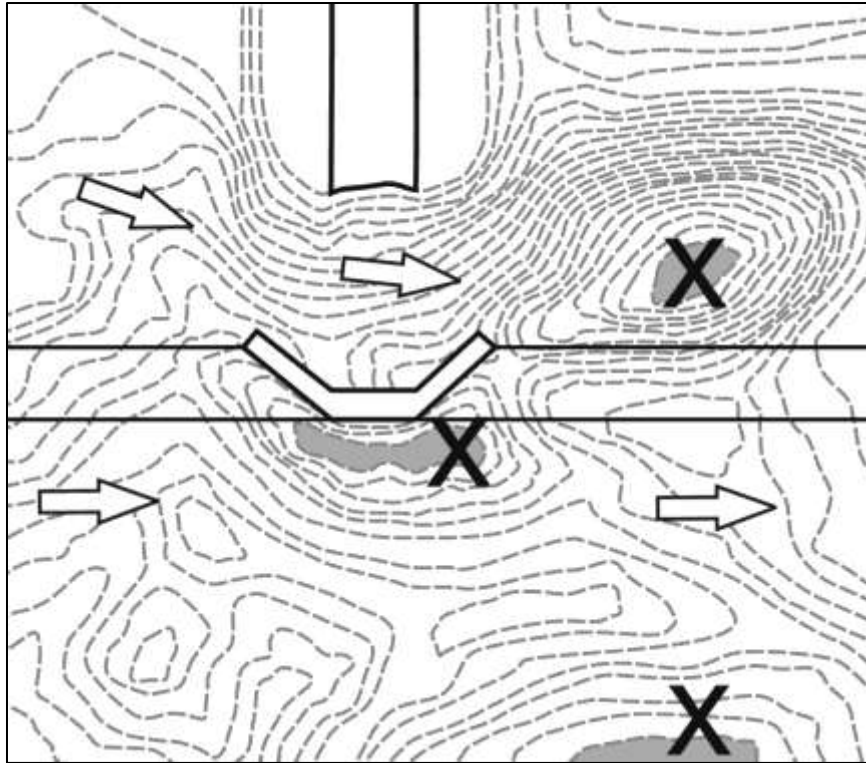
Figure 8-3. Three local maxima (X) of scour depths - Scour Condition A developed before the embankment breached, and then two scour-depth maxima developed downstream of the abutment once the embankment breached
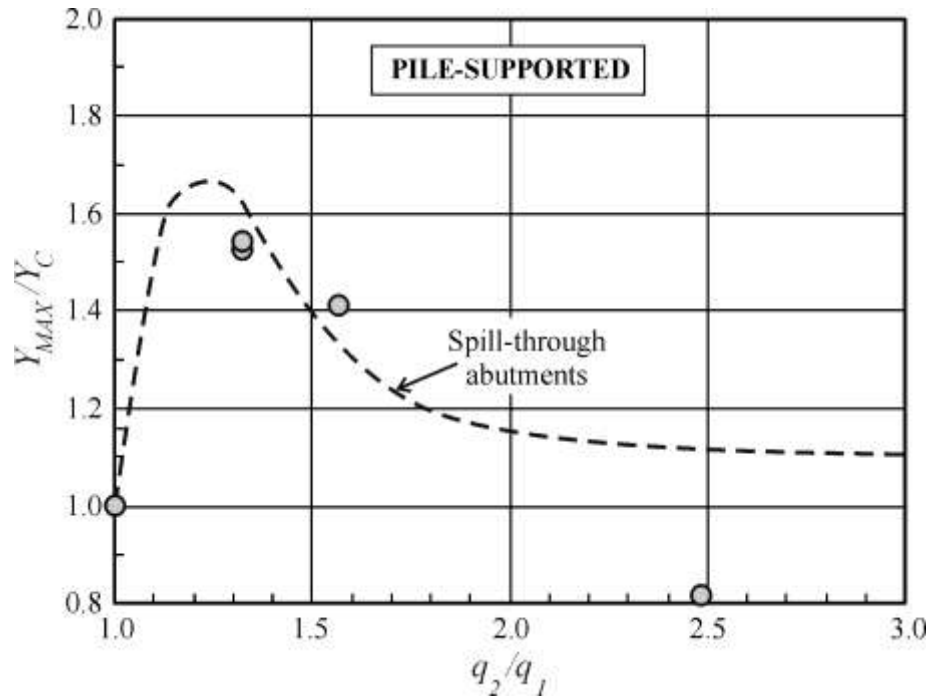
Figure 8-4. Variation of normalized maximum scour depth, Y_{MAX}/Y_C, for pile-supported, riprap-protected, wing-wall abutments on erodible floodplains (Scour Condition A). Also shown is an envelope curve (from Figure 7-3) encompassing the data obtained for the spill-through abutments on fixed floodplains

Figure 8-5. Variation of normalized maximum scour depth, Y_{MAX}/Y_C, for sheet-pile-supported wing-wall abutments on erodible floodplains (Scour Condition A). Also shown is an envelope curve (from Figure 7-3) encompassing the data obtained for the spill-through abutments on fixed floodplains
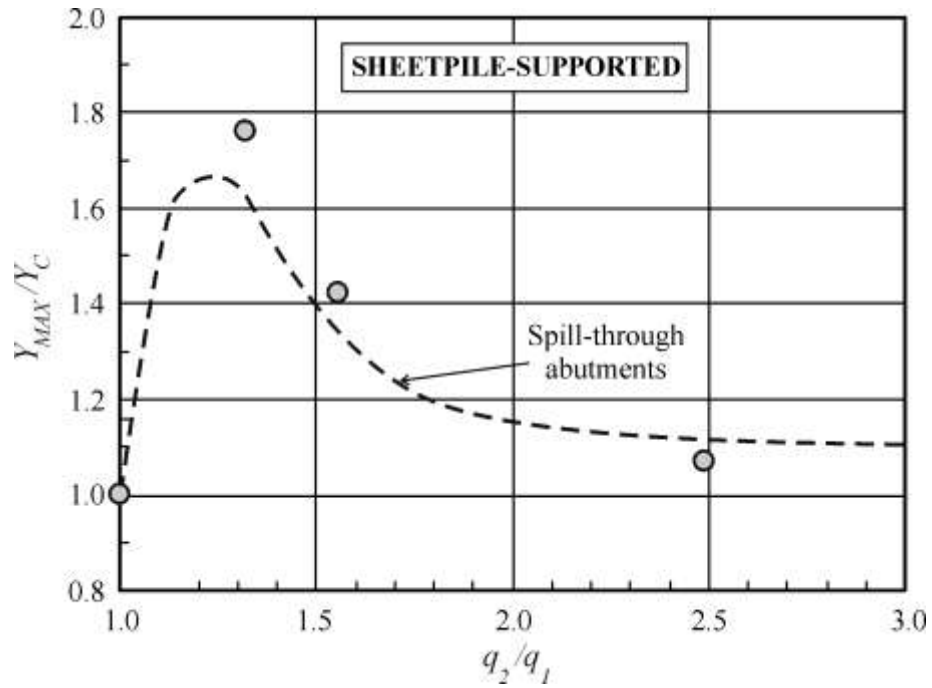
(a)

(b)

Figure 8-6. Scour hole around wing-wall abutment on a fixed floodplain with $B_f/0.5B = 0.43$; a view from the upstream side (a), and a view from the above (b)

(a)

(b)

Figure 8-7. Sour hole of wing-wall abutment on fixed floodplain with $B_f/0.5B$ = 0.43; a view from the upstream side (a), and a view from the above (b). The dark line indicates the initial bed elevation
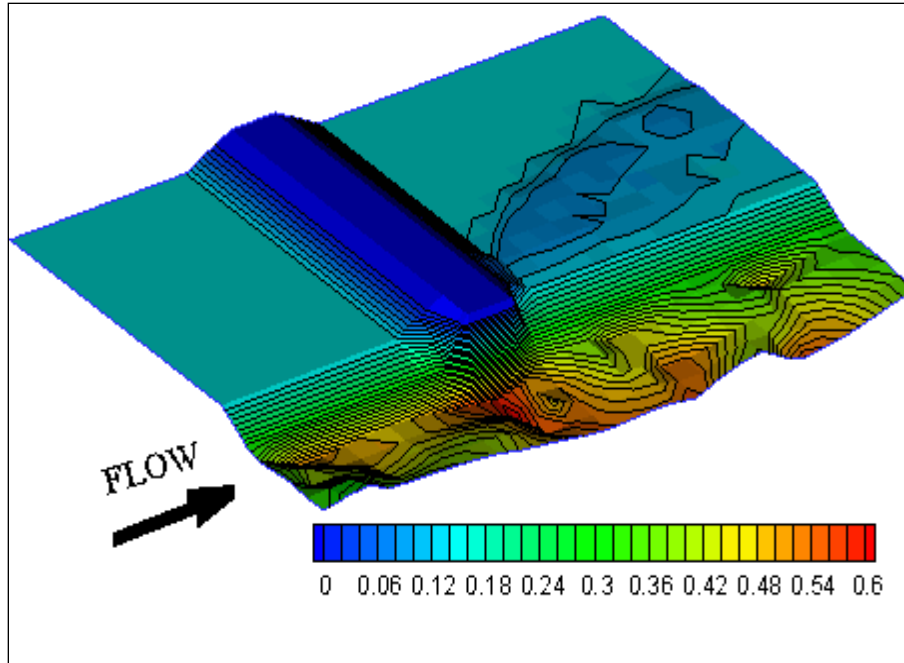
Figure 8-8. Bathymetry of resulting scour hole of wing-wall abutment on fixed floodplain with $B_f/0.5B = 0.63$. The scale represents elevation in meters

(a)

(b)

Figure 8-9. Scour hole developed at pile-supported, wing-wall abutment on erodible floodplain with $B_f/0.5B = 0.23$; a view from the upstream side (a), and a view from the abutment's front side (b)

(a)

(b)

Figure 8-10. Scour hole developed at pile-supported, wing-wall abutment on erodible floodplain with $B_f/0.5B = 0.43$; a view from the abutment's upstream corner (a), and, a view from the above (b)
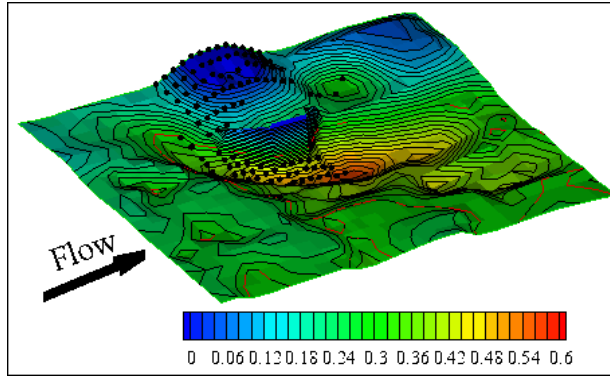
(a)

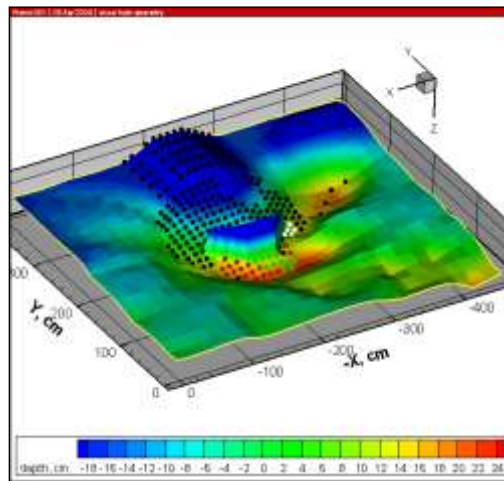

(b)

Figure 8-11. Scour hole developed at pile-supported, wing-wall abutment on erodible floodplain with $B_f/0.5B = 0.63$; a view of the upstream side (a), and a view from the above (b)

(a)

(b)
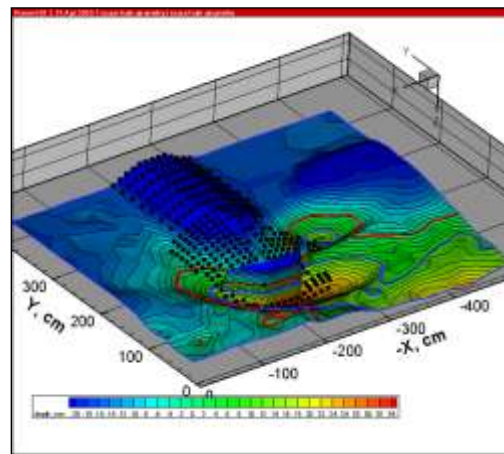
(c)

Figure 8-12. Bathymetry plots; measurements corresponding to photographs in Figures 8-9(a),
Figure 8-10(b), and Figure 8-11(c)
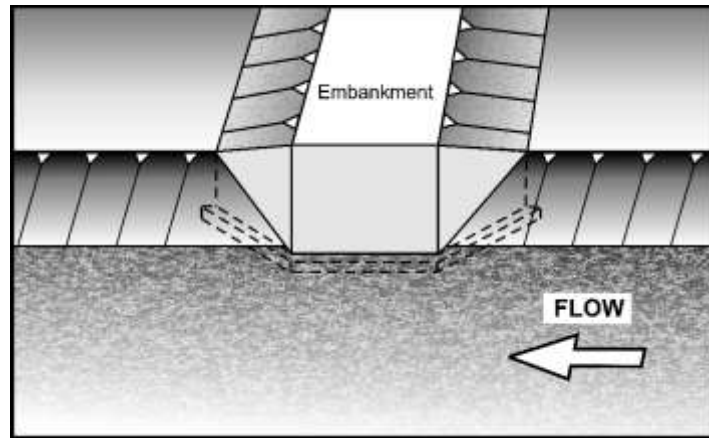
(a)
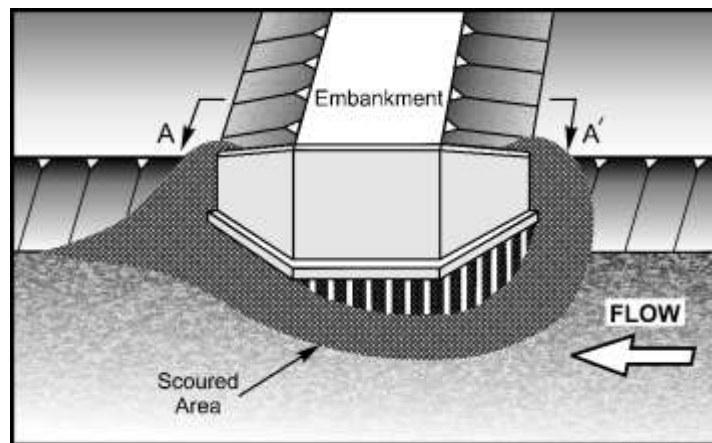
(b)
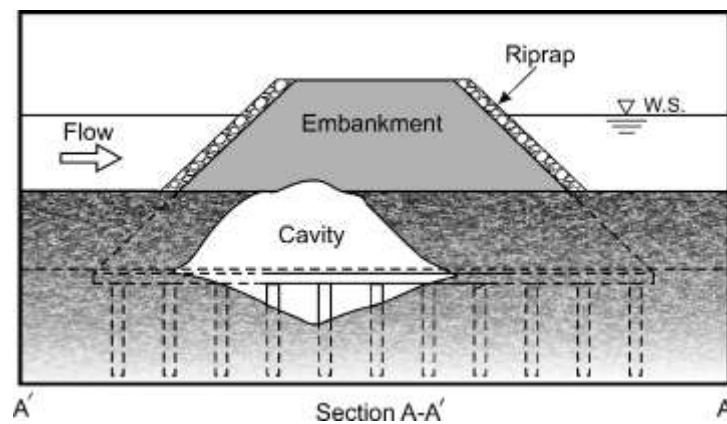
(c)

Figure 8-13. As scour exposes piles (a)-(b), embankment soil may be removed under the pile cap, forming a cavity behind the pile cap (c)

(a)

(b)

Figure 8-14. Resulting scour hole of wing-wall abutment on sheet piles with $B_f/0.5B = 0.23$; a view of the upstream side (a), and a view from the downstream side (b)
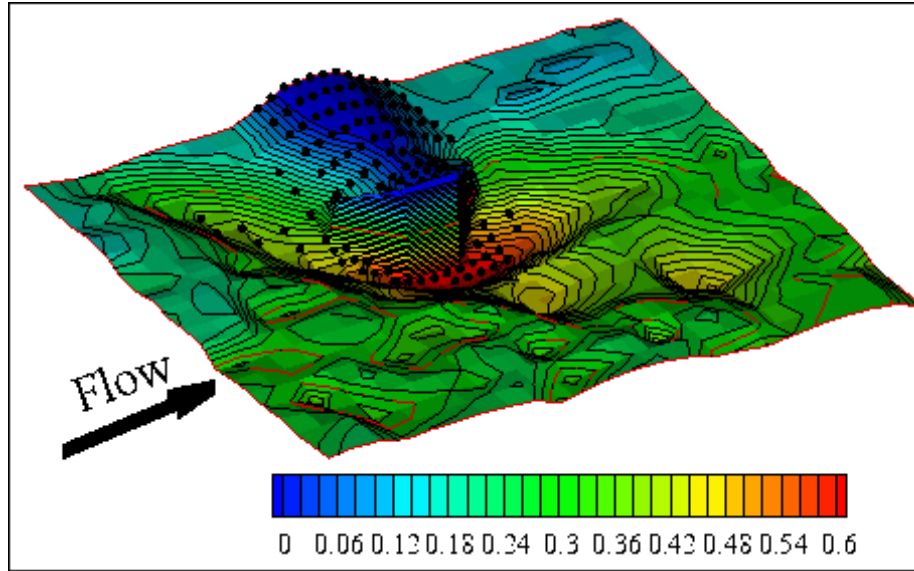
Figure 8-15. Contour plot of resulting scour hole of wing-wall abutment on sheet piles with B_f $/0.5B = 0.23$

Measured Scour Bathymetry	Scour Photos
(a-i) $B_f/0.5B = 0.23$	(a-ii) $B_f/0.5B = 0.23$
(b-i) $B_f/0.5B = 0.43$	(b-ii) $B_f/0.5B = 0.43$
(c-i) $B_f/0.5B = 0.63$	(c-ii) $B_f/0.5B = 0.63$
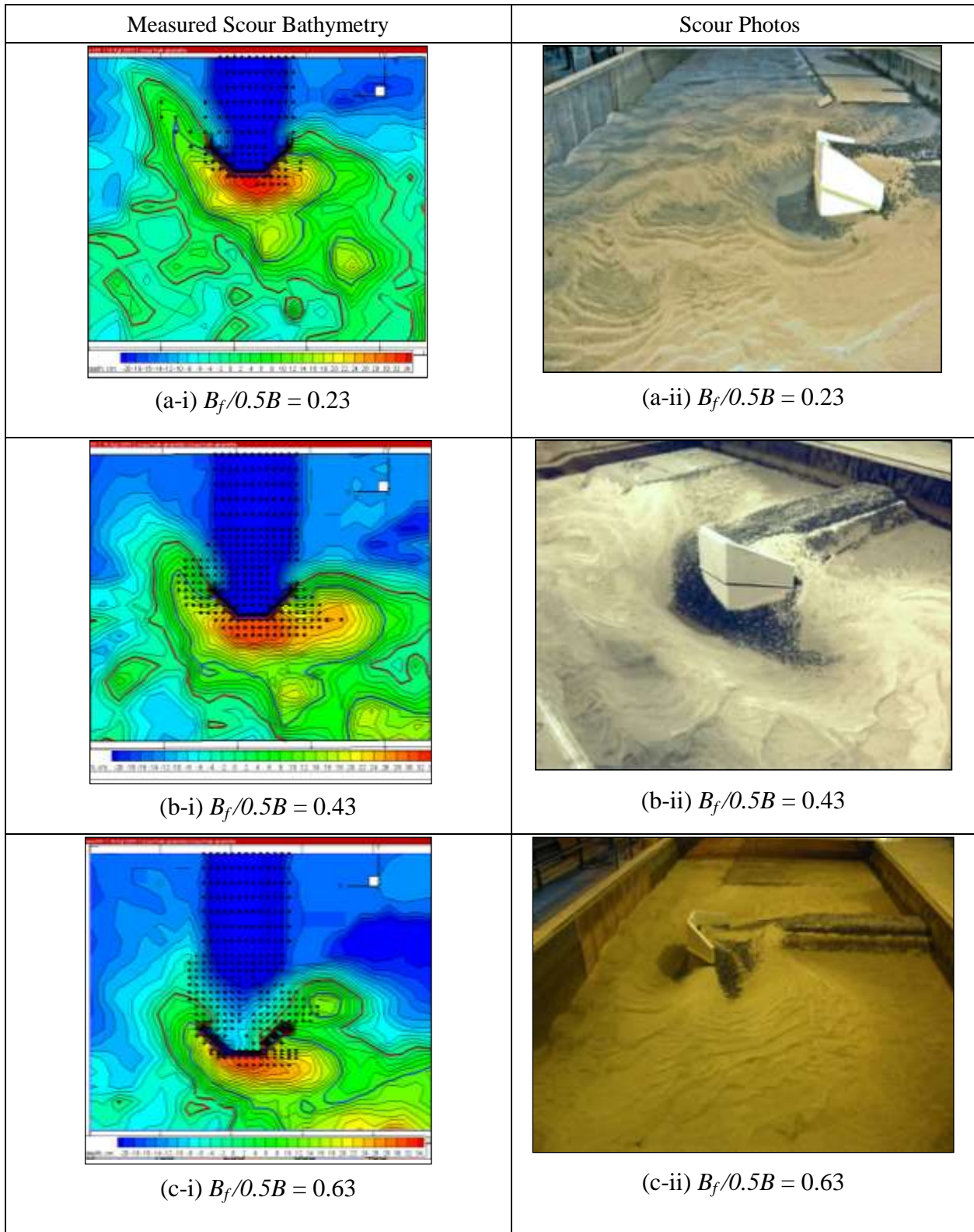
Figure 8-16. Resulting scour holes for sheet-pile-supported, wing-wall abutments on erodible floodplains; $B_f/0.5B = 0.23$(a), 0.43 (b), and 0.63 (c)

Capped Piles	Sheet Piles
(a-i) $B_f/0.5B = 0.23$	(a-ii) $B_f/0.5B = 0.23$
(b-i) $B_f/0.5B = 0.43$	(b-ii) $B_f/0.5B = 0.43$
(c-i) $B_f/0.5B = 0.63$	(c-ii) $B_f/0.5B = 0.63$
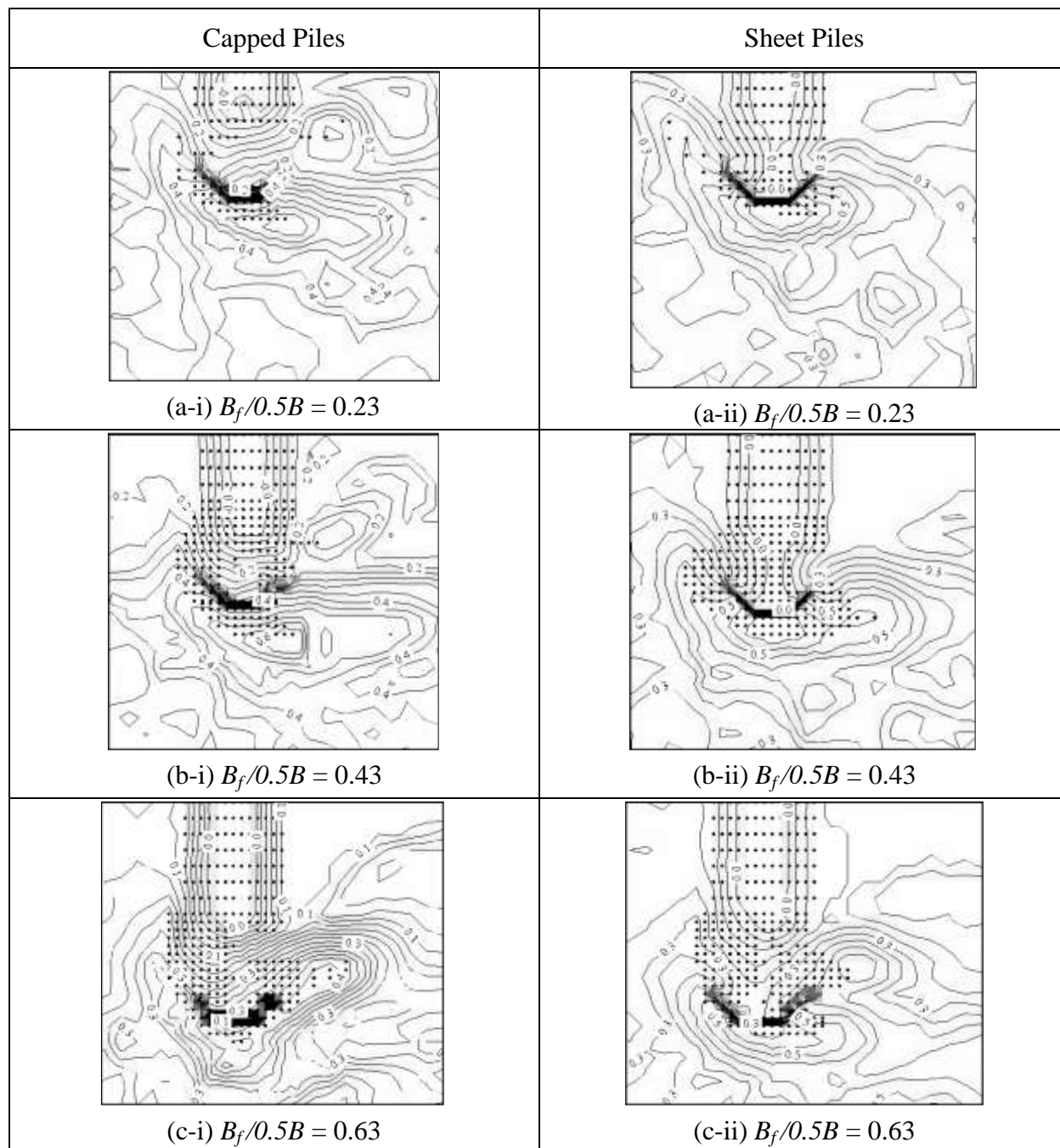
Figure 8-17. Contour plots of resultant scour geometry under Scour Condition A with capped piles and sheet piles; $B_f/0.5B$ = 0.23 (a), 0.43 (b), and 0.63 (c). Contours are drawn from water surface at a contour interval of 0.05 m.
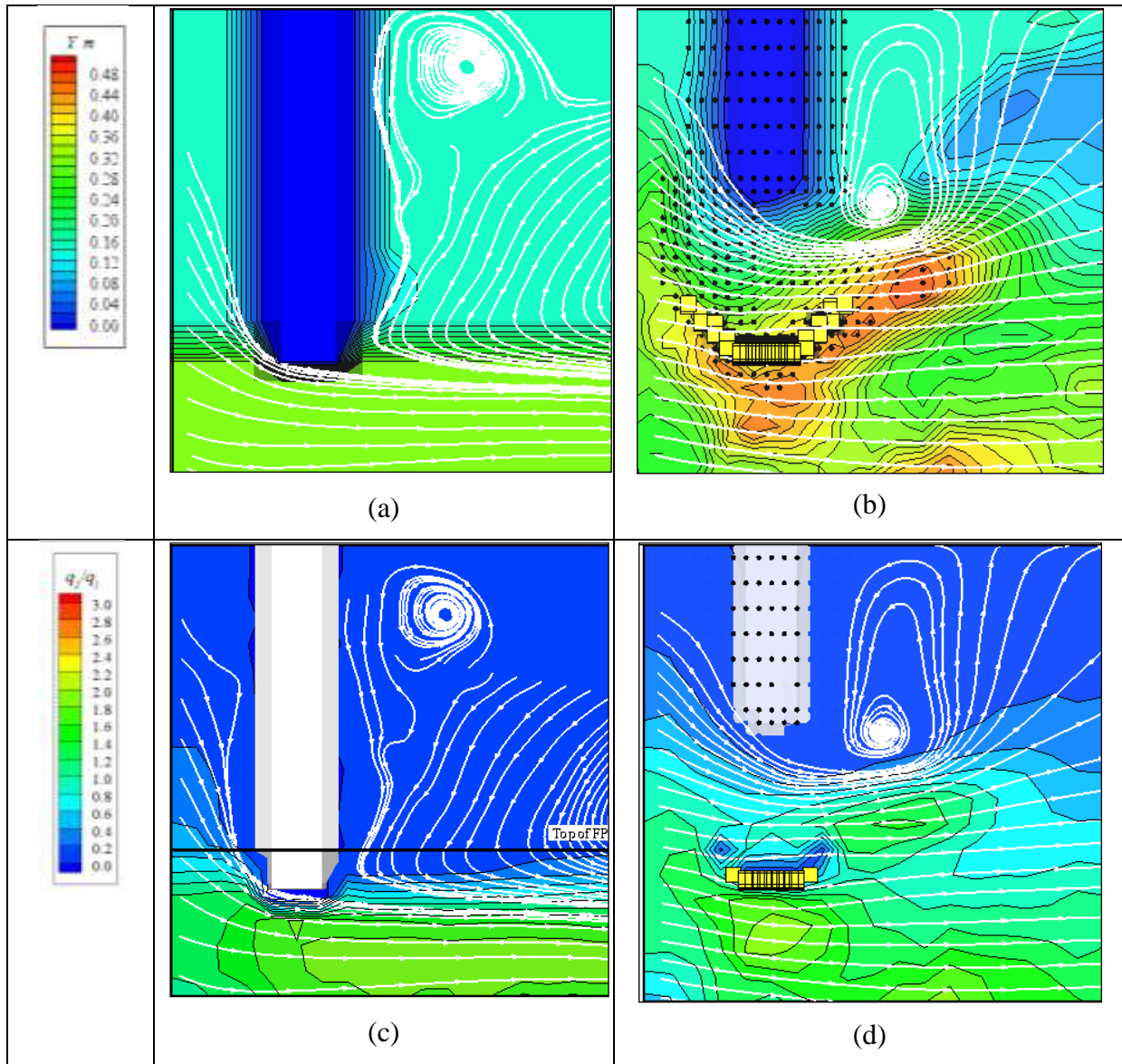
Figure 8-18. Flow fields around wing-wall abutment with $B_f/0.5B = 0.63$; flow pathlines and bathymetry at pre-scour condition (a), pathlines and bathymetry at equilibrium condition (b), pathlines and distribution of q_2/q_1 at pre-scour condition (c), and pathlines and bathymetry at equilibrium condition (d)

CHAPTER 9

LABORATORY RESULTS FOR SCOUR CONDITION B AT SPILL-THROUGH AND WING-WALL ABUTMENTS

9.1 Introduction

Scour Condition B is clear-water scour occurring when abutments are set well back on a floodplain or are in a rectangular channel. The two abutment situations are essentially the same, because flow around the abutments is essentially flow in a single channel, (not a compound) channel. Additionally, because most floodplain flows convey negligible sediment bedload over floodplains, it is assumed customarily that clear-water scour normally occurs at abutments and piers set well back on floodplains (e.g., Richardson and Davis, 1995; Melville and Coleman, 2000). Commensurate with this assumption, the present experiments were performed as clear-water scour.

This chapter describes the results of the flume experiments concerning scour at spill-through and at wing-wall abutments subject to Scour Condition B. As in Chapters 7 and 8, the results are presented in the sequence – scour-depth trends, observations and flow field. Because these two chapters show the scour trends for spill-through and wing-wall abutments to be essentially the same, this chapter presents the data obtained for both abutment forms. Figure 9-1 indicates the principal layout features and variables considered for abutments subject to Scour Condition B. Because $B_f \equiv 0.5B$, the abutment length parameter L/B_f can be restated as $L/0.5B$. Figure 4-1 indicates the general relationship between B_f and $0.5B$. Table 9-1 lists the scour-depth data obtained from the experiments.

9.2 Scour-Depth Trends

Figure 9-2 presents experimental relationships between the maximum flow depths Y_{MAX} and Y_C plotted versus the unit-discharge ratio q_{f2}/q_f, for the spill-through abutment and the wing-wall abutment. These relationships are practically the same as those found with Y_{MAX} and Y_C versus unit-discharge ratio q_{f2}/q_f in the case of Scour Condition A (see Figures 7-3 and 8-2). Here, q_f is

the average unit discharge of flow over the approach floodplain; q_{f2} is the average unit discharge through the bridge waterway at the abutment axis; Y_{MAX} is the maximum flow depth; and Y_C is calculated using Eq. (4-28), from Laursen's procedure (Laursen 1963).

To assess the depth-amplification factor, $\alpha_B = C_{TB}m_B^{6/7}$, expressed for Eq. (4-26), the ratio Y_{MAX}/Y_C is plotted in Figure 9-2 against the unit-discharge ratio q_{f2}/q_f for spill-through abutments and wing-wall abutments. This figure provides some important insights:

1. The data conform reasonably to the conceptual trend consistent with Figure 4-7, for varying abutment length in a channel of finite width;

2. At the lesser values of q_{f2}/q_f (and the flow contraction), Y_{MAX} substantially exceeds Y_C. Eventually, as the bridge waterway becomes more contracted, q_{f2}/q_f increases, and values Y_{MAX} approach Y_C. This portion of the trend reflects the dominance of scour caused primarily by flow contraction as opposed to that attributable to the local change in bed-form height in the contraction, combined with the turbulence generated by flow passing around the abutment and over the edge of the main-channel bank;

3. The values of Y_{MAX}/Y_C attain a maximum value of around 2.2 when $q_{f2}/q_f \approx 1.5$ for the spill-through abutments, and $Y_{MAX}/Y_C \approx 2.5$ when $q_{f2}/q_f \approx 1.1$ for the wing-wall abutments. These values are slightly larger than those of Scour Condition A shown in Figure 7-3 for spill-through abutments and Figure 8-2 for wing-wall abutments;

4. For the spill-through abutments, the Y_{MAX}/Y_C declines asymptotically to a value of about 1.1;

5. For the wing-wall abutments, Y_{MAX}/Y_C has the maximum value at the minimum unit-discharge ratio tested, then monotonically decreases to a level of about 1.4;

6. These results for the two abutment shapes (spill-through and wing-wall abutments) show almost the same trend when q_{f2}/q_f is larger than 1.5. However, when q_{f2}/q_f is smaller than 1.5, the value of Y_{MAX}/Y_C for the wing-wall abutment is greater than that for the spill-through abutment. This tendency shows that abutment shape becomes less important as

embankment length becomes longer. It is an influence mentioned by at least one earlier study (e.g., Dongol 1994);

7. The values of Y_{MAX} developed in the present rectangular channel were largely similar to those developed in the compound channel with erodible floodplain. This result is attributable to flow concentration during scour development. Flow concentration occurred for all the experiments in Scour Condition B; and,

8. An estimate of the peak value obtained using $Y_{MAX}/Y_C = 1.81C_{TB}$ (Eq. (4-33), $q_{f2}/q_f \rightarrow 0$, for the limiting condition of a finite-length abutment in a very wide channel can be extrapolated from the data:

   i. For the spill-through abutments, $Y_{MAX}/Y_C = 1.81C_{TB} \approx 2.0$

   ii. For the wing-wall abutments, $Y_{MAX}/Y_C = 1.81C_{TB} \approx 2.5$

   Here $Y_C = Y_1$, because no contraction scour occurs across the bridge waterway. The larger limiting value of Y_{MAX}/Y_C for the wing-wall abutments reflects the stronger turbulence generated by this bluffer form of abutment.

9.3 Geotechnical Limit to Maximum Scour Depth

As indicated in Chapters 7 and 8 for Scour Condition A, the maximum scour depth attainable at an abutment is limited by the geotechnical stability of the earthfill embankment at the abutment. For a given design flow, scour cannot deepen below this limit.

Figure 9-3 illustrates this limit in simple terms for an embankment formed of sand. As scour deepens, it reduces the stability of the earthfill embankment at the abutment, adjusting the embankment slope to its equilibrium slope. When the slope is exceeded, embankment material slides into the scour region (Figure 9-3a) and the flow transports it away. Further deepening leads to more slope instability and erosion, until eventually, the erosion extends to the abutment column. Because the cross section of flow increases (Figure 9-3b), further erosion results in breaching of the embankment and relaxation of the flow around the abutment.

It is possible to formulate the geotechnical limit to maximum scour depth. Figure 9-3 illustrates this limit. As indicated in Figure 9-3a, and found in the flume experiments, the location of deepest scour, d_{Smax}, was a radial distance, R, out from the abutment column. For the present study (and many abutment embankments), the constructed embankment slope was 2 horizontal to 1 vertical, such that the requirement for embankment slope stability, when the slope extends back to the abutment column, is

$$\theta_S = \tan^{-1}\left(\frac{E_H + d_{S\,max}}{R}\right) \tag{9-1}$$

where E_H is embankment height. Adjusting Eq. (9-1), gives an estimate for the limiting values of d_{Smax};

$$d_{S\,max} = R\tan\theta_S - E_H \tag{9-2}$$

The flume experiments showed that R varied with the abutment length parameter L/B_f (or essentially q_2/q_1), as indicated in Figure 9-4, which includes data from similar measurements reported by Melville et al. (2006) (and NCHRP Project 24-18) who studied the use of riprap aprons as an abutment-scour counter-measure. The two data sets are in reasonably good agreement. Melville et al. (2006) suggest for R,

$$\frac{R}{Y_f} = 4\left(\frac{L}{Y_f}\right)^{0.2} \tag{9-3}$$

Consequently, the limiting scour depth can be estimated as

9-4

$$d_{S\max} = 4\left(\frac{L}{Y_f}\right)^{0.2} Y_f \tan\theta_S - E_H \qquad\qquad (9\text{-}4)$$

In other words, the maximum scour depth at the abutment should not exceed the limit given by Eq. (9-4). Note that this limit can actually be attained, especially when θ_S is large, such as for an earthfill embankment formed of a compacted stiff clay. A larger scour depth leads to breaching of the embankment and flow relaxation through the bridge waterway (Figure 9-3b). As mentioned subsequently in Chapter 14, the limiting scour-depth analysis should be further investigated for a range of earthfill materials, along with varying combinations of compacted embankment earthfill and floodplain soils. The present Project was limited largely to uniform noncohesive sediment. The foregoing formulation of Eqs (9-1) through (9-4) is somewhat simplified, but is nonetheless indicative of how to estimate a limiting scour depth.

It could be noted for an analysis of abutment geotechnical stability that riprap presence does not enhance geotechnical stability. Riprap adds weight to the slope, but does not increase the shear strength of the earthfill forming the embankment.

For abutments on footing foundations, a limiting maximum scour-depth coincides with the undermining of the footing and the possible geotechnical collapse of the earthfill embankment behind the abutment column. This limit also could be formulated, at least in approximate terms. A formulation is not given here, but the photo shown subsequently in Figure 12-13a illustrates such a geotechnical collapse, and directly indicates how the formulation might be formulated.

9.4 Observations of Scour Processes and Bathymetry

The observations of Scour Condition B at spill-through abutments and wing-wall abutments show differences in the location of maximum scour for the two abutment forms.

Appendices B3 and B4 give visual records of scour development at riprap-protected, pile-supported spill-through and wing-wall abutments, respectively, subject to clear-water scour. Scour development at a riprap-protected, sheetpile-supported wing-wall abutment is illustrated in Appendix B5. A further sequence of photos in Appendix B6 illustrates the scour formed at a short, pile-supported wing-wall abutment.

9.4.1 Spill-Through Abutments

Figures 9-5a-d show overviews of the equilibrium scour condition associated with spill-through abutments for length parameter values $L/0.5B$ = 0.10, 0.30, 0.60, and 0.70. The following observations can be made from these figures:

1. The resulting scour forms were basically similar to those obtained with spill-through abutments placed on an erodible floodplain in a compound channel (Section 7.3.2). The deepest scour occurred immediately downstream from the abutment;

2. For relatively short abutments, the scour region was confined to around the abutment, with little or no scour occurring elsewhere in the channel;

3. As the length of the embankment, $L/0.5B$, increased, the scour region extended further across the channel. In effect, the plan dimensions of scour increased in scale as the abutment lengthened and the flow contraction increased. The lateral extent of scour is evident from the line drawn along the channel's centerline;

4. Also, as $L/0.5B$ increased, the size of the sand accumulation in the wake region behind the embankment became larger; and,

5. Also, as $L/0.5B$ increased beyond 0.60, the embankment breaches increased in width. As explained in Section 9.4, this effect occurred because the flow velocity (magnitude and angle) increased when $L/0.5B$ increased.

It is useful to look closely at scour development for a representative layout of abutment. In this respect, Figure 9-6 depicts the resultant equilibrium scour hole for a spill-through abutment with length parameter $L/0.5B = 0.50$. This photograph shows how scour at the upstream corner of the

abutment led to embankment failure there, and how riprap from the upstream side of the abutment failed and slid into the scour hole. The maximum depth of scour, though, developed adjacent to the abutment's downstream corner, and where flow contraction was greatest. Also, riprap stone in the scour hole partially armored the bed within the scour hole, and deflected the region of deepest scour further downstream.

The bathymetry measurements corresponding to Figure 9-6 are given in Figure 9-7. The black dots indicate riprap stone. The contour lines start from the water surface at 0 m with an increment of 0.015 m. The red curves indicate the bed level, 0.15 m below the water surface. Two black lines indicate cross sections at the embankment axis and at the location of the maximum scour, respectively. Figures 9-7a-b show a plan view and two cross sections of the channel bathymetry from Figure 9-6. The photograph in Figure 9-6 shows how local scour and contraction scour merge for abutments. If the conventional assumption of distinct contraction and local scour processes were correct, there would have been two scour-depth maxima: a maximum scour depth and a more-or-less uniform contraction scour depth across the channel. However, the data and the photograph show that a flat region cannot exist in the contraction area. The two cross-sectional profiles show a gradual variation of scour region, indicative of scour at a short contraction.

9.4.2 Wing-Wall Abutments

Basically the same observations made in Section 9.3.1 for scour at the spill-through abutments hold for scour at the wing-wall abutments. Figures 9-8 show how the equilibrium scour bathymetry varied with length of embankment for wing-wall abutments. However, there were two main differences:

1. During the early phase of scour, the maximum depth of scour was at the upstream side of the abutment. Eventually, as scour developed, the maximum scour occurred adjacent to the abutment's downstream corner; and,

2. Embankment breaching occurred for all the layouts of the wing-wall abutment tested, except for the shortest layout, $L/0.5B = 0.14$.

The development of scour at the abutment's leading corner is illustrated in Figure 9-9, which shows views of early scour development at a wing-wall abutment when $L/0.5B$ = 0.67. The black line on the wing-wall abutment indicates the initial level of the sand bed. This early stage of scour, lasting about 5 to 10 minutes produced deepest scour at the leading corner, and some accumulation of sand at the abutment's downstream corner. Such scour development is akin to scour development around a bluff pier; i.e., deepest scour at the front. As the experiment continued for 30 hours, however, the maximum scour deepened, and the accumulation of sand moved downstream from the abutment. The equilibrium scour region and its bathymetry are shown in Figures 9-10 and 9-11.

9.5 Flow-Field Observations

The flow pattern at the water surface around the abutments produced useful insights into scour development. As described in Chapter 6, the experiments involved extensive LSPIV measurements of the flow field around the abutment. To determine if the flow field remained steady as scour developed, flow-field measurements were made prior to scour development at an initial scour stage.

9.5.1 Spill-Through Abutment

The LSPIV measurements of the flow pattern at the water surface around the abutments produced useful insights into scour development. Figure 9-12 shows a series of surface flow fields giving flow pathlines and values of q_{f2}/q_f at the start of scour when $L/0.5B$ = 0.10, 0.20, 0.30, 0.50, 0.60, and 0.70. These insights are augmented by a set of figures, Figures 9-12a-f, 9-13a-b, and 9-14a-b, that shows the flow field changes associated with scour development for a selected representative abutment condition.

Once scour developed, flow was seen to be drawn to the scour region, as the LSPIV images in Figure 9-13a-b show. Figures 9-14a-b-f compare flow pathlines, flow bathymetry, and values of q_{f2}/q_f for the initial flat-bed and equilibrium-scour bathymetries when $L/0.5B$ = 0.50. Figures 9-

15a-b show the lateral distribution of q_{f2}/q_f at two cross sections at the start and end of scour: i.e., at the abutment axis, and the location of maximum scour depth. The equilibrium scour were taken 36 hours after the experiment's start. Figures 9-16a-b show essentially the same insights (flow pathlines, bathymetry, and values of q_{f2}/q_f for the initial flat-bed and equilibrium-scour bathymetries) when $L/0.5B = 0.67$. For instance, the Figure 9-16b shows that the location of the maximum value for q_{f2}/q_f remained approximately the same for the equilibrium-scour bathymetry as for the initial flat-bed, though the flow concentrated through the scour region. On the whole, these insights are similar to those obtained with flow around abutments paced in the compound channel (Section 7-4).

These sets of flow-field data, and data associated with the equilibrium scour, yield the following flow-related insights regarding the influence of increasing value of abutment length parameter, $L/0.5B$:

1. The figures show that a maximum value of q_{f2}/q_f occurred just downstream from the embankment, coinciding with eventually the location of deepest scour;

2. The overall magnitude of q_{f2}/q_f values increased as $L/0.5B$ increased;

3. The flow became more uniformly distributed across the channel through the bridge waterway as $L/0.5B$ increased;

4. Scour development concentrated flow at the region of deepest scour for a range of $L/0.5B$ values, just as resulted with the spill-through abutments in compound channels; and,

5. The large wake region formed behind the embankment enlarged as flow was drawn to the location of deepest scour.

9.5.2 Wing-Wall Abutment

Comparison of the flow fields associated with the wing-wall and spill-through abutments helps explain the differences in scour at the two abutments. The photographs in Figures 9-17a-b show flow streamlines as revealed by means of the LSPIV at the start of scour and at equilibrium

scour, for the wing-wall abutment, when $L/0.5B = 0.67$. The distribution of q_{f2}/q_f values through two cross sections at the wing-wall abutment are shown in Figures 9-18a-b for this abutment layout. The information in these figures is comparable to that shown in Figures 9-16a-b for the spill-through abutment. Since these two experiments had almost the same embankment length ($L/B = L/B_f = 0.67$), they had similar geometric contraction ratio in terms of the width of the whole channel and the length of the embankment.

A comparison of the flow fields yields the following insights:

1. Before scour, the distributions and values of q_{f2}/q_f are fairly comparable for the wing-wall and spill-through abutments, as evident in Figures 9-16a and 9-18a. However, the equilibrium scour conditions produced dissimilar distributions;

2. The flow patterns at the equilibrium-scour stage were substantially different for the two abutment forms. For the spill-through abutment (Figure 9-16b), the uniform flow region became narrower. On the other hand, for the wing-wall abutment (Figure 9-18b) the uniform flow region became wider as scour developed closer to the wing-wall abutment;

3. For the wing-wall abutment, the location of deepest scour was close to the front of the abutment, and therefore scour drew flow closer to the abutment. The maximum value of q_{f2}/q_f for the wing-wall abutment was about 4.5 at the location of maximum scour, in front of the abutment (Figure 9-18b);

4. For the spill-through abutment, the location of deepest scour was just out and downstream from the abutment's downstream corner. The maximum value of q_{f2}/q_f for the spill-through abutment was about 4.8 at the location of maximum scour depth (Figure 9-16b);

5. For the spill-through abutment, the flow pathlines were deflected out from the abutment. However, for the wing-wall abutment, the pathlines were drawn behind the abutment. Consequently, the scour region became wider for the spill-through abutment; and,

6. The flow separation region at the front of the spill-through abutment was not as well delineated as for the wing-wall abutment, and thus the wake region was not as well delineated for the spill-through abutment.

9.5.3 Influence of Main Channel Proximity

It is useful to consider briefly how the scour flow field associated with Scour Condition B is influenced by the proximity of a main channel. A comparison is possible using flow-field observations for an abutment of practically the same embankment length, but with two different settings, as indicated in Figures 9-19a, b for spill-through abutments:

1. One abutment in a compound channel built at $L/B_f = 0.50$, $B_f/0.5B = 0.63$, and $L/0.5B = 0.27$ (Figures 9-19a-i, a-ii); and,

2. One abutment on a rectangular channel set at $L/0.5B = 0.30$ (Figures 9-19b-i, b-ii).

Figures 9-19a, b show the pathlines (as white curves) and include the bathymetry as the background contours. They also show q_{f2}/q_f along the section where the maximum scour depth occurred. The principal point of the comparison is to show that flow concentration through the scour region occurred to a proportionately greater extent in the rectangular channel (Figure 9-19b-i, b-ii) than in the compound channel (Figures 9-19a-I, a-ii). When the main channel was relatively close to the abutment, the scour region extended across to the main channel such that floodplain flow did not concentrate quite as much in the scour region.

When the abutment extended sufficiently far across the floodplain of a compound channel that scour extended to bed of the main channel, the resultant extent of embankment failure and breaching was larger than embankment breaching triggered by scour limited to the floodplain alone. The greater elevation drop to the main-channel bed produced a larger area of embankment instability and failure, thereby creating a larger area of breaching than when scour was limited to the floodplain. Additionally, the larger area of instability caused breaching to occur faster at the abutment in the compound channel. For the conditions shown in Figures 9-20a, b, breaching happened about 2 hours after the start of scour in the compound channel, whereas it occurred after about 24 hours for the rectangular channel.

The differences in the timing of breaching caused the scour regions to differ. When the embankment breached before the scour was fully developed by the flow around the un-breached

abutment, the flow developed a different pattern from that before scour. Scour commensurately developed in accordance with the flow pattern. Eventually, the scour had reached its equilibrium condition. The new flow pattern did not significantly alter the scour bathymetry. However, when the embankment breached during an earlier stage of scour, the resulting scour bathymetry differed from that when breaching did not occur; e.g., compare Figure 9-20a with Figure 9-19a. However, when the embankment breached during a later stage of scour development, the scour bathymetry was similar to that at an unbreached embankment; e.g., compare Figure 9-20b with Figure 9-19b. The stability of the earthfill embankment was a significant factor influencing the flow field as scour developed.

9.6 Numerical Simulation of Flow Field

As done for flow around spill-through abutments in compound channels (Section 7.5), the numerical experiments using the two-dimensional, depth-averaged model FESWM-2D produced flow fields showing the distribution of unit discharge, as well as depth-average velocity and bed shear stress, commensurate with flow around an abutment on a wide floodplain or a broad rectangular channel. These simulations were run for the range $L/B_f = 0.05$ through 0.50 for spill-through abutments as well as for simple vertical-wall abutments. The vertical-wall simulations investigated flow-field sensitivity (at least in depth-averaged flow) to the abutment shape. A vertical wall abutment is geometrically similar to a wing-wall abutment, but with a wing angle of 0° relative to the bridge axis. Figure 9-21 illustrates the computational mesh used for one configuration of a spill-through abutment. Morales and Ettema (2010) fully detail the simulation.

The variation of unit discharge, q, for flow around three representative spill-through abutments, for which $L/B_f = 0.10$, 0.20, and 0.50, are presented in Figures 9-22a-c. These figures also show the streamlines associated with flow around the abutment. Evident in the figures is the increased contraction of flow with increasing L/B_f. A transverse profile of q, as shown in Figure 9-23, indicates that q quickly attains a maximum value, q_{MAX}, over a comparatively narrow peak, and then asymptotically declines to a constant value away from the abutment. Also shown in this figure is the transverse profile of flow vorticity, ϖ, defined as

$$\varpi = \left(\frac{\partial V}{\partial x} - \frac{\partial U}{\partial y} \right) \tag{9-5}$$

in which U and V are the streamwise (x) and transverse (y) components of velocity, respectively. The peak values of ϖ and q occur close together. This result is to be expected, given the sharp peak in the transverse distribution of q.

Values of the unit-discharge ratio q_{MAX}/q_{f2} were determined from the simulations, and are plotted versus q_{f2}/q_1 in Figure 9-24, which presents three curves; numerical results for spill-through abutments and vertical wall abutments, along with experimental results for spill-through abutments. These unit discharge terms are defined in Chapter 4. Figure 9-24 indicates the following findings:

1. Slightly higher values of q_{MAX}/q_{f2} were obtained for flow around the vertical wall abutments. However, the relatively modest difference in value suggests that abutment shape does not have a major effect on q_{MAX}/q_{f2};

2. The values of q_{MAX}/q_{f2} attain a broad peak when q_{f2}/q_1 varies from about 1.2 to 1.4;

3. The peak value of q_{MAX}/q_{f2} for spill-through and vertical-wall abutments are approximately 1.45 and 1.55, respectively; and,

4. The values of q_{MAX}/q_{f2} measured during the flume experiments with spill-through abutments lie below those determined from the numerical simulations. This result is attributable to the computational mesh being finer (narrower) than the flow width over which measurements were taken in laboratory experiments. As can be seen in Figure 19-24, the peak value of q_{MAX}/q_{f2} occurred at a fairly narrow band. The measurement width of the LSPIV and ADV velocity measurements were about 20mm, thereby exceeding the width in which the peak velocity and unit discharge occurred. The wider measurement of velocity leads to an averaging of flow velocity, and therefore a reduced estimate of velocity and q_{MAX}.

9.7 Comparison with ABSCOUR

The ABSCOUR method (Chang and Davis 1998, 1999), outlined in Section 5.7, is the prior scour-estimation method that most closely resembles the method developed in this project. ABSCOUR treats abutment scour as essentially inseparable from contraction scour. Scour Condition B is the condition enabling best comparison of ABSCOUR scour estimates and scour data from the present project, because the overall geometry of channel and abutment are similar to that considered in the development of ABSCOUR. One major difference between the experiments upon which ABSCOUR and present experiments is that the latter used abutments comprising an abutment column set amidst an erodible embankment. To account for this difference, the ABSCOUR estimates of Y_{MAX}/Y_C set the spiraling-flow coefficient $k_f = 1.0$; i.e., no spiral-flow amplification of scour depth is estimated using Eq. (5-35).

The magnitudes for Y_{MAX}/Y_C obtained from the present experiments with spill-through abutments (Figure 9-2) agree quite well with those obtained from ABSCOUR over the range $1 < q_{f2}/q_f \leq 2$; see Figure 9-25. For the ABSCOUR curve in this figure, the limit $q_{f2}/q_f = 1$ is based on flow contraction locally around an abutment in a wide channel. If this same convention were used for the data from the experiments in the present study, at $q_{f2}/q_f = 1$, Y_{MAX}/Y_C would match the ABSCOUR estimate. Note that, for the present experiments, $q_{f2}/q_f = 1$ implies no abutment intrusion into the channel; i.e., $L/0.5B = 0$. As q_{f2}/q_f exceeds about 2, ABSCOUR estimates of Y_{MAX}/Y_C increasingly differ from the trends shown by the present data.

For wing-wall abutments, the peak magnitude of Y_{MAX}/Y_C obtained from the present experiments (Figure 9-2) is somewhat less than that obtained using ABSCOUR at $q_{f2}/q_f = 1.2$, but the ABSCOUR and data curves trend in opposite directions for larger values of q_{f2}/q_f, Figure 9-25. The difference in the trends is attributable to ABSCOUR's use (Eq. (3-30)) of the relationship $Y_2/Y_1 \propto (q_{f2}/q_f)^2$, rather than $Y_2/Y_1 \propto (q_{f2}/q_f)^{6/7}$, as per Eq. (4-11).

Table 9-1. Data summary for tests with abutments subject to Scour Condition B

Spill-Through Abutment with Riprap-Protected Embankment				
$L/0.5B$	q_2/q_1	Y_{MAX} (m)	Y_C (m)	Y_{MAX}/Y_C
0.69	3.18	0.52	0.37	1.40
0.60	2.50	0.51	0.30	1.73
0.51	2.05	0.48	0.25	1.68
0.34	1.52	0.42	0.20	2.10
0.24	1.32	0.35	0.17	2.05
0.24	1.32	0.35	0.17	2.05
0.18	1.22	0.32	0.16	2.00
0.00	1.00	0.15	0.15	1.00

Wing-Wall Abutment with Riprap-Protected Embankment				
$L/0.5B$	q_2/q_1	Y_{MAX} (m)	Y_C (m)	Y_{MAX}/Y_C
0.68	3.05	0.48	0.36	1.34
0.59	2.41	0.47	0.29	1.61
0.42	1.72	0.45	0.22	2.05
0.42	1.72	0.44	0.22	2.00
0.14	1.16	0.39	0.16	2.50
0.00	1.00	0.15	0.15	1.00
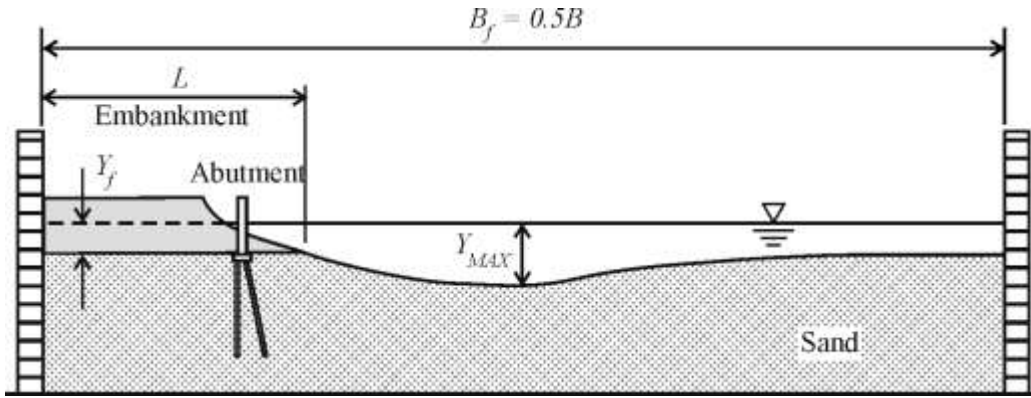
Figure 9-1. Principal variables measured for abutments subject to Scour Condition B, abutments set back on an erodible floodplain or in a rectangular channel
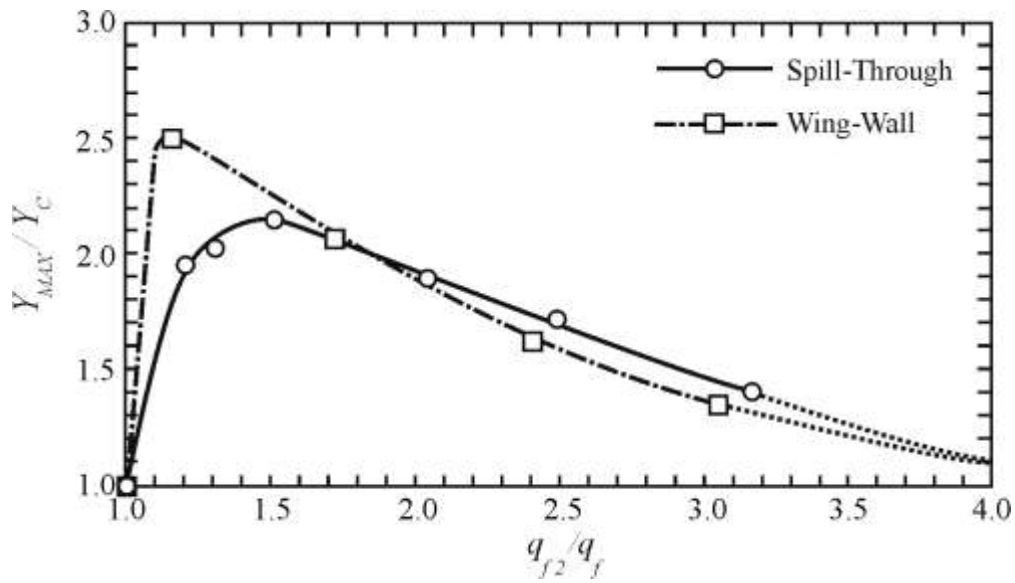
Figure 9-2. Relationships between flow-depth increase, Y_{MAX}/Y_C, and unit-discharge ratio, q_{f2}/q_f for spill-through abutments and wing-wall abutments, Scour Condition B
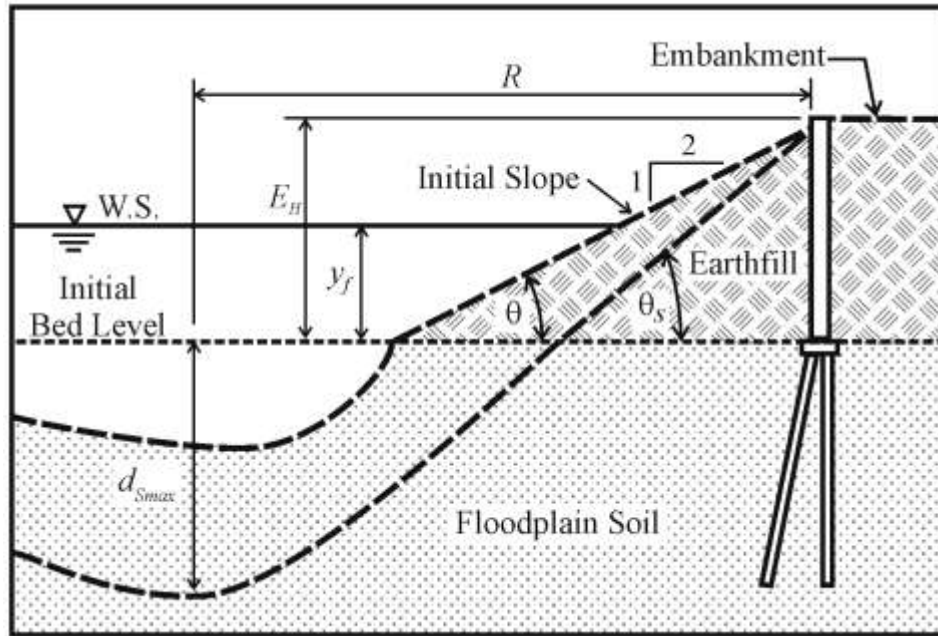
(a)
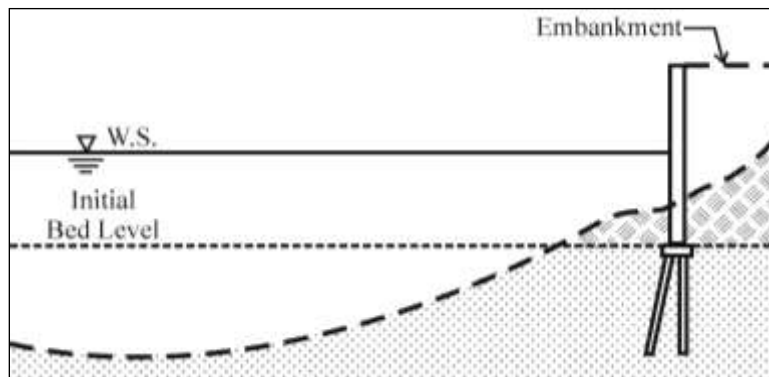
(b)

Figure 9-3. Deepening scour destabilizes the embankment face, causing the slope to fail geotechnically, and to erode back to a limiting condition. When the slope erodes back past the abutment column, the embankment breaches, and Scour Condition B attains an equilibrium state: the scour limit for an embankment face eroded back to an extent defined in terms of angle for embankment-slope stability, θ_S, and column position (a); and, embankment failure beyond this limit induces leads to embankment breaching and flow relaxation (b)
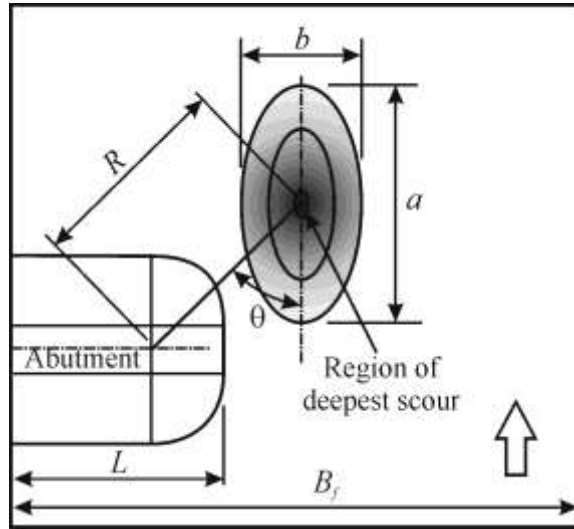
(a)
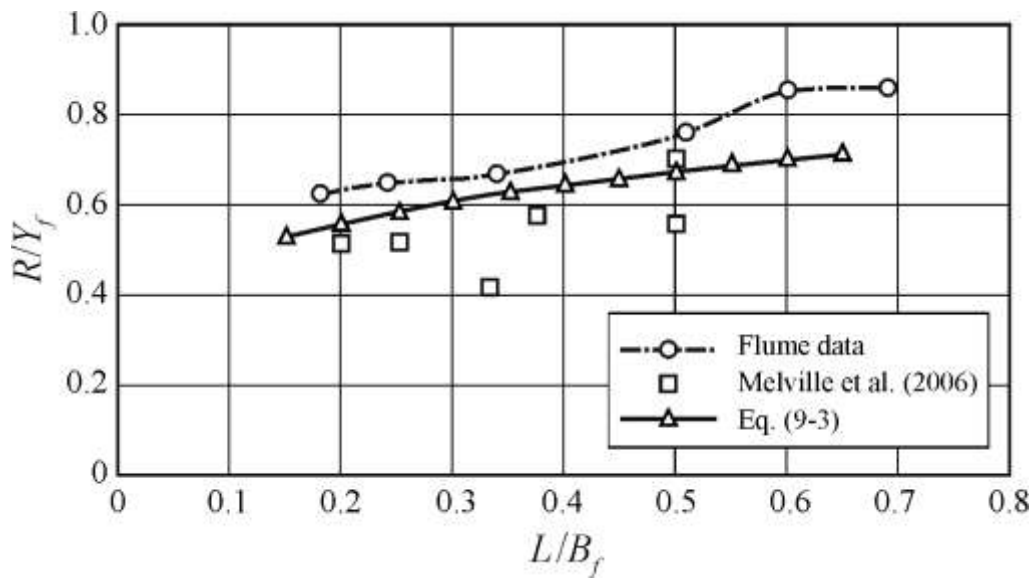
(b)

Figure 9-4. Definition sketch for distance, R, to deepest scour (a), and variation of R/Y_f versus L/B_f (b)

(a)

(b)

(c)

(d)
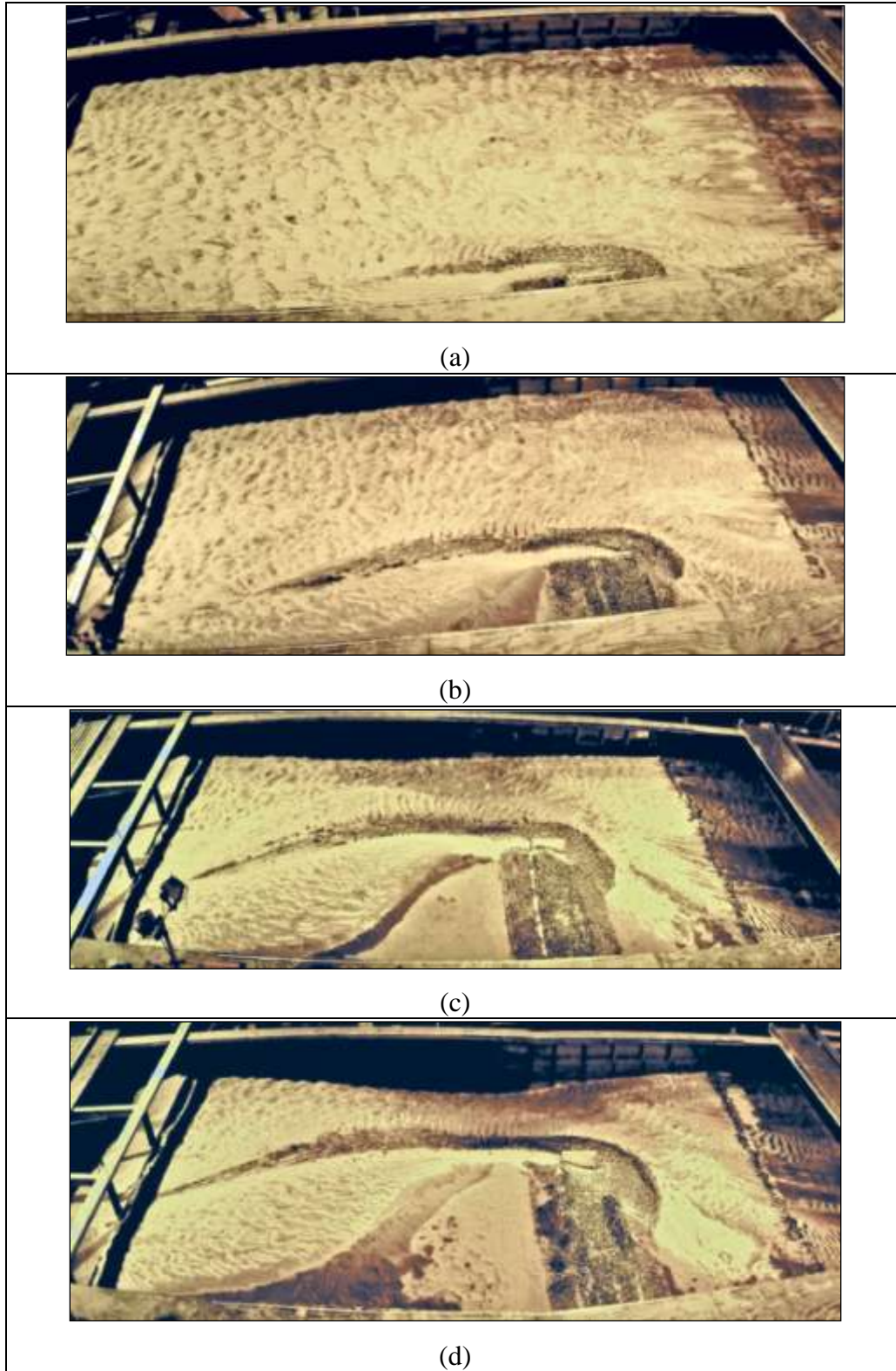
Figure 9-5. Top views of scour at a spill-through abutment with $L/0.5B = 0.1$ (a), 0.3 (b), 0.6 (c), and 0.7 (d)

Figure 9-6. Equilibrium scour hole at a spill-through abutment with *L/0.5B* = 0.5
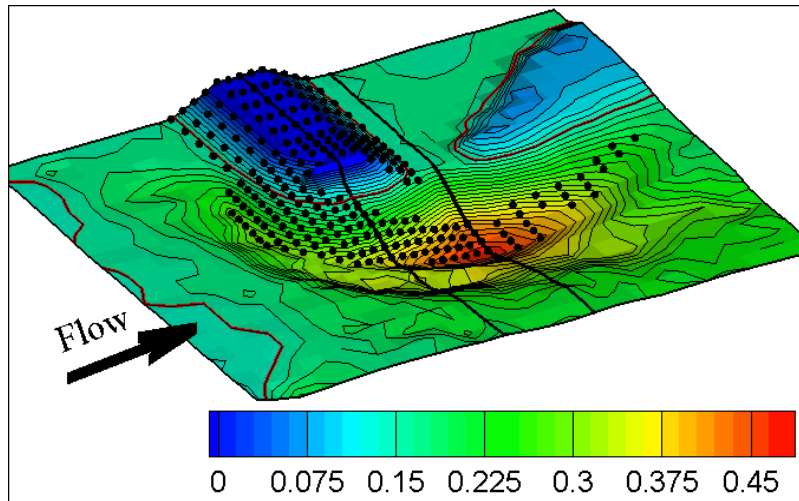
(a)
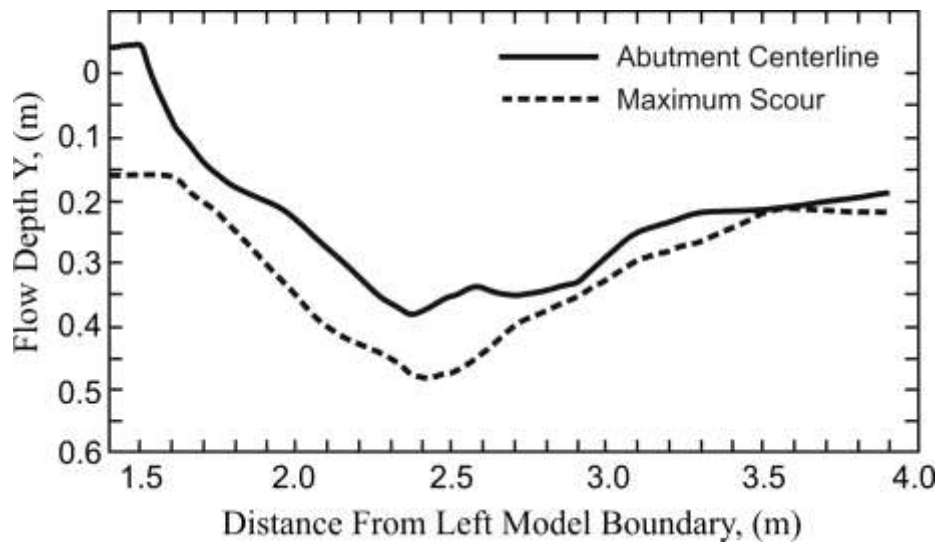
(b)

Figure 9-7. Bathymetry plot (a), and cross sections (b) for the scour region near a spill-through abutment on erodible floodplain with *L/0.5B* = 0.5 (Scour Condition B). The black dots in (a) indicate extent of riprap-stone disposition

(a)

(b)

(c)

(d)

Figure 9-8. Top views of wing-wall abutments with $L/0.5B = 0.14$ (a), 0.42 (b), 0.59 (c), and 0.67 (d)

(a)
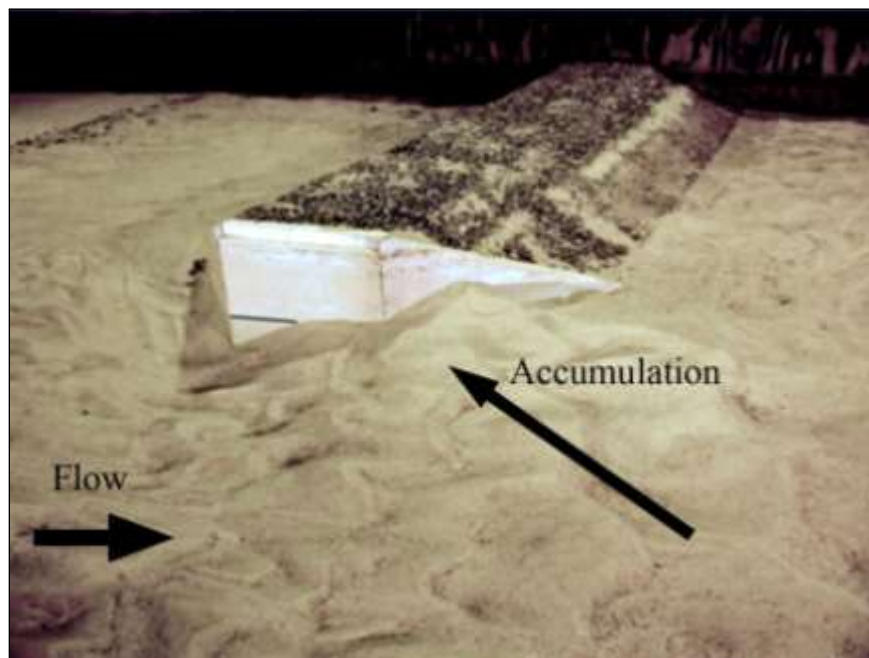
(b)

Figure 9-9. Upstream view (a), and side view (b) of scour hole with a wing-wall abutment: $L/0.5B = 0.67$ (after experiments of 5 minutes)

Figure 9-10. Resulting scour hole of a wing-wall abutment with *L/0.5B* = 0.67
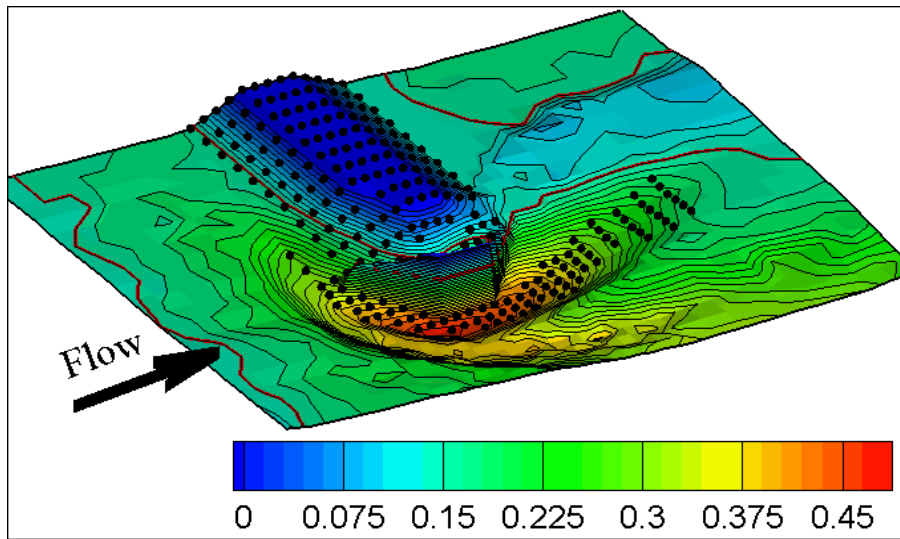
Figure 9-11. Contour plot of resulting scour hole of a wing-wall abutment with *L/0.5B* = 0.67.
The black dots in (b) indicate riprap-stone disposition. A red curve in (b) indicates 0.15 m from
the initial water level
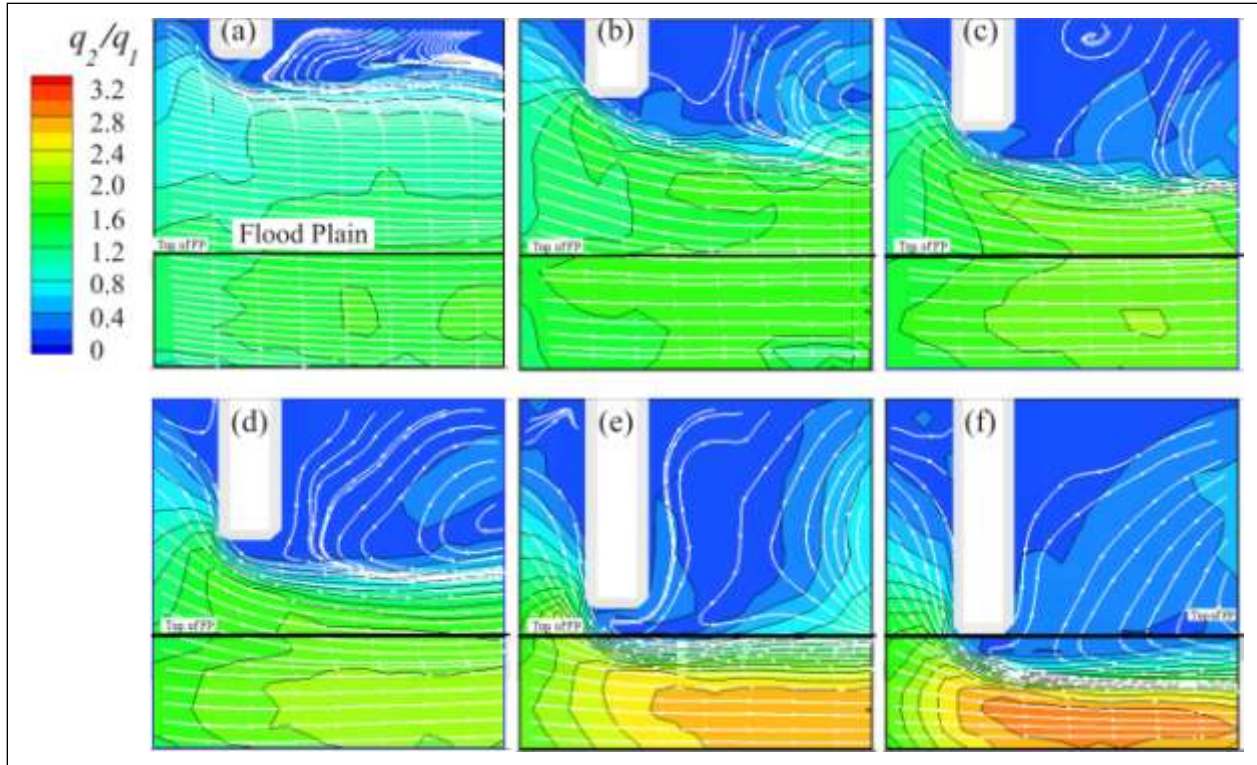
Figure 9-12. Surface flow patterns and q_{f2}/q_f distributions at pre-scour condition for spill-through abutments with $L/0.5B = 0.10$ (a), 0.20 (b), 0.30 (c), 0.50 (d), 0.60 (e), and 0.70 (f)

(a)   (b)
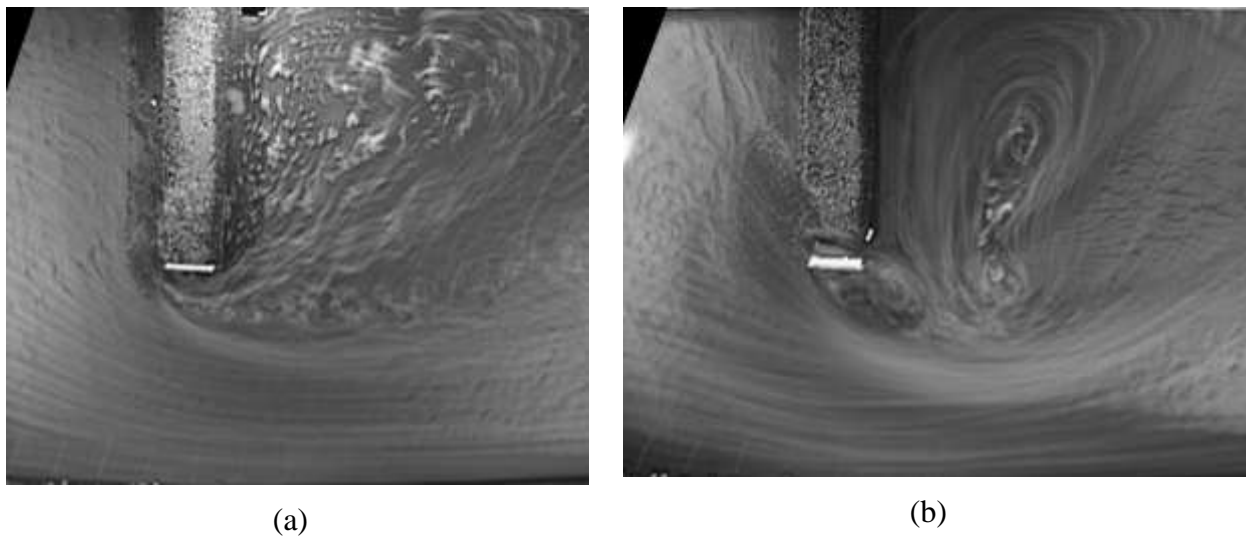
Figure 9-13. Surface flow patterns determined by LSPIV for a spill-through abutment with $L/0.5B = 0.5$; flow field before scour (a), and flow field associated with equilibrium scour (b)
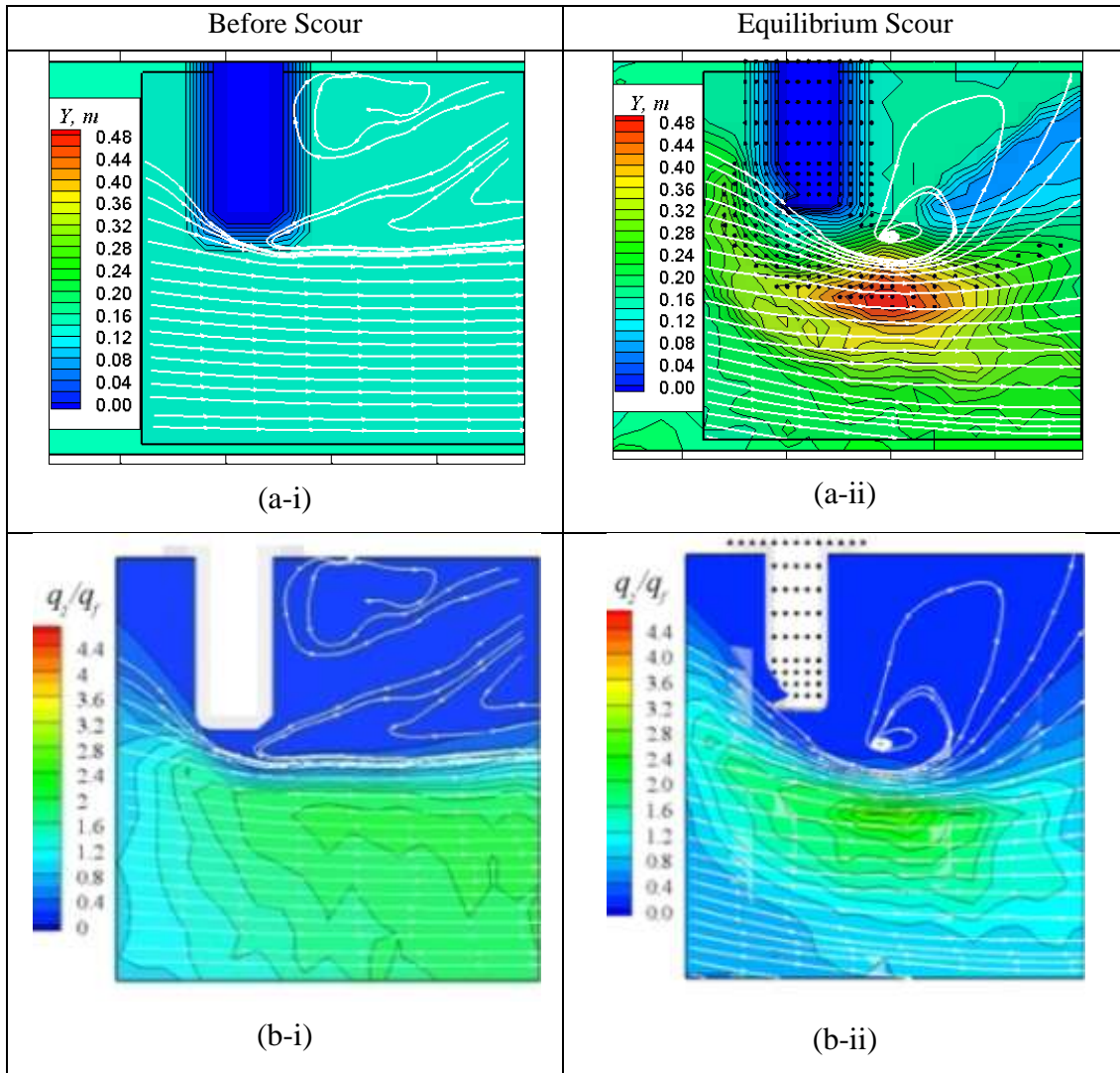
Figure 9-14. Flow fields around a spill-through abutment with *L/0.5B = 0.5* before scour and at equilibrium scour: pathlines and bathmetry before scour (a-i), and at equilibrium scour (a-ii); magnitude of q_{f2}/q_f and steam lines before scour (b-i), and at equilibrium scour (b-ii)
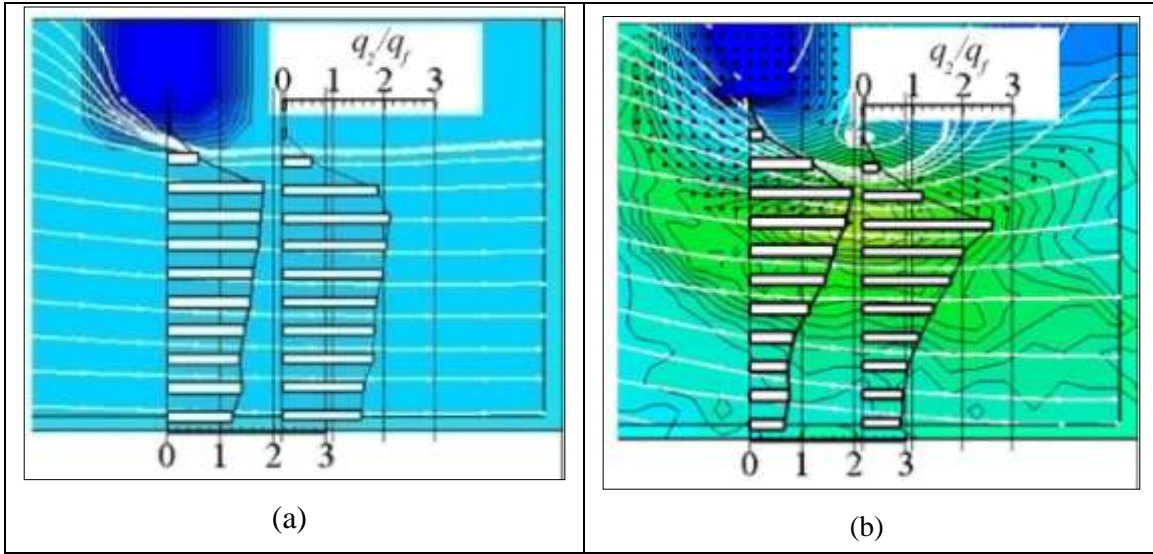
Figure 9-15. Flow pathlines, channel bathymetry, and transverse profiles of q_{f2}/q_f obtained for a spill-through abutment with $L/0.5B = 0.50$; before scour (a), and after scour (b). Note that scour development concentrates q_{f2}
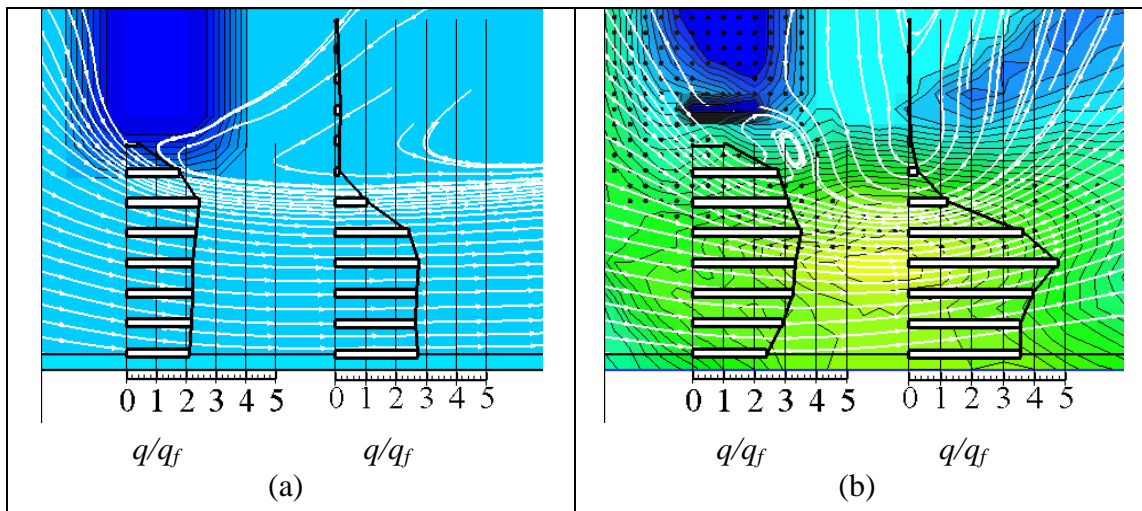
Figure 9-16. Flow pathlines, channel bathymetry, and transverse profiles of q_{f2}/q_f obtained for a spill-through abutment with $L/0.5B = 0.67$; before scour (a), and after scour (b)
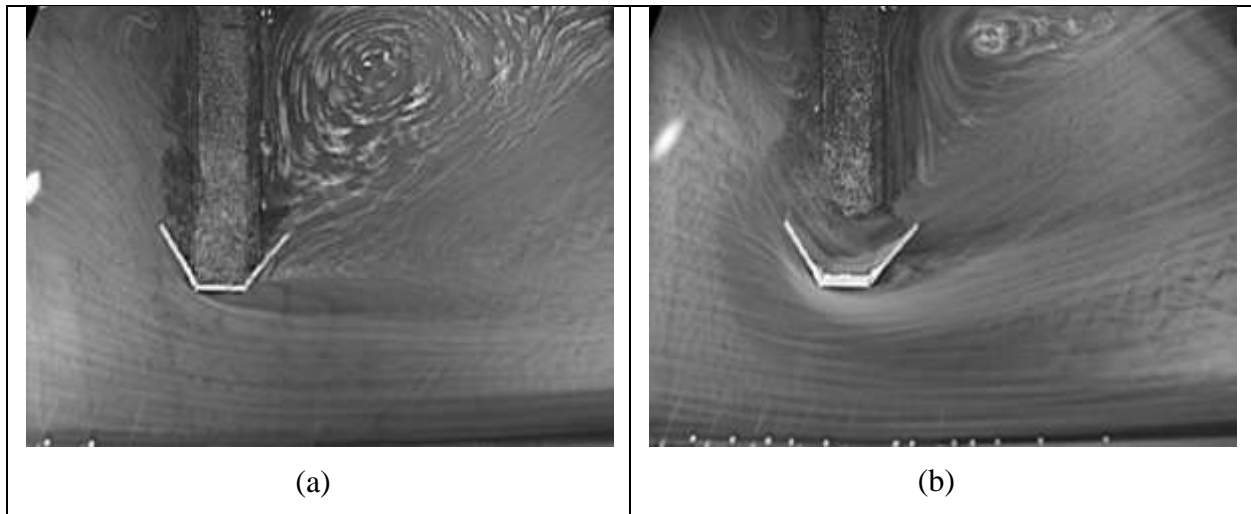
Figure 9-17. Surface-flow patterns determined by LSPIV for a wing-wall abutment with *L/0.5B* = 0.67; flow field before scour (a), and, flow field associated with equilibrium scour (b)
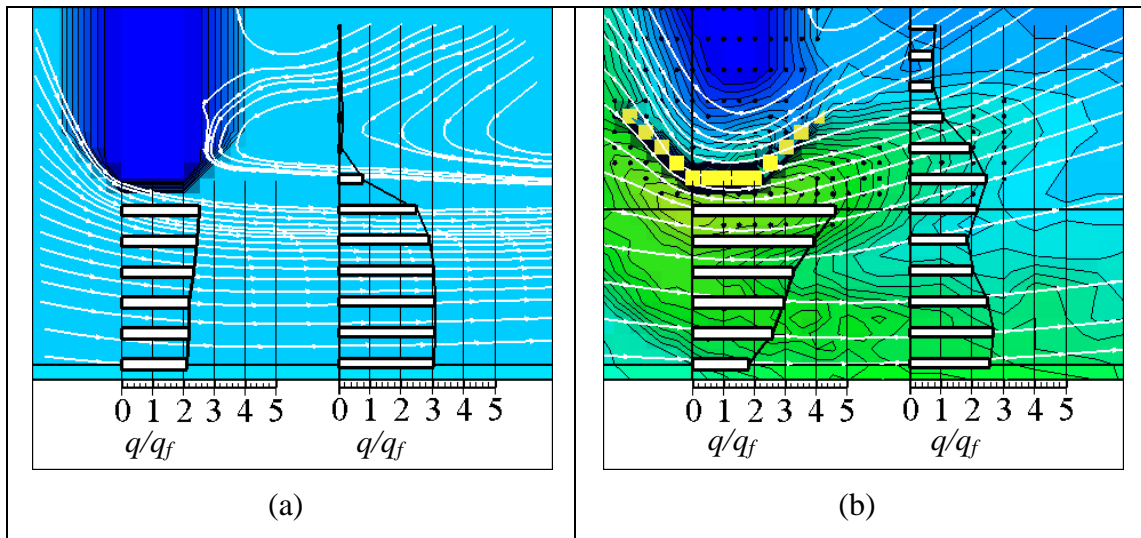
Figure 9-18. Flow pathlines, channel bathymetry, and transverse profiles of q_{f2}/q_f obtained for a wing-wall abutment with *L/0.5B = 0.67*; before scour (a), and after scour (b)

Before Scour	Equilibrium Scour
(a-i)	(a-ii)
(b-i)	(b-ii)
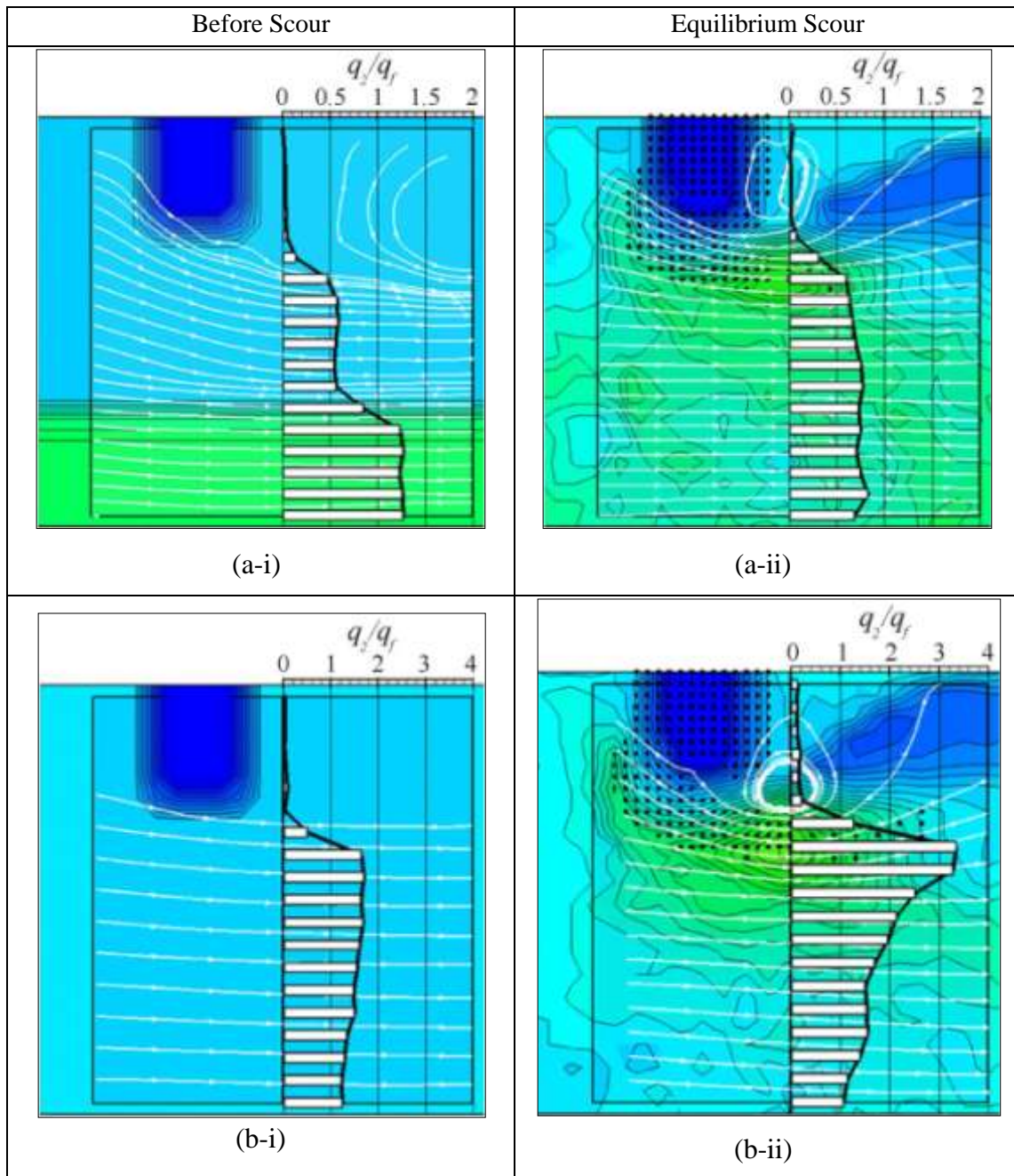
Figure 9-19. Comparison of distributions of q_{f2}/q_f along the maximum scour section in the compound channel for a spill-through abutment with $B_f/0.5B = 0.63$ and $L/B_f = 0.43$: before scour (a-i), and at equilibrium (a-ii); and in the rectangular channel with $L/0.5B = 0.30$; before scour (b-i), and at equilibrium (b-ii)

Pre-Scour	Equilibrium
(a-i)	(a-ii)
(b-i)	(b-ii)
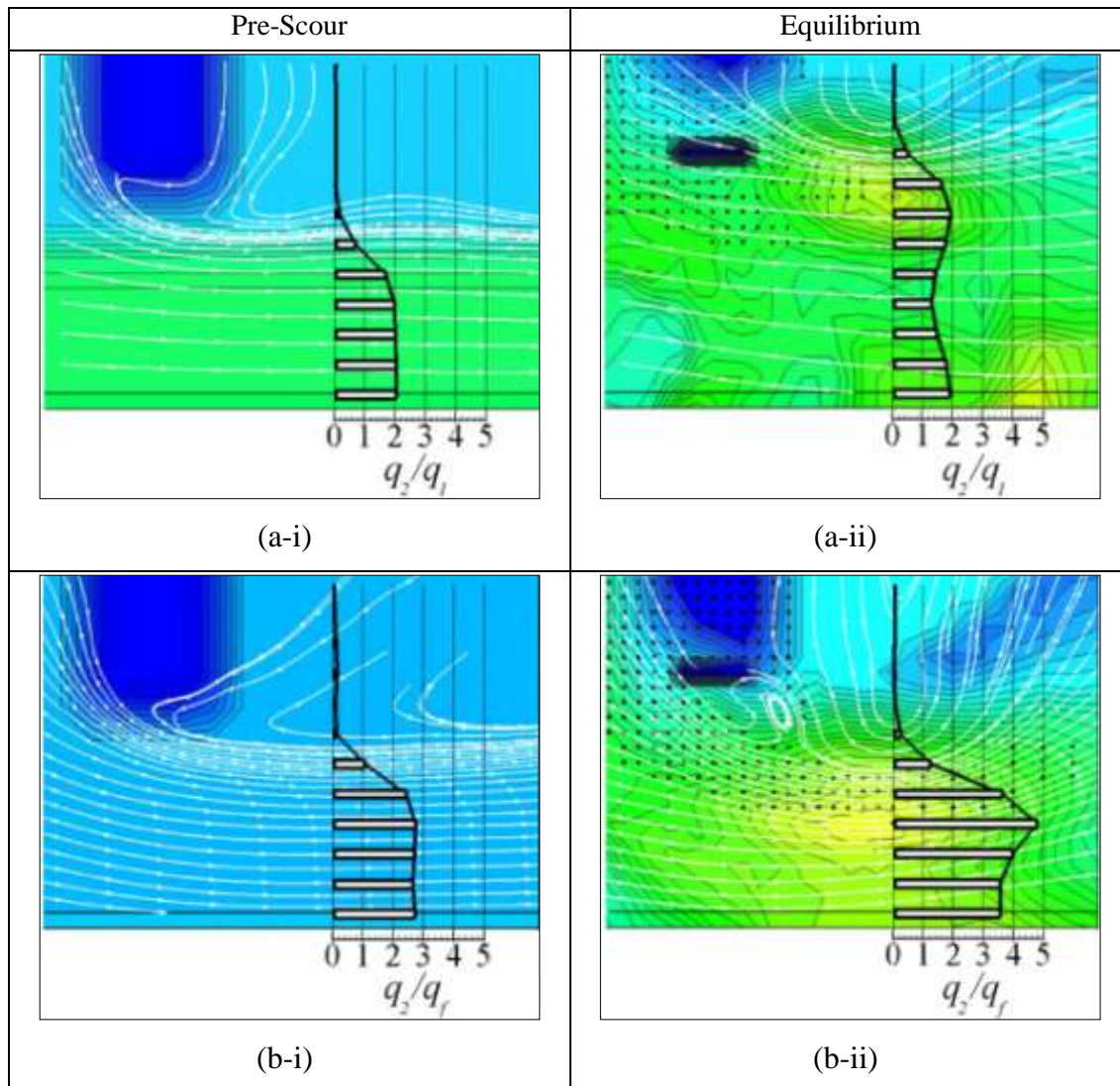
Figure 9-20. Comparison of distributions of q_{f2}/q_f along the maximum scour section in the compound channel for a spill-through abutment with $B_f/0.5B = 0.63$, and $L/B_f = 1.00$: before scour (a-i), and at equilibrium (a-ii); and in the rectangular channel with $L/0.5B = 0.30$; before scour (b-i), and at equilibrium (b-ii)
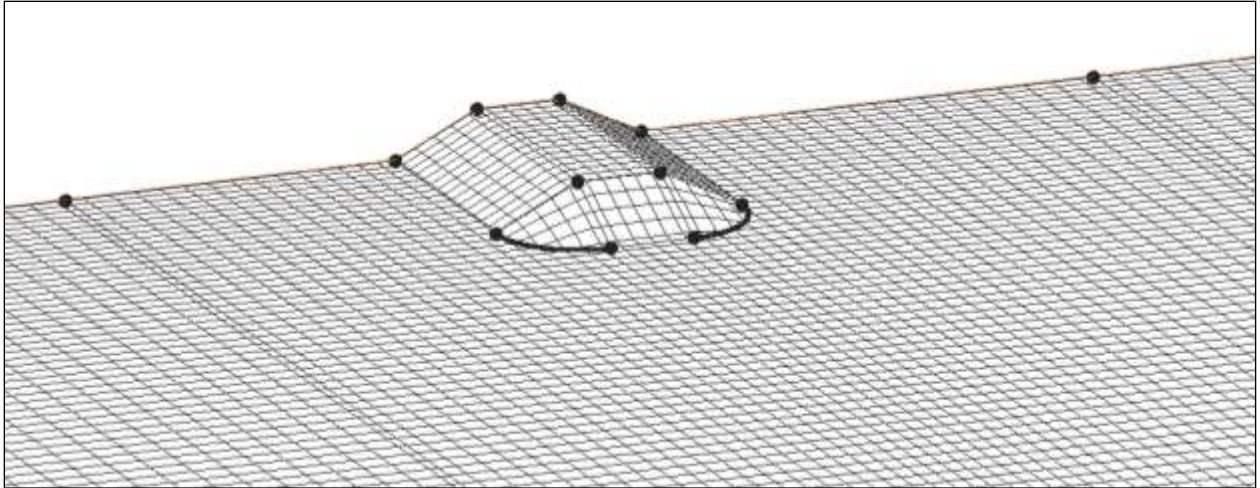
Figure 9-21. Sample computational mesh used for flow simulation using the numerical model FESWMS
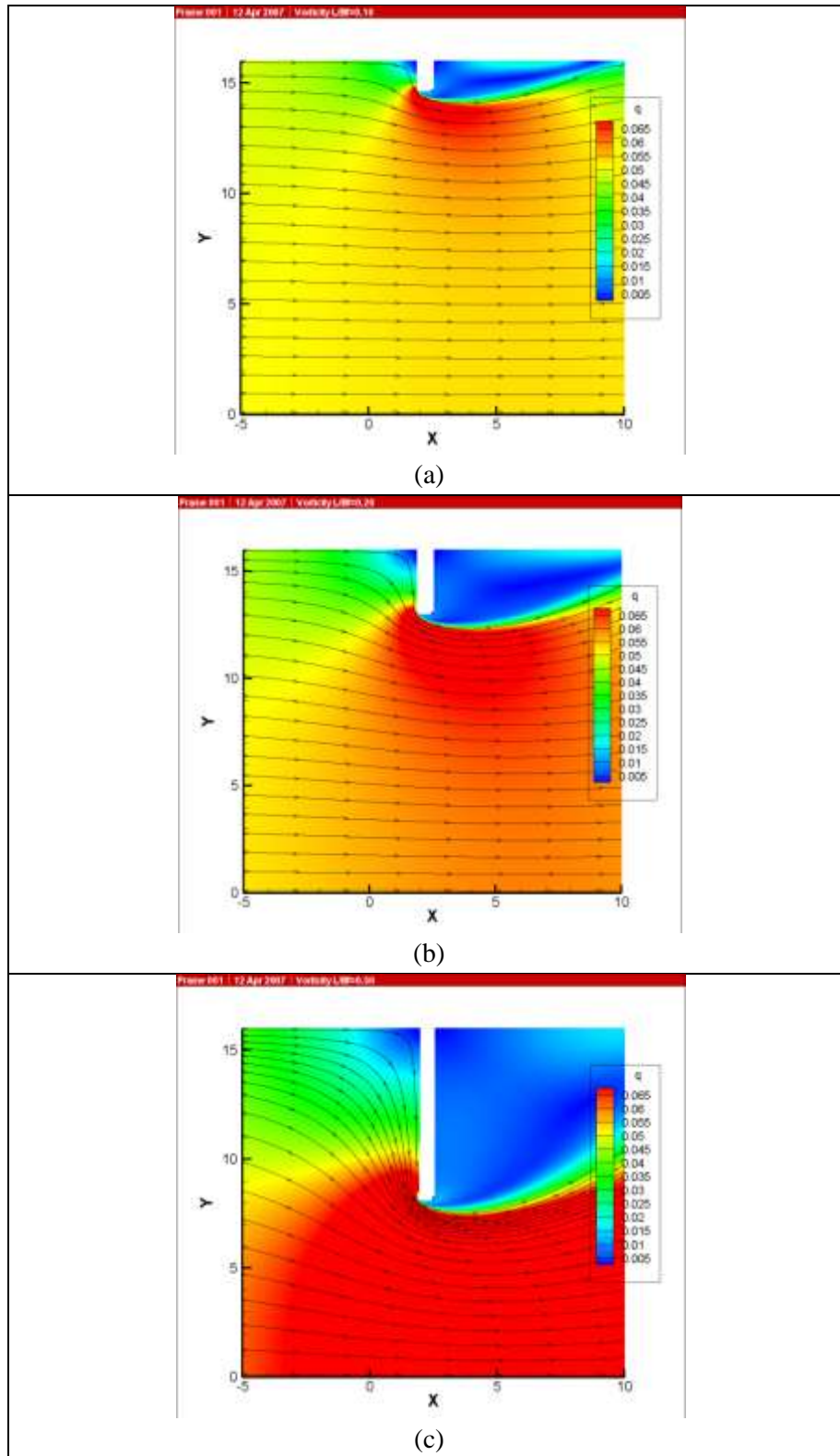
Figure 9-22. Numerical simulations of flow around representative abutment lengths with *L/0.5B*
= 0.10 (a), 0.20 (b), and 0.50 (c). Magnitudes of unit discharge, *q*, are indicated.
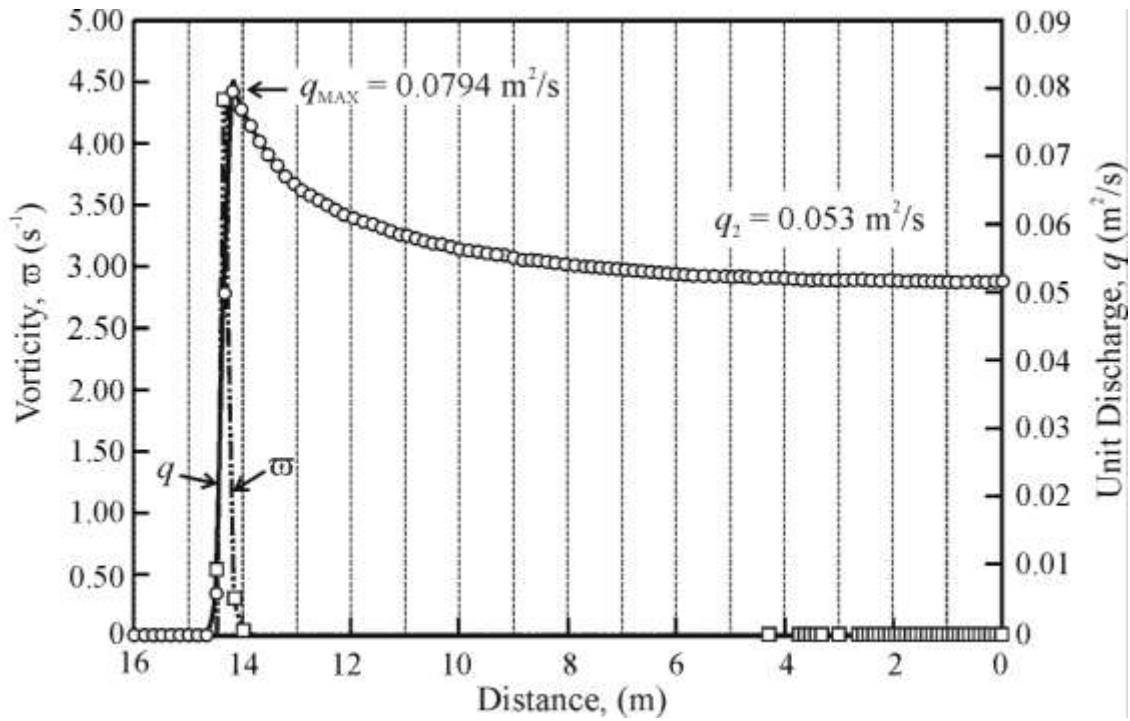
Figure 9-23. Transverse profiles of unit flow discharge, q, and vorticity, ϖ, with $L/0.5B = 0.10$
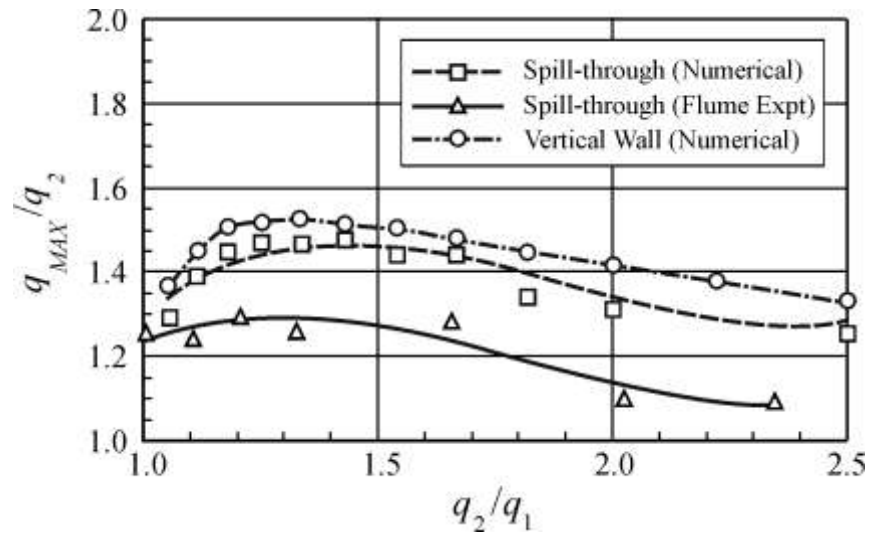
Figure 9-24. Comparison of numerical and experimental values for the variation of q_{MAX}/q_2 with q_2/q_1 for flow around spill-through abutments, and vertical wall abutments on a floodplain (or in a rectangular channel)
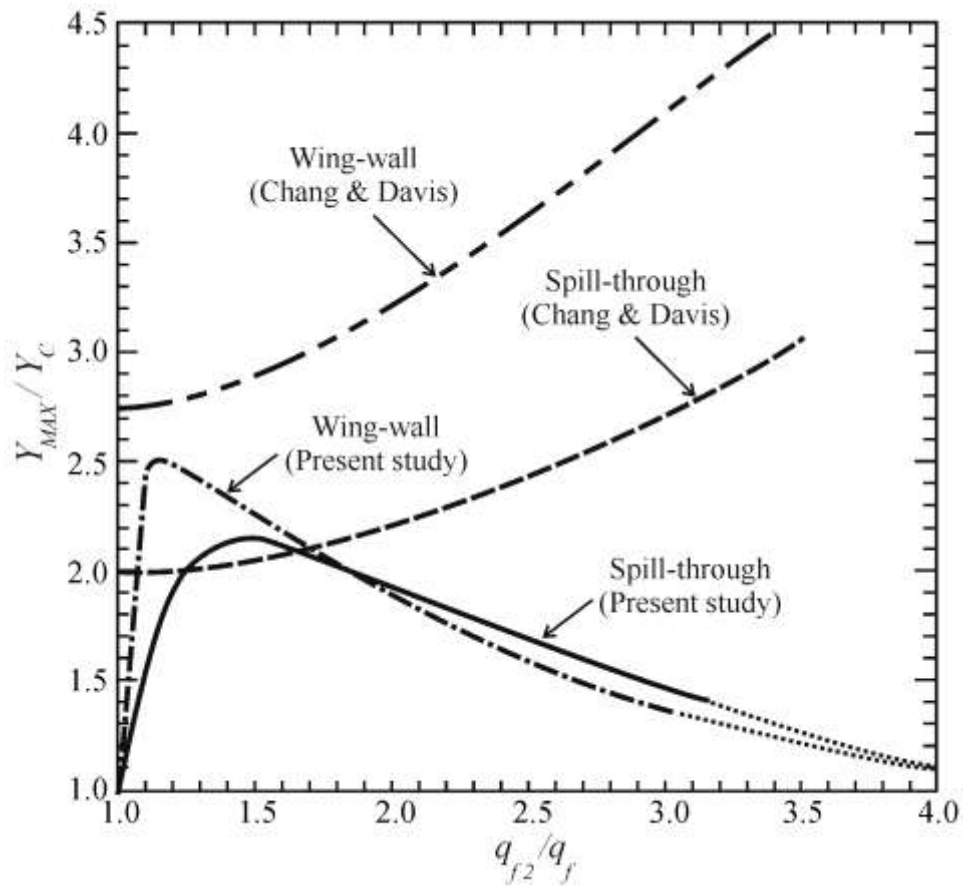
Figure 9-25. Comparison of trends for Y_{MAX}/Y_C versus q_2/q_1 for Scour Condition B; data from the present study, and values estimated using the ABSCOUR method proposed by Chang and Davis (1998, 1999). The comparison is for spill-through and wing-wall abutments

CHAPTER 10

LABORATORY RESULTS FOR SCOUR CONDITION C AT EXPOSED ABUTMENT COLUMNS

10.1 Introduction

This chapter presents the results obtained from the laboratory experiments investigating Scour Condition C, the most vulnerable of abutment scour conditions – the abutment is located in a readily erodible channel or floodplain, and the abutment's embankment lacks adequate (or any) protection by means of riprap or some alternative armoring cover. Scour Condition C leads to major breaching of the embankment, fully exposing the abutment column to further scour. When this happens, scour progresses at the abutment column as if the column were a pier (Figure 3-3).

Described first is scour development at abutments with unprotected embankments. Described next is scour development at an exposed pile-supported (spill-through and wing-wall shapes) subject to a range of flow parameters; notably, variable flow intensity (u_*/u_{*c}) and column alignment to flow (β). Figure 10-1 indicates the variables measured.

Taken together, the results presented lead to empirical equations for predicting maximum scour depth at exposed standard stub and wing-wall abutments. Variations on the equations occur for alternative designs of abutment columns. These equations are vital for determining the depths to which the pile or sheet-pile foundations of abutment columns should be placed.

10.2 Scour-Depth Trends

For abutments located on erodible floodplains, Scour Condition C led to the deepest scour at the foundation of each abutment column. Deeper overall scour occurred near the spill-through abutments and the wing-wall abutments subject to Scour Conditions A and B, but such scour either was at some distance from the abutments in the case of spill-through abutments (e.g., see Figure 7-10b or 7-11b) or never entirely exposed the abutment's foundation (e.g., see Figure 8-9b for Scour Condition A at a wing-wall abutment whose embankment is not fully breached).

Figure 10-2 shows data relating the depth parameter Y_{MAX} and the abutment-length parameter, L/B_f, for spill-through abutments and one wing-wall abutment, when $B_f/0.5B = 0.43$. Two values of Y_{MAX} are given for each value of L/B_f; one is at the abutment, and the other (Y'_{MAX}) is in the main channel. (Note that the parameter L/B_f serves as a surrogate for the flow parameter q_2/q_1, when all other parameters are constant.) Before embankment breaching occurred, scour occurred around the floodplain and in the main channel. Once the embankment was breached, flow around the abutment reduced, and the elevation of the main-channel bed remained more-or-less at its original level, with allowance for uncertainty associated with dune amplitude. The data for the spill-through abutment are re-plotted in Figure 10-3 as Y_{MAX}/Y_C versus q_2/q_1, to enable comparison with the Y_{MAX}/Y_C trends obtained for Scour Conditions A and B (Figures 7-3 and 8-2).

The extent of scour away from the abutment depended on the time required for the abutment's embankment to breach. Figure 10-4 relates this time to embankment length, expressed as L/B_f. The time given is up to the instant that flow began passing through the embankment. It was shorter for the longer embankments, because the rate of scour deepening increased with L/B_f. The maximum duration was 82 minutes for $L/B_f = 0.50$. Once a breach had formed, flow through the breach, further eroded the embankment and widened the breach. The process of breach widening took up to several hours in the model. Section 10-3 further discusses and illustrates the process. Embankment breaching caused the flow velocity at the abutment column to vary in magnitude and direction.

The following comments can be drawn from scour-depth data:

1. A central point is that scour at an exposed abutment column occurs as a local scour, akin to scour at a pier, and therefore varies the column's constructed shape. The single data point for the exposed column of the wing-wall abutment lies well above the data associated with the exposed spill-through abutment column, as shown in Figure 10-2. The column for the wing-wall abutment was much wider than that of the spill-through abutment, and thus produced a deeper scour;

2. Scour development varies with the time to breaching of the abutment's embankment. A longer time to embankment breaching enabled a deeper scour form of Scour Condition B to develop before Scour Condition C eventually developed;

3. Because the breaching time is a function of the strength of the earthfill forming the embankment, scour development and depth depend on embankment's earthfill strength;

4. As embankment breaching occurs, the flow field changes substantially, causing the flow velocities at the exposed abutment to vary in magnitude and direction. Accordingly, scour development at the exposed abutment column is unsteady; and,

5. Design estimation of scour depth at abutment columns must rely on semi-empirical relationships developed from laboratory data, such as presented later in this chapter.

10.3 Observations of Scour Processes and Bathymetry

The scour processes associated with Scour Condition C for spill-through and wing-wall abutments begin in much the same way as for Scour Conditions A and B but, as illustrated below and in Appendix B7, the processes proceed to breaching and complete washout of the embankment and exposure of the abutment column. The experiments simulated these processes suitably well.

10.3.1 Breaching of Spill-Through Abutments

Figures 10-5a-d show the development of Scour Condition C at an unprotected spill-through abutment, for the layout $L/B_f = 0.70$, and $B_f/0.5B = 0.43$. In addition, Appendix B7 shows scour development over time for an unprotected spill-through abutment. The abutment's embankments was constructed with the same sand used to form the floodplains, and was not protected with riprap. As can be seen from the photo sequence, the wetted sand above the water line behaved in a manner akin to cohesive soil; it was able to stand with a vertical face at and above the water line.

The ensuing set of stages characterized scour development for this representative case:

1. Flow was contracted around the abutment, scouring the floodplain there, as well as scouring the bed of the main channel. Initially, scour progressed as merging of Scour Conditions A and B;

2. Scour of the floodplain led to a side-slope failure at the embankment's front corner, and thereby started embankment breaching. For this experiment, the embankment breached in 13 minutes;

3. Once the embankment breached, flow widened the breach, washing out a major portion of the embankment, exposing the abutment's standard-stub columns like a pier; and,

4. Scour then developed locally around the standard-stub column.

Because the scour occurred in a clear-water condition, considerable time was needed for the scour hole to attain an equilibrium depth. The black line on the abutment in Figure 10-5d is the original surface level of the floodplain.

Though flow breached and washed out the embankment, and appreciably deep scour developed at the exposed abutment column, significant scour still occurred in the main channel for larger values of L/B_f and $B_f/0.5B$. The bathymetry plots in Figure 10-6 show the initial layout of an abutment (Figure 10-6a), and the resulting scour (Figure 10-6b), for the layout $L/B_f = 1.00$, with $B_f/0.5B = 0.43$. Scour Conditions A and C are evident in Figure 10-6b. The detailed embankment breaching and scour processes are:

1. Scour Condition A developed during the earlier stage of scour before the embankment breached. Had breaching taken longer, the maximum water depth in the main channel could have been deeper. Breaching led to Scour Condition C; and,

2. The bed level just upstream from the abutment became slightly elevated above its original level. This rise occurred because, once the embankment breached, the approach-flow velocity in the main channel just upstream from the abutment decreased, causing some bed sediment to deposit.

10.3.2 Breaching of Wing-Wall Abutments

The overall scour processes for the wing-wall abutment were the same as for the spill-through abutment, and resulted in the scour developing deepest beneath the wing-wall's upstream corner. By virtue of the shape of the wing-wall abutments, the scour bathymetry at the wing-wall abutment was more complicated than that for the spill-through abutment.

Figure 10-7 shows the development of Scour Condition C at an unprotected wing-wall abutment set at $L/B_f = 1.22$ (nominally 1), and $B_f/0.5B = 0.43$. The eventual equilibrium scour form is shown in Figure 10-7f, in which the black line on the wing-wall abutment marks the level of the main-channel bed before scour. Figure 10-8, which gives the bathymetry measurements corresponding to Figure 10-7e, shows that scour was deepest at the abutment, but it also shows that significant scour in the main-channel bed occurred. This latter region of scour was similar to that formed for the wing-wall abutment subject to Scour Conditions A and B; e.g., see Figures 8-9 and 9-9.

10.4 Scour at Exposed Abutment Columns

As mentioned earlier in this chapter, design estimation of scour depth at exposed abutment columns necessarily entails the use of semi-empirical relationships similar in nature to the relationships used to estimate depth of local scour at piers. Important parameters in this regard are a column's constructed form and length dimensions. Also important are the following parameters:

1. Flow intensity, expressed as shear velocity of approach flow normalized by particle-entrainment shear velocity (u_*/u_{*c}), at least for clear-water scour; and,

2. Column orientation relative to flow direction, β. The findings of experiments investigating these influences are presented and discussed here for the designs of pile-supported stub-abutment and wing-wall columns used in the current experiments. The influence of flow intensity was investigated for both clear-water and live-bed scour. The experiments were conducted using the two flumes described in Chapter 6.

The maximum scour depth at an exposed abutment column can be expressed in the form of a pier-scour relationship, as indicated by Eq. (4-33).

10.4.1 Influence of Flow Intensity

The influence of flow intensity, u_*/u_{*c}, on equilibrium scour depth at an exposed standard-stub column of a spill-through abutment, or a wing-wall column, was found to be the same as for scour at a pier. Figures 10-9 and 10-10 show the influence of flow intensity on scour at the model standard-stub abutment and wing-wall abutments, respectively. Scour depth increased as u_*/u_{*c} increased over the clear-water range, $0.5 \leq u_*/u_{*c} \leq 1.0$, for both column forms; the lower limit is based on findings generally reported in the literature (e.g., Melville and Coleman, 2000). Table 10-1 summarizes the data obtained from the present experiments, which include live-bed scour at the pier column. ; i.e., $1.0 \leq u_*/u_{*c} \leq 2.1$, the upper limit coinciding with values of u_* estimated the flow approaching the exposed abutment column during the abutment scour experiments. One test for each abutment column was conducted with the column placed in the main channel.

Figures 10-11a,b and 10-12a,b show photographs of clear-water scour and live-bed scour produced around the exposed standard-stub column and those produced around the exposed wing-wall column, respectively. Each pair of figures was for flow intensities $u_*/u_{*c} = 0.90$ and 1.26. The scour bathymetry is closely similar to scour holes formed at pile-supported piers.

For the live-bed cases associated with embankment breaching (i.e., $1.0 \leq u_*/u_{*c} \leq 2.1$), the flow intensities used for the column scour depth resulting from Scour Condition C were determined approximately for the pre-scour flow. The magnitudes of flow velocities, and thus u_*/u_{*c}, immediately upstream from the abutment were unsteady because the flow field changed as the embankment eroded. Accordingly, the flow intensity varied. Given the difficulties associated with a priori determination of u_* an exposed column, it is a practical expedient to use flow intensity at the pre-scour condition, or for design simply to assume live-bed scour. However, as live-bed scour conditions prevailed and scour depth is conveniently sensitivity to u_*/u_{*c}, exact determination of is unnecessary.

10-6

The data in Figures 10-9 and 10-10 show that d_{Smax} increased until $u_*/u_{*c} = 1.0$, then it dipped to about 70% of its peak value, with a wide range of uncertainties then occurring owing to bed-form presence. It is reasonable to use bed-form amplitude as an estimate of this uncertainty as indicated in Table 10-1. The data for Scour Condition C exhibit scatter associated with the presence of bed forms (dunes and ripples) in the vicinity of the abutment column. The local amplitude of bed forms near the column are included in Table 10-1. For some tests, column scour coincided with a bed-form trough, whereas for others scour was measured mid-amplitude. Continuous measurements of scour depth were not taken during the tests.

A further cause of scatter in scour-depth at a pier column is flow orientation at the column. Such scatter was greatest for the model wing-wall abutments, as evident in Figure 10-10. Flow breaching an embankment at an abutment column was not initially aligned with the column, but became more aligned as an embankment breach fully developed.

The scour depths predicted using the relationships proposed by Melville and Coleman (2000) and the HEC-18 equation (Richardson and Davis 1995) agree reasonably well with the data, though the HEC-18 equation overestimates slightly. Therefore, the pier-scour approach to scour-depth estimation for Scour Condition C, as suggested in Section 4.6, holds as valid.

The maximum values of scour depth at the model abutment columns can be approximated, in terms of column base (or pile-cap) width, for standard-stub columns as

$$d_{SOcolumn} \approx 1.7 b_{stub} \qquad\qquad (10\text{-}1)$$

And for wing-wall columns as

$$d_{SOcolumn} \approx 0.7 b_{wing} \qquad\qquad (10\text{-}2)$$

Here, b_{stub} and b_{wing} are the transverse widths of the abutment columns, as defined subsequently in Figure 10-16 and 10-17; for the models, the widths of the , $b_{stub} = 0.077$ m, and $b_{wing} = 0.48$ m (Figure 6-4 and 6-5 give prototype values. The lesser value of the coefficient for the wing-wall column reflects the angle of the wing-walls. Eqs 10-1 and 10-3 are approximate, and will vary with other abutment column designs.

10.4.2 Influence of Abutment Alignment

The scour data obtained with exposed standard-stub and wing-wall columns aligned at a range of angles agree with the trends generally known for scour at piers of fairly complex form. The scour data were obtained using $u_*/u_{*c} = 0.75$, with abutment alignment angle β varied from 0 to 15, 30°, 45°, and 90°. Figures 10-13, and 10-14 show the relationships between the maximum scour depths and abutment alignment, β, for the standard-stub and the wing-wall columns, respectively. For both columns, the minimum scour depth occurred when $\beta = 0˚$, and it increased monotonically to $\beta = 90˚$.

Scour depth for the standard-stub column was more sensitive to alignment angle than was the wing-wall column. By virtue of its broader width at $\beta = 0˚$, the scour depth at a wing-wall column at this alignment was greater than that at a standard-stub column similarly aligned. However, as β increased the scour depths approximately approach each other for the two columns. The scour depth for the wing-wall abutment aligned at $\beta = 90˚$ was only modestly greater than for the standard-stub column at the same alignment. Observations of scour development showed that exposure of the piles beneath the column relieved flow so as to weaken the downflow toward the bed at the front of the column, thereby somewhat diminishing the effect of column width and shape on eventual scour depth. This influence is illustrated in Figures 10-11 and 10-12 for the standard-stub and the wing-wall abutments aligned at $\beta = 0^o$, respectively; and, in Figures 10-15a,b for the two columns aligned at $\beta = 45˚$. The latter two figures reveal that pile width and configuration (also, elevation of pile cap) play a role determining eventual scour depth. The width and spacing of circular piles for both columns were the same, though the wing-wall column had more piles.

Figures 10-16 and 10-17 re-plot the data in Figures 10-13 and 10-14 in terms of an alignment factor, K_β, versus alignment angle, β. Here, K_β, is defined as the ratio of the local scour depth for the abutment column aligned at angle β relative to that when $\beta = 0$. Figure 10-16 compares the values of K_β, obtained for the standard-stub abutment with the commonly used set of alignment-factor curves proposed by Laursen and Toch (1956), who developed the curves using scour data obtained with simple rectangular piers extending at depth into a sand bed. The standard-stub column, though, comprises a rectangular column founded on a pile cap and pile cluster. The value of l/b_p for the column was 5.27, and its K_β values concur well with those Laursen and Toch suggest for $l/b_p = 6$. Though the column was supported by piles beneath the bed level, and the overall scale of scour depth magnitudes would be less than those for a rectangular column extending to depth within the bed, the curves show that the overall K_β trend for the standard-stub column is the same as for a rectangular block of similar proportions. No similar comparison and verification is immediately feasible for the wing-wall column. The K_β values given in Figures 10-16 and 10-17 are suggested for use in the design method described in Chapter 12.

Table 10-1. Effect of flow intensity on maximum scour depths at exposed standard-stub column and wing-wall column (constant alignment angle, $\beta = 0^o$)

Flow Intensity u_*/u_{*c} ("emb. breach" means value estimated from abut. scour expt.)	Maximum Scour Depth (m) ($\pm$ indicates bed-form amplitude)	
	Standard-Stub Abutment	Wing-Wall Abutment
0.75	0.08	0.21
0.80	0.09	0.24
0.90	0.11	0.27
1.00	0.12	0.29
1.10	-	0.27
1.26	0.08	0.19
1.29 (emb. breach)	0.09 ($\pm$ 0.005)	0.32, 0.23, 0.22, 0.16 ($\pm$0.10)
1.40 (emb. breach)	0.10 ($\pm$ 0.005)	-
1.55 (emb. breach)	0.13 ($\pm$ 0.015)	-
1.85 (emb. breach)	0.13 ($\pm$ 0.010)	-
2.10 (emb. breach)	-	0.32 (($\pm$0.02

10-10

Table 10-2. Effect of abutment alignment on maximum scour depths at exposed standard-stub column and exposed wing-wall column (constant flow intensity, $u_* / u_{*c} = 0.75$)

Abutment Angle β	Maximum Scour Depth (m)	
	Standard-Stub Abutment	Wing-Wall Abutment
0°	0.08	0.21
15°	0.13	0.22
30°	0.18	0.29
45°	0.22	0.29
90°	0.29	0.32
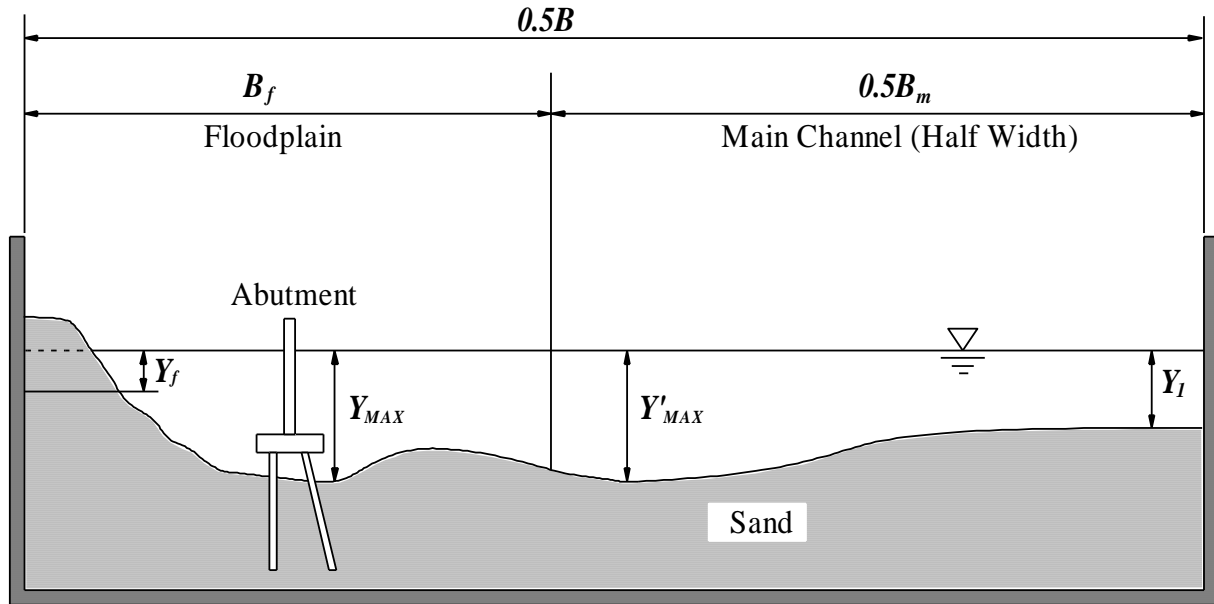
Figure 10-1. Principal variables measured for abutments subject to Scour Condition C
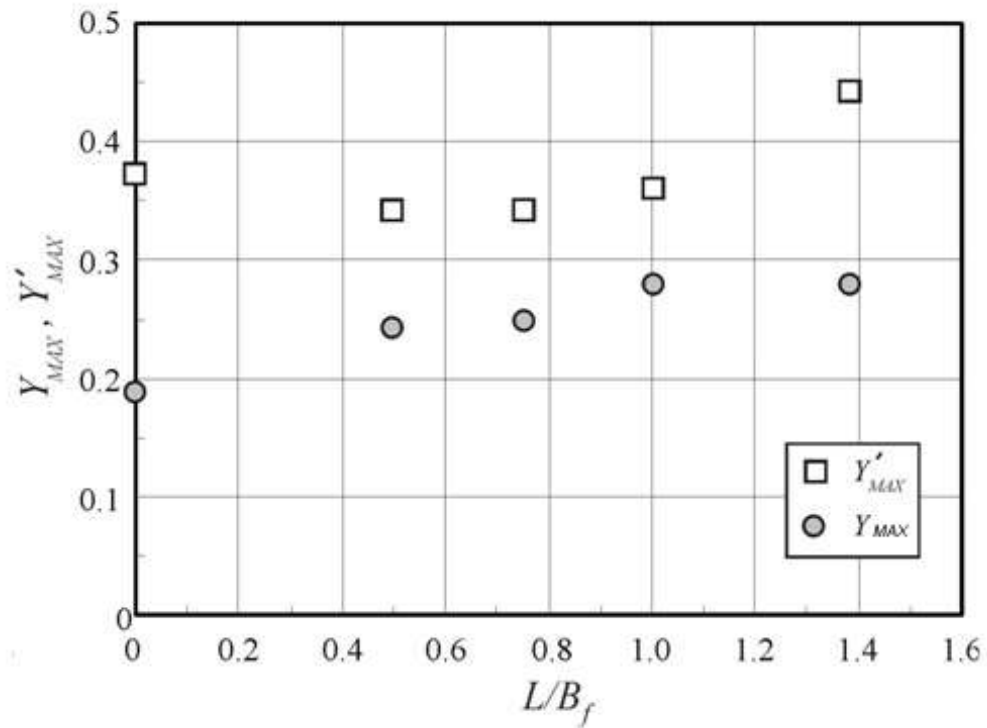
Figure 10-2. Relationship between Y_{MAX} and Y'_{MAX}, with L/B_f for exposed spill-through abutments. Note that embankment extends beyond floodplain when L/B_f exceeds 1
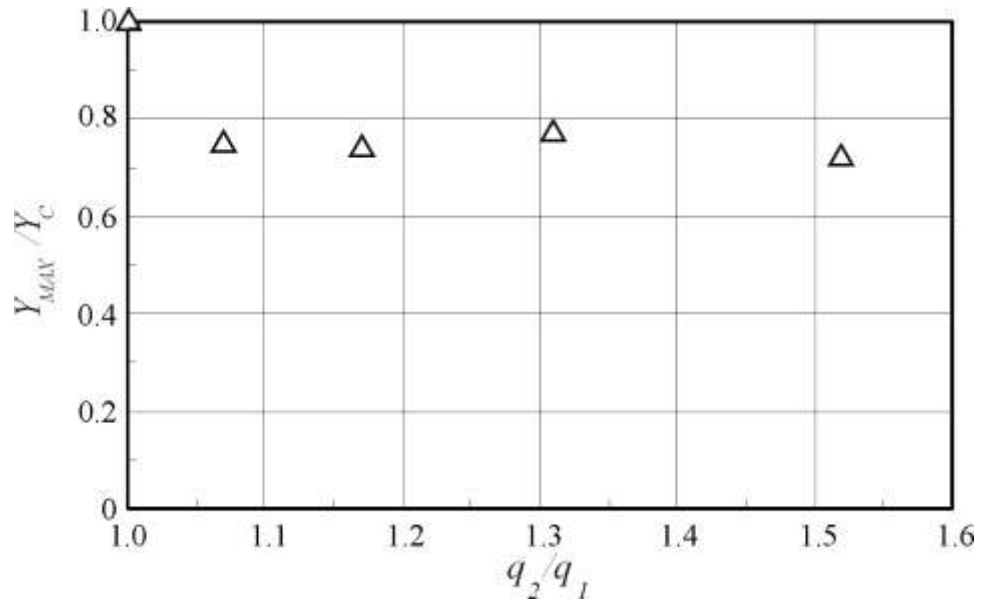
Figure 10-3. Relationship between Y_{MAX}/Y_C and q_2/q_1 for spill-through abutments
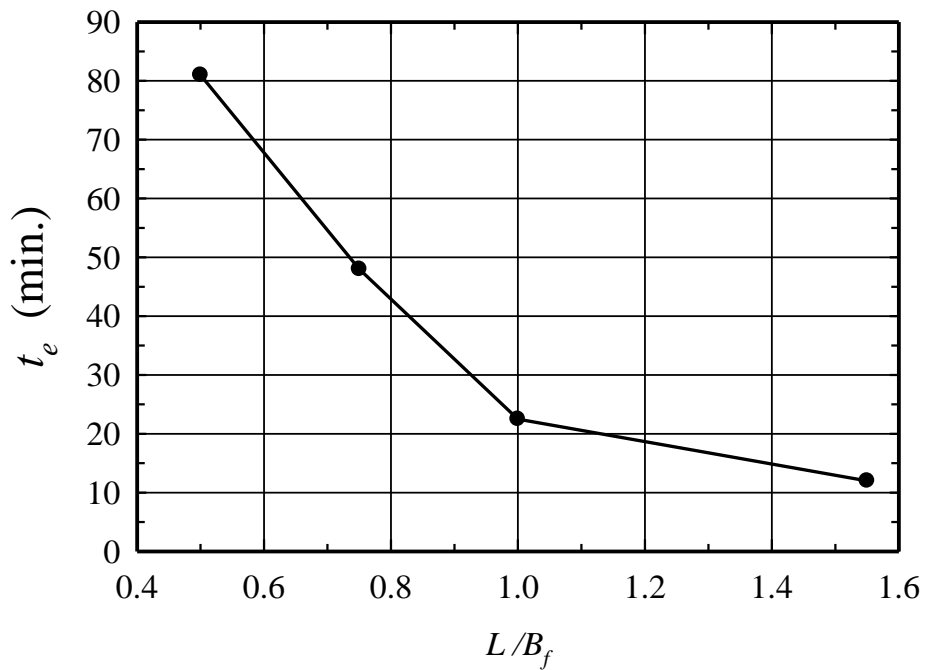
Figure 10-4. Variation of time to embankment breach, t_e, against L/B_f
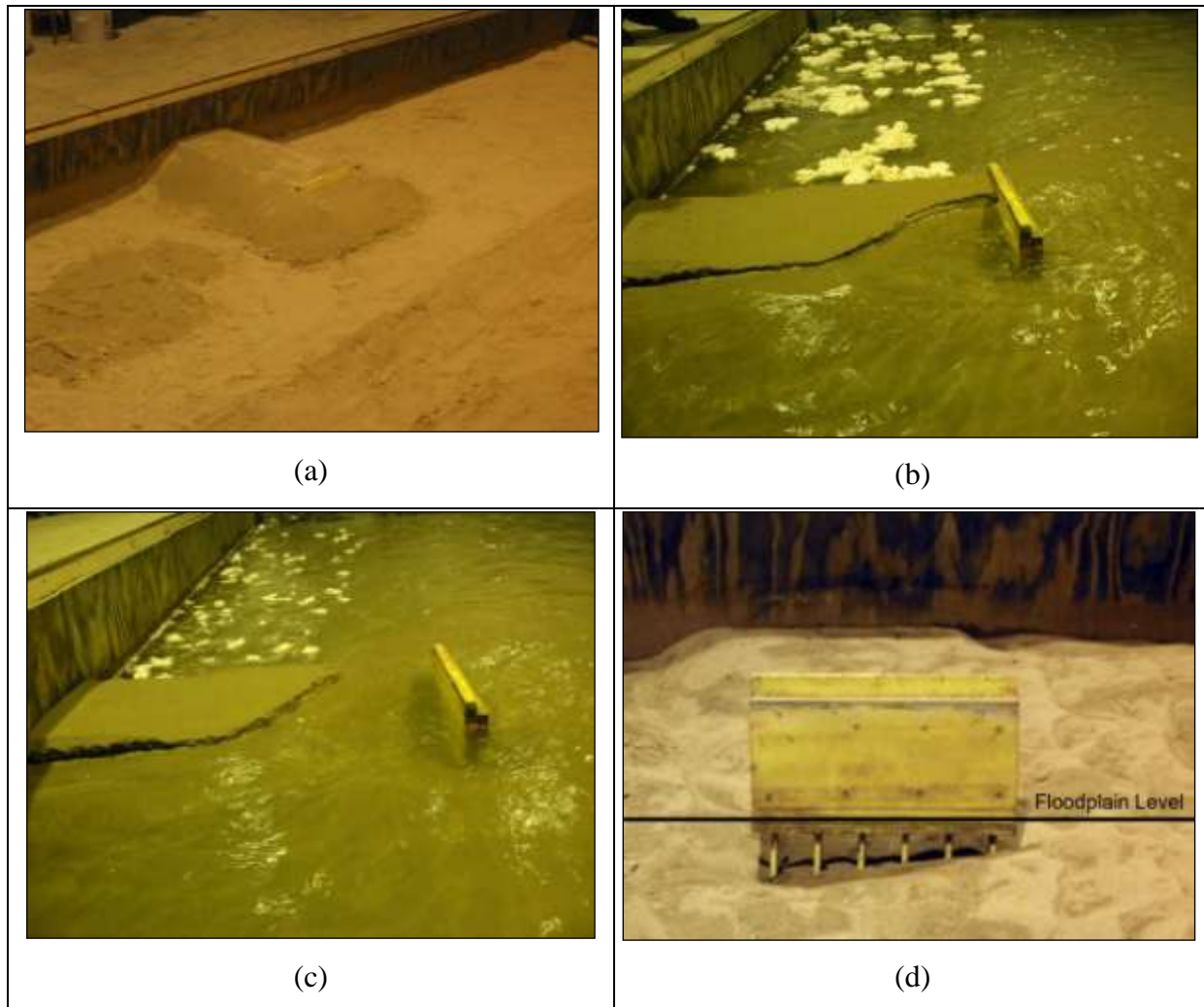
Figure 10-5. Scour development around standard-stub abutment under Scour Condition C with $B_f/0.5B = 0.43$ and $L/B_f = 0.70$; initial condition: $t = 0$ (a), initial embankment breach (b), embankment breach (c), and final scour hole at exposed abutment column (d)
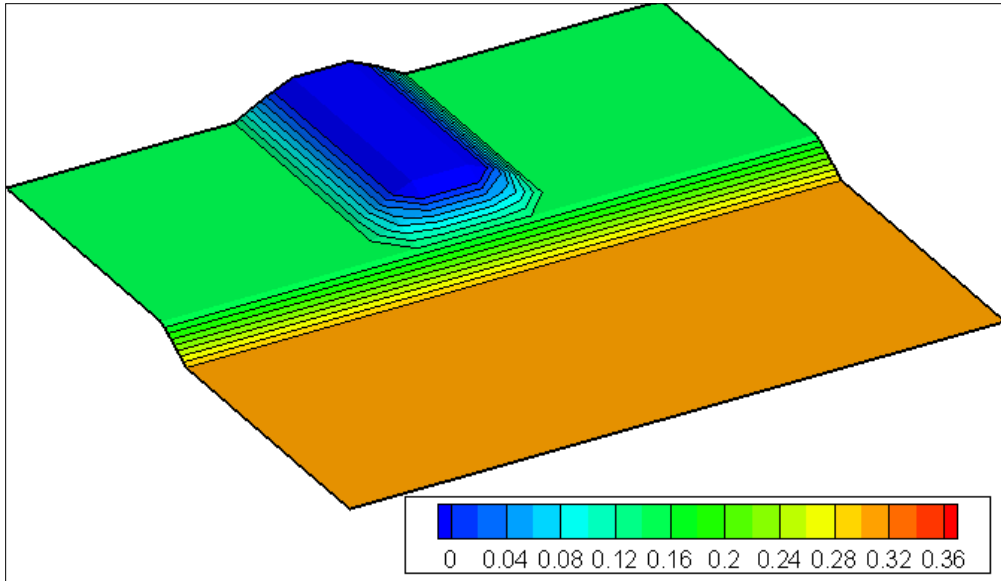
(a)
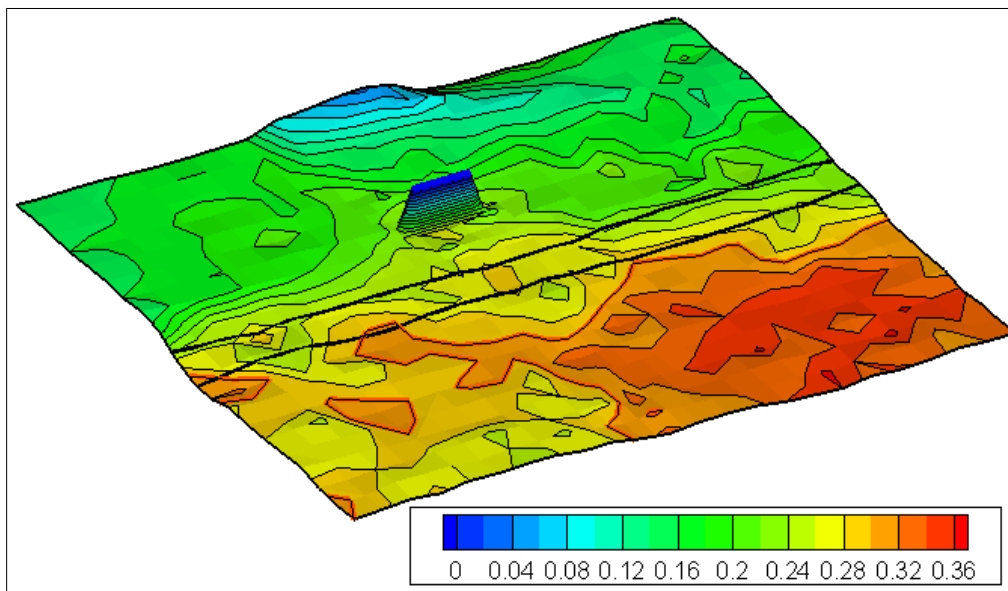
(b)

Figure 10-6. Initial layout of spill-through abutment (a), and resultant scour bathymetry (b) under Scour Condition C with $B_f/0.5B = 0.43$ and $L/B_f = 1.00$
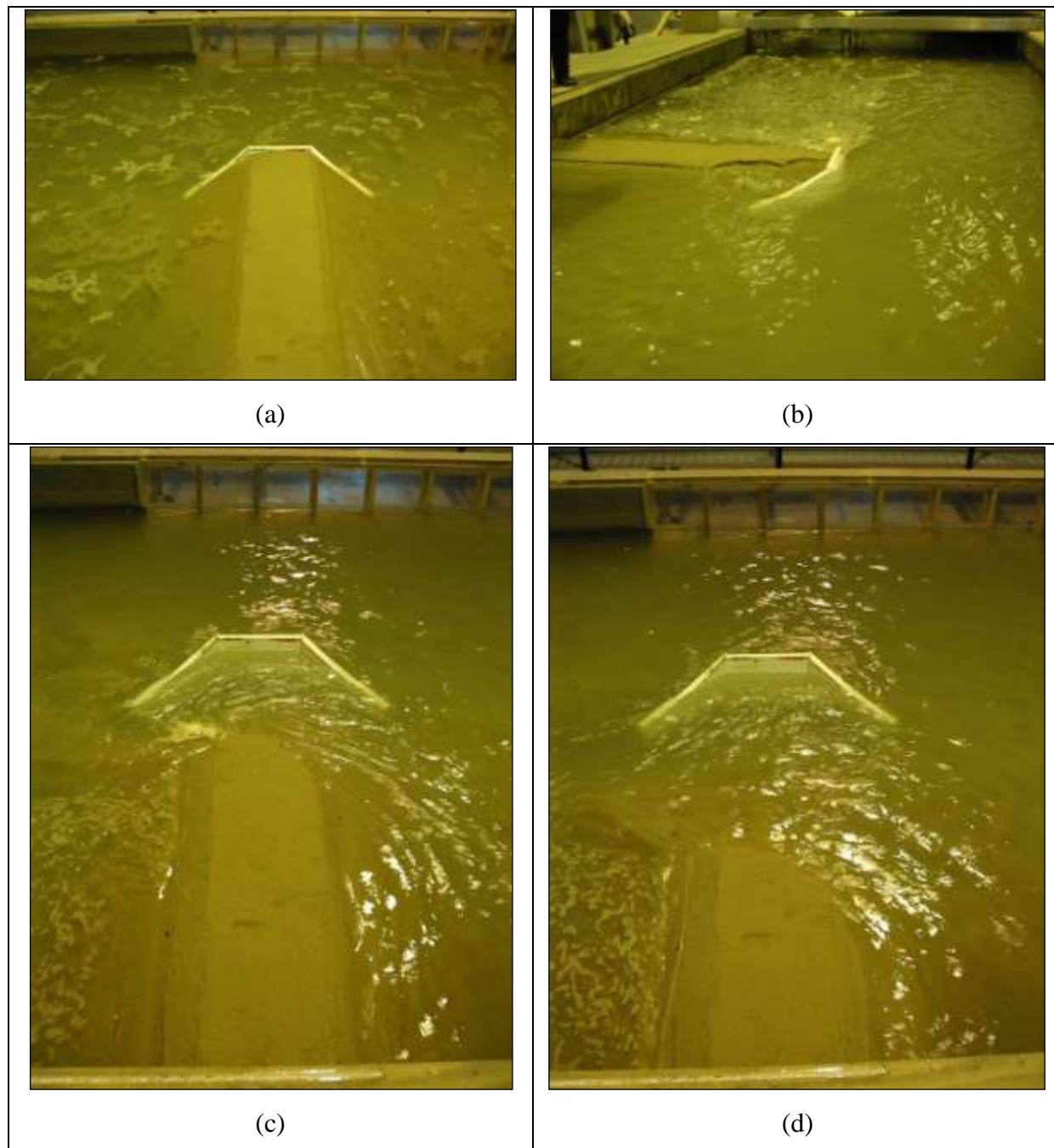
Figure 10-7. Development of Scour Condition C at unprotected wing-wall abutment set with $L/B_f = 1.22$, and $B_f/0.5B = 0.43$; initial stage (a), embankment eroding (b), embankment breached (c), and further development of embankment erosion (d)

(e)

(f)
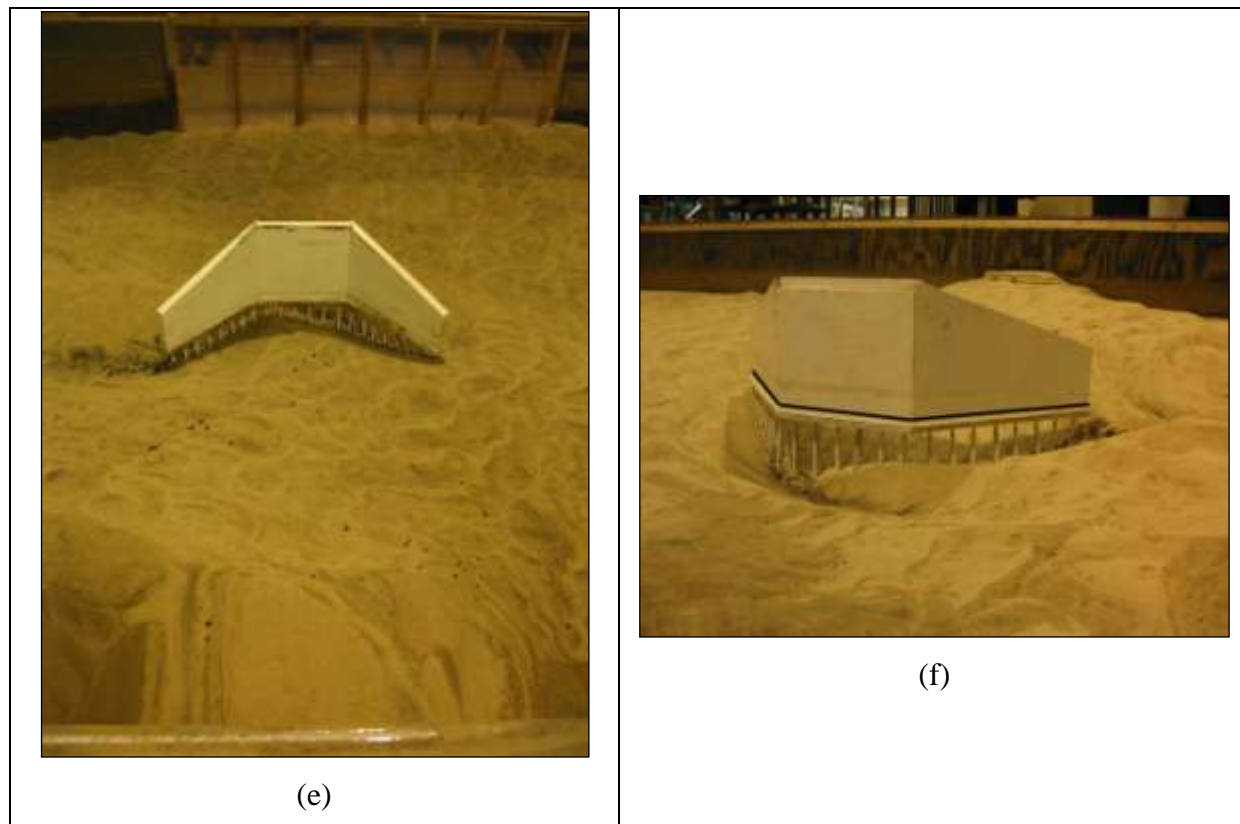
Figure 10-7 - continued. Development of Scour Condition C at unprotected wing-wall abutment set with $L/B_f = 1.22$, and $B_f/0.5B = 0.43$; exposed wing-wall abutment and breached embankment (e), and extensive scour around exposed abutment column (f)
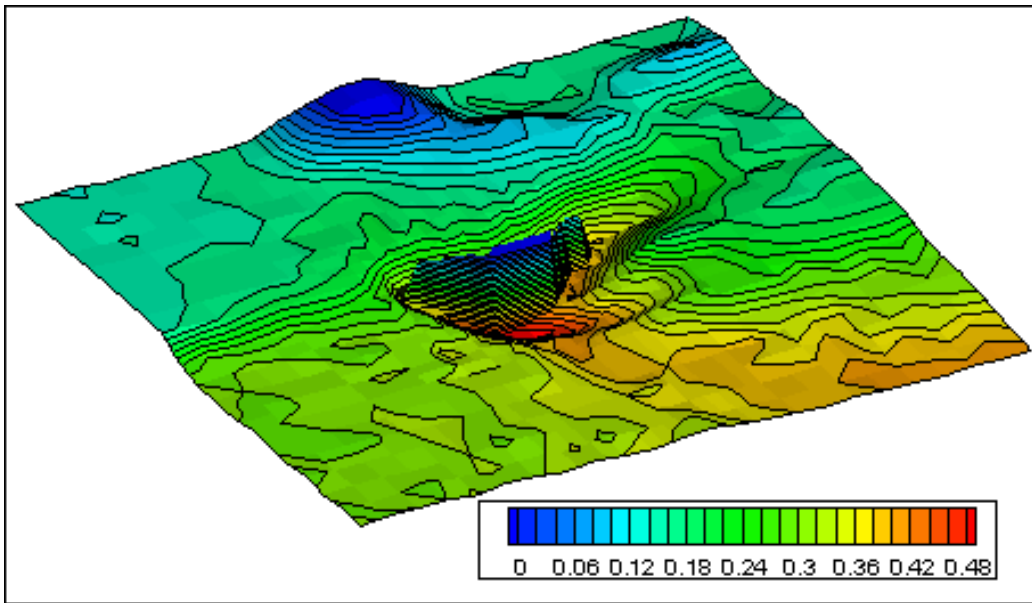
Figure 10-8. Resultant scour bathymetry around wing-wall abutment for Scour Condition C
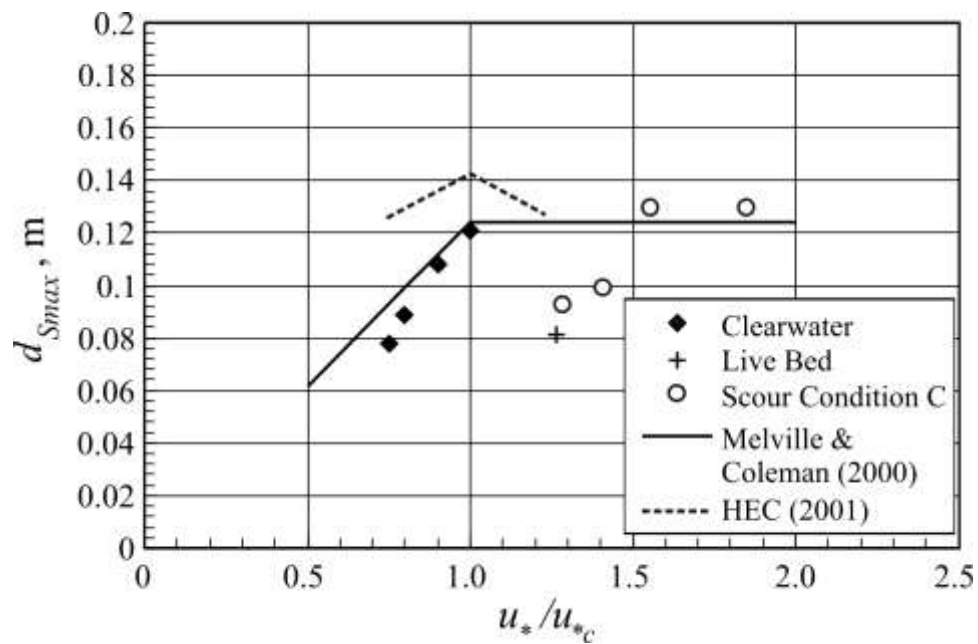
Figure 10-9. Influence of flow intensity, u_*/u_{*c}, on scour depth at exposed standard-stub column (HEC 2001 is from Richardson and Davis 2001)
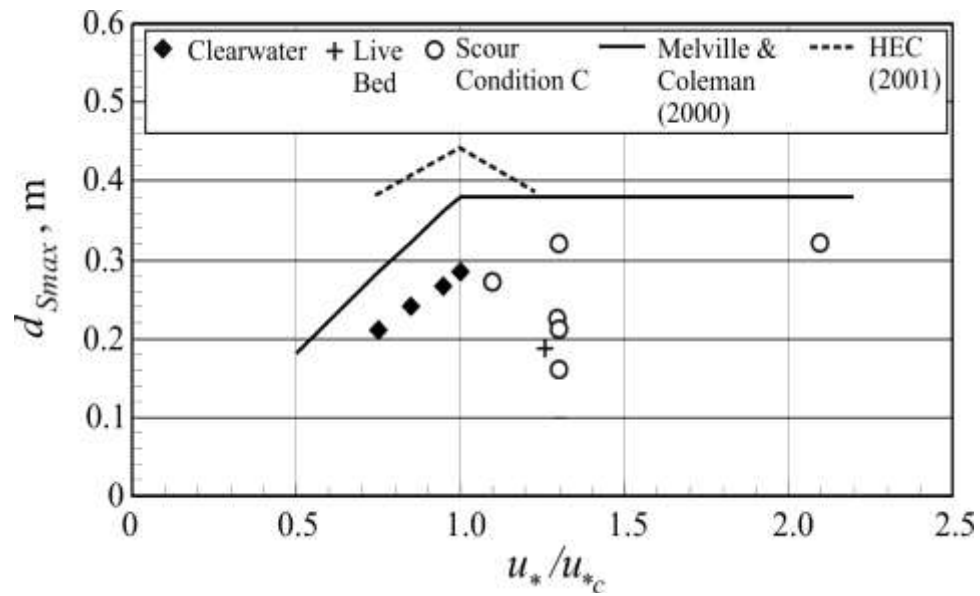
Figure 10-10. Influence of flow intensity, u_*/u_{*c}, on maximum scour depth at exposed wing-wall column (HEC 2001 is from Richardson and Davis 2001)

(a)
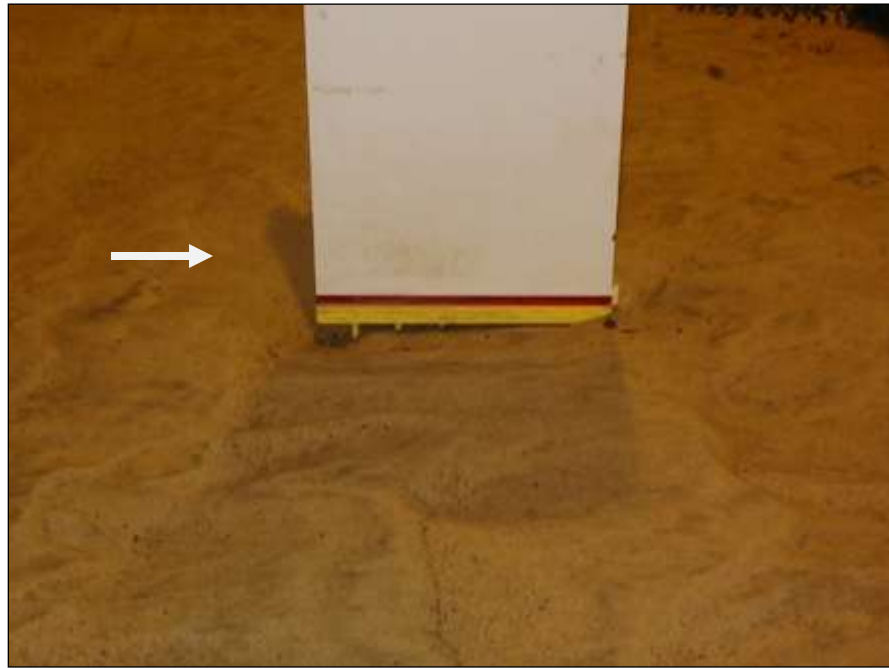
(b)

Figure 10-11. Scour holes produced by exposed standard-stub column with $\beta = 0^\circ$; (a) u_*/u_{*c} = 0.90, and (b) u_*/u_{*c} = 1.26
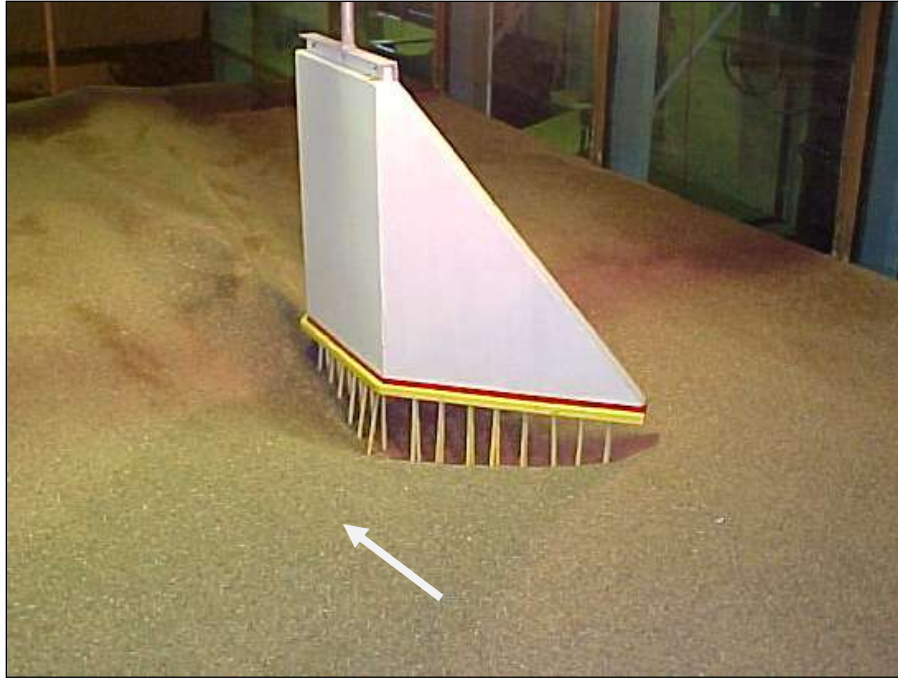
(a)
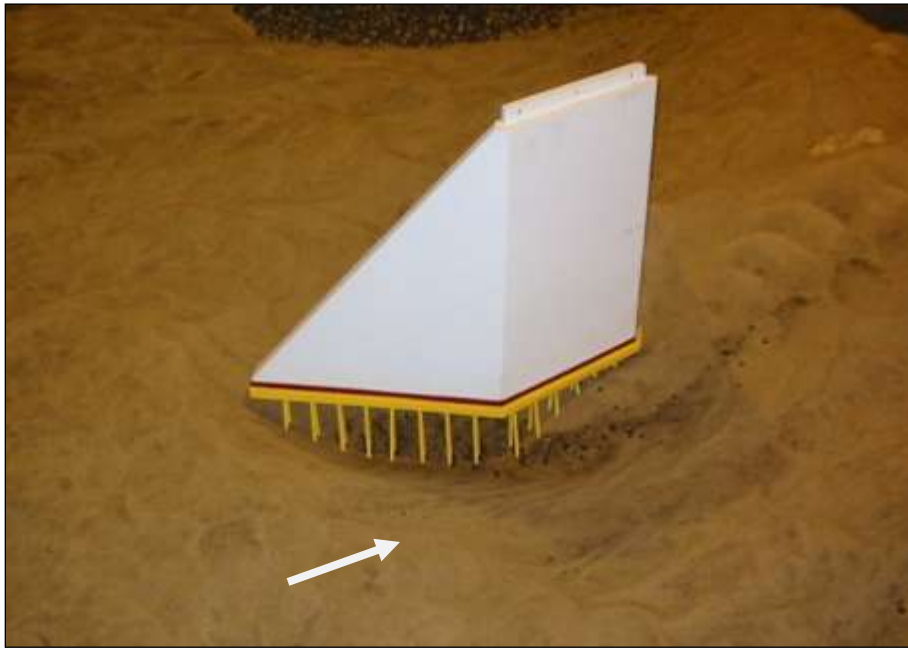
(b)

Figure 10-12. Scour holes produced by exposed wing-wall column with $\beta = 0^{\circ}$; (a) $u_*/u_{*c} = 0.90$, and (b) $u_*/u_{*c} = 1.26$
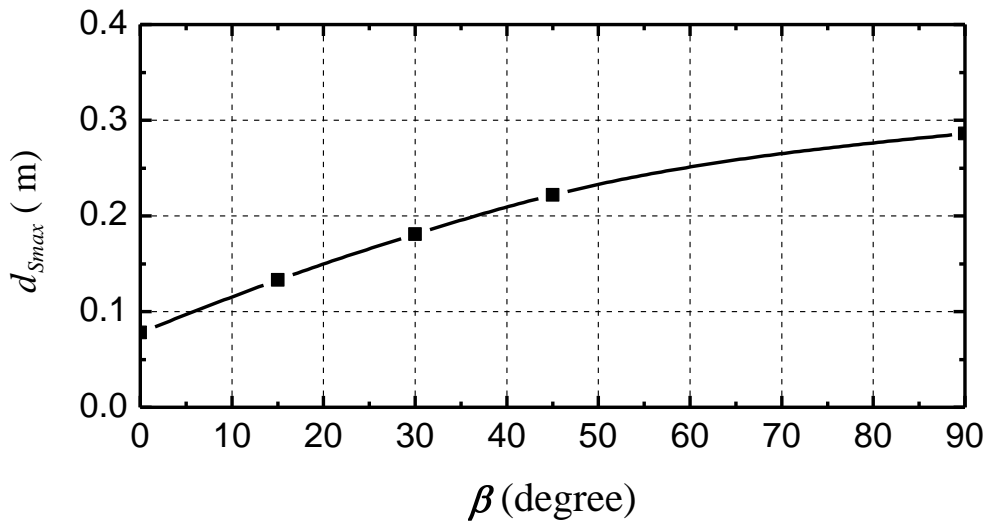
Figure 10-13. Maximum scour depth versus abutment alignment, β, for exposed standard-stub column
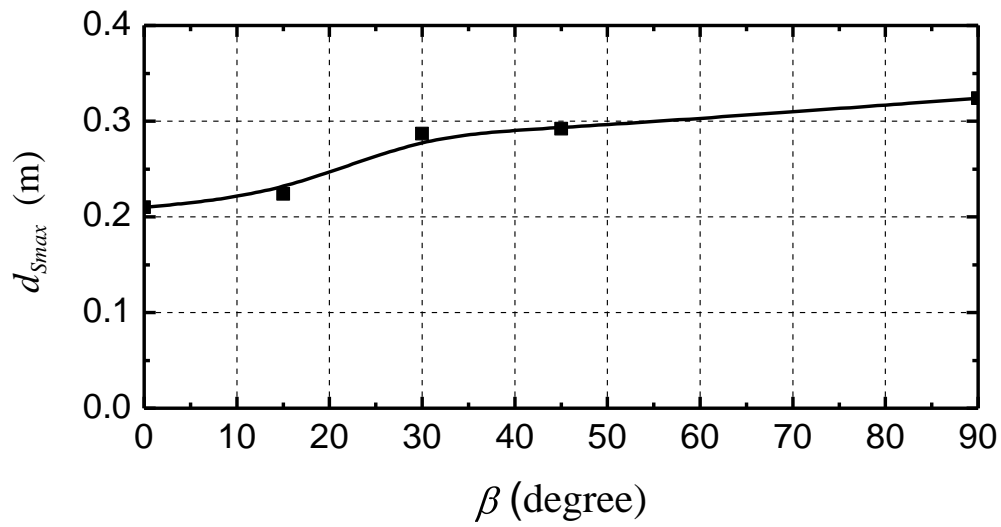
Figure 10-14. Maximum scour depth versus abutment alignment, β, for exposed wing-wall column

(a)

(b)

Figure 10-15. Views of scour holes with $\beta = 45^{o}$ to flow direction; standard-stub column (a), and wing-wall column (b)
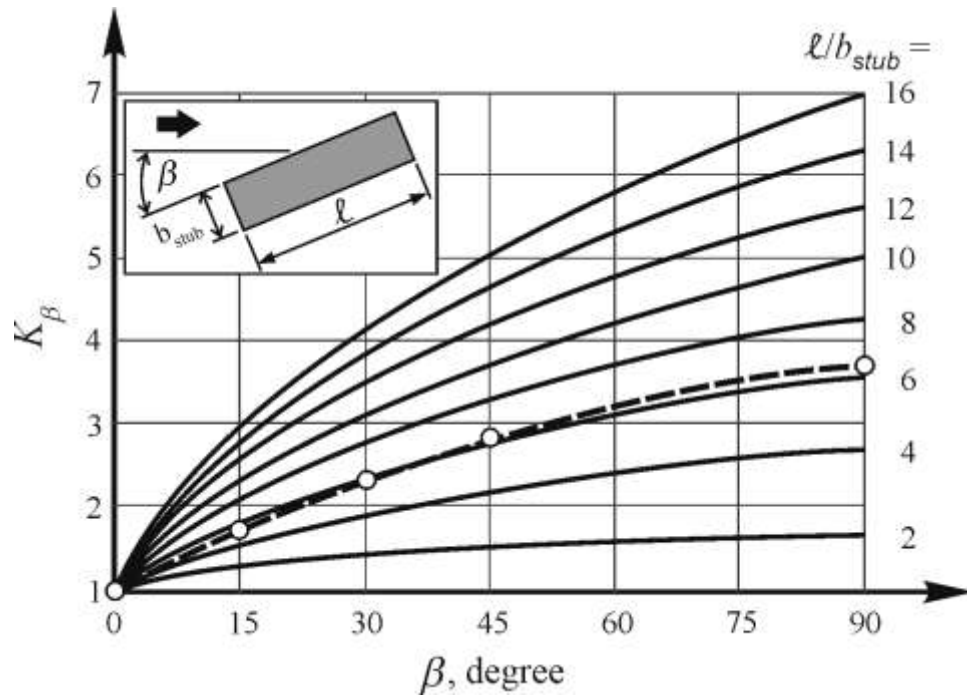
Figure 10-16. Variation of alignment factor, K_β, against abutment alignment angle, β, for standard-stub abutments; data (o) shown are plotted on the alignment factor diagram proposed by Laursen and Toch (1956)
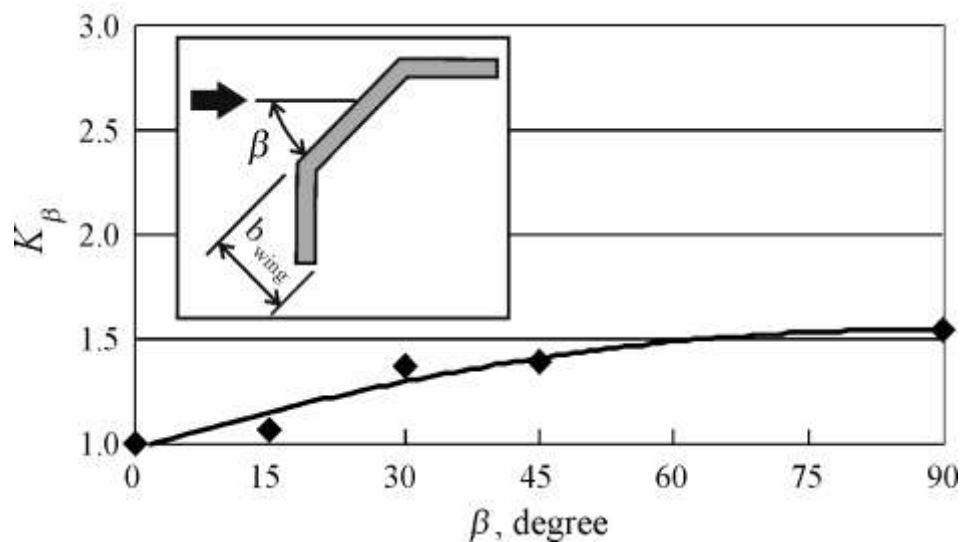
Figure 10-17. Variation of alignment factor, K_β, for wing-wall abutments

CHAPTER 11

PIER INFLUENCE ON ABUTMENT SCOUR

11.1 Introduction

The laboratory tests presented here address the influence of pier presence on abutment-scour for Scour Conditions A and B. Equally, they also yield data and insights regarding abutment influence on scour at a pier. The test results are given in terms of maximum scour depth at the scour hole for an abutment-pier combination, d_{Smax}, relative to the maximum scour depth at an abutment alone (no pier present), d_{Smax0}. Additionally, the results include the location of d_{Smax}, and the scour depth at the pier itself, d_{Spier}. The experiments were run with a pile-supported pier of standard design used by the Iowa Department of Transportation (Figure 6-14). One additional experiment was run with a large circular pier (model diameter = 0.2m), to ascertain whether a larger pier width substantially affects scour depth at an abutment.

A prime independent parameter varied in the results was L_p/Y_f, where L_p is pier distance from the abutment toe, and Y_f is flow depth at the abutment toe. For abutments on floodplains, Y_f is flow depth on the floodplain. Figure 11-1 shows these variables. If a channel has no floodplain, approach flow depth, Y_1, should be substituted for Y_f. The other parameters varied were the following combinations of abutment shape and layout:

1. Spill-through abutments on fixed floodplains (Scour Condition A);

2. Spill-through abutments on erodible floodplains (Scour Conditions A and B). The abutments were protected with a layer of simulated riprap stone, except in one test; and,

3. Wing-wall abutments on erodible floodplains (Scour Conditions A and B).

As the experiments showed that pier presence did not substantially increase scour depth for these combinations, additional experiments were not run for wing-wall abutments on fixed floodplains. Further, an experiment conducted with a pier near a wing-wall abutment for Scour Condition B (scour on floodplain) produced the same result as for the same the same pier proximity

arrangement under Scour Condition A with an erodible floodplain. The abutment scour forms obtained for the two Conditions were the same. Therefore, the tests were pursued using Scour Condition A with, and without an erodible floodplain.

11.2 Scour-Depth Trends for the Abutments

Presented here are the laboratory data on scour depths for the abutment and floodplain combinations investigated.

11.2.1 Spill-Through Abutment on Fixed Floodplain

Pier presence slightly increased scour depth at the spill-through abutment on the fixed floodplain, with $L/B_f = 1.00$, and $B_f/0.5B = 0.43$. Figure 11-2 shows, with the data expressed as ds_{max}/ds_{max0} versus L_p/Y_f, that pier presence increased scour depth by about 5% to 7%, but only over the range L_p/Y_f, = 0 to 6; i.e., the distance from abutment toe to pier (Figure 11-1) was within about $6Y_f$ (0.9m in the model), and when $L_p/Y_f = 0$, the pier was at the abutment toe on the floodplain. For larger values of L_p/Y_f, pier proximity had no substantial influence on maximum depth of abutment scour, and $d_{Smax}/d_{Smax0} = 1.0$.

Included in Figure 11-2 is an uncertainty margin reflecting the magnitudes of dune and ripple height, H, relative to the measured value of d_{Smax}. The band encompasses the heights of dunes moving along the approach channel. For all the experiments, slight differences in ds_{max}/ds_{max0} attributable to pier presence were well within the uncertainty band associated with dune height. No dunes, however, were located within the scour region. The results infer that the addition of half the estimated dune height at the abutment site sufficiently takes into account any scour depth increase caused by pier presence.

The results in Figure 11-2 indicate that abutment scour was dominated by the abutment flow field, and the local flow field produced by the pier only mildly amplified maximum scour depth when the pier was close to the abutment. The additional experiment conducted using a large circular cylinder to simulate a pier confirmed this finding. As evident by the pertinent data included in this figure, the presence of a cylinder of diameter (0.2m) equivalent to half the simulated deck width did not deepen the scour hole at the abutment.

11.2.2 Spill-Through Abutment on Erodible Floodplain

For the spill-through abutments on erodible floodplains, pier presence reduced maximum scour depth when pier distances were approximately less than about three time Y_f; i.e., $L_p/Y_f \leq 1$ or 3 for the two widths of floodplain ($B_f/0.5B = 0.43$ and 0.23, respectively). When the values of L_p/Y_f exceeded these values, pier presence had no discernable influence on abutment scour depth or location, and $d_{Smax}/d_{Smax0} = 1.0$. The data trends in Figures 11-3 and 11-4 show reductions in d_{Smax}/d_{Smax0} of about 10% and 20% for the two widths of floodplain when the pier was at the spill-slope toe ($L_p/Y_f = 0$).

The reductions in d_{Smax}/d_{Smax0} were less for the wider erodible floodplain at $B_f/0.5B = 0.43$, because an abutment located fully across a wider floodplain produced a deeper scour, and pier influence on abutment scour depth was less. Figure 11-5 compares pier influence for the two floodplain widths used. The influence, by and large, is within the error margin associated with dune height.

In comparison, for the fixed floodplain set at $B_f/0.5B = 0.43$, pier presence did not reduce scour depth but instead slightly increased it (Figure 11-2). A pier in close proximity to an erodible, riprap protected embankment provided a measure of abutment-scour protection.

11.2.3 Wing-Wall Abutment on Erodible Floodplain

The laboratory results obtained from the experiments with a pier adjacent to wing-wall abutments on an erodible floodplain ($B_f/0.5B = 0.23$) indicate that pier proximity, or L_p/Y_f, marginally increased depth of abutment scour, though the increase could be attributable to dune presence. This finding, shown in Figure 11-6, is consistent with the result obtained for the experiments with the spill-through abutments on a fixed floodplain (Figure 11-2). Though pier presence increased scour depth by about 5% to 7%, the scour depths are within the uncertainty margin associated with dune height. In brief, pier presence had no dramatic effect on abutment scour depth. Note that, because the abutment toe is directly below the abutment cap for a wing-wall abutment, the value of L_p for the first pier position was set at $3.5Y_f$ (Figure 11-6).

11.3 Scour-Depth Trends for Piers near Abutments

Because the model abutments developed a much deeper scour than did the pier, scour depth at the pier was dominated by abutment scour, when the pier was close to an abutment. Data are presented for the following pier situations:

1. Pier near a spill-through abutment on a fixed floodplain;
2. Pier near a spill-through abutment on an erodible floodplain. In all but one test, the abutment embankment was riprap protected; and,
3. Pier near a wing-wall abutment on an erodible floodplain. In all but one test, the abutment was pile supported. One test was run with the abutment column on a simulated sheet-pile

11.3.1 Pier near Spill-Through Abutment on Fixed Floodplain

Figure 11-7 plots d_{Spier}/d_{S0pier} versus L_p/Y_f, where d_{Spier} is the scour depth at pier with the abutment present, and d_{S0pier} is the scour depth at pier without the abutment. This figure shows that initially d_{Spier}/d_{S0pier} did not vary with L_p/Y_f, reflecting the fact that the pier was essentially enveloped by the flow-field features generated by abutment. Pier presence did not influence abutment scour depth substantially; d_{Spier} coincided with the abutment scour depth, d_{Smax}. In other words, abutment proximity fully dominated pier scour development and its depth.

As L_p/Y_f further increased, the abutment's influence decreased and so did pier scour depth. Eventually, when L_p/Y_f exceeded about 11 ~ 12, pier scour depth became equivalent to the local, pier-scour depth when no abutment was present; i.e., $d_{Spier}/d_{S0pier} = 1$.

The real concern for a pier located close to an abutment is that the depth of scour at the pier is determined primarily by abutment scour, which considerably exceeds the scour depth that would occur at the pier alone. The maximum scour depth at an isolated pier aligned with the approach flow was only about 15% of the maximum scour depth at the abutment for Scour Condition A, and $B_f/0.5B = 0.43$.

It is possible to normalize the curve in Figure 11-7 into a format that is useful for design estimation of scour at a pier close to an abutment. Chapter 12 subsequently presents this normalized curve. The curves limits entail basing pier scour estimation on abutment scour depth when a pier is close to an abutment; or on pier scour depth when the pier is distant from an abutment.

11.3.2 Pier near Spill-Through Abutment on Erodible Floodplain

The data on pier scour depth for piers near spill-through abutments on erodible floodplains gave a different trend than when the floodplain was fixed. Figure 11-8 expands Figure 11-7 with additional data for spill-through abutments on erodible floodplains. The two widths of erodible floodplain ($B_f/0.5B$ = 0.43 and 0.23, with L/B_f = 1) gave the same trend, with the data aligning.

When the pier was at the abutment toe, it was protected by embankment spill-slope soil and riprap, which failed and collected around the pier, and thereby preventing scour at the pier. However, when the pier was sufficiently distant from the abutment toe, so that failed spill-slope soil and riprap did not reach the pier, scour occurred at the pier. The maximum scour depth exceeded scour at an isolated pier (d_{S0pier}), but was considerably less than for the same pier position but with a fixed floodplain. Because the embankment eroded, and thus the depth and width of abutment scour was reduced, the reach of abutment influence on pier scour was less than when the floodplain was fixed.

The test run without riprap protection of the embankment, and the pier located such that L_p/Y_f = 0.53, resulted in the eventual washout of the embankment and the development of Scour Condition C at the abutment column. Scour was deeper at the abutment column than at the pier, for the reasons explained in Section 11.4.2.

11.3.3 Pier near Wing-Wall Abutment on Erodible Floodplain

The data on pier scour depth for piers near wing-wall abutments on erodible gave the same trend as for spill-through abutments on a fixed floodplain. Figure 11-8 also gives the data for wing-wall abutments on an erodible floodplain ($B_f/0.5B$ = 0.23, with L/B_f = 1). Because there was no spill-slope for the wing-wall abutment used, little if any embankment soil and riprap collected at

the pier. Erosion of the floodplain around the abutment, though, eased flow velocities and resulted in lesser scour depth at the abutment, as described in Chapter 8. The smaller scour at the abutment reduced the extent of abutment influence on pier scour.

The test run with the abutment column on sheet-pile support produced the same abutment scour depth as obtained without a pier close to the abutment. Accordingly the scour depth at the pier was commensurate with scour depth attributable to the abutment. This test was conducted with $L_p/Y_f = 3.5$.

11.4 Observations of Scour Bathymetry and Flow Field

The observations of scour bathymetry and the flow field help explain the data trends on scour depth.

11.4.1 Spill-Through Abutment on Fixed Floodplain

The set of photographs in Figure 11-9 show the scour bathymetry commensurate with the data in Figure 11-2. Pier presence moved the location of maximum scour depth slightly closer to the centerline axis of the model spill-through abutment for Scour Condition A. Also, for a fairly narrow range of pier locations ($2.0 < L_p/Y_f < 3.0$) pier presence widened the scour region. For example, as Figure 11-10 illustrates, when $L_p/Y_f = 3.2$, pier presence doubled the width of the scour region compared to when no pier was present. Pier presence in this distance range resulted in an interaction between abutment and pier scours.

The increase in Y_{Pmax}/Y_{MAX} (or scour depth) for the range of L_p/Y_f values investigated is attributable to the pier's action of increasing the amount of flow deflected around the toe of the spill-through abutment. Essentially, for $L_p/Y_f < 6$, pier presence increased the abutment's length, increased flow contraction through the bridge waterway, and thereby slightly deepened scour for Scour Condition A. This influence was evident in LSPIV images showing flow from the floodplain passing around the pier's outer side of the pier. The region of turbulence between the pier and the abutment indicated that relatively minor amount of flow passed in this region. As the pier was moved further away from the abutment's toe, more flow passed between the abutment and the pier, causing the pier's influence on abutment scour depth to diminish.

11-6

The results show that, even when a pier was adjacent to an abutment, the abutment flow field dominated abutment scour. Flow contraction around the abutment, and turbulence produced by flow passing around that abutment were primarily responsible for the scour. The pier slightly modified the flow field, but did not generate major additional turbulence structures that exacerbated scour. The pier's pile cap was also largely sheltered by a wake eddy formed by flow passing from the floodplain and entering the main channel.

Because it was found that pier proximity did not result in substantially deeper abutment scour for spill-through abutments on a fixed floodplain, additional tests were not conducted using wing-wall abutments.

11.4.2 Spill-Through Abutment on Erodible Floodplain

As for Scour Condition A at an abutment on a fixed floodplain, pier presence only slightly affected abutment flow field, which was marked by flow contraction around the abutment, and turbulence produced by flow passing around that abutment. The set of photographs in Figure 11-11 show the scour bathymetry commensurate with the data for the abutment layout $B_f/0.5B = 0.43$ (Figure 11-3), scour at a pier and a nearby spill-through abutment on an erodible floodplain. The photographs in Figure 11-12 provide a similar set of scour views commensurate with the data associated with abutment layout $B_f/0.5B = 0.23$ (Figure 11-4).

Pier presence caused the location of maximum scour depth to move closer to the axis of the bridge and thus closer to the abutment for experiments with the non-erodible abutment. However, for the experiments with an erodible floodplain, the maximum scour depth occurred a little downstream of the abutment as set of bathymetry measurements illustrated in Figure 11-13.

Additionally, pier presence exerted a protective influence when the floodplain was erodible and the abutment's embankment was protected by riprap. This influence entailed the pier blocking considerable amount of riprap stone from moving far from the abutment slope when the slope began failing. In so doing, the pier acted to maintain a greater area concentration of riprap stone around the base of the abutment, and thereby retarded scour development. As L_p/Y_f increased,

the amount of riprap stone blocked by the pier diminished, riprap stone was dispersed more sparsely over a larger area, causing a deeper scour to develop. When riprap stone was dispersed over a greater area, and scour deepened, the embankment became more prone to be breached.

As noted in Section 11.3.2, scour at an unprotected abutment with a pier at its spill-slope toe led to a deeper scour at the abutment column than at the pier. Figure 11-14 depicts the resulting scour for this situation. Observations of scour progression showed the pier to be sheltered in the flow separation region at the end of the abutment, while flow impinged directly against the abutment column as the embankment breached (Figure 11-14a). Once the embankment breached, the pier was partially sheltered by the wake as flow passed around the exposed abutment column. Consequently, a deeper scour occurred at the abutment column than the pier (Figure 11-14b).

11.4.3 Wing-Wall Abutment on Erodible Floodplain

Pier proximity to abutment on an erodible floodplain affected depth scour to a modest extent that is within the amplitude of dunes formed in the flume. As illustrated in Figure 11-6, a maximum increase in depth of about 7% occurred for this abutment arrangement. The corresponding scour bathymetries are shown in Figure 11-13. Pier presence slightly increased the width of the scour region, though not as much as for the spill-through abutments. In overall terms, scour was dominated by flow contraction around the abutment.

The tests showed that, when the abutment was on sheet-piles, a pier close to the abutment ($L_p/Y_f = 3.5$) did not alter abutment scour depth. Scour development was driven by the flow field close to the abutment.

11.5 Flow-Field Observations

The influence of pier proximity on abutment scour is describable in terms of the flow field developed by an abutment at a bridge waterway, and the erosion characteristics of the waterway boundary.

The LSPIV measurements of flow-field surface velocities support the scour-depth trends evident in Figure 11-1 through 11-4. Pier proximity to abutment exerted only a small effect on scour depth for each abutment condition. This finding confirms that abutment scour was dominated by the abutment flow field; i.e., by the contraction of streamlines around the abutment, and the large-scale turbulence produced by flow passing around that abutment.

The pairs of images in Figure 11-14 illustrate LSPIV images and the resulting velocity contours of the flow field before and after scour at a spill-through abutment with an adjacent pier. The development of scour deepened the flow depth, reduced flow velocity, and subsequently strengthened the eddy circulation in the wake region.

A shortcoming of the LSPIV method, though, is that it does not illuminate the flow structures within the flow around the pier and abutment. However, Figure 11-15 shows that the pier generated comparatively little turbulence. Moreover, when close to the abutment, the pier was skewed to its local approach flow, thereby presenting a larger width to the flow. The flow-field observations also indicate the pier close to the abutment acted to, in effect, lengthen the abutment. The two further pairs of photographs in Figure 11-15 illustrate how pier presence initially pushed the approach flow further away from the abutment, and then as scour developed pier presence deflected a small portion of flow between the abutment and the pier. Though the maximum scour depth did not differ substantially for an abutment with or without a pier close by, the modified flow around the abutment adjusted the wake flow field (e.g., comparison of Figures 11-15a-ii and b-ii.

An important practical question concerns the required value of the distance L_p before scour at a pier is beyond the influence of an abutment. This question has a two part answer:

1. By virtue of an abutment's contraction of flow through a waterway, a pier will be in a region of flow contracted an average amount as used to estimate long-contraction scour; and,

2. If sufficiently close to an abutment, a pier will be in a region (commensurate with a short contraction) of amplified flow contraction and abutment-generated turbulence structures

that produce abutment scour. A figure such as Figure 11-7 indicates for Scour Condition A that pier scour will be influenced by abutment scour if the pier is within a distance of about 11 times floodplain flow depth; i.e., if $L_p/Y_f < 11$, or thereabouts. Though lesser values of limiting L_p/Y_f are likely when the floodplain is erodible (Figure 11-8), this distance limit is a reasonable approximate guide.

The limit for L_p/Y_f suggested in item 2 above also can be assessed using measurements and numerical simulation of the flow passed an abutment. The set of profiles for unit discharge through the bridge waterway axis, q_2, presented in Figure 7-26 infers that the distance limit $L_p \approx 11Y_f$ is beyond the region of amplified contraction. For the floodplain flow depth used in the tests, $Y_f = 0.15$, the distance limit is 1.65m.

Flow field measurements made for Scour Condition B also suggest that the distance limit $L_p \approx 11Y_f$ is a reasonable, approximate guide. Figure 11-18, for example, shows distributions of q_2/q_f for flow around a spill-through abutment undergoing Scour Condition B. The distributions are for flow before scour and after scour. They show that, beyond $L_p \approx 11Y_f$, the values of unit discharge reduce and become level, and that the boundary bathymetry is away from the scour formed at the abutment.

While further work is needed to confirm or elaborate the distance limit for which a scour at a pier is unaffected by abutment scour, the approximate limit $L_p \approx 11Y_f$ is a useful guide.
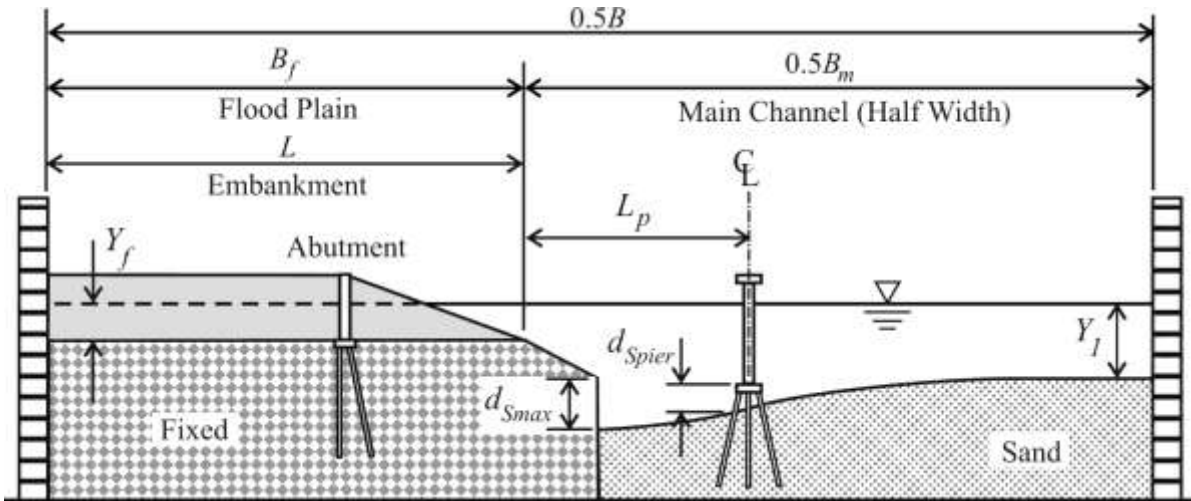
Figure 11-1. Variables considered in laboratory experiments regarding pier-proximity influence on abutment scour (here, $L/B_f = 1.0$; other experiments were run with $L/B_f < 1.0$)
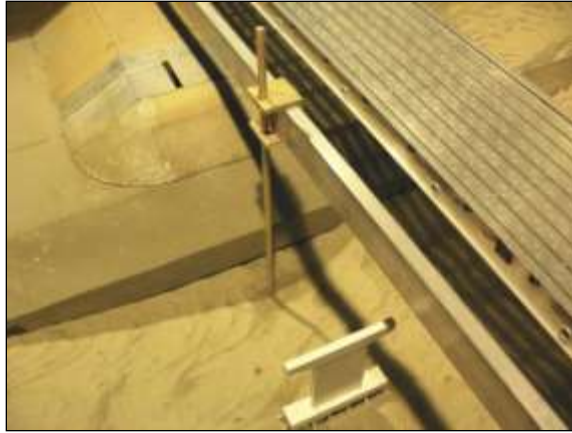
(a)
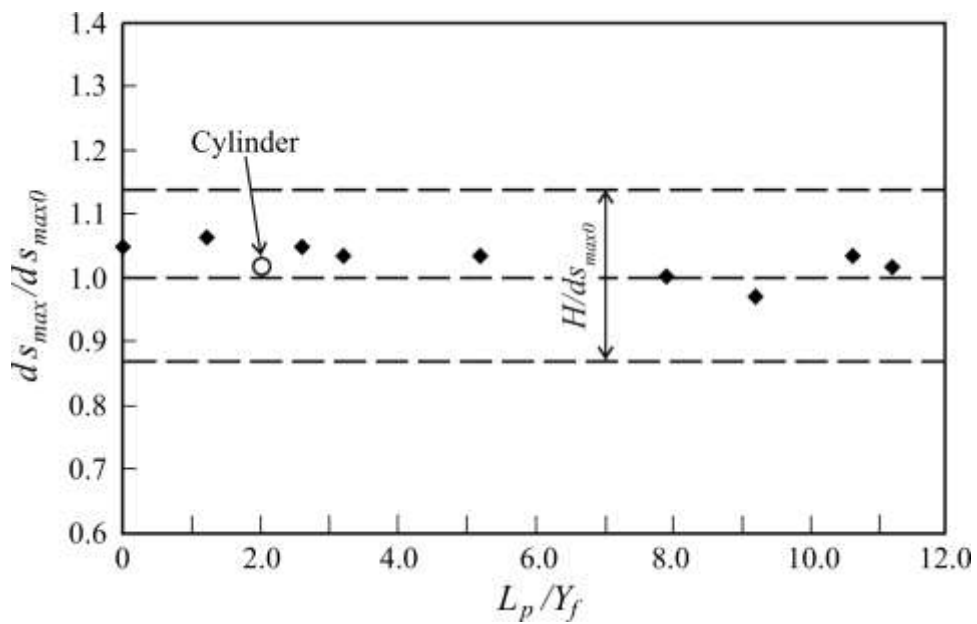
(b)

Figure 11-2. Influence of pier proximity on scour at a spill-through abutment on a fixed floodplain with $B_f/0.5B = 0.46$: (a) photo of scour; and, (b) variation of normalized flow depth, d_{Smax}/d_{Smax0}, with relative pier position, L_p/Y_f. Indicated are uncertainty margins associated with dune height in main channel, and ripple height in scour region. Note that Scour Condition A prevailed.

(a)
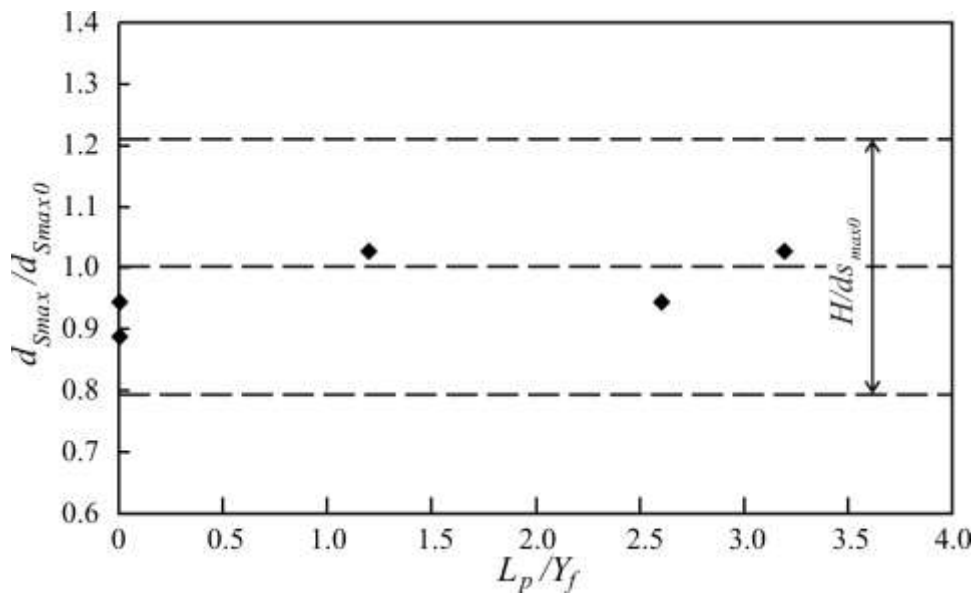
(b)

Figure 11-3. Influence of pier proximity on scour at a spill-through abutment on an erodible floodplain with $B_f/0.5B = 0.46$: (a) photo of scour; and, (b) variation of normalized flow depth, d_{Smax}/d_{Smax0}, with relative pier position, L_p/Y_f. Indicated are uncertainty margins associated with dune height in main channel, and ripple height in scour region. Note that Scour Conditions A and B prevailed

(a)
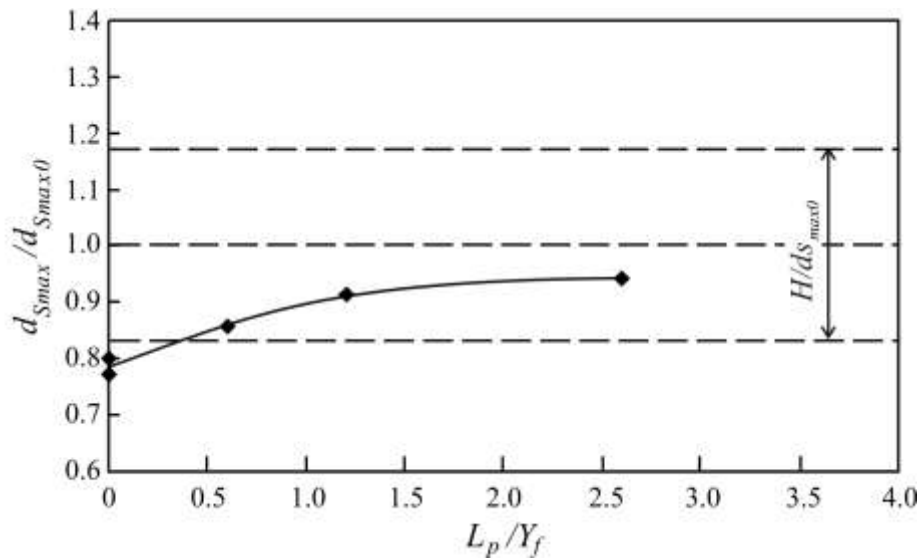
(b)

Figure 11-4. Influence of pier proximity on scour at a spill-through abutment on an erodible floodplain with $B_f/0.5B = 0.23$; (a) photo of scour; and, (b) variation of normalized flow depth, d_{Smax}/d_{Smax0}, with relative pier position, L_p/Y_f. Indicated are uncertainty margins associated with dune height in main channel, and ripple height in scour region. Note that Scour Conditions A and B prevailed.
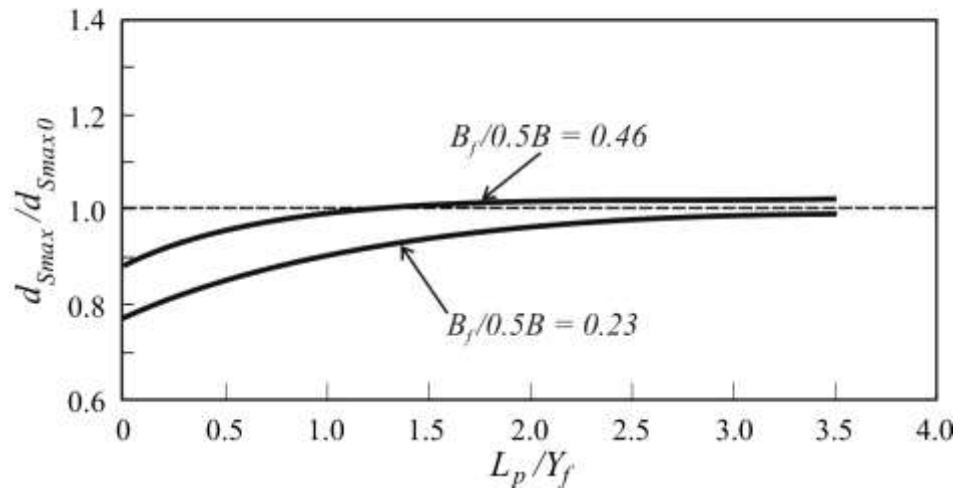
Figure 11-5. Pier influence on scour at spill-through abutments on erodible floodplains obtained with two floodplain widths, $B_f/0.5B = 0.3$, and $B_f/0.5B = 0.5$

(a)
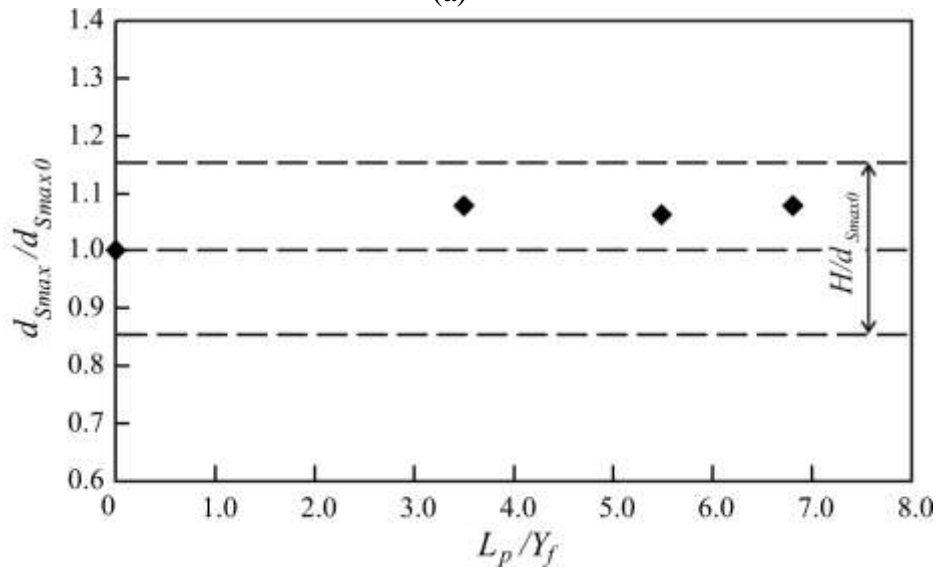
(b)

Figure 11-6. Scour at a pier close to a wing-wall abutment on an erodible floodplain with $B_f/0.5B = 0.23$: (a) photo of scour (a); and, (b) variation of normalized flow depth, d_{Smax}/d_{Smax0}, with relative pier position, L_p/Y_f. Indicated are uncertainty margins associated with dune height in main channel, and ripple height in scour region. Note that Scour Conditions A and B prevailed.
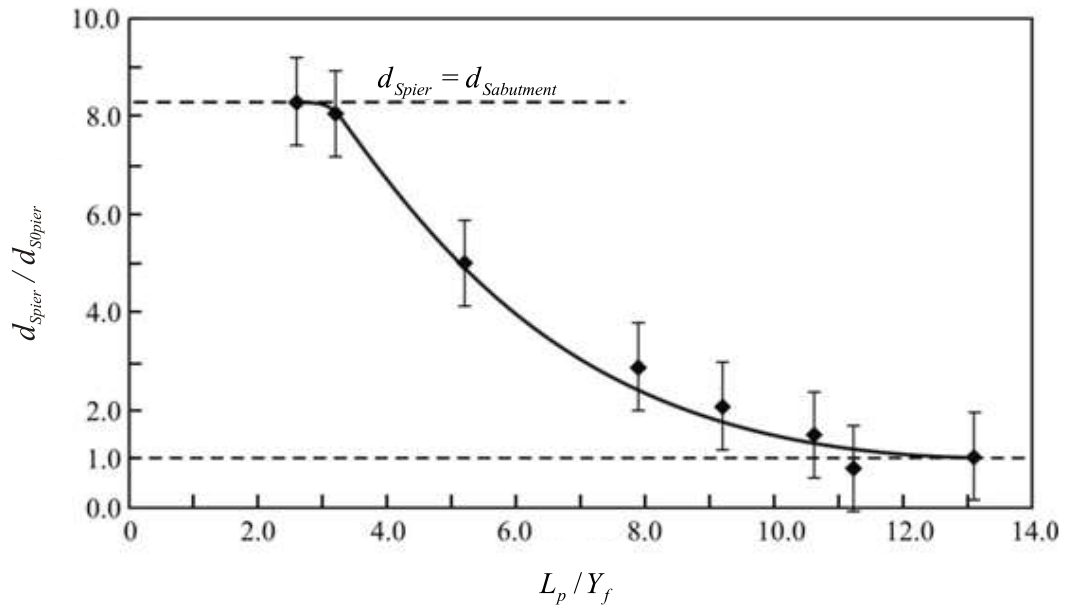
Figure 11-7. Variation of normalized scour depth at pier with position relative to a spill-through abutment on fixed floodplain (Scour Condition A). The smallest value of L_p/Y_f coincides with the toe of the spill-through abutment, at the edge of the fixed floodplain. The error bars indicate relative dune height.
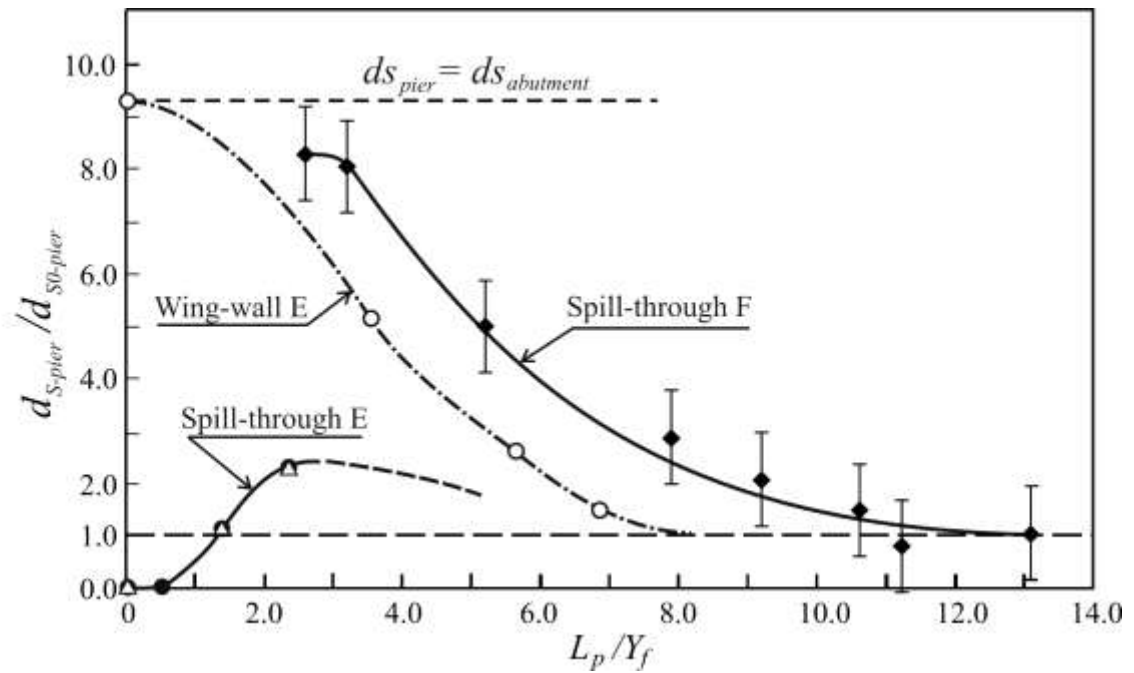
Figure 11-8. Variation of normalized scour depth at pier with position relative to a spill-through abutment on an erodible floodplain (Spill-through E), a wing-wall abutment on an erodible floodplain (Wing-wall E), and a spill-through abutment on fixed floodplain (Spill-through F, same as Figure 11-7). The error bars indicate relative dune height.

Expt.	L_p (m)	Before Expt.	After Expt.
(a)	0		
(b)	0.18		
(c)	0.38		
(d)	0.78		
(e)	1.18		

Figure 11-9. Effect of pier location on scour around fixed spill-through abutment on fixed floodplain with $B_f/0.5B = 0.43$
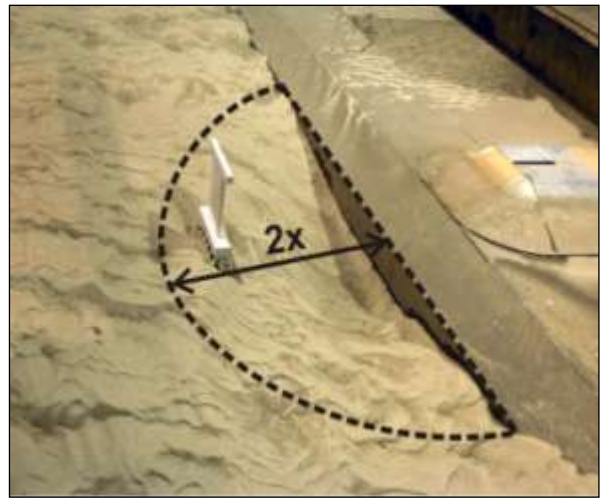
(a)   (b)

Figure 11-10. Effect of pier on scour width with $L_p/Y_f = 3.2$: (a) narrow scour width without a
pier; and, (b) twice as wider scour hole with a pier

Expt.	L_p (m)	Before Expt.	After Expt.
(a)	0		
(b)	0.18		
(c)	0.38		

Figure 11-11. Effect of pier location on scour around spill-through abutment on erodible floodplain with $B_f/0.5B = 0.43$

Expt.	L_p (m)	Before Expt.	After Expt.
(a)	0		
(b)	0.08		
(c)	0.18		
(d)	0.38		

Figure 11-12. Effect of pier location on scour around spill-through abutment on erodible embankment and erodible floodplain with $B_f/0.5B = 0.23$

(a) Fixed embankment; no pier

(b) Fixed embankment with pier ($L_p = 0$)

(c) Erodible embankment; no pier

(d) Erodible embankment with pier ($L_p = 0.18$m)

(e) Short erodible embankment; no pier

(f) Short erodible embankment with pier ($L_p = 0.38$m)
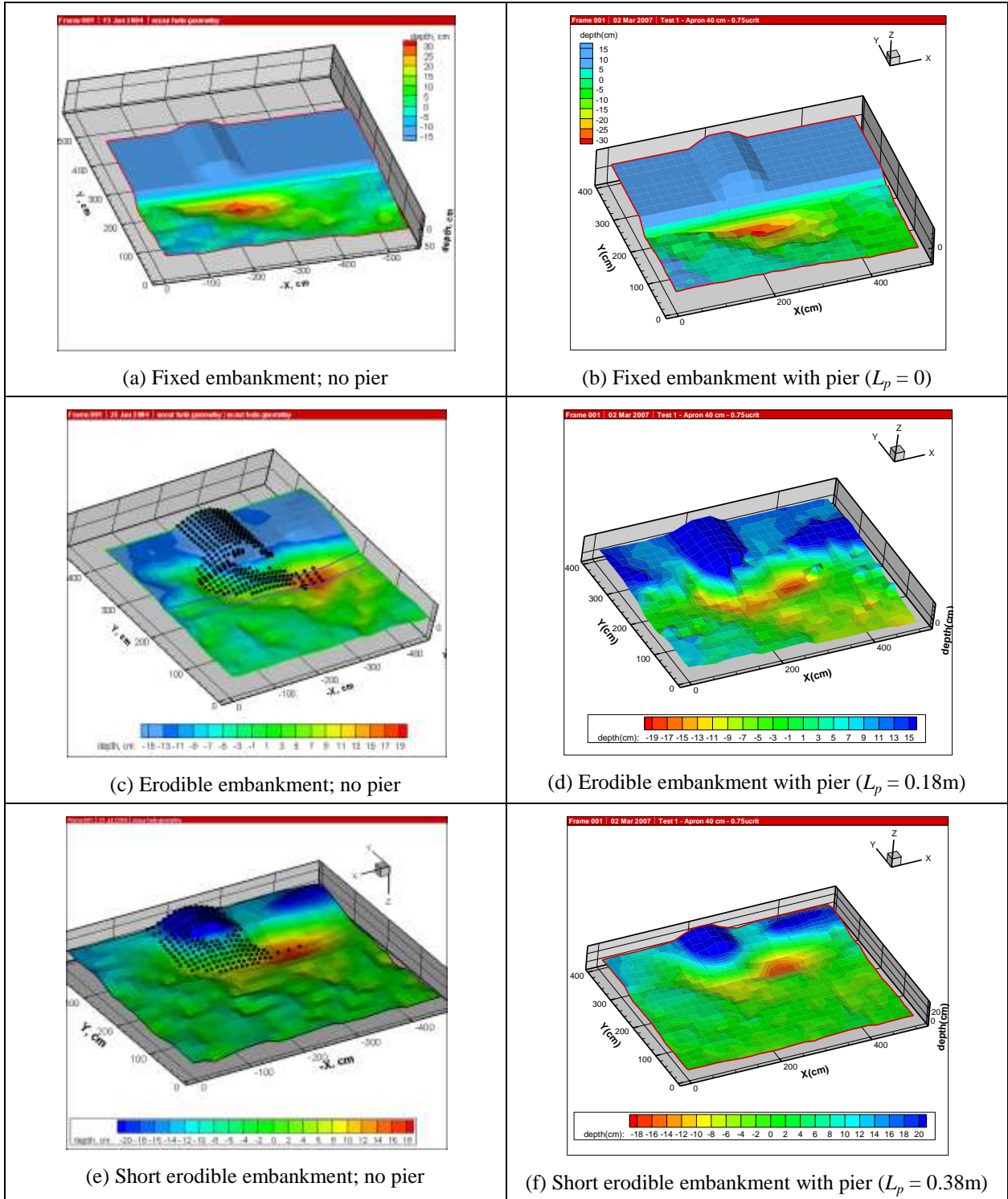
Figure 11-13. Isometric illustration of effect of pier presence on final bathymetry around spill-through abutment under different conditions of floodplain: $L_p = 0$ (b); $L_p = 0.18$ m (d); and, $L_p = 0.38$ m (f)

(a)
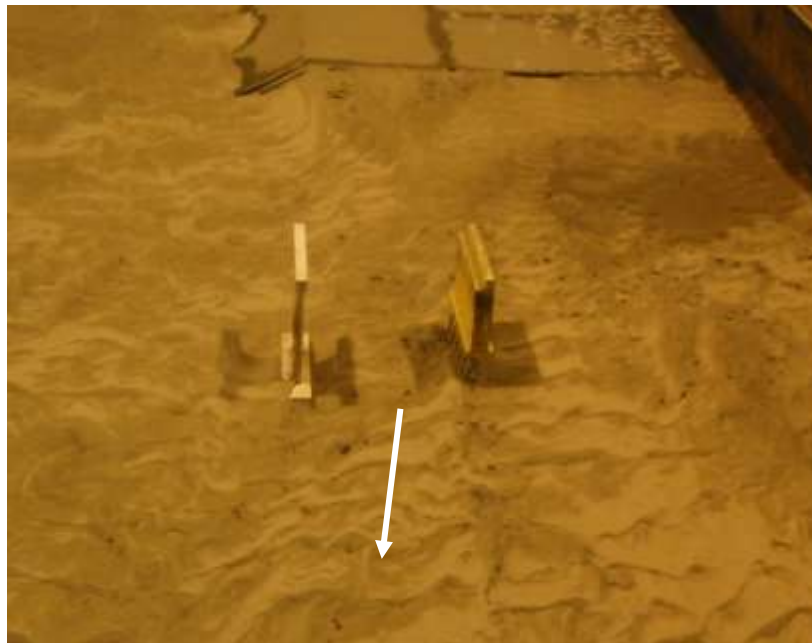
(b)

Figure 11-14. Scour at an unprotected spill-through abutment, with nearby pier ($L_p = 0.18$m), on an erodible floodplain: (a) scour progression after embankment breaching; and, (b) greater scour at abutment column than at pier

Expt.	L_p (m)	Before Expt.	After Expt.
(a)	0.52		
(b)	0.82		
(c)	1.02		

Figure 11-15. Effect of pier location on scour around short wing-wall abutment on erodible embankment and erodible floodplain with $B_f/0.5B = 0.23$

(a-i) Flow field before scour   (a-ii) Flow field after scour
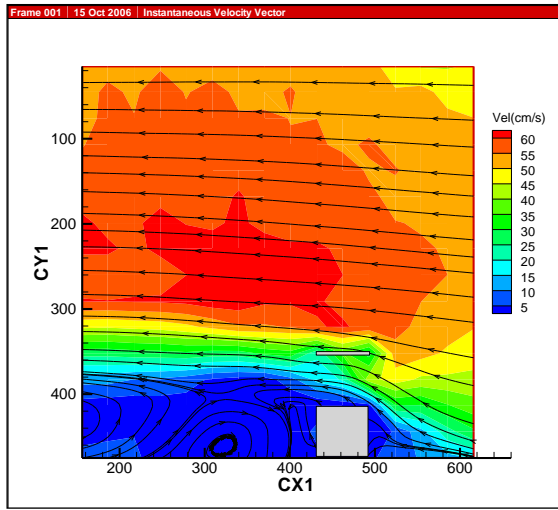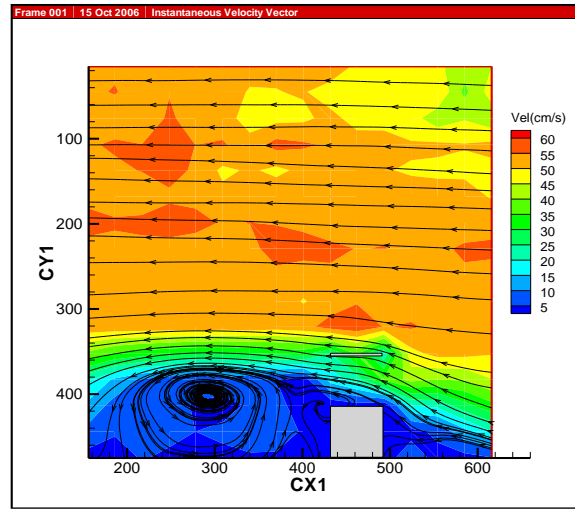
(b-i) Velocity contours and pathlines   (b-ii) Velocity contours and pathlines

Figure 11-16. LSPIV-determined flow fields and surface-flow velocity contours surrounding abutment and pier: before scour (a-i) and (b-i); and, after scour: (a-ii) and (b-ii).
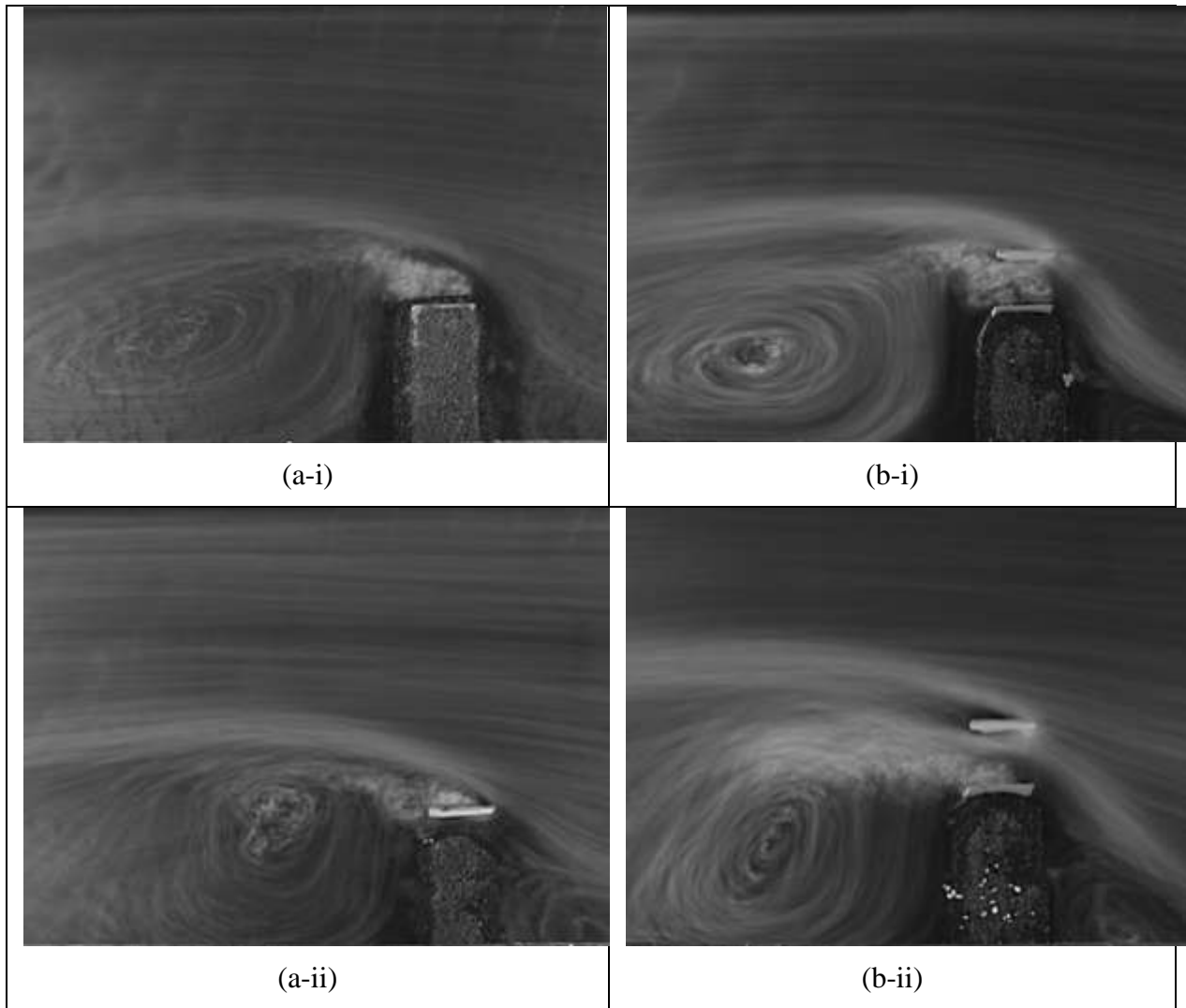
Figure 11-17. LSPIV illumination of surface flow fields around abutment and pier with $B_f/0.5B$ = 0.23: before scour: (a-i) and (b-i); and, after scour: (a-ii) and (b-ii)
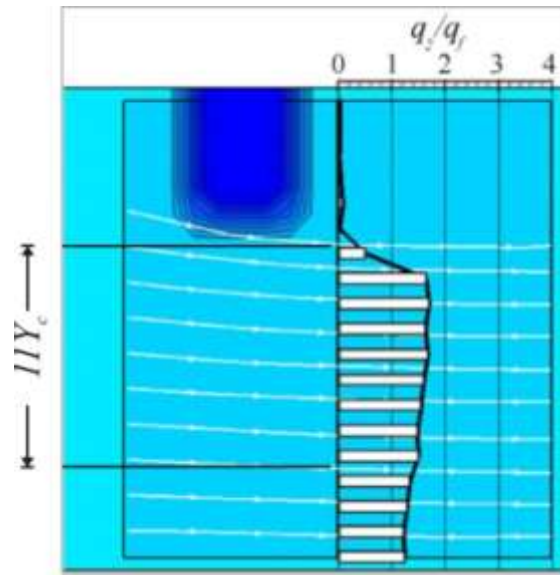
(a)
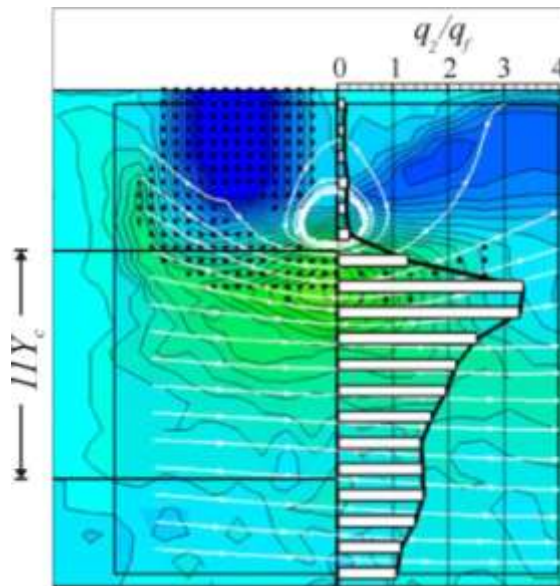
(b)

Figure 11-18. Cross-sectional distributions of unit discharge ratio q_2/q_1 for flow around a spill-through abutment in a rectangular channel (or Scour Condition B): (a) before scour, and (b) after scour. The distance $11Y_c$ from the abutment toe indicates the region of greatest contraction of flow associated with scour at the abutment

CHAPTER 12

DESIGN METHOD AND FIELD VERIFICATION

12.1 Introduction

Chapter 4 introduces the method, which was developed from the data and observations reported in Chapters 7 through 11. The present chapter presents the design method for estimating equilibrium scour depths at abutments exposed to three conditions of abutment scour:

1. Scour Condition A;

2. Scour Condition B; and,

3. Scour Condition C.

The method applies to abutments comprising earthfill embankments and having the following forms and abutment-column construction:

1. Spill-through abutments supported by piles;

2. Wing-wall abutments supported by piles; and,

3. Wing-wall abutments supported by sheet piles.

The design curves presented in Figures 12-1 through 12-4 indicate three limits, which lead to a bifurcating design curve in these figures:

1. For large flow contractions, abutment scour approaches, though moderately exceeds, the contraction scour depth estimated for flow in a long contraction;

2. However, for little or no contraction of flow ($q_2/q_1 \to 1$), the variation of L/B should be considered as either

   (i). L decreasing with constant B when $L/B \to 0$ (as for the experiments conducted in this project), or

(ii). *L* constant with *B* increasing when $L/B \to 0$. Practical constraints on flume width make this limit difficult to study in the laboratory. Nonetheless, as mentioned in Sections 7.2, 8.2, and 9.2, the peak values of Y/Y are reasonably close in magnitude to the scour depths estimated for scour locally at an abutment in a flow without contraction scour across the channel.

These limits are discussed with each figure.

The method also applies to bridge layouts for which a pier is located in close proximity to the abutment. Furthermore, the method includes a guide for estimating scour depth at a pier close to an abutment.

Close field verification of the accuracy of the methods for scour-depth estimation developed from laboratory experiments is complicated by the extensive variability of abutment site situations, and the major lack of field data on scour depths. Nevertheless, it is useful to determine, at least in approximate terms, how well the laboratory data obtained in this study compare with field data and observations of abutment scour. Additionally, it is useful to determine how well the estimation method developed before this study compared with the field data on scour depth.

12.2 Estimation of Scour Depth for Scour Condition A

The design scour depth for Scour Condition A, live-bed scour of the main channel of a compound channel, is estimated as an amplification of contraction scour; i.e., from Eq. (4-14) in Chapter 4,

$$Y_{MAX} = \alpha_A Y_C = C_{TA} m_A^{6/7} Y_C \qquad (12\text{-}1)$$

In terms of scour depth below the approach-bed level, Eq. (12-1) can be re-written as

$$d_{S\max} = Y_{MAX} - Y_1 = Y_1 \left[C_{TA} m_A^{6/7} \left(\frac{q_2}{q_1} \right)^{6/7} - 1 \right] \qquad (12\text{-}2)$$

In Chapter 4 this equation is Eq. (4-15). The issues now are estimation of α_A and Y_C, or q_2, m_A (or q_{MAX}), and C_{TA}. Eq. (4-13) defines Y_C (Laursen 1963).

Figures 12-1 and 12-2 give design curves showing values of α_A for spill-through abutments and wing-wall abutments, respectively. The curves were taken from the envelopes fitted around the data presented in Chapters 7 and 8; i.e., from Figures 7-3 and 8-2. As explained in Section 12.1, the curves in each figure bifurcate, when $q_2/q_1 \rightarrow 1$.

Further, the curves apply when a pier is close to an abutment, because the results presented in Chapter 11 show that pier proximity does not deepen abutment scour.

Also shown are values of dune amplitude $0.5H$ (in the scour area) normalized with Y_C. The maximum height, H, of dunes in the channel, and alluvial channels generally is approximately a third of the flow depth (Vanoni 1975).

The design curves in Figures 12-1 and 12-2 indicate the following considerations for scour-depth estimation:

1. For channel parameter ($B_f/0.5B$) values and abutment configurations similar to those tested in this Project, the bell-shaped curve in Figures 12-1 and 12-2 can be used to estimate Y_{MAX}/Y_C;
2. At the lowest values of q_2/q_1, and short abutments on a floodplain, scour depth in the main channel is associated with the troughs of dunes passing along the main channel. The trough locally lowers the bed at the abutment, such that Y_{MAX}/Y_C is approximately 1.15 (with bed-form wavelength $\lambda \approx 0.33 Y_C$);

3. For situations (not tested in this project) where an abutment is adjacent to a very wide main channel, such that scour is attributable only to the local flow field at the abutment when $q_2/q_1 \to 1$ (and $Y_C \to Y_1$), estimate scour depth using –

   (i) $Y_{MAX}/Y_C = Y_{MAX}/Y_1 = 1.8$ for spill-through abutments (Figure 12-1); and,

   (ii) $Y_{MAX}/Y_C = Y_{MAX}/Y_1 = 2.0$ for wing-wall abutments (Figure 12-2)

   [Note: these are upper-bound magnitudes, as discussed in Section 4.6.]

4. Note:

   (i). For the parameter ranges used in this Project, the influence of abutment shape (spill-through versus wing-wall) on α_A is greatest for the partial range of $1.05 < q_2/q_1 < 1.6$;

   (ii). At comparatively large values of q_2/q_1, Y_{MAX}/Y_C approaches 1.1, because scour is dominated by contraction scour; and,

   (iii) In overall terms, the two α_A curves for spill-through and wing-wall abutments align quite closely.

The design procedure for estimating d_{Smax} entails calculating q_2/q_1, based on known rate of water discharge and cross-sectional area of flow in the approach channel and in the bridge waterway. Then calculate Y_C by means of the relationship provided by Laursen (1960), or an alternative formulation, and determine α_A from Figure 12-1 or 12-2, in accordance with abutment shape (spill-through or wing-wall). Chapter 13 gives the detailed sequence of calculation steps used to estimate scour depths associated with Scour Conditions A.

With regard to the influence of pier proximity on scour depth, the findings discussed in Chapter 11 show that pier proximity does not substantially increase scour depth for spill-through abutments. The influence is within the uncertainty range associated with bed-form amplitude (Figures 11-2 and 11-3). Therefore Eqs. (12-1) and (12-2) are not modified to account for pier-proximity influence on scour depth.

As indicated in Section 9.3 for Scour Condition B, a maximum scour depth for Condition A can be estimated on the basis of the geotechnical stability of the earthfill embankment. The limit can

be assessed using the same considerations as underlie Eqs. (9-1) through (9-4) – scour can only deepen to the extent that the embankment remains geotechnically stable and does not breach.

12.3 Estimation of Scour Depth for Scour Condition B

The design scour depth for Scour Condition B, clear-water scour of the erodible floodplain of a compound channel, is estimated as an amplification of contraction scour; i.e., from Eq. (4-14) in Chapter 4,

$$(12\text{-}3)$$

where Y'_{MAX} is flow depth at the location of maximum scour, Y_{fC} is floodplain flow depth associated with clear-water flow through a long contraction. The coefficients C_{TB} and m_B are as defined above, but now apply to Scour Condition B. In normalized terms, using approach depth, Y_f, Eq. (12-3) is

$$\frac{Y'_{MAX}}{Y_f} = C_{TB}m_B{}^{6/7}\left(\frac{\tau'_f}{\tau_c}\right)^{3/7}\left(\frac{q_2}{q_f}\right)^{6/7} \tag{12-4}$$

and

$$d_{S\max} = Y'_{MAX} - Y_f\left[C_{TB}m_B{}^{6/7}\left(\frac{\tau'_f}{\tau_c}\right)^{3/7}\left(\frac{q_2}{q_f}\right)^{6/7} - 1\right] \tag{12-5}$$

Eqs. (12-4) and (12-5) correspond to Eqs. (4-27) and (4-29) in Chapter 4. The scour estimation issue now is assessment of α_B and Y_{fC}, or q_2, C_{TB}, and m_B.

Figures 12-3 and 12-4 give design curves showing values of α_B for spill-through abutments and wing-wall abutments, respectively. The values were taken from the envelopes fitted around the laboratory data presented in Chapter 9. The curves apply when a pier is close to an abutment, because the results presented in Chapter 11 show that pier proximity does not deepen abutment

scour. As explained in Sections 4.6 and 12.1, the curves in each figure bifurcate, when $q_2/q_1 \rightarrow$ 1.

The lower limit $q_2/q_1 = 1/(1-Y_f/B_f)$ in Figure 12-3 coincides with minimum value of the abutment length parameter, $L/B_f = 2Y_f/B_f$, whereby the full inclined slope of the abutment extends into the flow. The trends in Figures 12-3 and 12-4 are as follow:

1. For configurations of abutment and relative channel width similar to those tested in this Project, the bell-shaped curve in Figures 12-3 and 12-4 can be used to estimate Y'_{MAX}/Y_C;

2. As q_2/q_f increases as a partial abutment increasingly extends across a floodplain, α_B initially increases in response to increased values of C_{TB} and m_B. As q_2/q_f further increases, the values of Y'_{MAX}/Y_f reduce asymptotically to about 1.1. At this limit scour is dominated by contraction scour;

3. For situations (not tested in this project) where an abutment is in a very wide channel, such that scour is attributable only to the local flow field at the abutment when $q_2/q_f \rightarrow 1$ (and $Y_C \rightarrow Y_f$), estimate scour depth using –
   (i). $Y'_{MAX}/Y_C = Y'_{MAX}/Y_1 = 2.5$ for spill-through abutments, and (Figure 12-3); and,
   (ii). $Y'_{MAX}/Y_C = Y'_{MAX}/Y_1 = 2.75$ for wing-wall abutments (Figure 12-4)

   [Note: these are upper-bound magnitudes, as discussed in Section 4.6.]

4. Note:
   (i). The influence of abutment shape (spill-through versus wing-wall) on α_B is greatest for the partial range of $1/(1-Y_f/B_f) < q_2/q_f < 1.6$, as for Scour Condition A; and,
   (ii) In approximate terms, the two α_B curves for spill-through and wing-wall abutments align quite closely.

The design procedure for estimating d_{Smax} entails calculating q_2/q_f, based on known rate of water discharge and cross-sectional area of flow in the approach channel and in the bridge waterway. Then calculate Y_{fC} by means of the relationship provided by Laursen (1963), or an alternative formulation, and determine α_B from Figure 12-3 or Figure 12-4, depending on abutment shape.

Chapter 13 gives the detailed sequence of calculation steps used to estimate scour depths associated with Scour Conditions B.

The findings given in Chapter 11 show that pier proximity does not substantially increase scour depth for spill-through abutments. Instead, pier proximity mildly reduces abutment scour depth when a pier is very close to an abutment (Figures 11-3, 11-4, 11-5). The influence of pier proximity is within the uncertainty range associated with bed-form amplitude, and that indeed diminished scour depth when a pier was close to the abutment (Figure 11-4). Therefore, Eqs (12-3) through (12-5) are not modified to account for pier-proximity influence on scour depth.

However, for wing-wall abutments, the flume tests revealed that pier proximity increased scour depth by about 7%, for the range of proximal distances tested under Scour Condition B. Accordingly, it is suggested here that, for wing-wall abutments, Eq. (12-3) be modified as

$$Y_{MAX} = 1.07\alpha_B Y_{fC} \tag{12-6}$$

Alternatively, the scour depth estimate from Figure 12-4 could be increased by an amount equivalent to bed-form amplitude.

It is important to recall that scour can only deepen to the extent that the earthfill embankment at the abutment column remains geotechnically stable and does not breach. Breaching increases the cross-sectional area of flow through the bridge waterway, relaxes flow velocities, and prompt Scour Condition C. Eqs. (9-1) through (9-4) offer a simplified means of estimating this limiting scour depth.

12.4 Estimation of Scour Depth for Condition C

The design estimate of scour depth for Scour Condition C (scour at an exposed abutment column) is obtained using the following relationship developed from Eq. (4-33), which treats an exposed abutment column as being essentially a form of pier: i.e.,

$$d_{S\max} = K_I K_\beta d_{S0column} \tag{12-7}$$

Here, $d_{S0column}$ is the maximum depth of local scour at the abutment column when aligned with the flow direction ($\beta = 0$); and flow intensity parameter $u_* / u_{*c} = 1.0$, the value at which local scour depth normally is a maximum; K_I is a flow intensity coefficient; and K_β is an alignment coefficient. Values of K_I and K_β can be obtained from the curves given in Figures 12-5 and Figure 12-6 for the standard-stub columns (spill-through abutment) and wing-wall columns (wing-wall abutments); these figures stem from the laboratory data presented in Sections 10.4.1 and 10.4.2.

The value of $d_{S0column}$ for the standard-stub column and the wing-wall column founded in sand are given by Eqs. (12-8) and (12-9), based on the data obtained for the 1/30-scale models (Section 10.4.1). For standard-stub columns,

$$d_{SOcolumn} \approx 1.7 b_{stub} \tag{12-8}$$

And for wing-wall columns as

$$d_{SOcolumn} \approx 0.7 b_{wing} \tag{12-9}$$

Here b_{stub} and b_{wing} are the transverse widths of the abutment columns, as defined in Figure 12-6. The coefficients in Eqs 12-8 and 12-9 give reasonable estimates for the two designs of abutment column used in this project. The coefficients will vary with other abutment column designs.

If these abutment columns were founded in floodplain sediment or soil under design flow conditions for which the value of u_* / u_{*c} is less than 1, the values of $d_{S0column}$ should be reduced using the flow intensity coefficient, K_I. The value of u_* / u_{*c} may be less than 1 for flow over floodplains formed in cohesive soils, or non-uniform gravels, more resistant to erosion than the sand used in the present experiments.

The value of alignment coefficient K_β requires some judgment. Once the embankment is breached and the abutment column fully exposed, the abutment is more-or-less aligned with the

flow. However, there may be a period when the embankment is breached but the column not fully aligned with the flow. In this situation, the floodplain flow sweeps at an angle β around the abutment column. Design estimation of d_{Smax} then requires assessing β.

To complete the present design method, the data in Figures 10-16 and 10-17 of Chapter 10 are shown again (but without data) in Figures 12-6 as an alignment factor, K_β, versus flow alignment, β for standard-stub and wing-wall columns. Here, K_β is defined as the ratio of the local scour depth for the abutment column aligned at angle β relative to that when $\beta = 0$. Figure 12-6a compares the values of K_β obtained for the standard-stub abutment with the commonly used set of alignment-factor curves proposed by Laursen and Toch (1956), who developed the curves using scour data obtained with simple rectangular piers extending at depth into a sand bed. This figure suggests that Laursen and Toch's set of figures can be used for an abutment built similarly to the stub column used in this study (Figures 2-7 or 6-14). For stub columns whose pile cap is at an elevation well above the bed or floodplain levels (e.g., see Figure 3-5 and subsequently in Figure 12-10), scour depth must be estimated from similar laboratory data as this study obtained for the variables in Eq. (12-6).

12.5 Scour Depth at Adjacent Pier

The results presented in Chapter 11 show that, when a pier is close to an abutment, scour depth at the pier is governed primarily by scour depth at the abutment. Only when the pier position exceeded a distance of about 11 times floodplain flow depth, Y_f, was pier scour not significantly affected by abutment scour. This limit applies to Scour Conditions A and B. The data trend in Figure 11-7 can be used as an approximate design guide for estimating scour depth at piers adjacent to abutments. The guide is shown as Figure 12-7, which indicates the depth variation of pier scour between two well-defined limits. Though Figure 11-7 was developed for Scour Condition A for abutments on a fixed floodplain, Figure 11-8 indicates that the design curve in Figure 12-7 conservatively envelops pier scour data for Scour Condition A with an erodible floodplain. Scour at a pier near an abutment subject to Scour Condition B also can be estimated using Figure 12-7.

For a pier close to an abutment, scour depth is governed primarily by scour formed by flow around the abutment; this scour depth is d_{Smax}. However, for a pier distant from an abutment, scour depth is unaffected by the abutment; this scour depth is d_{S0pier}. The variation associated with pier scour depth can be stated in three sub-ranges:

$$— \tag{12-10a}$$

$$\overline{} \qquad — \tag{12-10b}$$

$$— \tag{12-10c}$$

These sub-ranges are evident in Figure 12-7, which plots the ratio d_{Spier}/d_{S0pier} against L_p/Y_f. The design examples in Section 12.7 show how scour-depth estimation should take into account pier proximity. As the data used for Figures 11-7 and 12-7 were obtained using one value of Y_f, some caution may be needed in using Figure 12-7 for all flow depths at a pier near an abutment.

12.6 Field Verification

Field verification of abutment-scour estimation presently is limited to approximate comparison. The same considerations complicating accurate estimation of scour depth at abutments inevitably complicate field verification of scour estimation methods. Many abutment sites are practically unique in their terrain, flow-resistance features, boundary sediments and soils, as well as details of their layout and construction. Additionally, case-studies of abutment scour commonly involve a geotechnical failure of the main-channel bank and/or the abutment's approach embankment. These considerations limit to approximate terms the accuracy of quantitative field verification of estimation methods.

12.6.1 Modes of Comparison

Two forms of field verification were used for the scour estimation method developed for this Project:

1. Visual comparison of abutment scour observed in the fields and the laboratory;

2. Quantitative comparison of abutment scour depths measured in the field and laboratory; and,

3. A scour-depth prediction equation proposed by Benedict (2003). His equation, based on field measurement of scour at abutments, is described in Section 5.6.

The principal sources of field observations and data used for the comparison are those reported by the United States Geological Survey (USGS), notably Mueller and Hitchcock (1998), Mueller and Wagner (2005), and Benedict (2003). An important point emerging from a review of field reports of scour at abutments is the relative scarcity of well-documented abutment scour cases.

12.6.2 Visual Comparison

Field observations reveal that scour at actual abutments generally conforms to the Scour Conditions A, B and C, as described in Chapters 7 through 11. Figures 3-5 through 3-8 illustrate field examples of scour conditions. Additional visual comparison is given by the sets of photographs compiled as Figure 12-8 through 12-13. These figures compare scour failures at actual abutments with those obtained in the laboratory flume experiments.

Figures 12-8 and 12-9 show the consequences of Scour Condition A for spill-through and wing-wall abutments, respectively. The scour region shown in the laboratory views would cause bank and embankment failures as depicted for the field cases. The illustrations of Scour Condition B, Figure 12-10, shows scour at a spill-through abutment with an earthfill embankment protected by grass cover. Scour led to slope failure and erosion of the abutment's earthfill face, partially exposing the abutment column. The corresponding laboratory test was with a riprap-protected embankment, and also resulted in the failure of the abutment's earthfill face. The riprap, though, protected the face, and caused scour to deepen further away from the abutment column than occurred for the field example. Figures 12-11 and 12-12 show field and laboratory examples of Scour Condition C, when the abutment column became fully exposed.

Taken together, the field observations also reveal the difficulties met when attempting to compare field and laboratory examples of scour, or even comparing field examples with each other. Besides differences in local site circumstances, it is difficult to get observations taken from the similar viewing perspectives. Moreover, the scour bathymetry associated with abutment failures seems rarely to get measured. In part, this lack occurs because of access difficulties, and because of the usual pressing practical need to stabilize and repair the abutment site; repair work quickly follows a scour failure.

The most noticeable feature of abutment scour evident in all of the field observations is the geotechnical failure of the bank and/or embankment slopes. The figures emphasize the important role of embankment strength in scour development. The geotechnical failure of the soils forming a channel bank or earthfill embankment alters, and typically relieves, the flow field causing scour. The importance of soil strength is underscored in the additional field observations given in Figure 12-13a-b, which show two modes of bank or embankment failure. In both cases, scour of the channel bed or floodplain resulted in embankment failure; a cuspate slip surface (Figure 12-13a) encompassing the abutment, and embankment sideslope failures (Figure 12-13b).

12.6.3 Quantitative Comparison

A difficulty complicating quantitative field verification of scour-depth estimation is the need for adequate field documentation of flow bathymetry, water levels, and velocities. The two sources of field data used in the present verification effort either provide adequate flow and bathymetry data (Mueller and Wagner, 2005), or give an envelope curve bracketing measured scour depths (Benedict 2003).

The field data were obtained from four bridge sites: Swift County Route 22 over the Pomme de Terre River, Minnesota; U.S. Route 12 over the Pomme de Terre River, Minnesota; Highway 25 over the Minnesota River, Minnesota; and State Highway 37 over the James River, South Dakota. The data, described in detail by Mueller and Wagner (2005), include flow velocity and bathymetry taken using an Acoustic Doppler Current Profiler (ADCP). An echo sounder also

was used to measure flow depths. These velocity and depth measurements were conducted during flood flow conditions at the bridge sites.

The empirical estimation relationship proposed by Benedict (2004) reflects the scour depth data measured for Scour Condition B, clear-water scour on floodplains in South Carolina. As pointed out in Section 5.6, he reports a significant number of bridge failures involving embankment breaching. However, his estimation relationship does not include these cases. The present study shows that the maximum scour depth with embankment breaching was smaller than that without embankment failure. Embankment breaching reduces flow in the region of scour, and if the geometry of the breached embankment had been measured and used in the prediction equations, then the predicted values of Y_{MAX}/Y_C would be smaller, and thereby closer to the value obtained from the experiments.

In addition, the present verification compared the field data on scour depth with the methods proposed by Melville and Coleman (2000) and Liu et al. (1961) for predicting scour depth at bridge abutments. The methods are described in Section 5.4 for Melville and Coleman (2000) and Liu et al. (1961). The data collected by USGS could be readily applied to these methods with a minimum amount of guesswork as to values of parameters not recorded by the USGS.

The field data from the four bridge sites Mueller and Wagner (2005), and the field data reflected by the empirical curve proposed by Benedict (2003), are compared in Figure 12-15 with the design curves presented in Figures 12-2 and 12-3. The comparison is in the format Y_{MAX}/Y_C versus q_2/q_1. The unit discharges q_1 and q_2 were determined using the velocity and bathymetry data for the four bridges. The values of Y_C were determined using the equation proposed by Laursen (1960) for live-bed scour, or Laursen (1963) for clear-water scour. Estimates of Y_{MAX} were obtained from the design curves proposed herein (Figures 12-2, 12-3, and 12-4),

The verification comparison shown in Figures 12-14 indicates the following points:

1. The field data align well with the design curves proposed in Figures 12-2 and 12-3. The design curves envelope the field data, though, at the larger values of q_2/q_1, the field data for the wing-wall abutments drop below the design curve for wing-wall abutments;

2. The field data values of Y_{MAX}/Y_C for the four sites reported by Mueller and Wagner (2005) are relatively small, and show only a modest increase with increasing q_2/q_1. Additionally, these field data show considerable scatter. These features of the field data are attributable to the variability of abutment site circumstances, and the difficulties in exact estimation of scour depth. Mueller and Wagner (2005) mention that the field data were measured at the bridge abutment. For the wing-wall abutment, as illustrated in Chapter 8, the maximum scour depth usually develops at the front of abutment, and therefore the flow depth observed by ADCP, most likely, detects the maximum flow depth around this area. However, for spill-through abutments the maximum scour depth usually occurred somewhat downstream from the centerline of bridge section (e.g., as shown by the figures in Chapter 9). Consequently, it is possible that the maximum scour depth measured at the bridge section does not represent the actual maximum flow depth around the spill-through abutment; and,

3. The scour estimates from the empirical curve proposed by Benedict (2004) vary also quite widely in magnitude for the estimated values, but come close to the design curve for wing-wall abutments. Most of the abutments associated with this curve are wing-wall abutments

In passing, it is useful to comment that values of Y_{MAX}/Y_C estimated using the methods proposed by Melville and Coleman (2000), Richardson and Davis (1995) and Liu et al. (1961) substantially exceed the field values of Y_{MAX}/Y_C.

12.6.4 Summary

Given the field limitations in adequate quantitative field verification of the proposed relationships for estimating scour depth at bridge abutments (Sections 12.2 - 12.4), the comparisons discussed earlier in Section 12.6 indicate that the proposed relations produce scour forms and depth estimates that reasonably concur with those observed at actual bridge

abutments. There remains a great need for further documentation of scour forms and bathymetries at abutments.
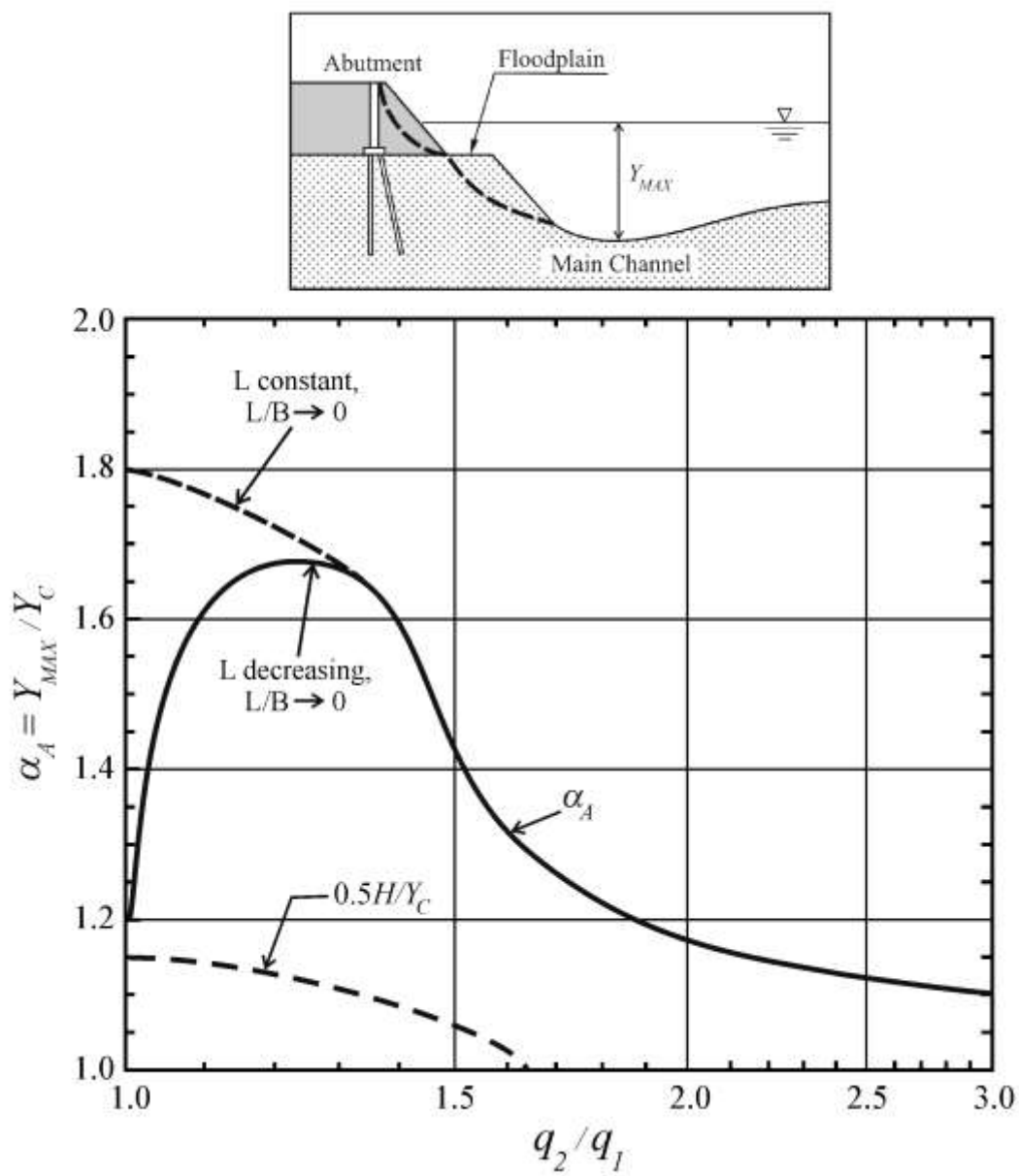
Figure 12-1. Design curve for short-contraction, scour-amplification factor, α_A, for spill-through abutments subject to Scour Condition A (fixed floodplain)
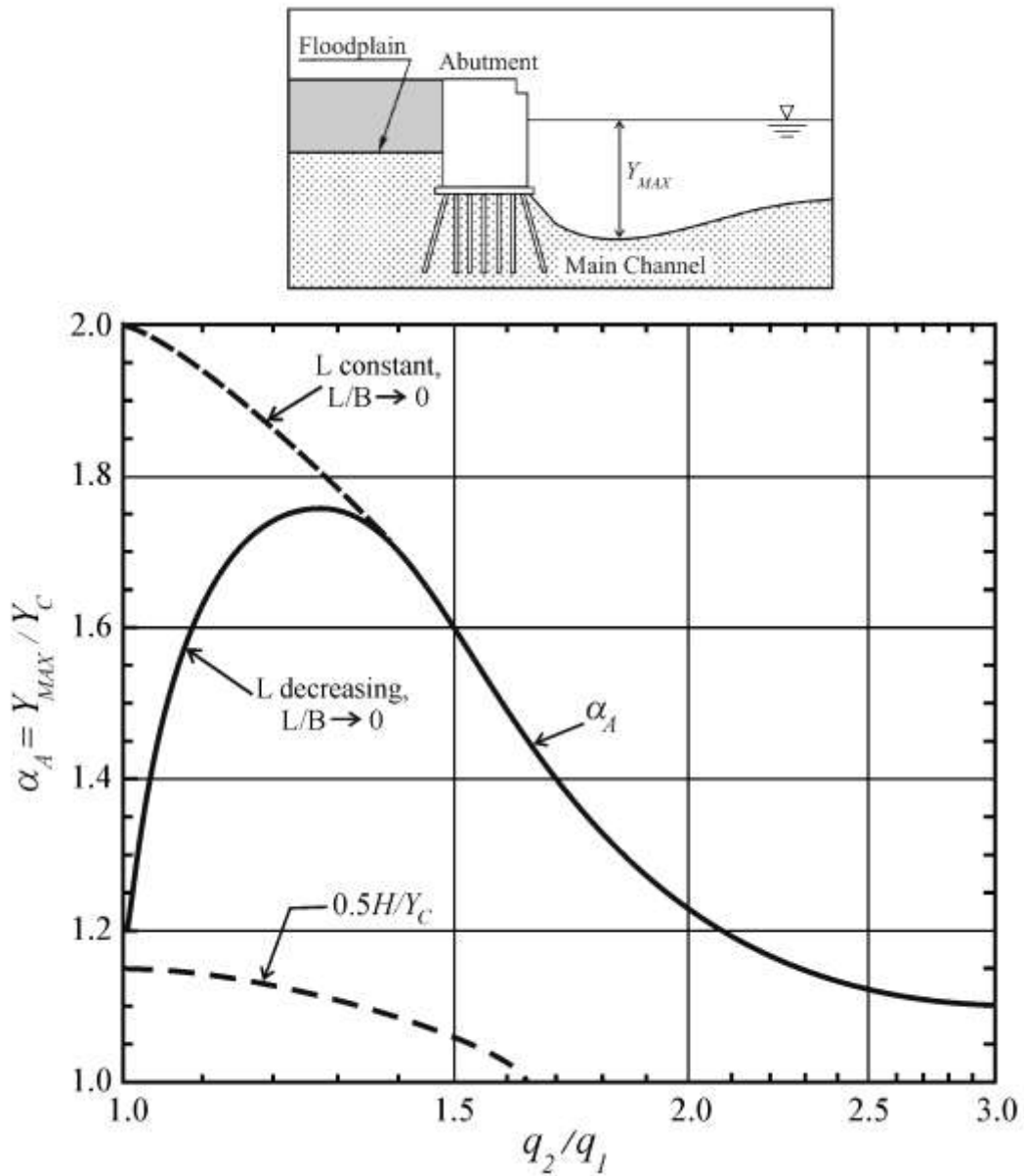
Figure 12-2. Design curve for short-contraction, scour-amplification factor, α_A, for wing-wall abutments subject to Scour Condition A (fixed floodplain)
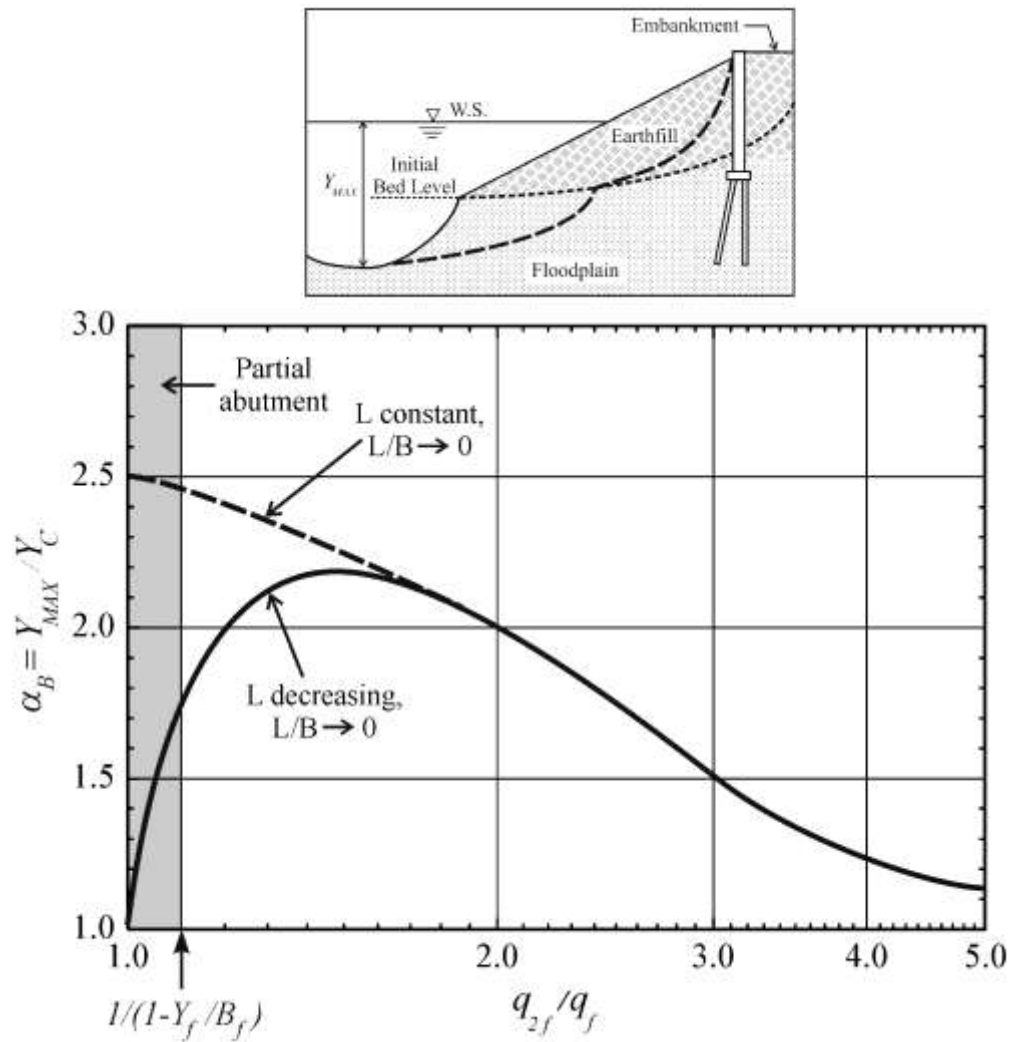
Figure 12-3. Design curve for short-contraction, scour-amplification factor, α_B, for spill-through abutments subject to Scour Condition B (abutment set back on a wide floodplain)
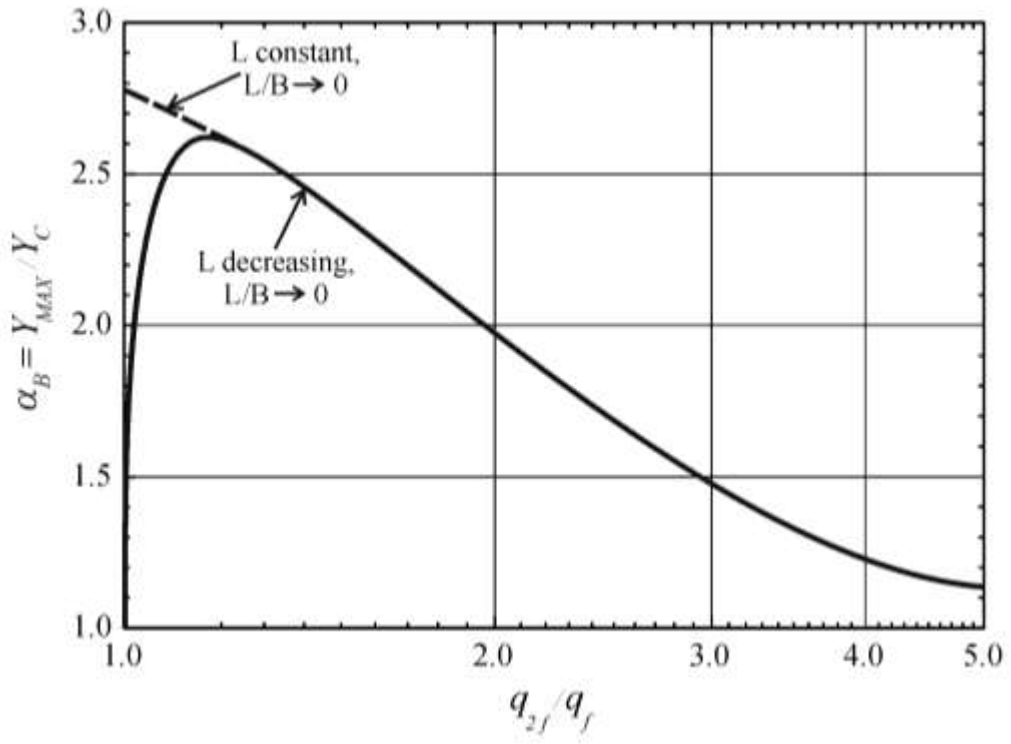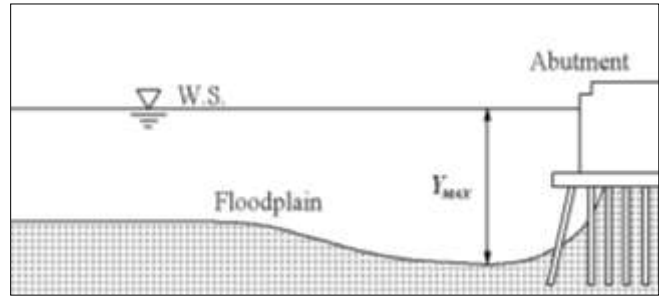
Figure 12-4. Design curve for short-contraction, scour-amplification factor, α_B, for wing-wall abutments subject to Scour Condition B (abutment set back on a wide floodplain)
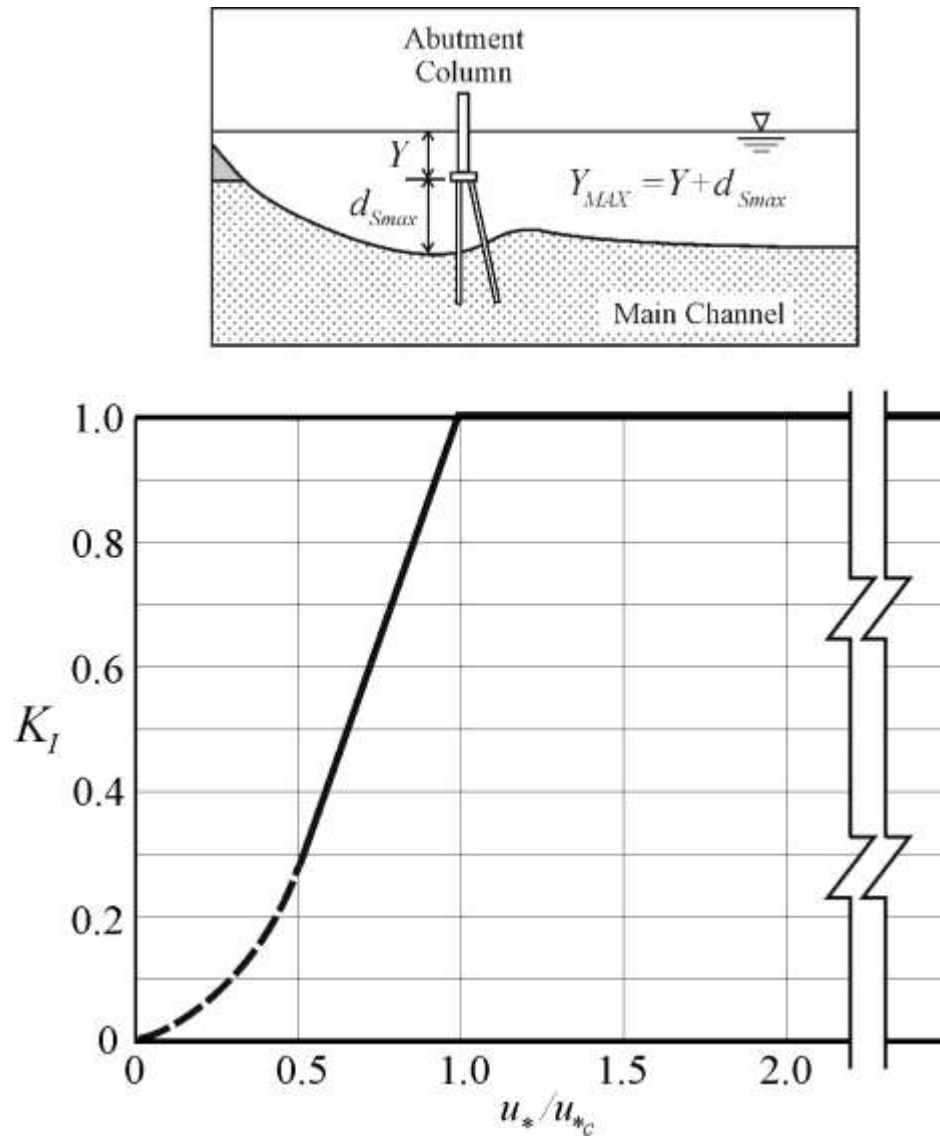
Figure 12-5. Design curve giving flow-intensity factor, K_I, for scour depth at exposed standard-stub and wing-wall columns (Figures 4-4 and 4-5 give details of column forms.)
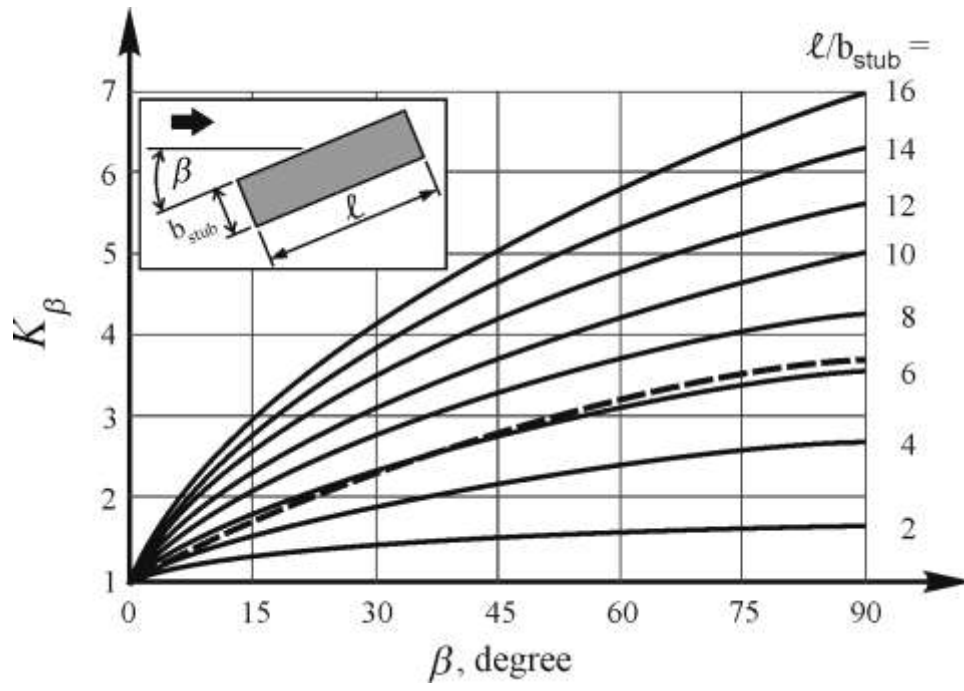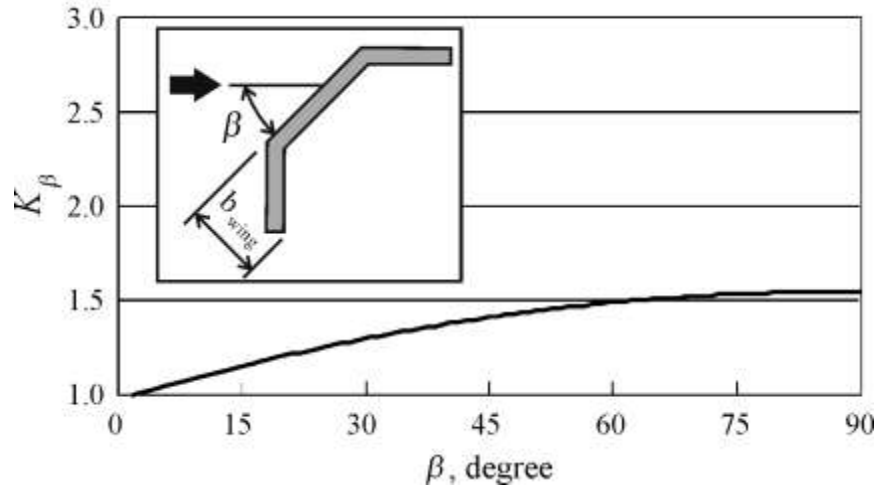
Figure 12-6. Design curves giving column-alignment factor, K_I, for standard-stub (a) or wing-wall (b) abutment columns (Figures 4-4 and 4-5 give details of column forms.)
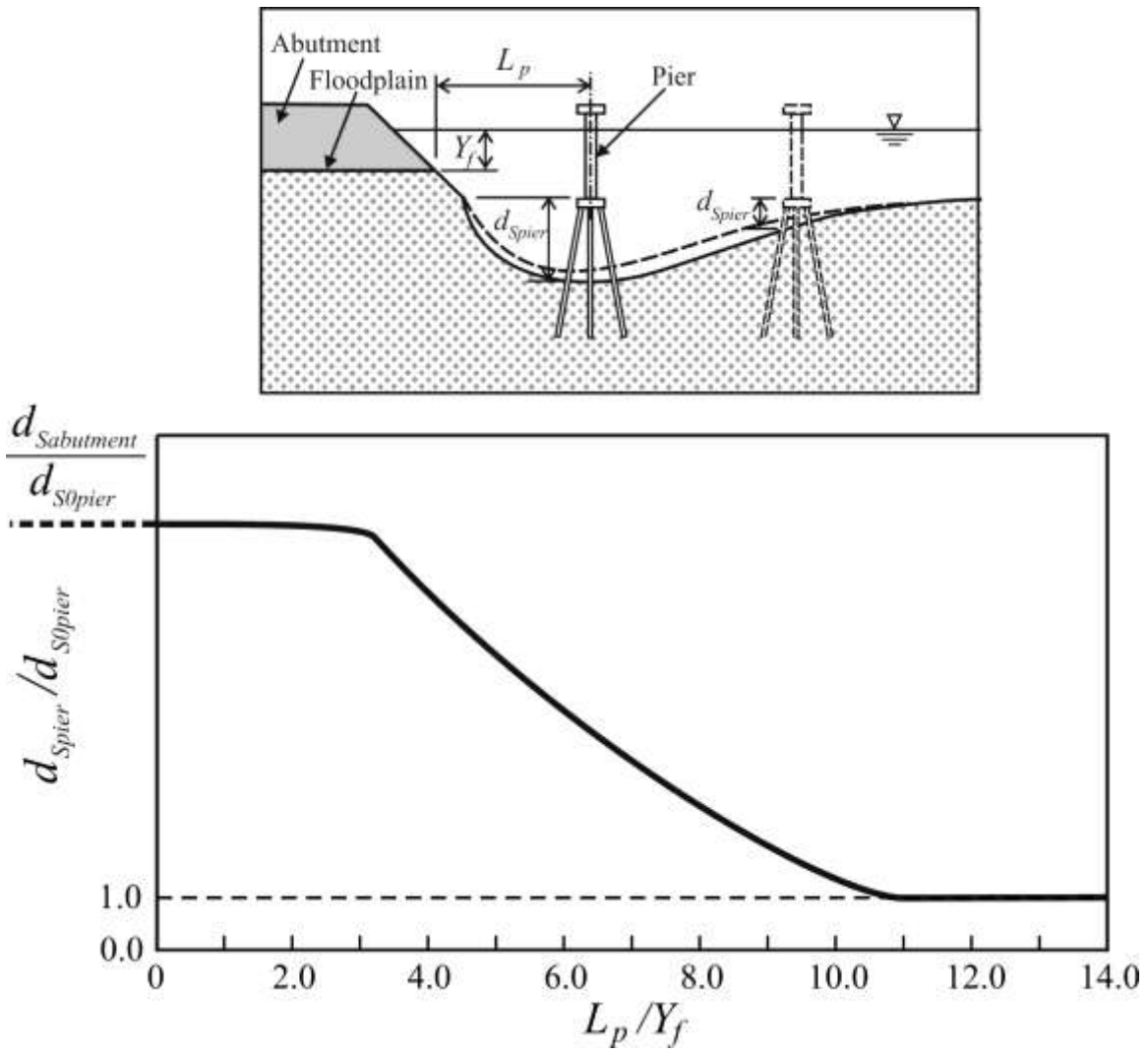
Figure 12-7. Design curve for estimating scour depth at a pier adjacent to an abutment subject to Scour Conditions A and B, or combination thereof (spill-through or wing-wall)

(a)

(b)
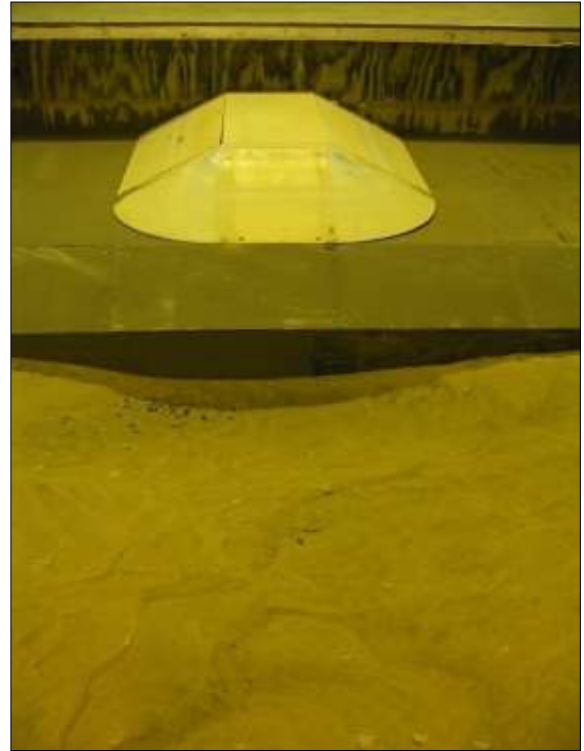
(c)

Figure 12-8. Observations of Scour Condition A for spill-through abutments on floodplains much less erodible than the main-channel bed. Field observations shown in (a) and (b) depict bank and embankment failures consequent to this scour condition; and, abutment scour under a comparable situation modeled in the laboratory flume is shown in (c), though the bank of the fixed floodplain was not allowed to fail in the model.

(a)

(b)

(c)

Figure 12-9. Observations of Scour Condition A for wing-wall abutments on floodplains much less erodible than the main-channel bed. Field observations shown in (a) and (b) depict bank and embankment failures consequent to this scour condition; and, abutment scour for a comparable situation modeled in the laboratory flume is shown in (c), though the bank of the fixed floodplain was not allowed to fail in the model

(a)   (b)

Figure 12-10. Observations of Scour Condition B for spill-through abutments on an erodible floodplain: a field observation of embankment failure consequent to this scour condition (a); and, a comparable scour situation modeled in the laboratory flume (b).

(a)   (b)

Figure 12-11. Observations of Scour Condition C for spill-through abutments on an erodible floodplain: a field observation of embankment failure consequent to this scour condition (a); and, a comparable scour situation modeled in the laboratory flume (b)

(a)

(b)

Figure 12-12. Observations of Scour Condition C for wing-wall abutments on an erodible floodplain: a field observation of embankment failure consequent to this scour condition (a); and, a comparable situation modeled in the laboratory flume (b)

(a)

(b)

Figure 12-13. These two figures illustrate the importance of embankment strength with respect to the development of abutment scour: (a) the slope failure of the embankment immediately behind a wing-wall abutment founded on a spread footing; and, (b) the extensive erosion of the earthfill embankment along the flank of a floodplain
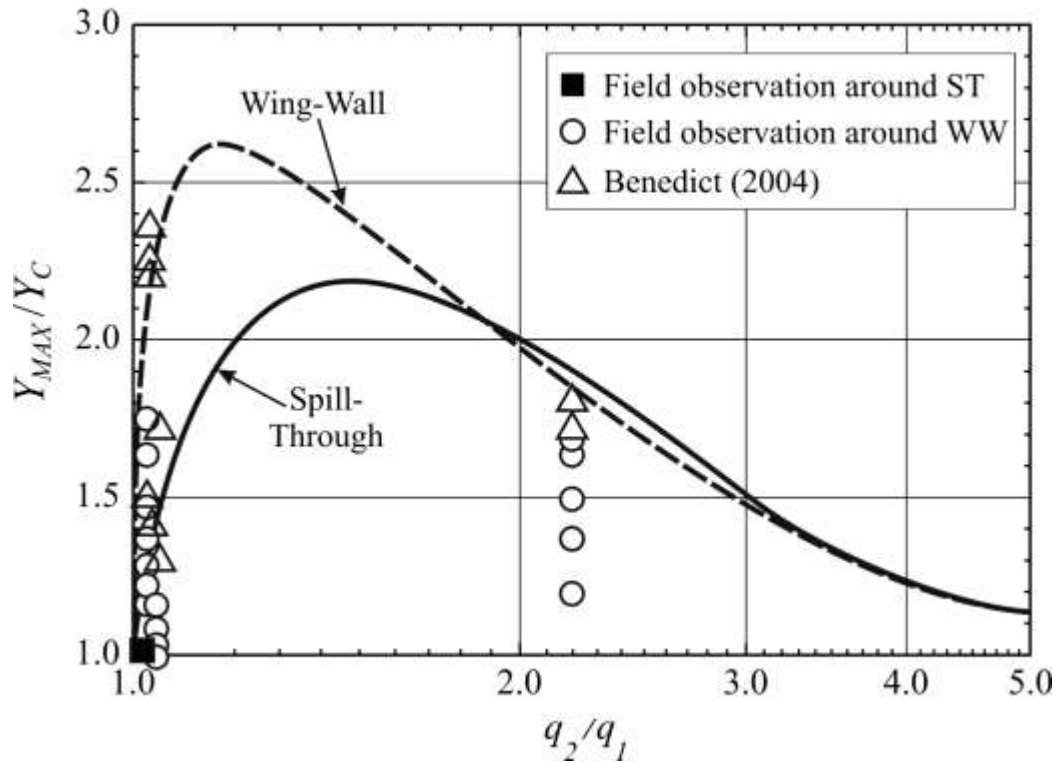
Figure 12-14. Comparison of field measurements of scour depth at spill-through and wing-wall abutments on erodible floodplain. The design curves are as proposed in Figures 12-3 and 12-4. The field observations are from Mueller and Wagner (2005) and (Benedict (2003)

CHAPTER 13

APPLICATION OF DESIGN METHOD

13.1 Introduction

This chapter shows in concept how the design method described in Chapter 12 applies to estimating equilibrium scour depths at abutments. The potential occurrence of Scour Conditions A, B, and C are considered for the following abutment situations:

1. A spill-through abutment whose embankment extends across the floodplain of a compound channel so as to be close to the main channel;

2. A spill-through abutment whose embankment extends a relatively short distance across the floodplain of a compound channel, so as to be distant from the main channel, or essentially is in a simple channel of approximately rectangular cross section;

3. A wing-wall abutment, supported on circular-section piles or on sheet piles, in a compound channel so as to be close to the main channel; and,

4. A wing-wall abutment whose embankment extends a relatively short distance across the floodplain of a compound channel, or is in a channel of essentially rectangular cross section.

The abutment forms and construction configurations are those given in Figures 6-4 for spill-through abutments and Figure 6-5 for wing-wall abutments. The adjoining pier is taken to have the design shown in Figure 6-14. For abutment situations 1 and 2, above, the floodplain is first considered to be far more resistant to erosion than the bed of the main channel, and then as resistant to hydraulic erosion as is the main-channel bed.

Figure 13-1 outlines the steps to implement the method. The steps relate the following considerations of abutment layout, shape, and construction to the possible occurrence of Scour Conditions A, B, and C:

1. **Abutment layout on a floodplain** (parameter, L/B_f). If L/B_f approaches 1, Scour Condition A may occur, for spill-through or wing-wall abutments. If L/B_f is less than about 0.75, Scour Condition B may occur. The suggested limit of 0.75 is selected from the experimental results presented in Chapters 7 and 8;

2. **Floodplain erodibility** (parameter, u_{*f}/u_{*fc}). If the floodplain is far less erodible than the main-channel bed ($u_{*f} \ll u_{*fc}$), such that the floodplain practically is fixed, scour is limited to Scour Condition A (when L/B_f approaches 1). If the floodplain is about as erodible as the main-channel bed ($u_{*f} \approx u_{*fc}$), Scour Condition B occurs, either with Scour Condition A (when L/B_f approaches 1) or alone (if L/B_f is less than about 0.75). The scour depth estimates for Conditions A and B are based on the relationships for short-contraction scour formulated in Chapter 4.

   If the abutment's approach embankment is prone to breach and expose the abutment column, Scour Condition C develops. The scour depth estimate for Condition C is estimated using the empirical curves obtained in Chapter 10.

   As noted in Section 4.3, in practical terms, significant uncertainty also attends estimation of shear velocity (or shear stress), and their critical values, for flow over floodplains.

3. **Purpose of scour-depth estimates**. The three scour conditions lead to two scour-depth estimates. These estimates should be compared and applied for two design purposes:

   (i)   To design the abutment's earthfill embankment so that it does not fail geotechnically when exposed to scour depths estimated for Conditions A or B; and,

   (ii) To design the abutment column's pile or sheet-pile supports so that they do not fail (i.e., continue to support the bridge deck) when exposed to a depth corresponding to the deepest scour estimated for Scour Conditions A, B, or C.

A critical consideration is that scour of the main-channel bed or the floodplain potentially leads to the geotechnical instability and collapse of the earthfill embankment at the abutment. For Scour Condition A, deepening scour may cause the bank of the main channel to collapse first, possibly then causing the abutment's embankment to collapse. Accordingly, as indicated in Figure 13-1, it is necessary to perform one to two bank-stability analyses for Scour Condition A, and one such analysis for Scour Condition B. Consequently, accurate estimation of scour depth at a bridge abutment entails assessing the limiting height (or slope steepness) for which the main-channel bank and the embankment at the abutment could remain standing as scour develops. Arguably for abutments supported by piles, this height (and slope steepness) limits maximum scour depth; i.e., as shown for Figure 9-4, Scour Condition B, the maximum scour depth results in the geotechnical failure of the embankment extending back to the abutment column.

Two further practical qualifications can complicate accurate scour-depth estimation, and must be mentioned before illustrating how to apply the design method.

1. The differing combinations of approach-channel morphology, local terrain topography, and flow-resistance features on floodplains (e.g., surface roughness, vegetation) affect approach-flow distribution. Variations of boundary sediments and soils at a site affect scour development. Together, these considerations introduce considerable uncertainty in scour depth estimation. To a large extent, numerical simulation (e.g., using a model like FESWMS) can address uncertainties associated with flow distribution at an abutment site. Much more sophisticated models are needed to address scour in channels formed in variable sediments and soils; and,

2. Abutments and their approach embankments can vary substantially in the details of their layout and construction. The findings of the present Project show, however, that the dominant scour process at abutments is the non-uniform contraction of flow passing around an abutment as if it were a short contraction.

The design guide for scour-depth estimation indicates when these foregoing qualifications need to be considered at decision points during scour depth estimation.

13.2 Design Steps Common to Scour-Depth Estimation for All Abutments

A series of design steps are common to scour-depth estimation for all bridge abutments. The steps ensue:

Step1. Determine the geometric configuration and dimensions of the bridge site (the compound channel in the bridge vicinity, layout and extent of the approach embankment, abutment form and construction, proximity and construction of adjoining pier [if any]);

Step 2. Determine the design discharge to be used, Q, and its commensurate average unit discharge of flow in the main channel, q_1, and over the floodplain, q_{f1}, (if one exists at the bridge site);

Step 3. Determine the corresponding average unit discharge through the bridge waterway, q_2;

Step 4. Calculate the long-contraction scour depth Y_C, associated with passage of the design flow through the bridge waterway. Depending on the abutment location in the channel at the bridge site (and thereby whether the contraction scour is of the live-bed or clear-water type) one of the following estimation relationships should be used:

  (i) For live-bed scour, use a relationship for Y_C such as that proposed by Laursen (1960), i.e., Eq. (4-14); and,

  (ii) For clear-water scour, use a relationship for Y_C such as that proposed by Laursen (1963), i.e., Eq. (4-24).

Step 5. At this point in the design process, enter Figure 13-1. It is necessary to consider the following factors:

(i). Length of embankment and abutment form (spill-through or wing-wall); and,

(ii). Floodplain's resistivity to erosion, if the abutment sits on a floodplain.

These factors are indicated as decision points in Figure 13-1, such that the next steps in design estimation vary in accordance with them.

13.3 Further Design Steps for Abutments Close to Main Channel

When the abutment is close to the main channel in a compound channel, Scour Condition A may occur. The findings from the laboratory experiments conducted for this Project indicate that Scour Condition A is likely when L/B_f equals or exceeds about 0.75. If the floodplain is erodible, Scour Condition B may occur in conjunction with Scour Condition A, but the resulting scour depth is less than for Condition A alone.

The further design steps are as follow (continuing the numbering sequence for the steps indicated in Section 13.2):

Step 6.   Estimate the scour depth associated with Scour Condition A, which occurs near the abutment and its embankment, but may not substantially expose the abutment column, unless scour actually causes the embankment to fail geotechnically:

(i) Use Eq. (12-1) and Figure 12-1 for a spill-through abutment;

(ii) Use Eq. (12-1) and Figure 12-2 for a wing-wall abutment on piles; and,

(iii) Use Eq. (12-1) and Figure 12-2 for a wing-wall abutment on sheet piles (note that the envelope includes data for pile and sheet-pile-supported wing-wall abutments).

Step 7.   Check the geotechnical stability of the bank of the main channel, and the earthfill embankment. Because scour locally heightens and steepens the river bank and the embankment, this step requires calculation to check bank and embankment stability. The relationships for this calculation are not given here, but rather in geotechnical texts (e.g. Lamb and Whitman 1974).

If scour were found to make the bank and embankment potentially unstable, leading to slope failure (such as the field example in Figure 3-5 for a spill-through abutment, or drawn in Figure 3-3), the abutment must be re-designed to be stable. Several options exist in this respect:

(i). For a bridge in design, widen the waterway opening to reduce Y_C; and,

(ii). Select a scour countermeasure method, such as described in NCHRP 24-18, Scour Countermeasures for Bridge Abutments (Barkdoll et al. 2007).

If the embankment were prone to geotechnical failure, scour estimation must consider the scour depth associated with Scour Condition C.

If scour did not cause concern for the stabilities of the main-channel bank and bridge embankment, it is left to the judgment of the designer to dimension the foundation of the abutment column so as to take into account the scour depth commensurate with Scour Condition C.

Step 8. Determine the scour depth associated with Scour Condition C, which occurs when embankment erosion is assumed to expose the abutment column:

(i) Use Eq. (12-7) with Figures 12-5 and 12-6a for scour at a standard-stub column of a spill-through abutment. In using Figure 12-6, it is necessary to assess the likely alignment of the abutment column relative to flow through the bridge waterway. [NOTE: a simplified, yet reasonable, estimate is to assume the flow is aligned with the column and gives the maximum clear-water scour. These assumptions are reasonable for flow through an abutment breached at the abutment column. Eq. (12-8) can then be used.];

(ii) Use Eq. (12-6) with Figures 12-5 and 12-6b for scour at a wing-wall column of a wing-wall abutment. This latter figure accounts for column alignment relative to flow direction. [NOTE: a simplified, yet reasonable, estimate is to assume the flow is aligned with the column and gives the maximum clear-water scour. These assumptions are reasonable for flow through an abutment breached at the abutment column. Eq. (12-9) can then be used.]; and,

(iii) For abutment columns differing in form from the standard-stub or wing-wall columns considered in this Project, estimate scour at the column as if estimating scour for a pier of approximately similar form. For instance, if the

pile cap for the stub abutment were located well above the floodplain (e.g., as in Figure 3-5), the scour estimate should be based on scour at a cluster of circular piles.

Step 9.   Consider the absolute lowest elevation attained by scour attributable to the scour depths for Scour Conditions A and C. Then decide whether this elevation should be used as the scour-depth estimate in designing the abutment's foundation.

13.4 Further Design Steps for Abutments Distant from the Main Channel

When the abutment is distant from the main channel in a compound channel, or is in a more-or-less rectangular channel, Scour Condition B occurs. The findings from the laboratory experiments conducted for this Project indicate that Scour Condition B occurs, and dominates scour when L/B_f is less than about 0.75. Scour Condition B may result in embankment breaching and, ultimately, in Scour Condition C.

The further design steps are as follow (continuing the numbering sequence for the steps indicated in Section 13-2:

Step 6.   Estimate the abutment scour depth associated with Scour Condition B:

(i) Use Eq. (12-3) and Figure 12-3 for a spill-through abutment, or

(ii) Use Eq. (12-3) and Figure 12-4 for a wing-wall abutment on piles. Also, use Eq. (12-6) when a pier is located within a distance $L_p/W < 3.0$ of the abutment.

Step 7.   Check the geotechnical stability of the earthfill embankment. Because scour locally heightens and steepens the river bank and the embankment, this step requires calculation to check bank and embankment stability. The relationships for this calculation are not given here, but rather in geotechnical texts (e.g. Lamb and Whitman 1974).

Step 8.   Determine the scour depth associated with Scour Condition C, which occurs when embankment erosion is assumed to expose the abutment column. The estimation relationships for this step are the same as for Step 8 in Section 13.3.

Step 9.   Consider the absolute lowest elevation attained by scour attributable to the scour depths for Scour Conditions B and C. Then decide whether this elevation should be used as the scour-depth estimate. Note that, for very short embankments, the scour depth associated with Condition C will always exceed that associated with Condition B, as discussed in Chapters 8 and 9.

13.5 Examples of Method Application

This section gives four examples of flow depth, and scour-depth estimation for spill-through abutments. Essentially the same estimate steps would be used for wing-wall abutments. As emphasized at the outset of this report, the scour-depth estimation method yields an estimate of maximum flow depth, Y_{MAX}, and scour depth, d_{Smax}.

13.5.1 Spill-Through Abutment in a Compound Channel

The embankment of a spill-through abutment is to extend across the floodplain of a compound channel such that $L/B_f = 0.85$. The main-channel and floodplain widths are 40.0m and 50.0m, respectively. The channel is symmetrical about its centerline. The floodplain comprises silty-clayey soils covered by grass and brush, whereas the bed of the main channel comprises medium-sized sand. The floodplain is judged to be relatively erosion resistant compared to the bed sediment.

For design flow conditions, flow depths in the main channel and on the floodplain are 3.0m and 1.5m, respectively; and the corresponding area-average velocity of flow through the main-channel and on the floodplain are estimated to be 1.75m/s and 0.4m/s, respectively

Consideration 1 indicates that the following two scour depths should be estimated:
   (i)   Scour Condition A (Figure 12-1); and,

(ii)   Scour Condition C (Figure 12-5).

Consideration 2 indicates that Scour Condition likely will not occur, because the floodplain is far less erodible than is the main-channel bed.

Steps 1 through 5 yield the following values for the abutment site:

- Section-average unit discharge for the main channel, $q_1 = 5.3$ m^2/s;

- Section-average unit discharge for the axis of the bridge waterway, $q_2 = 7.3$ m^2/s;

- Flow concentration through the bridge waterway gives $q_2/q_1 = 1.4$;

- Figure 12-1 gives $\alpha_A = 1.6$; and,

- For live-bed long-contraction scour, Eq. (4-14) gives contraction scour depth, $Y_C = 3.95$ m.

Step 6 gives a scour-depth estimate for Scour Condition A:

- From Eq. (12-1) and Figure 12-1, $Y_{MAX} = 6.3$ m; and,

- Estimated maximum scour depth = 6.3 m − 3.0 m = 3.3 m, below the initial bed level adjacent to the abutment.

Step 7 entails *Consideration 3*, bank and embankment stability. This step requires a slope-stability estimate of the main-channel bank and the embankment face. The actual details of this step are beyond the scope of the present Project. However, the analysis given in Section 9.3 could be used to serve as a geotechnical check on the limit of scour depth. The 3.2-m scour depth indicated above would suggest a high probability of main-bank collapse. The laboratory tests for this Project indicate that embankment failure will result in a lesser scour depth.

Step 8, Scour Condition C, assumes embankment failure leading to exposure of the abutment column. For a standard-stub column identical to that shown in Figure 6-4, and aligned with the approach flow, Eq. (12-8) gives a scour-depth estimate (below the floodplain level)

- $d_{Smax} = 1.7b_{stub} = 1.7 \text{x} (1.4\text{m}) = 2.4$ m, below the floodplain level at the column

Step 9 requires comparing which of the scour depth estimates for Conditions A and C gives the lower elevation of scour near the abutment, and then choosing an elevation for use in designing the abutment column. In this respect, the laboratory tests conducted for the Project indicate that Scour Condition C leads to the greater depth at the actual abutment column. Scour Condition A may give the overall lower elevation of scour, but is located away from the abutment column and likely triggers the geotechnical instability of the embankment (e.g., as evident in Figure 7-12). The designer may exercise judgment in selecting either scour depth in designing the abutment column.

To accommodate the uncertainties associated with scour-depth estimates for Scour Conditions A and C, the designer may wish to include a safety factor. This consideration is left up to the particular agency conducting the bridge design; no safety factor is suggested herein.

13.5.2 Spill-Through Abutment Set Well Back on a Floodplain
The embankment of a spill-through abutment is to extend 30m across a 70m-wide floodplain of a compound channel, symmetrical about its centerline. The floodplain comprises sand covered by patchy vegetation, such that the floodplain is judged to be readily erodible. For design flow conditions, flow depth over the floodplain is 1.5m, with a corresponding area-average velocity of flow estimated to be 1.0 m/s, respectively.

Considerations 1 and 2 indicate that the following two scour depths should be estimated:
    (i) Scour Condition B (Figure 12-3); and,

    (ii) Scour Condition C (Figure 12-5).

Steps 1 through 5 yield the following values for the abutment site:

- Section-average unit discharge for the approach floodplain, $q_f = 1.5$ m²/s;

- Section-average unit discharge for the axis of the bridge waterway, $q_2 = 2.6$ m²/s;

- Flow concentration through the bridge waterway gives $q_{2f}/q_f = 1.75$;

- Figure 12-3 gives $\alpha_B = 2.1$;

- At the limit of clear-water scour on the approach floodplain the shear stress exerted by the flow would nominally equal the critical shear stress for erosion of the floodplain, so that $\tau_f/\tau_c \approx 1$. As noted in Section 4.3, exact estimation of τ_f/τ_c is a significant difficulty for floodplains; and,

- For live-bed long-contraction scour, Eq. (4-28) gives contraction scour depth, $Y_C = 2.4$ m, below the floodplain level at the abutment.

Step 6 gives a scour-depth estimate for Scour Condition B

- From Eq. (12-3) and Figure 12-3, $Y_{MAX} = 5.1$ m; and

- Estimated maximum scour depth = 5.1 m − 1.5 m = 3.6 m, below the floodplain level at the abutment.

Step 7 entails *Consideration 3*, bank and embankment stability. This step requires a slope-stability estimate of the main-channel bank and the embankment face. The actual details of this step are beyond the scope of the present Project, though the analytical considerations are laid out in Section 9.3. A 3.6m scour depth would suggest that the abutment's embankment be threatened with geotechnical instability. The laboratory tests for this Project indicate that embankment failure will result in a lesser scour depth.

Step 8 assumes embankment failure leading to exposure of the abutment column. For a standard-stub column identical to that shown in Figure 6-4, and approximately aligned with the flow, Eq. (12-8) gives a scour-depth estimate (below the floodplain level)

- $d_{Smax} = 1.7b_{stub} = 1.7\text{x}(1.4 \text{ m}) = 2.4 \text{ m}$, below the floodplain level at the column

Step 9 requires comparing which of the scour-depth estimates for Conditions B and C gives the lower elevation of scour near the abutment, and then choosing an elevation for use in designing the abutment column. In this respect, the laboratory tests conducted for the Project indicate that Scour Condition C leads to the greater depth at the actual abutment column. Scour Condition B may give the overall lower elevation of scour, but located away from the abutment column (e.g., as evident in Figure 9-6). The designer must exercise judgment in selecting either scour depth in designing the abutment column.

13.5.3 Spill-Through Abutment with Pier at Toe of Embankment Face

The abutment in sub-section 13.5.2 has a pier located at the toe of its embankment face. The pier is identical to that in Figure 6-14. Of interest is the scour depth at the abutment and the pier; both the abutment and the pier are set well back on the floodplain.

The findings in Chapter 11 (Figure 11-5) indicate that pier presence mildly reduces scour depth for Scour Condition B. The reduction is slight, and need not be factored into the depth estimate for abutment scour. Therefore scour remains at 3.6 m for Scour Condition B.

The scour depth at the pier should be estimated as being that attributed to the abutment, as per Figure 12-7, because the scouring flow field is dominated by the abutment. Therefore the pier scour depth can be estimated as 3.6 m.
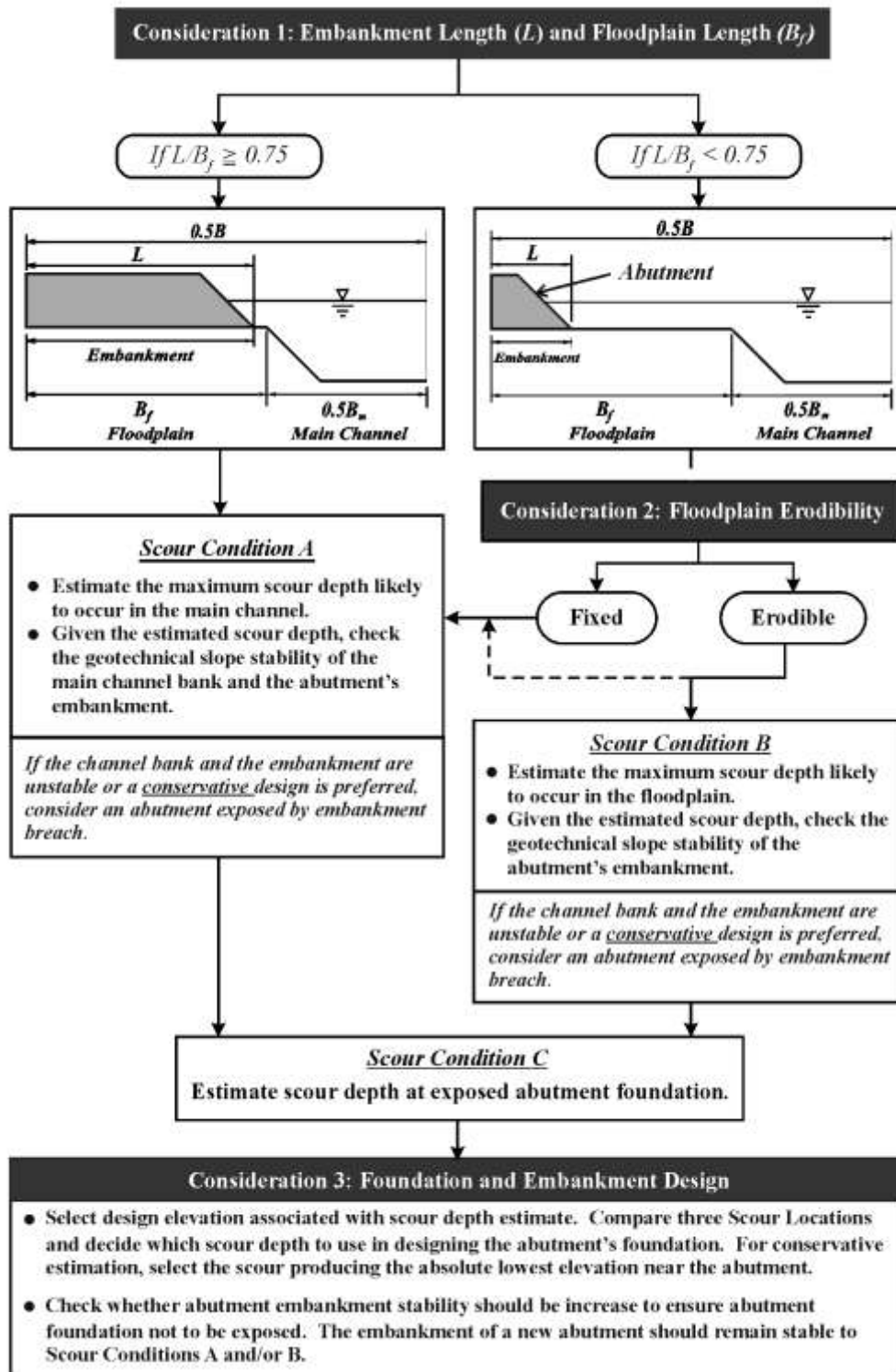
Figure 13-1. Flow chart outlining considerations in estimating scour depth at abutments

CHAPTER 14

CONCLUSIONS AND RECOMMENDATIONS

14.1 Introduction

This chapter presents the Project's principal conclusions and recommendations addressing its objectives as listed in Section 1.2. The principal objective was to develop a new approach for estimating abutment scour. Also presented are suggestions regarding aspects of abutment scour that require further investigation.

The Project involved flume experiments conducted with common standard designs of abutments in compound and simple channels. The experiments included the influences on scour of floodplain and embankment erodiblity, as well as of pier proximity. The abutments comprised an abutment column set amidst an earthfill embankment, as described in Chapter 2. To bracket the variation in the erodibility of floodplain soils and compacted earthfill embankments, the laboratory embankments simulated a fixed (non-erodible) embankment on a fixed floodplain: a riprap-protected erodible embankment on a readily erodible floodplain, and, an unprotected readily erodible embankment on a readily erodible floodplain. These differences in abutment layout and construction can result in different scour conditions, as described in Chapter 3.

The extensive new insights into scour processes obtained were utilized in developing the new method for estimating realistic scour depths at abutments. The method, introduced in Chapter 4, presented in Chapter 12, and applied in Chapter 13, takes into account important practical influences, notably abutment layout and construction, as well as the erodibilities of the floodplain (or channel bank) upon which the abutment is located and the compacted earthfill embankment approach to an abutment.

The new design approach replaces the old notion of linearly combining bridge-waterway contraction scour and local scour at the abutment structure, a notion that the Project's flume experiments do not support. Instead, the new method views abutment scour as essentially scour at a short contraction, for which the combined influences of non-uniform distribution of flow

passing around an abutment, and the generation of large-scale turbulence in flow, passing around an abutment are intrinsically linked. Accordingly, it is not meaningful physically to treat abutment scour as the linear combination of a contraction scour depth and a local scour depth, as currently assumed in many publications on abutment scour.

Prior relationships for scour-depth estimation neither adequately take into account practical considerations of bridge abutment layout and construction, nor the intrinsic linkage between so-called contraction scour and local scour, as critically reviewed in Chapter 5. As would be expected, most prior investigations of abutment scour focused on greatly simplified situations of scour. Practically all prior relationships for scour-depth estimation treat abutments and their approach embankments as being fixed, solid structures extending deep into the bed. However, few abutments are built like that. Consequently, prior scour-estimation relationships and guidelines are of dubious accuracy, and therefore do not extrapolate to field abutment situations. Prior scour relationships commonly do not take into account significant scour processes, and over-estimate scour depths at bridge sites.

To be kept in mind for scour depth estimation at abutments are the large number of uncertainty sources confounding accuracy in estimation. Accurate values of critical shear stress for vegetated floodplain soils surrounding an abutment is but one major source of uncertainty. The present project focused on the somewhat simplified situation of main-channel and floodplain boundaries composed of noncohesive sediment. Conduct of the project, though, also treated the common situation where the floodplain comprises vegetated soils and is far more resistant to erosion than the main-channel bed.

14.2 Conclusions about Scour Processes

The Project's main conclusions regarding scour processes and conditions, along with scour-depth trends, and flow-field observations ensue.

14.2.1 Scour Processes and Conditions

1. Abutment scour is essentially a form of scour at a short contraction. Accordingly, scour is closely influenced by flow distribution through the short contraction and by turbulence structures generated, and dispersed, by flow entering the short contraction;

2. Provided that the approach embankment of an abutment does not breach, so that flow passes through it, abutment scour principally develops as a local amplification of contraction scour associated with flow through a long contraction;

3. Abutment presence contracts flow non-uniformly across a bridge waterway. However, in situations of short abutments adjoining relatively wide channels, flow contraction scour decreases in accordance with two limits:

   (i). If channel width is constant and abutment length decreases, scour depth at the abutment approaches zero; or,

   (ii). For a full abutment form of constant length in a channel of increasing width, scour depth at the abutment approaches a limiting value associated with scour around an abutment in a very wide channel. This scour depth may be estimated approximately in terms of local flow contraction around the abutment itself.

   This second limit can be difficult to simulate by means of hydraulic models replicating the full form and usual construction of actual spill-through and wing-wall abutments, because most laboratory flumes are insufficiently wide;

4. Abutment scour entails hydraulic erosion followed by geotechnical failure of the main-channel bank and earthfill embankment around the abutment column. Normally, abutment structures are pier-like structures built from concrete or steel, around which an earthfill embankment is formed; and,

5. Abutment scour may involve three distinct scour conditions, herein termed Scour Conditions A, B, and C. These scour conditions, described in Chapters 3, and 7 through 9, were observed in the flume experiments and at actual bridge sites:

   (i). Scour Condition A occurs as scour of the main channel portion of a compound channel;

(ii). Scour Condition B is scour of the floodplain, and occurs for abutments set well back from the main channel; and,

(iii). Scour Condition C is the scour form that develops when breaching of an abutment's embankment fully exposes its abutment-column structure such that scour develops at the abutment column as if it were a pier.

14.2.2 Scour-Depth Trends

1. For Scour Condition A, a useful analytical framework with which to relate maximum flow depth (incorporating maximum scour depth), Y_{MAX}, to flow conditions and boundary sediment or soil is to plot the dimensionless parameters Y_{MAX}/Y_C and q_2/q_1. Here, Y_C is the flow depth estimated for live-bed flow through a long contraction; q_2 is the area-average unit discharge of flow through the bridge section; and, q_1 is the area-average unit discharge of flow through the main channel upstream from the bridge site. At lower values of q_2/q_1, scour depth (and Y_{MAX}/Y_C) is governed by the local flow field around an abutment. However, for large values of q_2/q_1, scour development is governed by flow contraction, so that Y_{MAX}/Y_C asymptotically approaches about 1.1. The approximate 10 percent increase is attributable to local concentration of flow and turbulence generated by flow around the abutment;

2. Scour depths for Scour Condition A reduce when the bank of the main channel and the abutment's embankment are erodible, because bank and embankment failure increase the flow area through the bridge waterway, thereby reducing flow velocities near the abutment;

3. The location of deepest scour commonly was where the axis of the abutment intersected with the bank of the main channel. For small q_2/q_1, the region of deepest scour is close to the bank of the main channel. As q_2/q_1 increases, flow constriction at the abutment increases, and scour at the abutment access becomes increasingly more uniform across the main-channel bed;

4. Abutment alignment did not appreciably affect Y_{MAX}/Y_C for the range of abutment layouts investigated under Scour Condition A. The variations in Y_{MAX}/Y_C were well within the amplitude variation of dune height;

5. For Scour Condition B, a useful analytical framework with which to relate maximum flow depth (incorporating maximum scour depth), Y_{MAX}, to flow conditions and boundary sediment or soil is to plot the dimensionless parameters Y_{MAX}/Y_C and q_{f2}/q_f. Here, Y_C is the flow depth estimated for clear-water flow through a long contraction; q_{f2} is the area-average unit discharge of flow through the bridge section on the floodplain; and, q_f is the area-average unit discharge of flow over the floodplain upstream of the bridge site. The trend for Y_{MAX}/Y_C versus q_{f2}/q_f is essentially the same as described in Item 1 for Y_{MAX}/Y_C and q_2/q_1;

6. The scour-depth trends for wing-wall abutments and spill-through abutments are similar, though with the following differences –

   i.   A peak maximum scour depth at wing-wall abutments exceeds that for spill-through abutments; and,

   ii. When flow contraction governs scour, the scour depths at wing-wall and spill-through abutments are comparable.

7. For Scour Condition C, scour depths must be estimated in a semi-empirical manner similar to that used for estimating scour depth at a pier of complex geometry. Scour is governed by the highly three-dimensional flow field developed at an exposed, pier-like column.

8. The scour-depth trends for scour Conditions A and B differ substantially from those estimated using ABSCOUR, the prior method that most closely resembles the method developed herein. However, for values of flow contraction within about q_2/q_1 (or q_{f2}/q_f) < 2, the magnitudes of Y_{MAX}/Y_C are reasonably comparable, provided the (ABSCOUR) coefficient for a spiraling-flow effect is set at 1.

14.2.3 Flow Field

1. The flow field around an abutment has essentially the same characteristics as flow fields through short contractions. Notably, flow distribution is not uniform and generates large-scale turbulence;

2. As the abutment length or L/B_f increased, the orientation of flow near the embankment on the floodplain swung more parallel to the embankment axis before turning through the bridge opening. Also, the flow became more uniformly distributed across the main channel through the bridge waterway;

3. Measurement and observation of the flow field, by means of LSPIV and ADV, reveal that the flow field can change substantially as scour progresses. Scour development at abutments can cause flow to concentrate in the region of scour. This concentration locally amplifies contraction scour;

4. Scour development may geotechnically destabilize the earthfill embankment at an abutment, causing the embankment to experience a geotechnical slope-stability failure. Flow subsequently eroding the exposed earthfill may breach the embankment. When an embankment breaches, and flow passes through the embankment, flow velocities decrease through the bridge opening. Scour Conditions A and B then cease developing;

5. For Scour Condition C, the quantitative estimation equations were adapted from the prediction equation for estimating the maximum scour as the pier-like structure from previous studies, and the current study shows good performance in terms of estimating the scour depth; and,

6. The geotechnical strength of the soils forming the bank of a main channel, and the compacted earthfill of an abutment's approach embankment influence the depth of scour that can develop at abutments. Besides scour deepening only to the extent that flow no longer erodes bed sediment or floodplain soil, scour can deepen only as long as the adjacent bank or embankment remain stable.

14.2.4 Influence of Pier Proximity

1. The flume data show that pier presence does not dramatically affect scour depth at an abutment. However, when a pier is at the toe of a spill-through abutment, pier presence may decrease scour depth by as much as 22%. This reduction occurs because the pier redistributes flow away from the abutment;

2. Abutment scour dominates scour at a pier close to an abutment. Therefore, pier-scour equations are not applicable for a pier close to abutments. The experiments show that abutment scour over-rides pier scour when a pier is within about 3 times floodplain flow depth form the toe of an abutment;

3. Scour at a pier is increased by pier proximity when a pier is within a distance of about 11 times floodplain flow depth from the toe of an abutment;

4. A high degree of accuracy is not practicable for estimating maximum scour depth at bridge abutments, because most abutments are located in compound channels whose geometry is fairly complex and whose channel is formed of various materials occupying different locations within a bridge site. Sands may form the bed of a main channel; silts and clay may predominate in riverbanks and underlying floodplains; and rocks may have been placed as riprap protection for the abutment, as well as sometimes along adjoining riverbanks. The scour-depth estimation method developed during the present study gives a reasonable estimate of scour depth. That depth should be increased by a safety factor for design purposes. The magnitude of the safety factor will depend on the economics associated with bridge construction. The present report does not suggest values for a pertinent safety factor, because the particular agencies conducting design estimations for scour depth must decide such values;

5. Heterogeneity associated with the shear strength of the floodplain or embankment might affect the selection of the scour conditions. However, as far as Y_{MAX} is concerned, for Scour Conditions A and B, those uncertainties do not have a strong influence. For Scour Condition C, the uncertainty associated with the structural detail of abutments influences scour-depth estimation for the abutment column; and,

6. The Project's findings, in terms of scour processes, and methods for predicting scour depth, are supported by field observations and data.

14.3 Recommendations for Scour-Depth Estimation

In accordance with the three scour conditions mentioned in Section 14.2.1, the Project has established that two maximum depths of scour are of interest for abutment design –

    i.   ***Maximum scour as near-abutment amplification of contraction scour***. The flume experiments show that the maximum scour depth develops essentially as a near-abutment amplification of contraction scour, the amplification caused by the increased flow velocity and turbulence local to the abutment and its approach embankment.   This depth occurs when an abutment's embankment has not breached, such that the flow is contracted around the abutment.

    ii.   For an abutment in a compound channel, the deepest scour should be checked at two locations: in the main channel if the abutment is close to the main channel, and, on the floodplain if the abutment is well set back from the main channel. The two locations coincide with Scour Conditions A and B.

    iii.   ***Maximum scour as local scour at fully exposed abutment structure***.   The experiments show that the deepest scour at the abutment column itself occurs when the embankment has breached so that the abutment column (e.g., standard stub or wing-wall) is fully exposed as if it were a pier; i.e., for Scour Condition C.

The foregoing conclusions led to the ensuing recommendations for estimating scour depth at bridge abutments:

1. For Scour Condition A at spill-through abutments and wing-wall abutments, use the design curves given in Figures 12-1 and 12-2, respectively;

2. For Scour Condition B at spill-through and wing-wall abutments, use the design curves in Figures 12-3 and 12-4, respectively;

3. For Scour Condition C at stub-columns (spill-through abutments), use Figures 12-5 and 12-6a to estimate the influences of flow intensity and flow alignment on scour depth;

4. For Scour Condition C at wing-wall-columns (wing-wall abutments), use Figures 12-5 and 12-6b to estimate the influences of flow intensity and flow alignment on scour depth;

5. When a pier is close to an abutment, the scour depth at the pier can be estimated using Figure 12-7; and,

6. The design curves indicated above in items 2 -– 5 do not include a safety factor. When estimating scour depth for design purposes, the designer must select a safety factor they deem appropriate for the abutment.

14.4 Recommendations for Further Research

Abutment scour involves more influences than could be investigated during this Project. The following recommendations are given for further research investigation:

1. The shear strength of the earthfill comprising an embankment has a significant effect on scour development and equilibrium depth. Further experiments should be conducted using simulated embankments that have a range of shear strengths. Shear strength would scale with the length scale of the experimental set up;

2. Other parameters should be varied, such as water-surface elevation, and size, uniformity of sediment forming the main channel bed, and surface roughness as well as the floodplain;

3. Scour of abutments on floodplains formed of cohesive soil is an important topic for further investigation. It is likely that scour takes much longer to develop for cohesive soil, as has been shown for scour at piers in cohesive soil;

4. Figure 4-6 delineates a grey region where abutment scour depth varies with the combined influences of several parameters. The present project examined scour trends for selected set of parameter ranges. Considerable scope still exists for further experimentation with other parameter ranges beyond those used in the present project;

5. Given all the scour-process insights produced from this project, it will be useful to re-visit field observations of scour cases at actual abutments. In so doing, it will be valuable to relate observed scour cases to the Scour Conditions this report describes; and,

6. Three-dimensional numerical modeling of flow would provide useful insights into how flow and scour evolve at a bridge abutment. In the long run, such modeling may alter again the design approach taken by engineers. The present Project was limited to two-dimensional modeling of flow.

REFERENCES

AASHTO, (1992). "Highway drainage guidelines." Vol. VII, Hydraulic Analyses for the Location and Design of Bridges, American Association of State Highway and Transportation Officials, Washington, D.C.

Barkdoll, B., Ettema, R., and Melville, B. (2007). "Countermeasures to protect bridge abutments from scour." Report 587, National Cooperative Highway Research Program, Transportation Research Board, Washington, D.C.

Bearman, P. W. (1984). "Vortex shedding from oscillating bluff bodies." Annual Review of Fluid Mechanics, Vol. 16, 195-222.

Benedict, S. (2003). "Clear-water abutment and contraction scour in the coastal plain and Piedmont provinces of South Carolina, 1996-99." Water-Resources Investigations *Report* 03-4064, U. S. Geological Survey, Columbia, South Carolina.

Biglari, B., and Sturm, T.W. (1998). "Numerical modeling of flow around bridge abutments in compound channel." *J. Hydr. Engrg*, ASCE, 124(2), 156.

Blench, T., (1962), Discussion of "scour at bridge crossings", by E.M. Laursen: Transactions of American Society of Civil Engineers, 127, 180-183.

Breusers, H.N.C., and Raudkivi, A.J. (1991). Scouring. *IAHR Hydraulic Structures Design Manual 2*, IAHR.

Cardoso, A. H., and Bettess, R. (1999). "Effects of time and channel geometry on scour at bridge abutments." *J. Hydr. Engrg.*, ASCE, 125(4), 388-399.

Chang, F., and Davis, S. (1998), "Maryland SHA procedure for estimating scour at bridge abutments, part 2-clear water scour," Proc. of Water Resources Engineering, '98, ASCE, Memphis, TN, pp. 169-173.

Chang, F. and Davis, S., (1999), "Maryland SHA procedure for estimating scour at bridge waterways, part 1 – live bed scour." In *Stream Stability and Scour at Highway Bridges*, (Eds) Richardson, E. and Lagasse, P., American Society of Civil Engineers, Reston VA, pp 401-4011.

Chow, V.T. (1959). Open Channel Hydraulics, McGraw-Hill, New York.

Cinotto, P., and White, K.E. (2000). "Procedures for scour assessments at bridges in Pennsylvania." *Open-File Report* 00-64, Pennsylvania Dept of Transportation, with US Geological Survey, PA.

CIRIA (2002). "Manual on scour at bridges and other hydraulic structures." *Pub*. 551, Construction Industry Research and Information Association, London, Britain.

Dargahi, B. (1989)."The turbulent flow field around a circular cylinder." *Experiments in Fluids*, No. 8, 1-12.

Dargahi, B. (1990). "Controlling mechanism of local scouring." *J. Hydr. Engrg*, 116(10), 1197-1214.

Dietz J. W., (1969). Kolkbildung im feinem oder leichter Sohlmaterialen bei strömenden Abfluss." Mitt. Theodor Rehbock Flussbaulab, Karlsruhe, Heft 155, Germany.

Dongol, D.M. (1994). "Local scour at abutments." *Report* 544, Dept. of Civil Engineering, University of Auckland, Auckland, New Zealand.

Ettema, R. (1980). "Scour at Bridge Piers." *Report* 215, Dept. of Civil Engineering, University of Auckland, Auckland, New Zealand.

Ettema., R., Muste, M. (2004). "Scale effects in flume experiments on flow around a spur dike in flatbed channel." *J. Hydr. Engrg*., ASCE, 130(7), p. 635.

Ferziger J.H., and Peric M. (2002). *Computational methods for fluid dynamics*, Third edition. Springer-Verlag, Berlin, Germany.

FHWA (2004). "Enhanced Abutment Scour Studies of Four Compound Channels" *U.S. Department of Transportation*, Federal Highway Administration, Research, Development, and Technology, Publication No. FHWA-RD-99-156, McLean, VA.FHWA-RD-99-156

Field, W. G. (1971). "Flood protection at highway openings." *Engineering Bulletin* CE3, University of Newcastle, NSW.

Froehlich, D.C. (1989). "Local scour at bridge abutments." *Proc*. ASCE National Hydraulic Conference, Colorado Springs, Colorado, 13-18.

Froehlich D C. (2002). *User's Manual* for FESWMS Flo2DH - Two-dimensional Depth-averaged Flow and Sediment Transport Model, Release 3, Publication No. FHWA-RD-03-053, Federal Highway Administration, McLean, VA.

Fujita, I., Muste, M., and Kruger, A. (1998). "Large-scale particle image velocimetry for flow analysis in hydraulic applications". *J. Hydr. Res*., 36(3), 397-414.

Garde, R, Subrmanaya, K., and Nambudripad, K. (1961). "Study of scour around spur dikes." *J. Hydr. Engrg*., ASCE, 118(4), 23-37, Discussion 88(2), 161-192.

Gill, M.A. (1972). "Erosion of Sand Beds Around Spur Dikes," *J. of the Hydraulics Division*, ASCE, 98(HY9), pp. 1587-1602.

Hjorth,P. (1975). "Studies of the nature of local scour." *Bulletin Series A,* No. 46, Dept. of Water Resources Engineering, Univ. of Lund, Sweden.

Hobbs, B.W. (2005)," Two-dimensional numerical simulation of flow in a steep-gradient stream: implications for sediment transport and habitat conditions." Master's Thesis, the University of Iowa, Iowa City.

Hoffmans G.J., and Booij, R. (1993). "The influence of upstream turbulence on local scour holes." *Proc.* IAHR 25th Congress, Tokyo, Japan.

Hoffmans, G.J., and Verheij, H.J. (1997). *Scour Manual.* A.A. Balkema, Rotterdam, The Netherlands.

Holnbeck, S. R., Parrett, C., and Tillinger T. N. (1993). "Bridge scour and change in contracted section, Razor Creek, Montana." *Hydraulic Engineering* '93, ASCE, Part 2(of 2), 2249-2254.

Hoyt, J. W., and Sellin, R.H.J. (2000). "Three-dimensional visualization of large structures in the turbulent boundary layer." *Experiments in Fluids*, 30(3), 295-301.

Kouchakdeh, S., and Townsend, D. R. (1997a). "Maximum scour depth at bridge abutments terminating in the floodplain zone." *Can. J. Civ. Engrg.,* 24(6), 996-1006.

Kouchakdeh, S., and Townsend, D. R. (1997b). "Influence of lateral momentum transfer on bridge abutment scour." *Proc.* 27th IAHR Congress, Theme A, San Francisco, August 10-15, 190-195.

Kouchakdeh, S., and Townsend, D.R. (1998). "Bridge abutment scour in compound-shaped river channels." *Proc.* Stream Stability and Scour at Highway Bridges, ASCE, Reston, VA, 417-427.

Kwan, T.F. (1984). "Study of abutment scour." Rept. 328, Dept of Civil Engineering, University of Auckland, Auckland, New Zealand.

Kwan T F, (1988), A study of abutment scour. Rept. No. 451, School of Engineering, University of Auckland, Auckland, New Zealand.

Lagasse, P.F., and Richardson, E.V. (1999). "Compendium of stream stability and bridge scour papers." *ASCE Publications*, Reston, VA.

Lamb, H. (1932). Hydrodynamics. 6th Edition, Cambridge University Press, Cambridge, UK.

Lamb, T. W. and Whitman, R.V., (1974), Soil Mechanics. John. Wiley and Sons Inc., New York.

Laursen, E.M. (1960). "Scour at bridge crossings." *J. Hydr. Div.*, ASCE, 86(2), 39-54.

Laursen, E.M. (1963). "An analysis of relief bridge scour." *J. Hydr. Div.*, ASCE, 86(2), 93-118.

Laursen, E.M., and Toch, A. (1956). "Scour around bridge piers and abutments." *Bulletin* No.4, Iowa Highways Research Board, Ames, Iowa, U.S.A.

Lim, S.Y. (1997). "Equilibrium clear-water scour around an abutment". *J. Hydr. Engrg.*, ASCE, 123(3), 237-243.

Liu, H.K., Chang, F., and Skinner, M. (1961). "Effects of bridge constriction on scour and backwater." *Report* CER60HKL22, Engineering. Research Center, Colorado State University, Colorado.

Lombard, P. J. and Hodgkins, G.A. (2008). "Comparison of Predicted and Observed Abutment Scour at Selected Bridges in Maine." Scientific Investigations Report 2008–5099, U.S. Geological Survey, Reston VA.

Melville, B.W., (1975). "Local scour at bridge sites." *Report* No. 117, School of Engineering, University of Auckland, Auckland, New Zealand.

Melville, B.W. (1992). "Local scour at bridge abutments." *J. Hydr. Engrg.*, ASCE, 118(4), p.615.

Melville, B.W. (1995). "Bridge abutment scour in compound channels." *J. Hydr. Engrg.*, ASCE, 121(12), p. 863.

Melville, B.W., and Coleman, S.E. (2000). *Bridge Scour*, Water Resources Publications, Colorado, U.S.A., 550p.

Morales, R. and Ettema, R. (2010). "Insights from Depth-Averaged Flow Models Applied to Bridge Abutments." Report 2010-7, Mountain Plains Transportation Consortium, Laramie, Wyoming.

Mueller, D.S., and Hitchcock, H.A. (1998) "Scour measurements at contracted highway crossing in Minnesota, 1997." *Proc.* 1998 Int. Water Res. Engrg. Conf., Part 1 (of 2) Aug 3-7, v1, ASCE, pp.210.

Mueller, D.S., and Wagner, C. R. (2005). "Field observations and evaluations of streambed scour at bridges" *Report* FHWA-RD-03-052, Federal Highway Administration, Washington, D.C.

Neill, C.R. (1973). *Guide to Bridge Hydraulics*, Roads and Transportation Assoc. of Canada, Univ. of Toronto Press, Toronto, Canada.

Palaviccini, M. (1993), Predictor Model for Bridge Abutments. PhD Thesis, The Catholic University of America, Washington, D.C.

Raudkivi, A.J. (1999). *Loose Boundary Hydraulics*, A.A. Balkema, Rotterdam, The Netherlands.

Rice, C.E., Kadavy, K.C., Robinson, K.M. (1998). "Roughness of loose rock riprap on steep slopes." *J. Hydr. Engrg.*, 124(2), 179-185.

Richardson, E.V., Simons, D.B., and Julien, P.Y. (1990). "Highways in the river environment participant notebook." Federal Highway Administration Publication FHWA-HI-90-016, Washington D.C., 650p.

Richardson, E.V., Harrison, L.J., and Davis, S.R. (1991). "Evaluating scour at bridges." *Report No. FHWA-IP-90-017 HEC 18*, Federal Highway Administration, Washington, D.C.

Richardson, E.V., and Davis, S.R. (1995). "Evaluating Scour at Bridges." *Publication No. FHWA HI-96-031,* Federal Highway Administration, Arlington, VA.

Richardson, E.V., and Davis, S.R. (2001). "Evaluating Scour at Bridges." *Hydraulic Engineering Circular* No. 18, 4th Ed., Federal Highway Administration, Arlington, VA.

Richardson, E.V., and Lagasse, P.F. (eds.) (1999). "Stream stability and scour at highway bridges - compendium of papers, ASCE Water Resources Engineering Conferences 1991-1998." ASCE, Reston, VA.

Rouse, H., (ed.) (1950). *Engineering Hydraulics*, John Wiley and Sons, New York.

Straub, L. G., (1934). "Effect of channel-contraction works upon regime of movable bed streams." *Transactions*, the 15th Annual Meeting, Part II, American Geophysical Union, Washington, D.C., 454-463.

Sturm, T.W., and Janjua, N.S. (1993). "Bridge abutment scour in a floodplain." *Conf. Proc. Hydr. Engrg*, ASCE, p.761.

Sturm, T.W. ,and Sadiq, A. (1996). "Bridge abutment scour in floodplain with backwater." *Conf. Proc. Hydr. Engrg.*, ASCE, Session BS-5.

Sturm, T. (1997), Unpublished preliminary results of a hydraulic laboratory study of contracted flow in a compound channel. Georgia Institute of Technology, Atlanta.

Sturm, T.W., and Chrisochoides, A. (1997). "Local scaling of bridge abutment scour in compound channels." *Conf. Proc. Hydr. Engrg.,* ASCE, p.196.

Sturm, T.W. (1998). "Abutment scour in compound channels." *Proc.* Stream Stability and Scour at Highway Bridges Conference, ASCE, Reston, VA, p. 443.

Sturm, T.W., and Chrisochoides, A. (1998a). "Abutment scour in compound channels for variable setbacks." *Conf. Proc.* Water Resources Engineering, ASCE, p.174.

Sturm, T.W., and Chrisochoides, A. (1998b). "One-dimensional and two-dimensional estimates of abutment scour prediction variables." *Transportation Research Record,* 1647, Nov., p.18.

Vanoni, V.A., (ed.) (1975). *Sedimentation Engineering*, *ASCE Manuals and Reports on Engineering Practices*, ASCE 54, New York, NY.

Williamson, C.H.K. (1996). "Vortex dynamics in the cylinder wake." *Annual Review of Fluid Mechanics,* 28, 477-539.

Yalin, M.S. (1992). *River Mechanics*, Pergamon, Oxford, Britain.

Yu, G., and Lim, S.Y. (2002). "Flow and scouring in main channel due to abutments." *Proc.* 1st International Conference on Scour at Foundations, Texas.

Zaghloul, N. A, (1983), "Local scour around spur dikes." Journal of Hydrology, 60, Issue 1-4, 123-140.

APPENDIX A

SURVEY OF DEPARTMENTS OF TRANSPORTATION

A.1. Introduction

To obtain substantiating information about scour processes observed in the field, an early task for the Project entailed conducting a survey of Departments of Transportation (DOT) to ascertain their field experience with abutment scour. The survey entailed compilation and distribution of a fairly simple questionnaire, whose main results are summarized here. The survey focused on obtaining information for use in selecting the types of abutment configuration and scour condition of principal interest for the laboratory flume experiments to be conducted.

The survey comprised a series of four questions focused on the following aspects of abutment scour:

1. Alignments of bridge abutments relative to main channels and floodplains;
2. Locations of scour areas relative to abutments;
3. Erodibility of floodplain soils; and,
4. Scour experience at bridge abutments.

The survey questionnaire was sent to 50 state agencies. Survey replies were received from 31 states, including two replies each from Arkansas, Illinois, and Virginia. Additionally, the Project was in contact with Mr. Stephen Benedict, who is with the South Carolina office of the U.S. Geological Survey (USGS). For the past six years he has worked on several research projects investigating field observation of abutment scour at selected sites in South Carolina. The USGS, in cooperation with the South Carolina Department of Transportation, had collected 209 observations of clear-water abutment scour at 146 bridges in South Carolina. Benedict amassed data on abutment scour, with case study information pertaining to scour depth ranging from 0 to 23.6 ft (7.2 m) in depth. Additionally, he has been working with these data to develop tools for assessing abutment depths of scour. His work is published in Benedict (2003).

Useful reports obtained in the course of the survey and interactions with other researchers actively studying scour problems are Parola et al. (1998), Newman (1996), and Fischer (1995). The report by Parola et al. describes the extensive scour damage caused by the major flooding event in the upper Mississippi River Basin during 1993. The second report describes bridge-scour problems in Georgia consequent to a major storm in 1994. The third report describes scour conditions observed across Iowa. Additionally, the Pennsylvania DOT provided the team a copy of its procedures for scour assessment at bridges (Cinotto and White 2000).

With regard to abutment position in a channel (Figure A-1), the survey sought input on the relative frequency of three general layouts (here termed types) of alignment:

1. Abutment layout Type 1, no floodplain, abutment in essentially a rectangular channel ($B_f = 0$);
2. Abutment layout Type 2, abutment set back on a floodplain ($L/B_f < 1$); and,
3. Abutment layout Type 3, abutment extending across a floodplain and into the main channel ($L/B_f > 1$).

The input responses from each state were provided in terms of the approximate percentage of abutments associated with each layout.

A.2. Survey Findings

The survey led to the following conclusions:

1. The great majority of abutment layouts coincide with Type 3, though substantial percentages of abutments were reported to be Type 1 or 2. The percentages varied from state to state. In approximate overall terms, most bridge abutments are located fully or partially on floodplains (82%);
2. A relatively high percentage of Abutment Type 1 (Figure A-1) was reported for Connecticut (60%), Massachusetts (79%), Michigan (80%), Rhode Island (50%), and

Texas (60%). It is noted here that Type 1 layout also is common in Maine (Lombard and Hodgkins, 2008). The South Carolina DOT reported that Type 1 abutments built in swamps without any inundated channels are normally spill-through abutments with riprap placed on the end fills and on the side slopes of the embankments for 30ft (10m) beyond the edge of the bridge;

3. A relatively high percentage of Abutment Type 2 was reported for California (70%), Minnesota (80%), and Pennsylvania (60%);

4. A relatively high percentage of Abutment Type 3 was reported for Arkansas (90%), Illinois (97%), Georgia (100%), Iowa (100%), Louisiana (100%), Mississippi (100%), Missouri (95%), Montana (100%), Nebraska (100%), New Mexico (90%), Ohio (75%), Oklahoma (97%), Oregon (85%), South Carolina (80%), Tennessee (75%), and Virginia (94%);

5. With regard to abutment scour conditions, the survey showed more or less evenly distributed responses among Scour Conditions A and B. This finding expresses a difficulty faced in preparing the Project's laboratory test plan, because of the variability of abutment scour conditions. It indicates that indeed several scour conditions must be investigated;

6. The survey indicated that erodible conditions of floodplain soils are highly variable as compared with main-channel beds, which usually comprise alluvial sediment;

7. Scour Conditions A and B sometimes occur owing to sand-mining activities and lateral shifts of the main channel;

8. The causes of Scour Conditions A and B scour were reported as being difficult to determine, probably due to local scour around abutment or contraction scour and/or a combination of both;

9. Scour Conditions A and B occur when embankment protection fails, and are compounded by drift (woody debris) accumulations against bridge substructures;

10. Scour Condition A is mentioned as occurring at "box bridges";

11. Embankment failures for Scour Condition A occur immediately adjacent to the bridge abutment, which makes it hard to determine whether it was abutment scour or embankment scour. Condition A (and combined Conditions A and B) was also reported to occur when road-side drainage ditches cut into the fill slope and channel migration

threatens roadway fill. Frequent overtopping over embankment associated with low bed grades was associated with Scour Condition B. Although it is not common, scour was reported to occur by wave action from ocean, lakes, or flooding rivers; and,

12. The preponderance of abutment failures attributable to scour occurs for small bridges. In many cases, scour was aggravated by factors such as change in channel alignment, or inadequate maintenance of bank conditions in the vicinity of an abutment. This observation is of substantial importance as it indicates the on-going necessity of effective monitoring of all bridge waterways; small and large.

These conclusions were used in planning the schedule of laboratory experiments conducted for the Project.
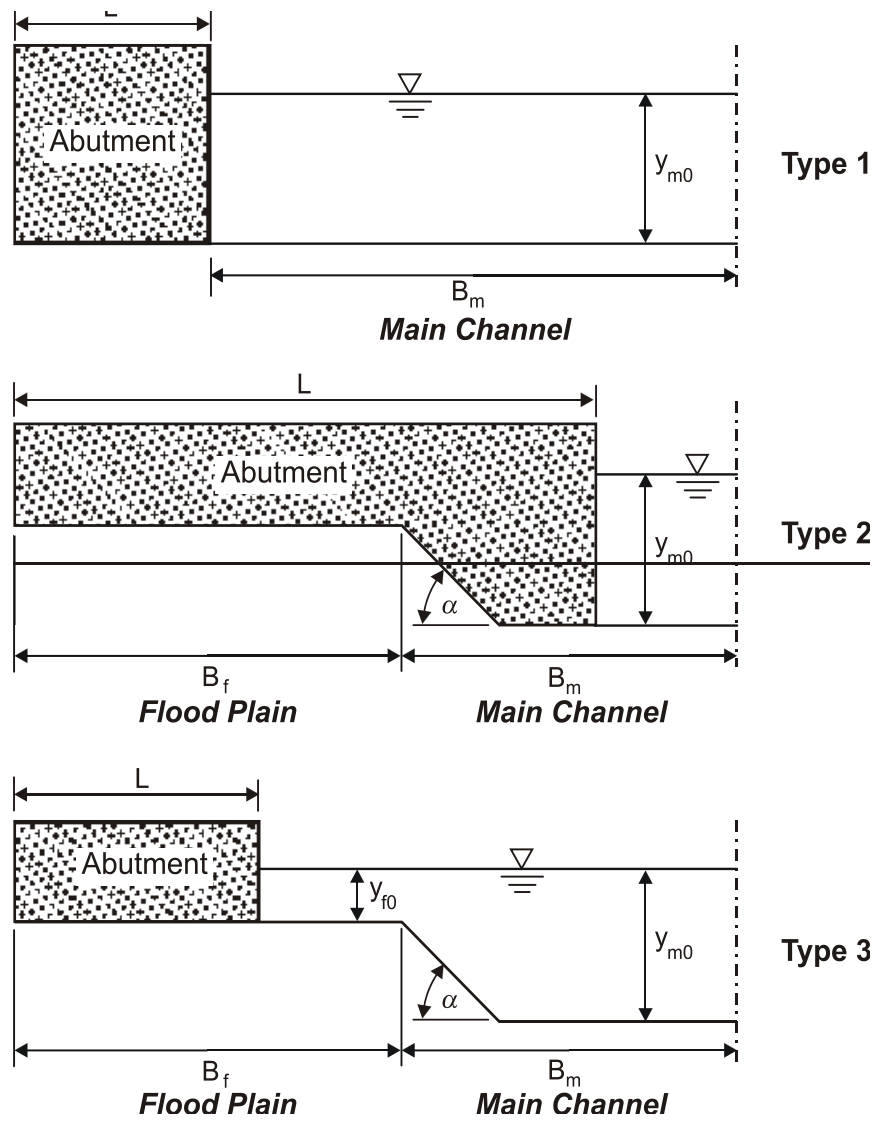
Figure A-1. This figure was used in the Survey question regarding general location and extent of abutments in river channels (main and floodplain). It applies to both spill-through and wing-wall abutments.
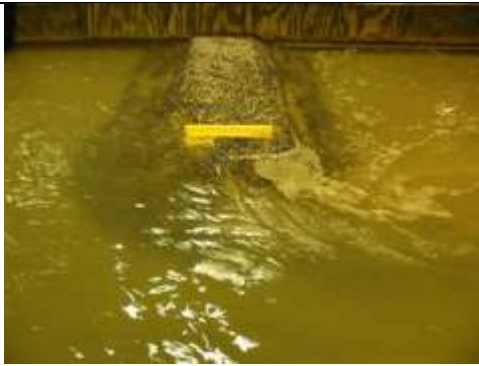
APPENDICES B

PHOTOS OF SCOUR DEVELOPMENT AT ABUTMENTS

The ensuing appendices, B1 through B7, give photo sequences of scour development at abutments as observed during the laboratory experiments. The appendices were selected to provide a representative sample of observations.

APPENDIX B1: Scour Development at a Riprap-Protected Spill-Through Abutment on an Erodible Floodplain ($B_f/0.5B = 0.63$, $L/B_f = 0.70$)

Time elapsed (min.)	Top view	Front and side views
Initial set up		
0		
6		

33		
63		
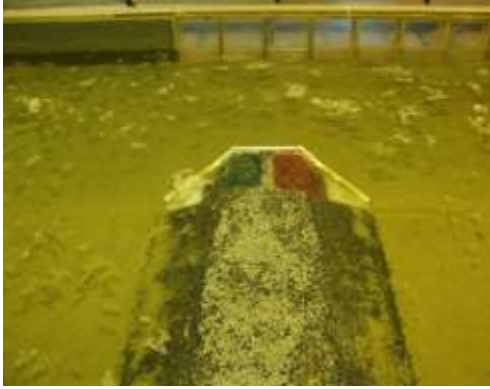
292		
964		
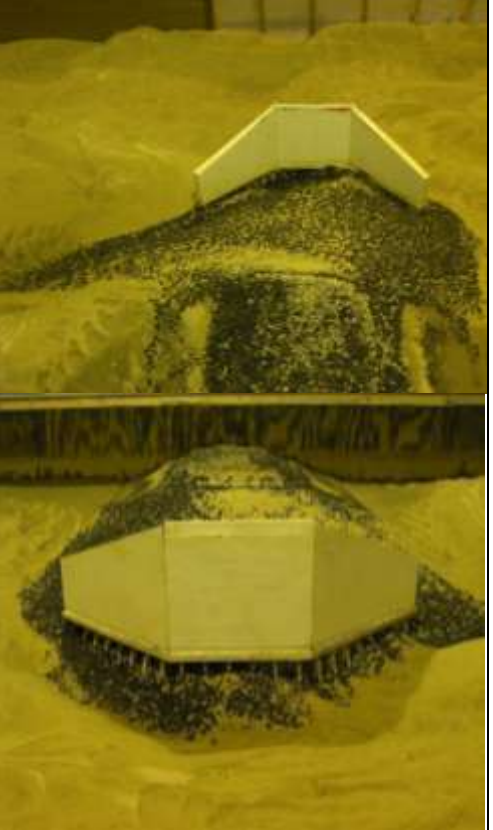
1,445		
1,684		

Final views (1,690)		
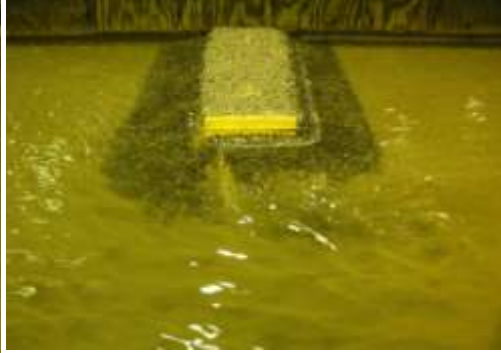
APPENDIX B2: Scour Development at a Riprap-Protected Wing-Wall Abutment on an Erodible Floodplain ($B_f/0.5B = 0.43$, $L/B_f = 1.19$)

Time elapsed (min.)	Side view	Top view
Initial set up		
0		
10		

15		
45		
80		
130		

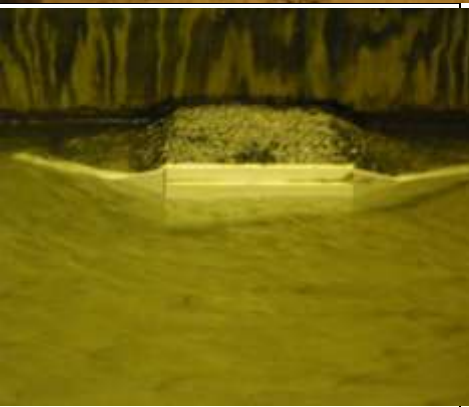| 190		
1,680		
Final view (1,700)		

APPENDIX B3: Scour Development at a Spill-Through Abutment in a
Rectangular Channel or Set Well Back on a Floodplain (*L/*0.5*B* = 0.50)

Time elapsed (min.)	Top view	Front and side views
0		
10		

| 20 | |
| 62 | |

| 178 | |
| 390 | |

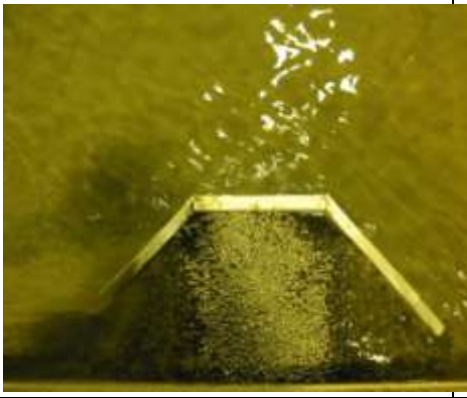|		
1,260		
2,307		
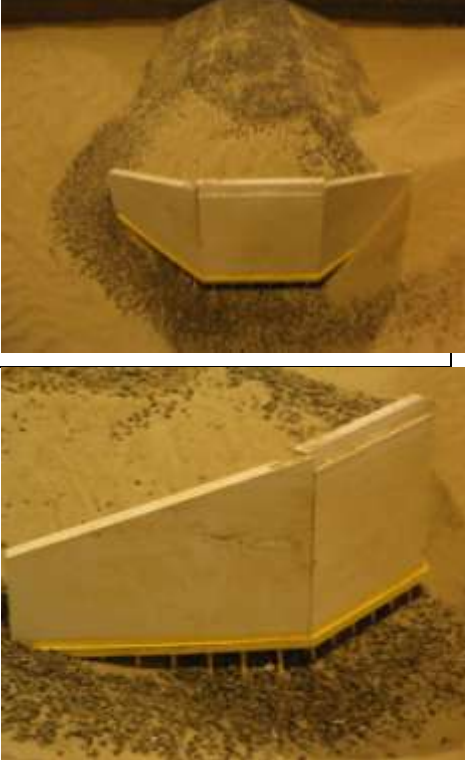
Final view	

APPENDIX B4: Scour Development at a Pile-supported Wing-wall Abutment in a Rectangular Channel or Set Well Back on a Floodplain (*L*/0.5*B* = 0.67)

Time elapsed (min.)	Top view	Side view
Initial set up		
30		
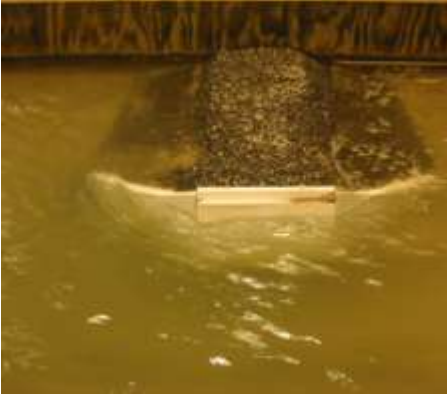
60		
135		

180		
240		
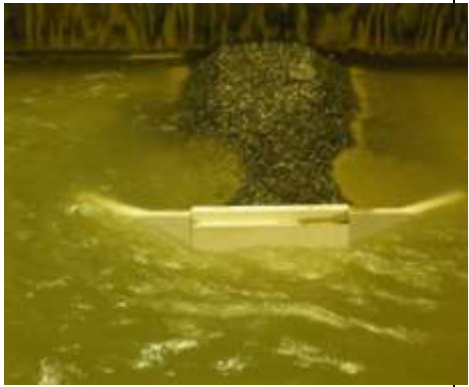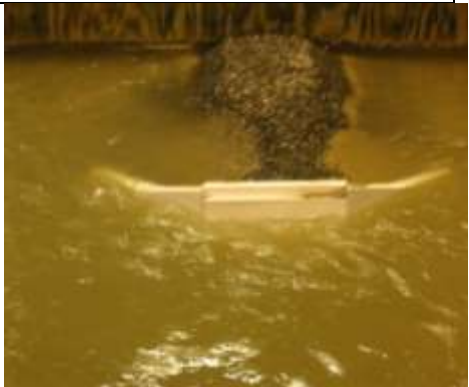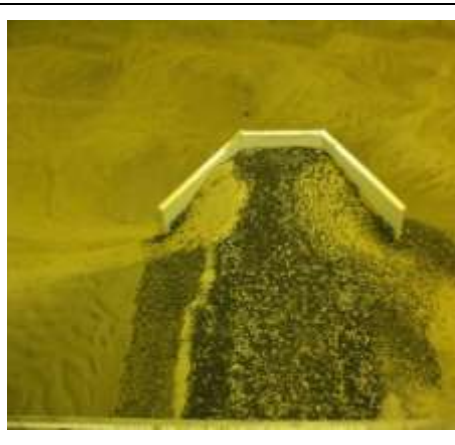
541		
1,140		

Final view		
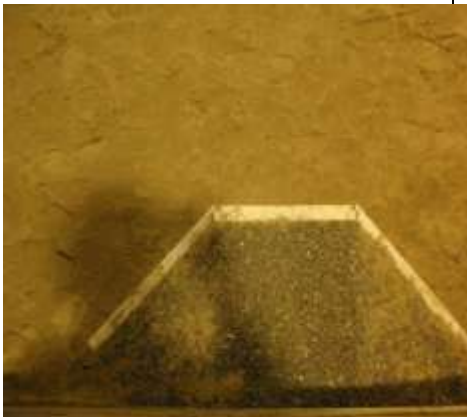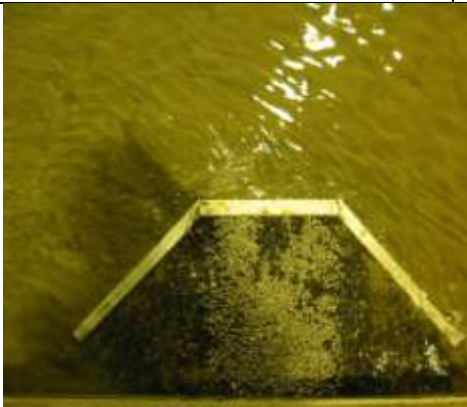
APPENDIX B5: Scour Development at a Sheet-Pile-Supported Wing-Wall Abutment in a Rectangular Channel or Set Well Back on a Floodplain (*L*/0.5*B* = 0.30)
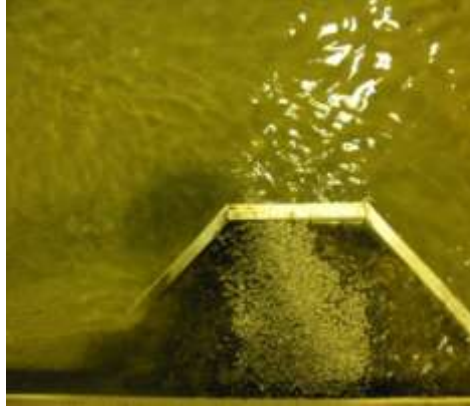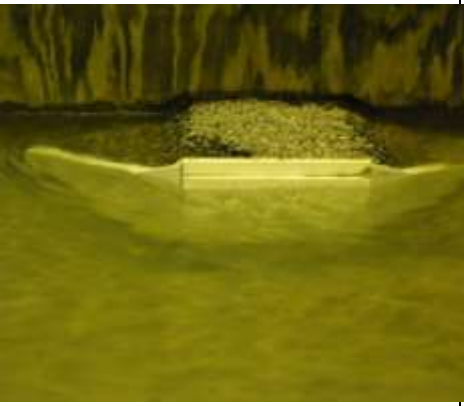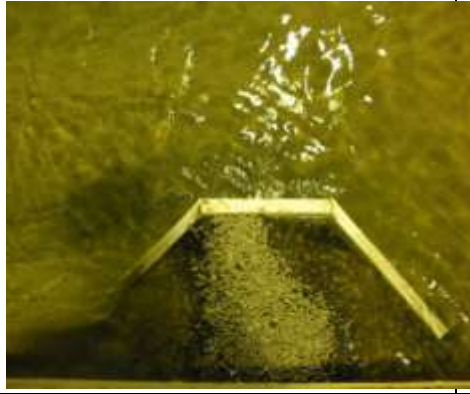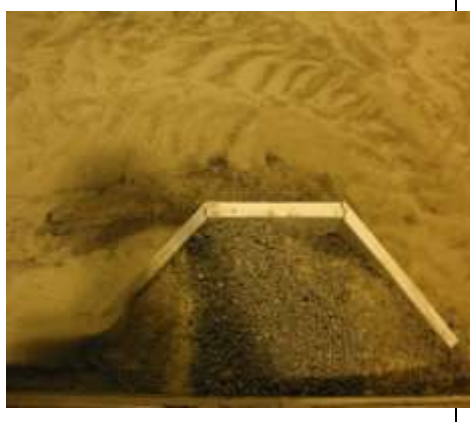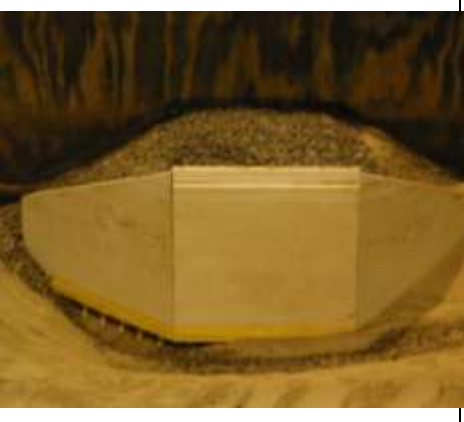
Time elapsed (min.)	Top view	Side view
30		
180		
570		

1,535		
1,680		
Final view		
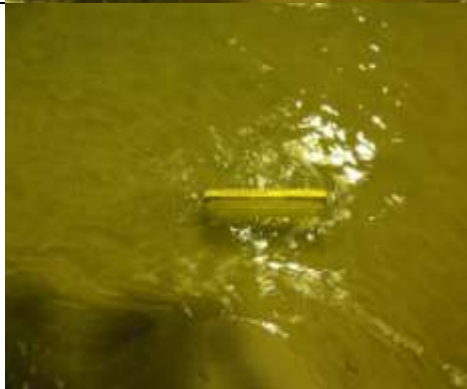
APPENDIX B6: Scour Development at a Riprap-protected, Pile-Supported, Wing-wall Abutment in a Rectangular Channel or Set Well Back on a Floodplain (*L*/0.5*B* = 0.14)

Time elapsed (min.)	Top view	Side and front views
Initial set up		
10		
720		

1,050		
2,180		
Final 2,185		

APPENDIX B7: Scour Development at an Unprotected Spill-Through Abutment in an Erodible Compound Channel ($L/0.5B = 0.43$)

Time elapsed (min.)	Top view	Front or side view
Initial set up		
0		
10		
30		

56		
60		
70		
92		

116		
197		
158		
Final view		

APPENDIX C

SCALE EFFECTS ASSOCIATED WITH TURBULENCE SIMILITUDE IN LABORATORY EXPERIMENTS ON SCOUR

C.1 Introduction

A concern that has plagued prior methods for estimating abutment scour depths, and is an expressed concern for the laboratory experiments on abutment scour conducted in the present Project, is the propensity for such methods to substantially over-predict scour depths. Such over-prediction has been attributed to the fact that the methods are based largely on flume tests using small-scale models, as is the case for the present Project. Scour of a sediment bed around a structure such as a bridge abutment involves a complex flow field marked by large-scale turbulence structures generated by flow around the abutment – notable structures are the horseshoe vortex, surface roller, and wake vortices, as illustrated in Figure C-1 for a simple circular cylinder. The laboratory-based equations used for predicting local-scour depths at cylinders, and abutments, inadequately account for the similitude considerations in the scaling of the frequency and vorticity of large-scale turbulence structures, notably the wake vortices, generated by flow around hydraulic structures. A consequence of inadequate scaling of large-scale turbulence is that flume experiments with small-scale models (the simplest being circular cylinders) can produce larger values of equilibrium scour depth relative to structure size than usually are observed in the field.

The present Project conducted a brief set of auxiliary tests to obtain insights showing that two parameters, and thereby the similitude of coherent turbulence structures, substantially influence equilibrium scour depth. The two parameters describe the frequency of vortex shedding and the amount of vorticity in the wake of an abutment. The insights are substantiated by means of a series of flume experiments conducted with a simple circular cylinder to determine whether the frequency of vortex shedding and wake vorticity influence the scour development and equilibrium scour depth. The experiments involved a set of circular cylinders of differing diameter placed in the same approach flow. Circular cylinders were used because their geometric simplicity enabled clearer definition of large-scale turbulence form and frequencies.

C.2 Similitude

The interaction of flow field and bed sediment around a cylindrical structure is conveniently discussed in terms of non-dimensional parameters that characterize the similitude of water and sediment movement in the local flow field around a circular cylinder. For a steady free-surface approach flow over a planar bed of uniform, spherical, cohesionless sediment, the pertinent variables are (Figure C-1) –

$$\rho, \mu, u_{*0}, g, u_{*c}, d, y_0, D$$

in which ρ and μ are fluid density and dynamic viscosity respectively; u_{*0} is shear velocity, y_0 is undisturbed approach flow depth, g is gravitational acceleration, d is representative grain size, u_{*c} is critical shear velocity for bed sediment entrainment, and D is cylinder diameter. The variables correspond to the following set of independent parameters developed using y_0, u_{*0} and ρ as the normalizing variables:

$$\left(\frac{u_{*0}}{u_{*c}}, \frac{U_0^2 f}{gD}, \frac{\rho U_0 D \sqrt{f}}{\mu}, \frac{D}{d}, \frac{D}{y_0} \right)$$

For the dimensional analysis leading to these parameters, use is made of U_0/D where the Darcy-Weisbach resistance coefficient $f = F(d/y_0)$ in accordance with fully turbulent flow over the approach bed; and U_0 is mean velocity. Equilibrium scour depth, d_{se}, (measured from undisturbed mean bed level) can be functionally related to the parameters; i.e.,

$$\frac{d_{se}}{D} = \varphi_1 \left(\frac{U_0}{U_c}, \frac{U_0^2 f}{gD}, \frac{\rho U_0 D \sqrt{f}}{\mu}, \frac{D}{d}, \frac{D}{y_0} \right) \tag{C-1}$$

Prior laboratory studies (e.g., Breusers and Raudkivi, 1991; Hoffmans and Verheij, 1997; Richardson and Davis, 1995; and Melville and Coleman, 2000) essentially use the functional relationship

$$\frac{d_s}{D} = \varphi_2\left(\frac{U_0}{U_c}, \frac{D}{d}, \frac{D}{y_0}\right)$$
(C-2)

which lacks parameters $\dfrac{\rho U_0 D \sqrt{f}}{\mu}$ and $\dfrac{U_0^2 f}{gD}$. For convenience, these two parameters can be stated simply as $\dfrac{\rho U_0 D}{\mu}$ and $\dfrac{U_0^2}{gD}$, with coefficient f dropped since it is embodied in the variables U_0 and y_0. The parameter D/B expresses cylinder blockage of the channel, an effect that is well understood.

Comparison of Eqs. (C-1) and (C-2) suggests that resolution of scale-issue requires ascertaining the influence of the parameters $\dfrac{\rho U_0 D}{\mu}$ and $\dfrac{U_0^2}{gD}$ on scour depth, as their influences remain largely unconsidered. These two parameters can be interpreted as expressing similitude in the frequency and strength of eddies shed from a cylinder. Given the range of length scales commonly used in scour experiments, Reynolds number in terms of viscous effect is unlikely to have direct bearing on scour depth. However, Reynolds number also influences the frequency of shedding, n, which can be estimated using the relationship between Strouhal number (St) and Reynolds number (Re) for flow around circular cylinders;

$$\frac{nD}{U_0} = \varphi_3\left(\frac{\rho U_0 D}{\mu}\right)$$
(C-3)

For the typical values of cylinder diameters and flow velocities used in flume experiments, as well as for cylindrical piers in a river, Re lies between 10^3 to 10^5, such that $St \approx 0.2$. Thus for cylinders in the same approach flow ($U_0 = $ constant), the frequency of vortex shedding, n, is inversely proportional to cylinder diameter. In other words, smaller cylinders in the same flow generate eddies at a greater rate.

The parameter $\dfrac{U_0{}^2}{gD}$ is in effect a normalized expression of vorticity of wake vortices, with vorticity defined as twice the rotation vector, ω. For a wake vortex, ω is related to the tangential velocity and eddy radius, r;

$$\omega \approx \frac{U_0}{r} \tag{C-4}$$

The representative radius, r, of flow around a circular cylinder is proportional to cylinder diameter, i.e., $r \propto D$. The ratio U_0/D accordingly expresses the scale of vorticity in wake vortices shed from a cylinder in an approach flow of nominal velocity U_0. Wake vorticity can be normalized in terms of D and g as

$$\left(\frac{U_0}{D}\right)\sqrt{\left(\frac{D}{g}\right)} = \frac{U_0}{\sqrt{gD}} \tag{C-5}$$

which squared gives $\dfrac{U_0{}^2}{gD}$. The parameter $\dfrac{U_0{}^2}{gD}$ also emerges from the Euler equation applied to water-surface profile across an eddy (Figure C-2); i.e.,

$$\frac{U_0{}^2}{r} = -\frac{1}{\rho}\frac{\partial}{\partial r}(p + \rho g Y) \tag{C-6}$$

in which Y is water depth, p is pressure, and r is radius of wake vortex. Simplifying, as pressure, $p = 0$ at a free surface,

$$\frac{U_0{}^2}{gr} = -\frac{1}{\rho}\frac{\partial Y}{\partial r} \tag{C-7}$$

in which $-\dfrac{\partial Y}{\partial r}$ is the gradient of the water-surface depression in a vortex shed by flow around the circular cylinder in an approach flow with velocity, U_0; r is the radial distance measured from the centre of the vortex, whose diameter scales (approximately) with D. Eqs. (C-5) and (C-7) imply that narrower cylinders (or small hydraulic models of abutments) in the same approach flow produce stronger eddies.

Though numerous studies have examined the coherent turbulence structures generated by flow around cylinders (e.g., Bearman, 1984 and Williamson, 1996), few studies have examined the influence of coherent turbulence structures on local scour. The writers found Dargahi's work (Dargahi 1989, 1990) to come closest to their own. Dargahi (1989) began by studying the vortex systems formed by a cylinder on a flat bed. He looked at the interaction of the horseshoe vortex and wake vortices, observed that the shedding frequency of horseshoe vortices is close to the shedding frequency associated with the cylinder's Strouhal number, and concluded that the two vortex shedding mechanisms are connected. Also, he observed that wake vortices cause bursts to occur downstream of the cylinder. Dargahi (1990) studied vortex shedding for a cylinder placed in a deformable bed, and found essentially the same vortex shedding behavior as for the fixed flat bed. His observations, together with those reported from scour development around circular cylinders (e.g., Hjorth 1975, Melville 1975, Ettema 1980) and bed-sediment transport generally (e.g., Yalin, 1992), indicate that vortices increase sediment entrainment and movement.

In essence, most laboratory experiments of scour at cylinders overlook the fact that there are three independent length scales in such experiments; cylinder diameter, sand-particle diameter, and flow depth. The three lengths lead to dynamic-similitude parameters that cannot be satisfied concurrently: a particle entrainment parameter, and parameters describing velocity and pressure gradients. The practical upshot is inadequate similitude of large-scale turbulence generated by flow around cylinder.

C.3 Approach
To confirm that similitude of large-scale turbulence structures is an important influence on flume data concerning local-scour depths at circular cylinders, the writers undertook a series of related

flume experiments in which the parameters $\frac{\rho U_0 D}{\mu}$ and $\frac{U_0{}^2}{gD}$ were varied by altering cylinder diameter D. The experiments entailed placing a series of cylinders in the same approach flow, measuring the equilibrium scour depth at each cylinder, then determining the variation of, d_{se}/D, with D; six values of D were used. Velocity measurements were performed for five of the cylinders to assess the frequency and spectral strength (or energy) associated with wake vortices shed from the cylinders. For two cylinders, further measurements were taken to ascertain the maximum vorticity of the wake vortices shed from the two cylinders. Also, flow-visualization experiments were done with one cylinder to view how wake vortices entrain and move sediment from the scour hole. The velocity and vorticity measurements were used to explain the trend obtained between d_{se}/D and D, and thereby to illuminate the significance of similitude in turbulence structures as expressed in the parameters $\frac{U_0{}^2}{gD}$ and $\frac{\rho U_0 D}{\mu}$.

C.4 Flume Experiments

Experiments were done using a re-circulating flume whose test section is 2.5-m deep, 3-m wide, and 21-m long (Figure C-3). The cylinders were placed in a 5-m long, 1.0-m deep sediment recess filled with coarse uniform sand. The median diameter of the sand was $d = 1.05$ mm, and u_{*c} was estimated to be 0.025 m/s (based on the Shields diagram). The approach flow to the test section was tripped by means of roughness blocks so as to produce an approach velocity profile that conformed to a fully turbulent open-channel flow. Table C-1 summarizes the approach-flow condition and cylinder sizes used. The approach flow and sediment were chosen so that the results of the experiments would not be significantly affected by the flow-depth and sediment coarseness factors described by Melville and Coleman (2000) and others. Also, the Reynolds number associated with depth-average flow velocity around the cylinders was in the Strouhal subcritical flow regime in terms of wake-vortex shedding ($St \approx 0.2$).

The shedding frequency of the large scale coherent structures in the wake of cylinders was found by performing power spectrum analysis of the velocity measurements taken in the wake of five cylinders using acoustic Doppler velocimetry (ADV). Initially, the ADV was checked as to whether it had enough temporal resolution to capture large scale eddies in the wake. Measurements were located at ($2.5D$, $1.5D$) relative to the centre of each cylinder; here, the first coordinate is in the downstream direction, while the second one is in the transverse direction,

with the origin of the coordinates is the bed-level center of the cylinder location (see Figure B-1). The measurement location was 0.75 m above the bed elevation. The sample size of 5,000 was taken at a sampling rate of 20Hz. Power spectrum plots were obtained from velocity time-series data using fast-Fourier-transform (FFT) analysis.

Large-scale particle-velocimetry (LSPIV) measurements were made to determine the strength and extent of the vortical structures behind the cylinder. The measurements were made at the flow free surface behind two cylinders (D = 64 mm and 114 mm). Flow-surface seeding was done with 2-mm diameter polypropylene beads as tracers. Image recording was done by means of a digital video camera that produced geometrically non-distorted images. In-house developed software provided instantaneous velocities and velocity-derived quantities (temporal mean, turbulence intensity, and temporal vorticity). The LSPIV procedure is described by Fujita et al. (1998).

A digital video camera also was set up at the side of the flume so as to record the flow features and particle movements associated with scour development around one cylinder (D = 172 mm). A non-dispersive dye was used to visualize wake vortices shed from the cylinder in several horizontal planes below the water surface. The dye produced strands of a shear-thickening, high extensional viscosity mixture designed to be slow to disperse (Hoyt and Sellin, 2000). The dye wand was placed upstream of the cylinder, centered with respect to the cylinder and at several elevations above the bed.

C.5 Results

The experiments yielded data and observations on equilibrium scour depth, frequency and intensity of wake vortices, wake flow field, along with sediment entrainment and movement from the scour hole.

C.5.1 Equilibrium Scour

Figure B-4 shows that the equilibrium scour depth normalized with cylinder diameter, d_{se}/D, was larger for the smaller cylinders, and that d_{se}/D varied almost inversely with D, at least for the range of cylinder sizes considered. The intensity or vorticity of eddies formed by flow around

each cylinder, expressed as $\dfrac{U_0^2}{gD}$, increases as D decreases; $\dfrac{U_0^2}{gD}$ is larger for the smaller cylinders, as given in Table 2. Note that, as the approach flow was the same for all the tests, Figure C-4 could be viewed as d_{se}/D plotted versus pier Reynolds number, $\dfrac{\rho U_0 D}{\mu}$. Additionally, Figure C-5 shows that d_{se}/D decreased as the normalized value of vorticity, $\dfrac{U_0^2}{gD}$, decreased; as U, f, and g were constant for the experiments, $\dfrac{U_0^2}{gD}$ = (constant)/D. These results support the writers' suggestion that inadequate similitude of large-scale turbulence influences the values of d_{se}/D obtained from laboratory experiments.

C.5.2 Frequency and Intensity of Shed Vortices

The power spectra for the streamwise component of flow velocity at the measurement point for five of the six cylinders are shown in Figure C-6. Table C-3 summarizes the maximum frequencies in each of the distributions. The frequencies correspond to the formation of the wake vortices shed from the boundary layer formed from each cylinder. The data in Figure C-6 and Table C-3 show that the frequency of shedding, and the vorticity of shed vortices, increased as cylinder diameter decreased. Figure C-7, which relates dominant frequency of vortex shedding to cylinder diameter delineates the trend more clearly.

The power associated with the peak frequency for the power-spectrum distribution indicates the strength of vorticity of wake vortices formed by the cylinder. In turn, the strength of wake vorticity expresses the capacity of wake vortices to entrain and move bed sediment from the flanks and rear of each cylinder. Table C-3 also summarizes the peak power values in the power spectrum plots. Figure C-8 shows that, as cylinder diameter increased, the power associated with the peak frequency decreased. This result supports the notion that smaller cylinders generate wake vortices of greater vorticity. Note that, although the measured power value for the 64 mm cylinder is shown in Figure C-8, the power was lower than the level expected, because the size of the ADV probe had become large compared to the size of the wake vortices.

C.5.3 Wake Vorticity

To better understand the influence of cylinder diameter on the vorticity of wake vortices and turbulence behind the cylinders, it is useful to illustrate the vorticity contours of the flow field behind two cylinders differing in diameter. The time-average structure of the wake vortices is revealed from plots of instantaneous vorticity plots determined using LSPIV measurements taken immediately behind two cylinders (Figures C-9a,b).

The plots illuminate the wake vortices formed from each cylinder. The vortex center was taken as the location of maximum vorticity for the wake vortices evident in Figures C-9a,b. The two vorticity plots use the same contour range and are in the same scale. Two dominant vortices are observable in the figures: a clockwise-rotating vortex and a counterclockwise-rotating vortex. Comparison of the shading density of the clockwise-rotating vortices (at the lower left corners of the frames) indicate that the eddy produced by the small cylinder ($D = 64$mm) is of much higher vorticity than the wake vortex formed by the large cylinder ($D = 114$mm), and thus the former eddy is indeed more intense. The magnitude of maximum, vertical out-of-plane vorticity (ω_z) was measured for the clockwise-rotating eddy observed for each cylinder. The maximum value of ω_z in the wake of the small cylinder was 24.52s/m, whereas the value estimated for the larger cylinder was 11.17s/m. As cylinder diameter approximately doubled, ω_z was about halved.

C.5.4 Wake-Vortex Visualization

As the scour hole initially developed around the 172mm-diameter cylinder, the horseshoe vortex actively entrained and moved sediment. Additionally, the wake vortices vigorously conveyed entrained sediment away from the scour hole, though the trajectories of entrained particles did not directly follow the bed, but rather followed spiral paths projected from the horseshoe vortex and connecting with the wake vortices. The spiral paths often caused individual sediment particles to be lifted as much as 80% of the flow depth behind the cylinder (Figure C-10).

When the wake vortices moved downstream from the cylinder, they weakened in intensity, with the consequence of particles dropping back to the bed. This effect, occurring in the cylinder's overall wake, resulted in the formation of a dune-like mound behind the cylinder. As the scour deepened, the vortices played an increasingly important role in moving sediment out of the scour

hole. The turbulence bursts occurring with wake-vortex impingement on the bed were the main flow events causing sediment ejection from the scour hole (Figure C-10). Once the equilibrium scour depth had more-or-less been attained, bed particles were moved only by the intermittent bursts caused by eddy impingement.

The use of dye revealed the vortices as well (Figure C-11). The average size of each vortex was estimated from each snapshot by following the vortex path. A comparison of the diameter of the vortices indicates the change in the structure of the vortex over the flow depth. Table C-4 shows that the vortex sizes were similar in planes 500 mm and 300 mm above the bed, but smaller in the plane 100 mm above the bed. These observations indicate the vortices observed using LSPIV were suitably representative of the coherent eddy system formed by the cylinder along most of its length.

C.5.5 Adjustment Factor for Wake-Vorticity Similitude

The data from the present study can be plotted so as to give the value of an adjustment factor for use in accounting for the miss-scaling of the coherent turbulent structures. Figure C-12 shows the resulting plot. In constructing the plot, the largest diameter cylinder tested (D = 0.4 m) was taken as reference diameter reasonably representative of prototype circular piers and piles (D_0), which commonly have diameters ranging from about 0.5 m to 1.0 m in diameter. Since modeling is performed with small cylinders, other cylinders act as model cylinders in laboratory conditions. Application of the correction factor to the scour depths obtained for each of the cylinders used in the experiments gives the same scour depth relative to cylinder diameter: d_s/D = 1.15 when u_*/u_{*c} = 0.80. The plot, along with the following equation drawn from it, provide a way to correct scour-depth estimates obtained from small-scale cylinders in experiments conducted with bed-sediment entrainment as primary similitude criterion:

$$K_W = 0.95(D_0 / D)^{-0.26}$$
(C-8)

with D_0 here taken as 0.40m. Though the present study was limited in the range of cylinder sizes used, and it did not investigate scour at narrow cylinders (large D_0/D), the writers anticipate that the plot in Figure C-12 levels off for large values of D_0/D. At such values, the bed-sediment

becomes increasingly rough relative to cylinder diameter, and leads to diminished scour depth relative to cylinder diameter (e.g., Melville and Coleman 2000). Though developed from clear-water scour, Eq. (C-8) expresses a general correction that is useful for adjusting also scour depths associated with live-bed scour.

C.6 Summary and Implications for Abutment-Scour Models

The experiments show the importance of considering similitude of large-scale turbulence structures generated by flow around cylinders, and thereby more complex structures like abutments, when conducting flume experiments on local scour. The experiments show that, for the same approach flow, d_{se}/D decreases as cylinder diameter increases (Figure C-4). The reduction in d_{se}/D coincides with, and is attributable to, reductions in the shedding frequency and vorticity of wake-vortices as cylinder diameter increases (Figures C-7 and C-8). An adjustment factor is needed to account for similitude of turbulence structures generated by flow around a cylinder. The results suggest using Figure C-12 for this purpose, though further data and work are needed to confirm and perhaps extend this figure.

The need for an adjustment factor arises because of a scale effect essentially attributable to the use of three independent length scales in local-scour experiments; cylinder diameter (or abutment width), bed-particle diameter, and flow depth. The three lengths lead to dynamic-similitude parameters that cannot be satisfied concurrently. One consequence is inadequate similitude of large-scale turbulence generated by flow around a cylinder during local-scour experiments.

The importance of turbulence structures on scour was confirmed by way of the further series of experiments involving ADV and LSPIV measurement of the flow in the cylinder wake, as well as from a set of flow-visualization experiments. ADV spectral analysis showed that in the same approach flow conditions, smaller cylinders shed eddies more frequently than do large cylinders. This finding is in agreement with the constancy of Strouhal number, 0.2, for the range of Reynolds numbers considered ($Re = 2.9 \times 10^4$ to 1.86×10^5).

LSPIV applied to two cylinders, differing in diameter by a factor of about 2, showed that the maximum vorticity of wake flow behind the smaller cylinder is about twice that for the larger

cylinder. This finding indicates that, for the same approach flow, a small cylinder has more capacity to remove scoured sediment compared to a large cylinder because it produces stronger eddies. The sediment particles entrained by the flow in the wake can be lifted up to near the free surface in the spiral upwelling caused by wake vortices.

The experiments imply that prior, flume-based equations for estimating equilibrium-scour depths at cylinders (or similar structures used to model bridge abutments) in a sediment bed scour may not adequately account for the similitude in coherent turbulence structures generated by flow around cylinders. The results from the experiments help in explaining why proportionately larger scour depths may occur for smaller cylinders, and smaller-scale abutment models, in flume experiments on local scour.

The question arises as to which length associated with an abutment should be used in the parameter $\dfrac{U_0^2}{gD}$ for similitude of turbulence structures generated by flow around abutments. It is suggested that D in the parameter be replaced with W, the top width of the abutment; i.e., $\dfrac{U_0^2}{gW}$.

Top width essentially is set as the roadway width, which is more-or-less standard. The energy head developed at the upstream face of an abutment corner dissipates around the end of the abutment and in the wake region. The width used in the abutment scour experiments (see Chapters 7 through 11) equaled or exceeded the width of the widest cylinder used in the present auxiliary experiments, thereby indicating that the present abutment-scour experiments were not by as substantially affected by scale effects attributable to large-scale turbulence as would have been smaller models. The 0.40m-wide abutment models were in a size range for which such scale effects would be negligible, in accordance with Figure C-12. Also, the abutment scour experiments (Chapters 7 through 11) showed that scour was predominantly governed by flow contraction and flow distribution rather than by large-scale turbulence. Therefore, the scour depths obtained for the abutment-scour experiments are in appropriate proportion with the size of the abutments simulated in the experiments.

Table C-1. Experimental conditions for scour experiments

Average Velocity U_0 (m/s)	u_*/u_{*c}	Pier Diameter D (mm)	Flow Depth Y (mm)	Reynolds Number Re
0.46	0.80	406	1000	1.86E+05
0.46	0.80	305	1000	1.39E+05
0.46	0.80	241	1000	1.10E+05
0.46	0.80	172	1000	7.84E+04
0.46	0.80	114	1000	5.22E+04
0.46	0.80	64	1000	2.90E+04

Table C-2. Results of the scour-depth experiments

D (mm)	d_{se} (mm)	Time to Equilibrium Scour (hours)	U_0^2/gD
406.4	435.4	48	0.049
304.8	368.4	24	0.066
241.3	313.4	24	0.083
171.5	258.0	24	0.117
114.3	184.6	24	0.175
63.5	110.5	24	0.316

Table C-3. Eddy frequency and peak power measurements

Pier Diameter (mm)	Peak Frequency (Hz)	Peak Power (cm^2/Hz)
406	0.16	1800
241	0.36	4400
172	0.55	5800
114	0.81	8500
64	1.59	3500

Table C-4. Comparison of eddy size in different planes in pixel units on video

Elevation above Bed (cm)	Eddy Diameter (pixels)
10	105
30	130
50	127
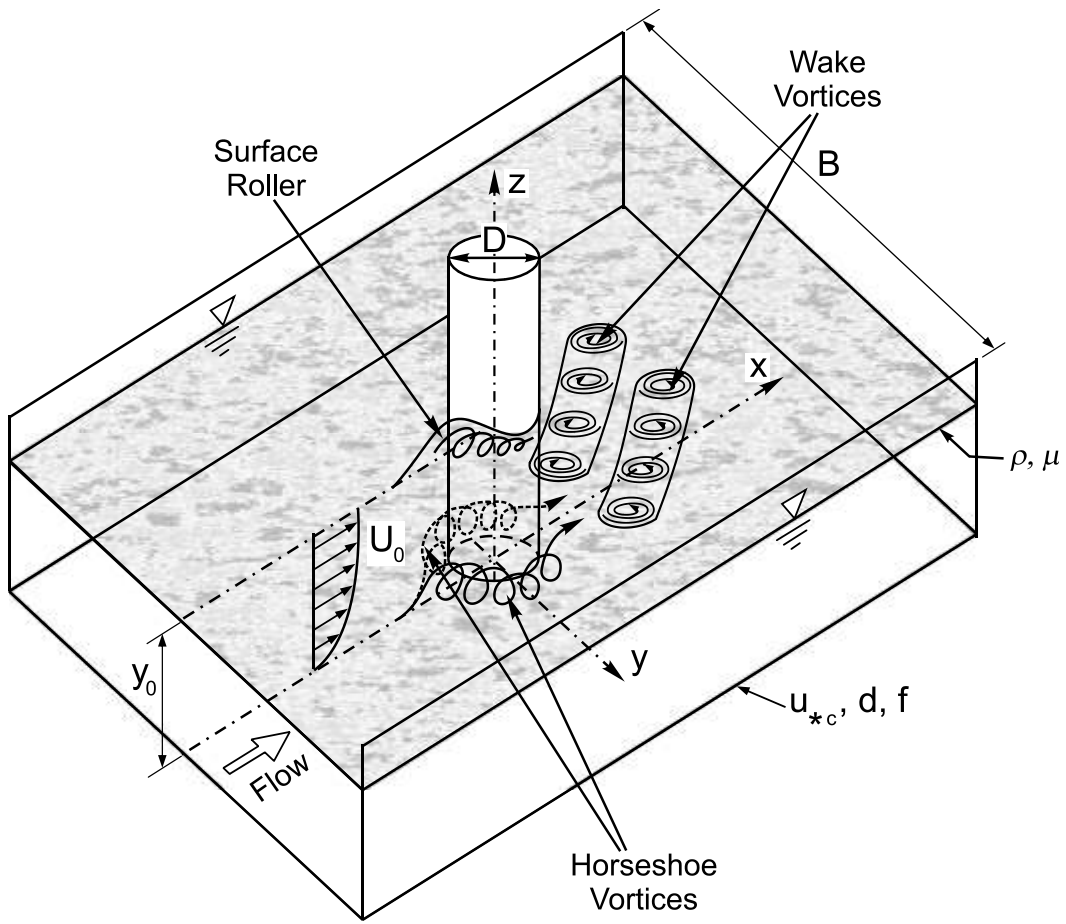
Figure C-1. Schematic of large-scale turbulence structures at circular pier
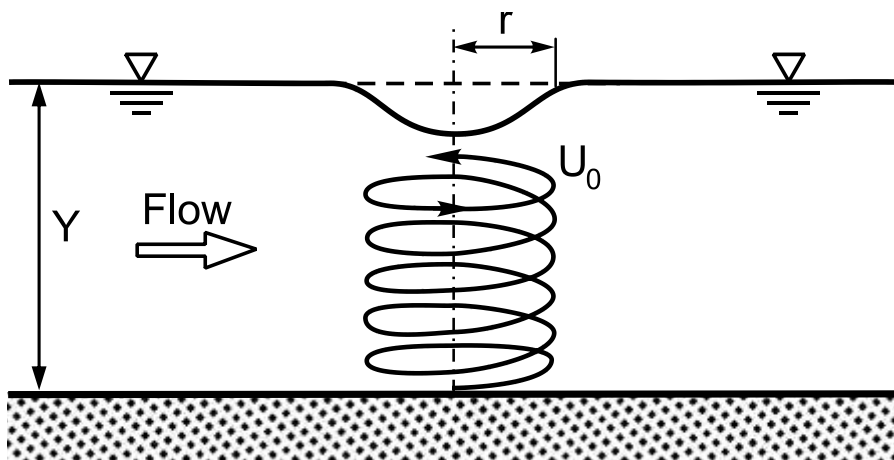
Figure C-2. Water-surface profile associated with a free-surface eddy
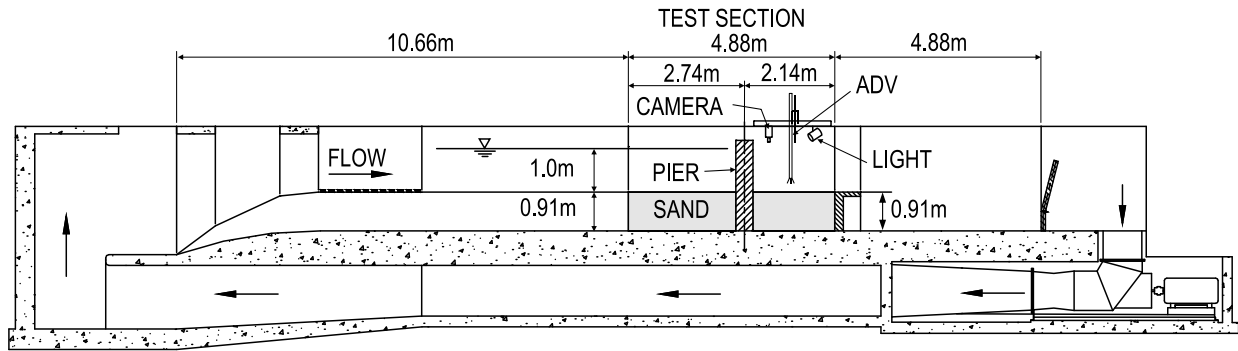
Figure C-3. Flume and experiment layout (side view)
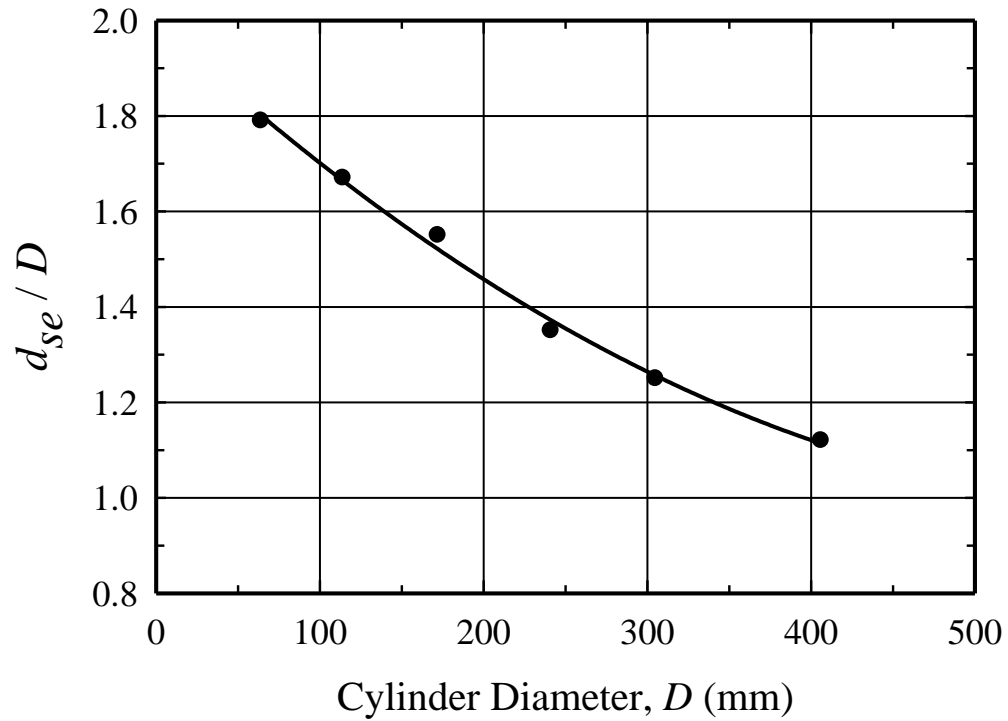
Figure C-4. Variation of d_{se}/D with D; essentially d_{se}/D versus $(\rho U/\mu)D$ for the same approach flow
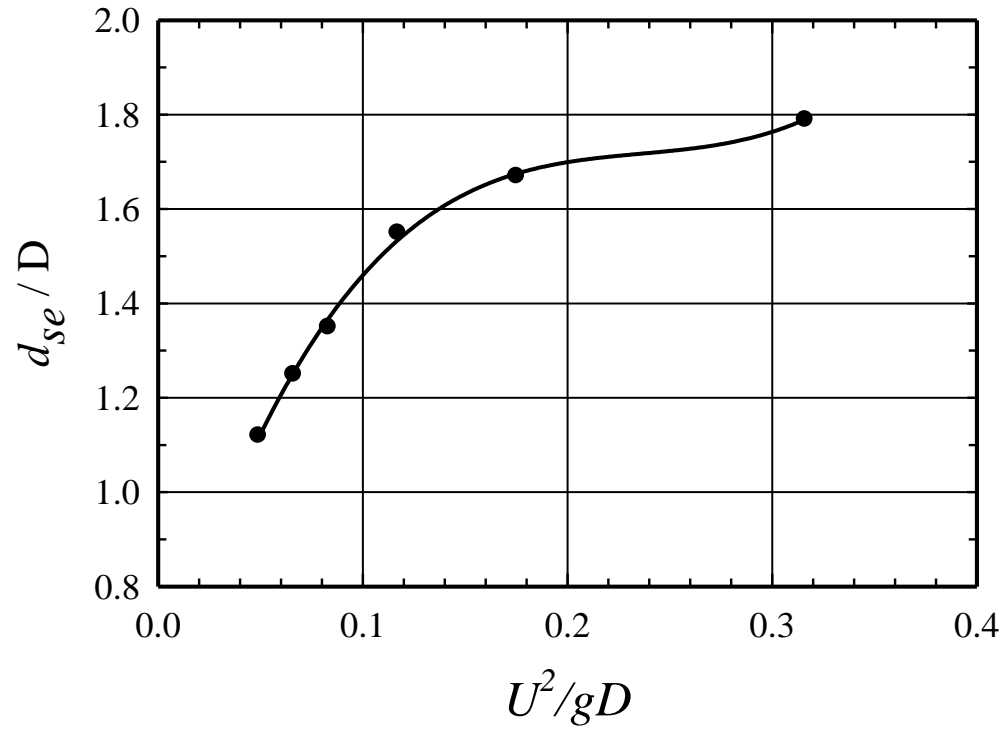
Figure C-5. Variation of d_{se}/D with U^2/gD
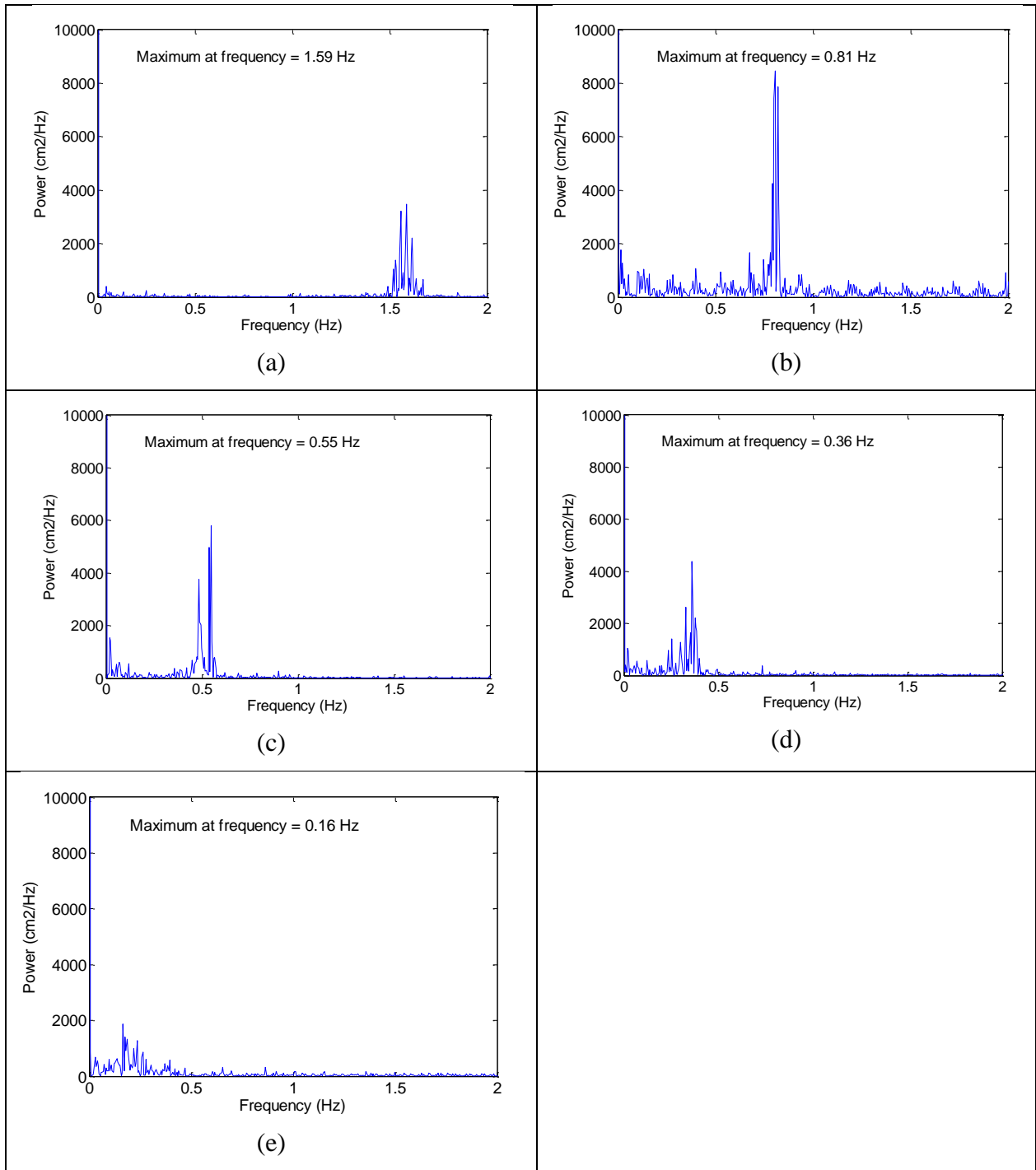
Figure C-6. Power-spectrum plots for velocity measurements for five-cylinder diameters: *D* = 64 mm (a); *D* = 114 mm (b); *D* = 172 mm (c); *D* = 241 mm (c); and, *D* = 406 mm (e)
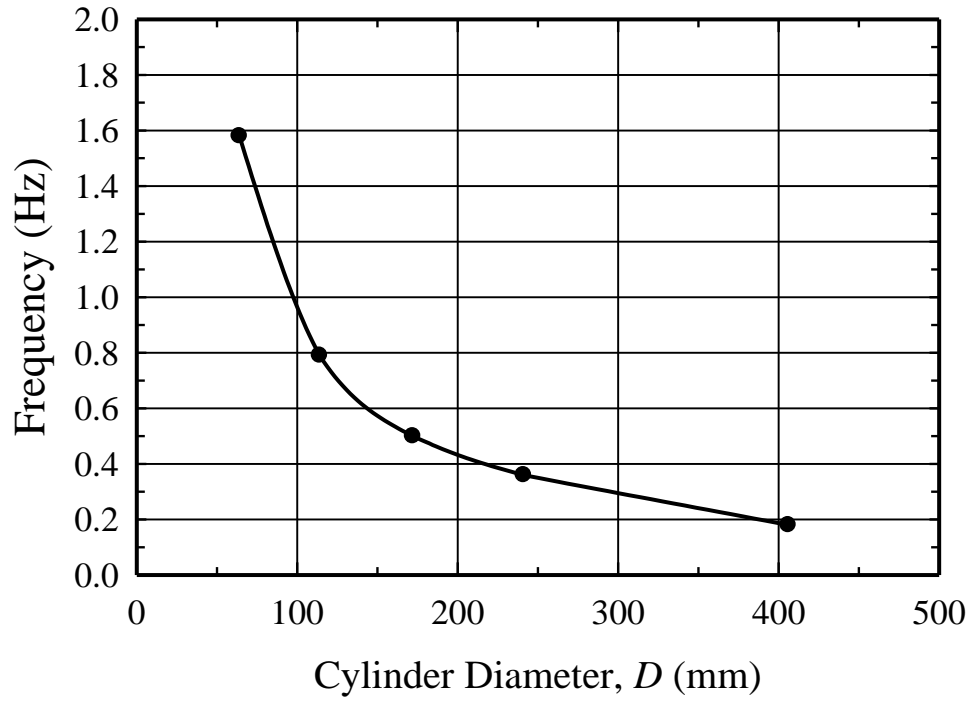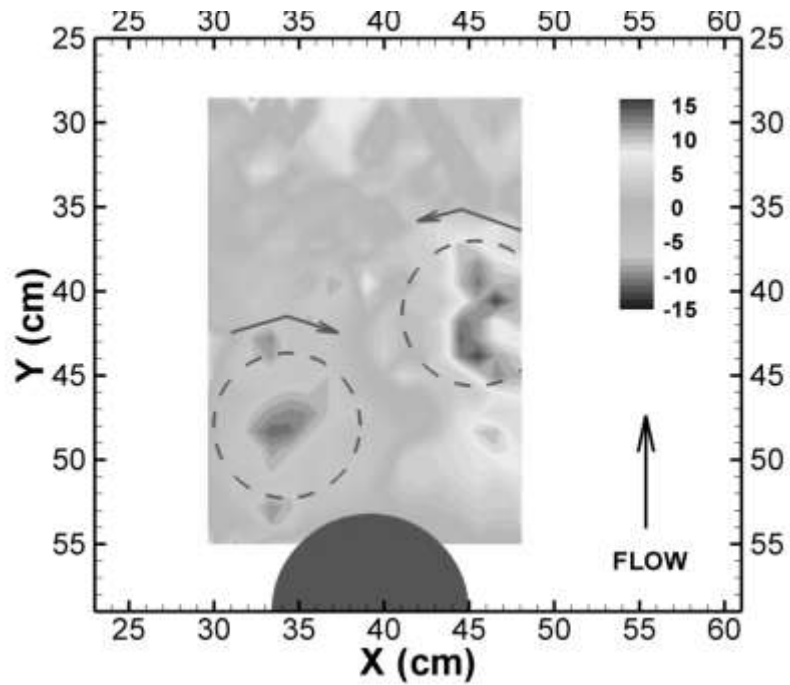
Figure C-7. Eddy shedding frequency versus cylinder diameter
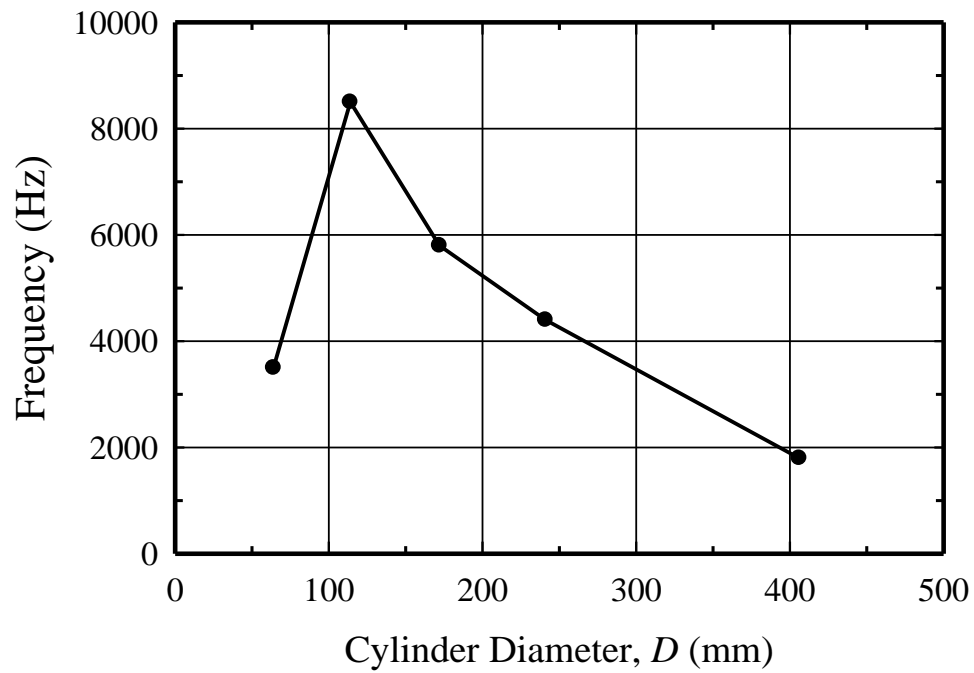
Figure C-8. Power-spectrum peak versus cylinder diameter
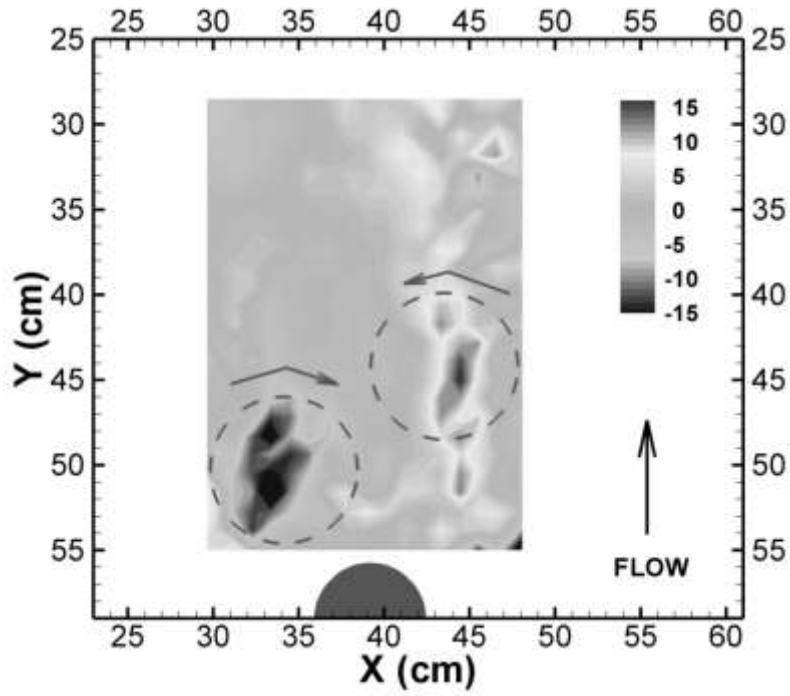
(a)

(b)

Figure C-9. Instantaneous contour of vorticity on x-y plane within cylinder wake: $D = 64$ mm
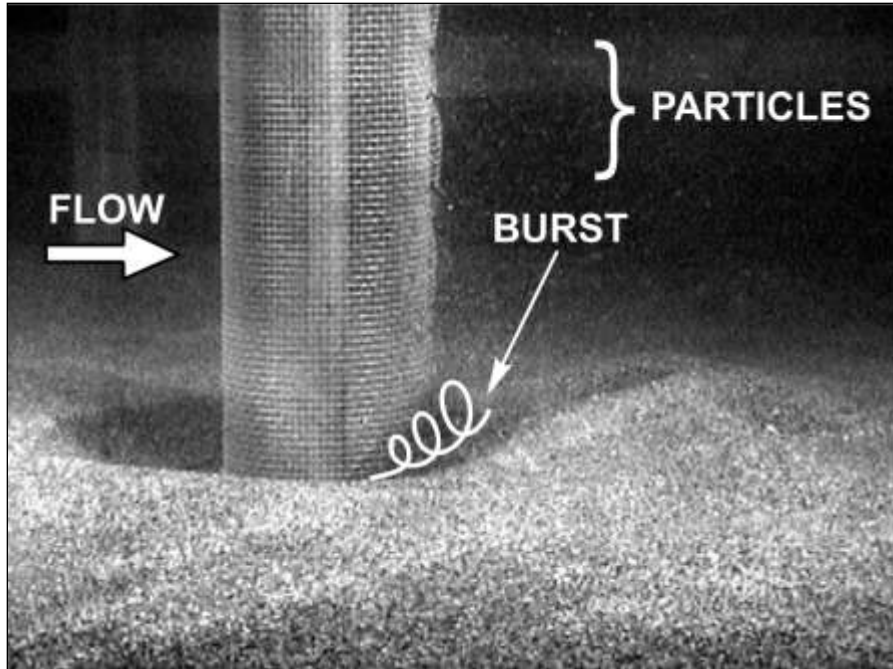(a); and, $D = 114$ mm (b)

Figure C-10. Snapshot from video, showing turbulent burst lifting bed particles into the water column behind cylinder
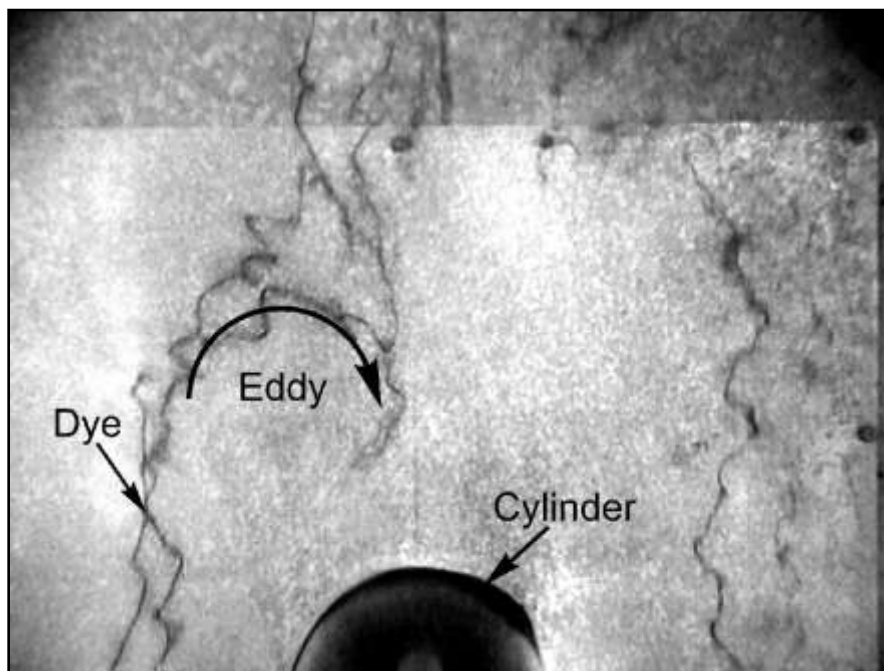

Figure C-11. Snapshot from video, showing an eddy (dye wand was located 300 mm above bed)
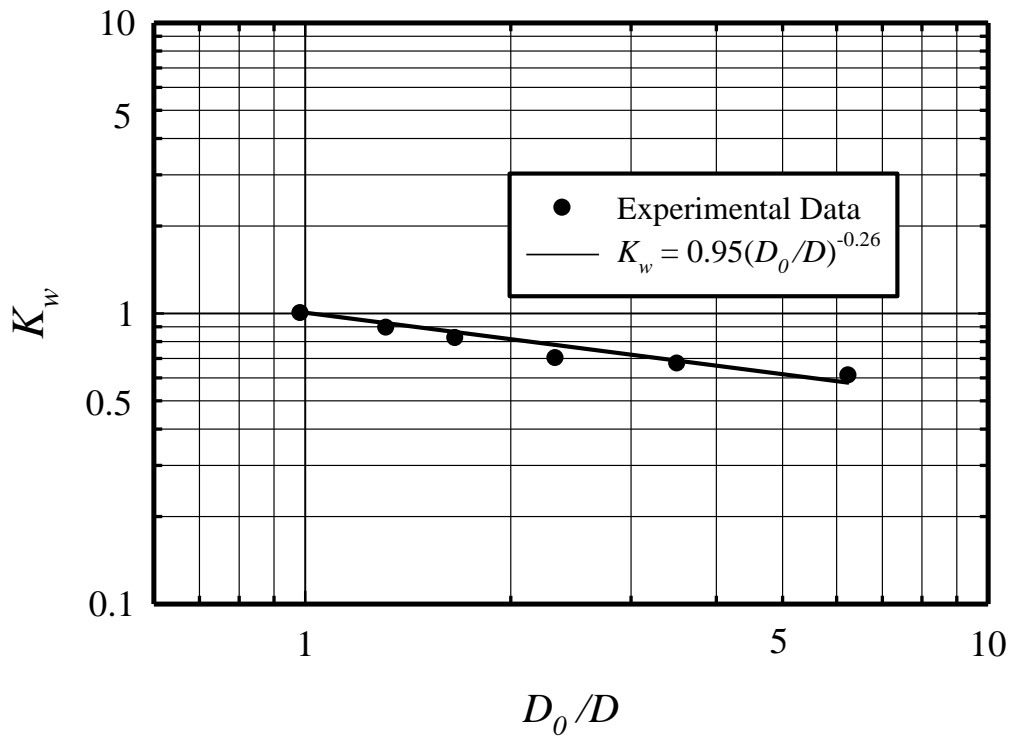
Figure C-12. Adjustment factor, K_w, to account for inadequate similitude of large-scale turbulence structures